

Plastic shrinkage cracking of blended cement concretes under hot weather conditions

Taofiq Olatunbosun Abiola

Civil Engineering

September 2002

Abstract

In order to inhibit the deterioration of concrete structures in the Arabian Gulf environment, emphasis has been shifted from the requirements of concrete strength towards to its durability, especially the selection of materials. Towards this end, silica fume and other types of blended cement materials are being used. However, silica fume cement concrete is also more susceptible to plastic shrinkage cracking, and under hot weather conditions, this cracking could be further aggravated. This research was conducted to investigate the effect of the type and dosage of silica fume and other blended cements on the plastic shrinkage cracking of concrete. The effect of cement type, super plasticizer type, temperature relative humidity and wind velocity on the plastic shrinkage strains, cracking and the microstructure were conducted. Additional studies to evaluate the effect of the type of silica fume on the early age properties, such as the compressive strength; the split tensile strength and the ultrasonic pulse velocity were also conducted.

Results of this research indicated that it is the fineness of the silica fume and its state of densification that determine its plastic shrinkage strain response. The fineness of the silica fume must be evaluated in terms of not only its specific surface area, but also its average pore radius.

The plastic shrinkage strain increased with increasing temperature and wind velocity and decreasing relative humidity. The decrease in the relative humidity presented the most severe condition that promoted higher plastic shrinkage strains and cracks. A threshold value of plastic shrinkage strain was determined in plain and blended cement that will initiate plastic shrinkage cracks. This threshold value was found to be independent of the exposure conditions.

The type of super plasticizer had a significant effect on the plastic shrinkage strains in silica fume cement concretes. The effect of the fineness of the silica fume played the most important role in determining the plastic shrinkage strains in the concrete. Incompatibility between the type of super plasticizer and the silica fume cement concrete was also noted. Statistical analysis of the early age properties, such as the compressive strength, split tensile strength and pulse velocity of plain and blended cements suggested that the material variability as represented by the type and dosage of silica fume was comparable to that of plain cement concrete.

INFORMATION TO USERS

This manuscript has been reproduced from the microfilm master. UMI films the text directly from the original or copy submitted. Thus, some thesis and dissertation copies are in typewriter face, while others may be from any type of computer printer.

The quality of this reproduction is dependent upon the quality of the copy submitted. Broken or indistinct print, colored or poor quality illustrations and photographs, print bleedthrough, substandard margins, and improper alignment can adversely affect reproduction.

In the unlikely event that the author did not send UMI a complete manuscript and there are missing pages, these will be noted. Also, if unauthorized copyright material had to be removed, a note will indicate the deletion.

Oversize materials (e.g., maps, drawings, charts) are reproduced by sectioning the original, beginning at the upper left-hand corner and continuing from left to right in equal sections with small overlaps.

ProQuest Information and Learning
300 North Zeeb Road, Ann Arbor, MI 48106-1346 USA
800-521-0600

UMI[®]

NOTE TO USERS

This reproduction is the best copy available.

UMI[®]

**PLASTIC SHRINKAGE CRACKING OF BLENDED
CEMENT CONCRETES UNDER HOT WEATHER
CONDITIONS**

BY

Taofiq Olatunbosun Abiola

A Thesis Presented to the
DEANSHIP OF GRADUATE STUDIES

KING FAHD UNIVERSITY OF PETROLEUM & MINERALS

DHAHRAN, SAUDI ARABIA

In Partial Fulfillment of the
Requirements for the Degree of

MASTER OF SCIENCE

In

Civil Engineering
September 2002

UMI Number: 1411737



UMI Microform 1411737

**Copyright 2003 by ProQuest Information and Learning Company.
All rights reserved. This microform edition is protected against
unauthorized copying under Title 17, United States Code.**

**ProQuest Information and Learning Company
300 North Zeeb Road
P.O. Box 1346
Ann Arbor, MI 48106-1346**

بِسْمِ اللَّهِ الرَّحْمَنِ الرَّحِيمِ

**PLASTIC SHRINKAGE CRACKING OF BLENDED
CEMENT CONCRETES UNDER HOT WEATHER
CONDITIONS**

TAOIFIQ OLATUNBOSUN ABIOLA

MS Thesis

**KING FAHD UNIVERSITY OF PETROLEUM AND
MINERALS**

September 2002

This copy of the thesis has been submitted on the conditions that anyone who consults it is understood to recognize that its copyright rests with its author and that no quotation from the thesis and no information derived from it may be published without proper permission from the author and his Thesis Advisor.

**KING FAHD UNIVERSITY OF PETROLEUM AND MINERALS
DAHHRAN, SAUDI ARABIA**

DEANSHIP OF GRADUATE STUDIES

This thesis, written by
TAOIQI OLATUNBOSUN ABIOLA

under the direction of his Thesis Advisor, and approved by his Thesis Committee, has been presented to and accepted by the Deanship of Graduate Studies, in partial fulfillment of the requirements of the degree of:

**MASTER OF SCIENCE IN CIVIL ENGINEERING
(STRUCTURES)**

Thesis Committee

Dr. Omar S. B. Al-Amoudi (Chairman)

Hamad I. Al-Abdul Wahhab
Dr. Mohammed Maslehuddin (Co-Chairman)

Prof. Abdullah Al-Musallam (Member)

Dr. Maher Bader (Member)

Dr. Mesfer Al-Zahrani (Member)

Dr. Hamad. I. Al-Abdul Wahhab

Department Chairman

Prof. Osama A. Jannadi

Dean of Graduate Studies

Date: 6/10/2002



Dedicated to

Me, I and Myself,

A milestone, of profound memory,

More than a ripple in the sea

ACKNOWLEDGEMENT

All praise is due to Allah, subhana wa ta'aala, Who gave me this patience and the strength and determination to complete this work successfully. I seek His mercy, favor and forgiveness upon His noble prophet Muhammad sallalahu alaiyhi wa sallam. I would like to thank King Fahd University of Petroleum & Minerals for giving me opportunity to pursue my graduate degree here, providing excellent research facilities and financial assistance during the course of my MS program.

I am thankful to my thesis advisor Dr. O. S. B. Al-Amoudi for his constant encouragement and for having what I call 'the right attitude' throughout the course of this research and a Professor of Civil Engineering in general. I also wish to thank him for his making all the financial and material resources at his disposal available throughout the course of this research.

My special sincere appreciation, indebtedness and thanks go to my thesis co-advisor Dr. Mohammed Maslehuddin for his invaluable help and advice. I acknowledge his untiring efforts, constant encouragement and unlimited support, concern, valuable time and, patience, guidance and critical review of the thesis during all its stages. I am grateful to my committee members Dr. Mesfer Al-Zahrani for his constant concern, and interest and personal understanding. I also thank Prof. Abdullah Al-Musallam and Dr. Maher Bader for their valuable comments and interest.

I am also thankful to the existing and past Chairman of the Department, Dr. Hamad I. Al-Abdul Wahhab, and Dr. Sahel N. Abdul-Jauwad respectively, and other faculty members for their cooperation, throughout the duration of my stay in KFUPM. I express my sincere appreciation and thanks to Mr. Hassan Zakariya for his help throughout the experimental stages of this work. I am also grateful to Dr. Ibrahim Asi who was in charge of all Civil Engineering Equipment, Mr. M. M. Khan, Mr. Omar Ahmad, of the various Civil Engineering Laboratories. Mr. Yones C. Solander and his team at the Central Workshop who fabricated the moulds used in the experiment, Mr. Farid and his team at RI who resuscitated most of the electronic equipment when they broke down, Dr. Ashraf Ali and Mr. Khalid and Mr. Rahat Saeed of the Petroleum Refining Section, RI, who assisted with the nitrogen adsorption. Mr. Barri, Mr. Shameem, Mr. Ibrahim and Mr. Rizwan of the Engineering Analysis Section RI, for the equipment I borrowed from them. I am also thankful to Mr. Saeed Al-Selais and Mr. Ibrahim Maghrabi of the Maintenance Department who were always on-hand and willing to fix the chamber whenever it broke down, and Mr. M. Abdul-Waris of the same department who assisted me with his own experience and helpful comments on the experimental setup.

I express my thanks to all my friends, the Nigerians as well as those from the Indian sub-continent, for making my stay at KFUPM a memorable one. I'll also like to appreciate the contributions of my friends and family back home, in the USA and South Africa.

TABLE OF CONTENTS

ACKNOWLEDGEMENT	vi
TABLE OF CONTENTS	vii
LIST OF TABLES	xiv
LIST OF FIGURES.....	xviii
ABSTRACT (ENGLISH)	xxvi
ABSTRACT (ARABIC)	xxvii
1 INTRODUCTION.....	1
1.1 CONCRETE DURABILITY UNDER HOT WEATHER CONDITIONS OF THE ARABIAN GULF	1
1.2 NEED FOR THIS RESEARCH.....	7
1.3 RESEARCH OBJECTIVES	9
2 LITERATURE REVIEW.....	11
2.1 CONCRETE DURABILITY UNDER HOT WEATHER CONDITIONS OF THE ARABIAN GULF	11
2.2 CRACKING IN CONCRETE.....	15
2.2.1 Crack Formation due to Desiccation.....	17
2.2.2 Crack Formation due to Temperature Gradients.....	19
2.3 PLASTIC SHRINKAGE CRACKING OF CONCRETE	20
2.3.1 Factors Affecting Plastic Shrinkage Cracking	24

2.4 SILICA FUME CONCRETE.....	31
2.4.1 Characteristics of Silica Fume.....	32
2.4.2 Silica Fume in the Arabian Gulf	34
2.4.3 Silica Fume Production and Delivery Forms	34
2.4.4 Plastic Shrinkage of Silica Fume Cement Concrete.....	37
2.4.5 Effect of Silica Fume on the Mechanism of Plastic Shrinkage Cracking .	39
2.4.6 A Model for Plastic Shrinkage.....	42
2.5 SUPERPLASTICIZERS	45
2.5.1 Interaction of Superplasticizers and Cement Matrix	47
2.5.2 Effect of Superplasticizer Dosage and Type of Cement	49
2.5.3 Effect of Superplasticizers on Silica Fume Concrete.....	49
2.5.4 Compatibility of Silica Fume with Superplasticizers.....	50
2.5.5 Superplasticizers, Silica Fume and Hot Weather	52
2.5.6 Characterization of the Interaction between Superplasticizers and Plain and Blended Cement Concretes	53
2.5.7 Modified Lignosulfate Polymer (MLP)	54
2.5.8 Sulfonated Naphthalene Polymer/Formaldehyde (SNP/SNF)	57
2.5.9 Polycarboxylic Ether (PCE).....	59
2.6 MICROSTRUCTURE OF CONCRETE	62
3 EXPERIMENTAL PROGRAM	73
3.1 MATERIALS	74
3.1.1 Coarse Aggregates.....	74

3.1.2	Fine Aggregates.....	75
3.1.3	Cement	75
3.1.4	Silica Fume.....	75
3.1.5	Superplasticizer	76
3.2	MIX DESIGN	77
3.3	CURING CONDITIONS	77
3.4	EXPERIMENTAL PROCEDURE	77
3.4.1	Preparation of Materials and Moulds.....	78
3.4.2	Mixing Process.....	79
3.5	MONITORING AND DATA ANALYSIS.....	80
3.5.1	Plastic Shrinkage Cracking	80
3.5.2	Plastic Shrinkage Strain and Temperature Measurements	80
3.5.3	Drying Shrinkage Strain.....	81
3.5.4	Compressive and Split Tensile Strengths.....	82
3.5.5	Ultrasonic Pulse Velocity.....	82
3.5.6	Pore Size Distribution and Specific Surface Area	83
4	RESULTS AND DISCUSSIONS	113
4.1	PLASTIC SHRINKAGE STRAIN	113
4.1.1	Effect of Cement Type on Plastic Shrinkage Strain.....	114
4.1.2	Discussion on the Plastic Shrinkage Strain	123
4.2	EFFECT OF EXPOSURE CONDITIONS ON PLASTIC SHRINKAGE STRAIN	133

4.2.1	Effect of Temperature on Plastic Shrinkage Strain	133
4.2.2	Effect of Relative Humidity on Plastic Shrinkage Strain.....	133
4.2.3	Effect of Wind Velocity on the Plastic Shrinkage Strain.....	134
4.2.4	Discussion on the Effect of Exposure Conditions on Plastic Shrinkage Strain	134
4.3	PLASTIC SHRINKAGE CRACKING.....	141
4.3.1	Effect of Blended Cement Type on Plastic Shrinkage Cracking	141
4.3.2	Effect of Exposure Conditions on Plastic Shrinkage Cracking.....	142
4.3.3	Discussion on Plastic Shrinkage Cracking.....	143
4.4	TIME TO ACHIEVE MAXIMUM STRAIN	152
4.4.1	Discussion on the Time to Achieve Maximum Strain	153
4.5	DRYING SHRINKAGE	157
4.5.1	Drying Shrinkage of Mortar Bars.....	157
4.5.2	Discussion on Drying Shrinkage of Mortar Bars	158
4.5.3	Drying Shrinkage of Concrete Slabs.....	168
4.5.4	Discussion on the Drying Shrinkage of Concrete Slabs	169
4.5.5	Comparison of Drying Shrinkage values	186
4.6	TEMPERATURE DISTRIBUTION IN CONCRETE SLABS	188
4.6.1	Effect of Cement Type	188
4.6.2	Discussion on the Effect of Cement Type.....	189
4.6.3	Effect of Exposure Conditions on the Temperature Variation.....	195
4.6.4	Discussion on the Effect of Exposure Conditions on Peak Concrete	

Temperature	197
4.7 ULTRASONIC PULSE VELOCITY IN CONCRETE SLABS	203
4.7.1 Discussion on the Pulse Velocity in the Concrete Slabs	203
4.8 EFFECT OF SUPERPLASTICIZERS ON THE PLASTIC SHRINKAGE STRAIN	208
4.8.1 Maximum Strain.....	208
4.8.2 Discussion on the Maximum Shrinkage Strains	209
4.8.3 Time to Achieve Maximum Strain Values.....	210
4.8.4 Compatibility of Superplasticizer with Silica Fume	210
4.8.5 Effect of Superplasticizers on Plastic Shrinkage Cracking.....	211
4.9 PORE SIZE DISTRIBUTION AND SPECIFIC SURFACE AREA OF PLAIN AND BLENDED CEMENT CONCRETES.....	218
4.9.1 Variation of Pore Volume with Pore Radius for Silica Fume Cements..	218
4.9.2 Variation of Pore Volume with Pore Radius for Plain, Fly Ash and Superpozz® Cements	219
4.10 PROPERTIES OF SILICA FUME CONCRETE AT EARLY AGES	225
4.10.1 Ultrasonic Pulse Velocity.....	225
4.10.2 Discussion of Pulse Velocity Results.....	226
4.10.3 Compressive Strength	227
4.10.4 Discussion on Compressive Strength Results	228
4.10.5 Correlation between Compressive Strength and Pulse Velocity.....	240
4.10.6 Discussion on the Relationship between Compressive Strength and Pulse	

Velocity.....	243
 4.10.7 Split Tensile Strength of Silica Fume Cement Concrete	253
 4.10.8 Discussion on the Split Tensile Strength of Plain and Blended Cement Concretes	259
 4.10.9 Correlation between the Split Tensile Strength and Compressive Strength of Blended Cements	259
 4.10.10 Discussion on the Relationship between the Split Tensile and Compressive Strength of Plain and Blended Cement Concretes.....	261
5 CONCLUSIONS AND RECOMMENDATIONS	267
 1.1 CONCLUSIONS	267
 5.1.1 Effect of Type and Dosage of Blending Material on Plastic Shrinkage Strain	269
 5.1.2 Effect of Exposure Conditions on Plastic Shrinkage Strain and Cracks.	269
 5.1.3 Incompatibility between Superplasticizer and Silica Fume Cement Concrete	271
 5.1.4 Temperature Distribution in Concrete Slabs	272
 5.1.5 Drying Shrinkage	272
 5.1.6 Pulse Velocity of Concrete Slabs.....	273
 5.1.7 Strength of Concrete at Early Ages	273
 5.1.8 Correlation between the Compressive Strength and Pulse Velocity in Blended Cement Concretes.....	275
 5.1.9 Correlation between the Split Tensile Strength and Compressive Strength	

.....	275
5.1.10 Effect of Type of Superplasticizer on the Plastic Shrinkage Strain.....	276
5.2 RECOMMENDATIONS	277
5.3 FUTURE STUDY	278
6 REFERENCES.....	280

LIST OF TABLES

Table 3.1: Grading of coarse aggregates used in all mixes.....	86
Table 3.2: Chemical analysis of Type I Portland cement used in all mixes.	86
Table 3.3: Sources of silica fume and fly ash selected for evaluation in this study.....	87
Table 3.4: Properties of Pechiney® (Ludun, France) silica fume.....	88
Table 3.5: Properties of EFACO® (Egypt) silica fume.	89
Table 3.6: Properties of ELKEM® (Norway) silica fume.	90
Table 3.7: Properties of BINASILICA® (SABAYEC, Jubail) silica fume.....	91
Table 3.8: Properties of BISLEY® (South Africa) silica fume.	92
Table 3.9: Properties of Lethabo® fly ash from South Africa.....	93
Table 3.10: Properties of Superpozz® from South Africa.....	94
Table 4.1: Maximum plastic shrinkage strain in the blended cement concretes at different dosages, exposed to a wind velocity of 15 km/hr, temperature of 45 °C and RH of 35%.....	122
Table 4.2: Specific surface area and bulk density of silica fume cement concrete.....	128
Table 4.3: TPV, APR and plastic shrinkage strain (7.5% silica fume dosage).	128
Table 4.4: TPV, APR and plastic shrinkage strain (7.5% silica fume dosage).	129
Table 4.5: Variation of plastic shrinkage strain with temperature in the concrete specimens exposed to a wind velocity of 15 km/hr and relative humidity of 50%. 137	137

Table 4.6: Variation of plastic shrinkage strain with relative humidity in the concrete specimens exposed to a wind velocity of 15 km/hr and temperature of 45 °C.....	137
Table 4.7: Variation of plastic shrinkage strain with wind velocity in the concrete specimens exposed to a relative humidity of 50 % and temperature of 45 °C.....	137
Table 4.8: Plastic shrinkage cracking in blended cement concretes exposed to a temperature of 45 °C, wind velocity of 15 km/hr and relative humidity of 35%..	146
Table 4.9: Variation of plastic shrinkage cracks with temperature in the concrete specimens exposed to a wind velocity of 15 km/hr and relative humidity of 50%.	147
Table 4.10: Variation of plastic shrinkage cracks with relative humidity in the concrete specimens exposed to a wind velocity of 15 km/hr and temperature of 45 °C.....	147
Table 4.11: Variation of plastic shrinkage cracks with wind in the concrete specimens exposed to a relative humidity of 50 % and temperature of 45 °C.	147
Table 4.12: Relationship between SSA, APR and plastic shrinkage cracking.	148
Table 4.13: Time to achieve maximum plastic shrinkage strain in plain and blended cement concretes.	156
Table 4.14: Maximum drying shrinkage in plain and blended cement mortars.....	161
Table 4.15: Maximum drying shrinkage in plain and blended cement concrete slab specimens.	176
Table 4.16: Summary of time to peak temperatures for plain and blended cement concretes.....	191
Table 4.17: Effect of exposure temperature on the time to achieve peak concrete	

temperature.....	199
Table 4.18: Effect of exposure relative humidity on the time to achieve peak concrete temperature.....	199
Table 4.19: Effect of exposure wind velocity on the time to achieve peak concrete temperature.....	199
Table 4.20: Summary of the ultrasonic pulse velocity test results after 90 days on the concrete slab specimens.	207
Table 4.21: Maximum plastic shrinkage strains in Series IV mixes (temperature of	214
Table 4.22: Optimum dosage of SNP (Conplast M432 MS) superplasticizer used in Series IV mixes (temperature of 45°C, RH of 35% and wind velocity of 15 km/hr)......	214
Table 4.23: Optimum dosage of MLP (Sika-520) superplasticizer used in Series IV mixes (temperature of 45°C, RH of 35% and wind velocity of 15 km/hr).....	214
Table 4.24: Optimum dosage of PCE (Glenium-51) superplasticizer used in Series IV mixes (temperature of 45°C, RH of 35% and wind velocity of 15 km/hr).	215
Table 4.25: Optimum dosage of SNF (EUCON 537 MS) superplasticizer used in Series IV mixes (temperature of 45°C, RH of 35% and wind velocity of 15 km/hr).	215
Table 4.26: Specific surface area, total pore volume and average pore radius of plain and blended cements after 56 days.	221
Table 4.27: Correlation coefficients for the relationship between pulse velocity and compressive strength for Type 1 silica fume cement concrete.	246
Table 4.28: Correlation coefficients for the relationship between pulse velocity and	

compressive strength for Type 2 silica fume cement concrete.	246
Table 4.29: Correlation coefficients for the relationship between pulse velocity and compressive strength for Type 3 silica fume cement concrete.	246
Table 4.30: Correlation coefficients for the relationship between pulse velocity and compressive strength for all types of silica fume cement concretes.	247
Table 4.31: Correlation coefficients for the relationship between pulse velocity and compressive strength for plain, fly ash and Superpozz® cement concretes.	247
Table 4.32: Correlation coefficients for the variation of split tensile strength with time of silica fume cement concretes (silica fume dosage: 7.5%).	256
Table 4.33: Correlation coefficients for variation of the split tensile strength with time of plain, fly ash and Superpozz® cement concretes.	256
Table 4.34: Relationship between split tensile and compressive strength for silica fume cement concretes (silica fume dosage: 7.5%).	264
Table 4.35: Relationship between split tensile and compressive strength for plain, fly ash and Superpozz® cement concretes.	264

LIST OF FIGURES

Figure 2.1: Variation of temperature and relative humidity in Riyadh [21].	65
Figure 2.2: Variation of temperature and relative humidity in Damman [21].	66
Figure 2.3: Variation of temperature and relative humidity in Jeddah [21].....	67
Figure 2.4: Effect of ambient conditions on the rate of water evaporation [19]......	68
Figure 2.5: PW curve, PW_E and the change in DWs [62].....	69
Figure 2.6: Schematic illustration of the interaction between a cement (muti-phase mineral system) and a chemical admixture (multi-component organic system) [94].	69
Figure 2.7: Dimensional range of solids and pores in hydrated cement paste [104].	70
Figure 2.8: Typical pore size distribution for paste in a high-strength concrete [105]....	71
Figure 2.9: Typical porosities using nitrogen adsorption method for various types of concretes at the age of 28 days [105].	72
Figure 3.1: Effect of cement type on plastic shrinkage strain and cracking.	95
Figure 3.2: Effect of environmental conditions on plastic shrinkage strain and cracking.	96
Figure 3.3: Effect of exposure conditions on concrete quality.	97
Figure 3.4: Effect of exposure conditions on split tensile strength.....	98
Figure 3.5: Effect of superplasticizer on plastic shrinkage strain.	99
Figure 3.6: Plan view of setup.....	100

Figure 3.7: Elevation view of setup	101
Figure 3.8: Grading of coarse aggregates used in all mixes.....	102
Figure 3.9: Types of physiosorption isotherms used in the BDDT classification [107].	103
Figure 3.10: Photographic documentation of the exposure chamber.....	104
Figure 3.11: Photographic documentation of the humidifier.....	105
Figure 3.12: Humidifier outlet.....	106
Figure 3.13: Mechanical humidity gauge.....	106
Figure 3.14: Electronic humidity gauge.....	107
Figure 3.15: Temperature and relative humidity controllers.....	108
Figure 3.16: Experimental setup showing the LVDTs, thermocouple wires and wind blower.....	109
Figure 3.17: Crack microscope	110
Figure 3.18: DEMEC gauge and gauge stud bar.....	111
Figure 3.19: Data logger.....	111
Figure 3.20: Slab surface showing drying shrinkage studs and a nearby crack.....	112
Figure 4.1: Plastic shrinkage strain in Type 1 silica fume cement concrete exposed to a temperature of 45°C, RH of 35% and wind velocity of 15 km/hr.	116
Figure 4.2: Plastic shrinkage strain in Type 2 silica fume cement concrete exposed to a temperature of 45°C, RH of 35% and wind velocity of 15 km/hr.	117
Figure 4.3: Plastic shrinkage strain in Type 3 silica fume cement concrete exposed to a temperature of 45°C, RH of 35% and wind velocity of 15 km/hr.	118
Figure 4.4: Plastic shrinkage strain in Type 4 silica fume cement concrete exposed to a	

temperature of 45°C, RH of 35% and wind velocity of 15 km/hr.	119
Figure 4.5: Plastic shrinkage strain in Type 5 silica fume cement concrete exposed to a temperature of 45°C, RH of 35% and wind velocity of 15 km/hr.	120
Figure 4.6: Plastic shrinkage strains in plain, fly-ash and Superpozz® cement concretes, exposed to a temperature of 45°C, RH of 35% and wind velocity of 15 km/hr.	121
Figure 4.7: Variation of the plastic shrinkage with bulk density and specific surface area of blended cement concretes for 7.5% silica fume cement concrete.	130
Figure 4.8: Variation of the plastic shrinkage strain with the average pore radius for plain and blended cements.	131
Figure 4.9: Variation of the plastic shrinkage strain with the total pore volume for plain and blended cements.	132
Figure 4.10: Variation of the plastic shrinkage strain with temperature in Type 1 silica fume cement concrete (7.5%), exposed to a RH of 50% and wind velocity of 15 km/hr.	138
Figure 4.11: Variation of the plastic shrinkage strain with the relative humidity in Type 1 silica fume cement concrete (7.5%), exposed to a temperature of 45°C and wind velocity of 15 km/hr.	139
Figure 4.12: Variation of the plastic shrinkage strain with the wind velocity in Type 1 silica fume cement concrete (7.5%), exposed to a temperature of 45°C and a RH of 50%....	140
Figure 4.13: Plastic shrinkage cracks in Type 4 silica fume cement concrete (10%	

replacement) exposed to a temperature 45 °C, wind velocity of 15 km/hr and RH of 35%.....	149
Figure 4.14: Plastic shrinkage crack in Type 1 silica fume cement concrete (10% replacement) exposed to a temperature 45 °C, wind velocity of 15 km/hr and RH of 35%.....	149
Figure 4.15: Plastic shrinkage crack in Type 1 silica fume cement concrete (5% replacement) exposed to a temperature 45 °C, wind velocity of 15 km/hr and RH of 35%.....	150
Figure 4.16: Threshold value of plastic shrinkage strain where cracking may occur for plain and blended cement concretes under hot weather conditions.	151
Figure 4.17: Drying shrinkage of Type 1 silica fume cement mortars.	162
Figure 4.18: Drying shrinkage of Type 2 silica fume cement mortars.	163
Figure 4.19: Drying shrinkage of Type 3 silica fume cement mortars.	164
Figure 4.20: Drying shrinkage of Type 4 silica fume cement mortars.	165
Figure 4.21: Drying shrinkage of Type 5 silica fume cement mortars.	166
Figure 4.22: Drying shrinkage of Superpozz® and fly ash cement mortars.....	167
Figure 4.23: Drying shrinkage of Type 1 silica fume concrete slabs.....	177
Figure 4.24: Drying shrinkage of Type 2 silica fume concrete slabs.....	178
Figure 4.25: Drying shrinkage of Type 3 silica fume concrete slabs.....	179
Figure 4.26: Drying shrinkage of Type 4 silica fume concrete slabs.....	180
Figure 4.27: Drying shrinkage of Type 5 silica fume concrete slabs.....	181

Figure 4.28: Drying shrinkage of plain, fly ash and Superpozz® concrete slabs.....	182
Figure 4.29: Drying shrinkage strains vs. APR for silica fume dosages of 5%.....	183
Figure 4.30: Drying shrinkage strains vs. APR for silica fume dosages of 7.5%.....	184
Figure 4.31: Drying shrinkage strains vs. APR for silica fume dosages of 10%.....	185
Figure 4.32: Temperature variation in Type 1 silica fume cement concretes with time.	192
Figure 4.33: Temperature variation in Type 2 silica fume cement concretes with time.	192
Figure 4.34: Temperature variation in Type 3 silica fume cement concretes with time.	193
Figure 4.35: Temperature variation in Type 4 silica fume cement concretes with time.	193
Figure 4.36: Temperature variation in Type 5 silica fume cement concretes with time.	194
Figure 4.37: Temperature variation in plain, fly ash and Superpozz® cement concretes with time.....	194
Figure 4.38: Effect of exposure temperature on concrete temperature in the concretes exposed to a RH of 50% and wind velocity of 15 km/hr (Type 1 silica fume at a dosage of 7.5%).	200
Figure 4.39: Effect of relative humidity on the concrete temperature, in the concretes exposed to a temperature of 45°C and wind velocity of 15 km/hr (Type 1 silica fume at a dosage of 7.5%).	201
Figure 4.40: Effect of wind velocity on the concrete temperature in the concretes exposed to a temperature of 45°C and a RH of 35% (Type 1 silica fume at a dosage of 7.5%).	202
Figure 4.41: Maximum strain values in Series IV mixes (three types of silica fume at a constant dosage of 7.5% using four different types of superplasticizers).	216

Figure 4.42: Time to achieve maximum strain values in three types of silica fume at a constant dosage of 7.5% and plain cement concrete using four different types of superplasticizers.	217
Figure 4.43: Typical plot of pore volume versus pore radius for plain and Type 1 silica fume cement pastes.	222
Figure 4.44: Variation of the pore volume with the pore radius for the various types of silica fume cement pastes at a constant dosage of 7.5%.	223
Figure 4.45: Variation of the pore volume with the pore radius for the plain, fly ash and Superpozz® cement pastes.....	224
Figure 4.46: Variation of pulse velocity with time in Type 1 silica fume cement concrete.	232
Figure 4.47: Variation of pulse velocity with time in type 2 silica fume cement concrete.	233
Figure 4.48: Variation of pulse velocity with time in Type 3 silica fume cement concrete.	234
Figure 4.49: Variation of pulse velocity with time in plain, fly ash and Superpozz® cement concretes.	235
Figure 4.50: Variation of compressive strength with time in Type 1 silica fume cement concrete.	236
Figure 4.51: Variation of compressive strength with time in Type 2 silica fume cement concrete.	237
Figure 4.52: Variation of compressive strength with time in Type 3 silica fume concrete.	

Figure 4.53: Variation of compressive strength with time in plain, fly ash and Superpozz® cement concretes.	239
Figure 4.54: Relationship between compressive strength and pulse velocity for Type 1 silica fume cement concrete (temperature of 45 °C, a RH of 35% and wind velocity of 15 km/hr).	248
Figure 4.55: Relationship between compressive strength and pulse velocity for Type 2 silica fume cement concrete (temperature of 45 °C, a RH of 35% and wind velocity of 15 km/hr).	249
Figure 4.56: Relationship between compressive strength and pulse velocity for Type 3 silica fume cement concrete (temperature of 45 °C, a RH of 35% and wind velocity of 15 km/hr).	250
Figure 4.57: Relationship between compressive strength and pulse velocity for plain, fly ash and Superpozz® cement concrete (temperature of 45 °C, a RH of 35% and wind velocity of 15 km/hr).	251
Figure 4.58: Relationship between compressive strength and pulse velocity for all three types of silica fume cement concrete (temperature of 45 °C, RH of 35% and wind velocity of 15 km/hr).	252
Figure 4.59: Variation of the split tensile strength with time for silica fume cement concretes at dosages of 7.5% (temperature of 45 °C, RH of 35% and wind velocity of 15 km/hr).	257

Figure 4.60: Variation of the split tensile strength with time for plain, fly ash and Superpozz® cement concretes (temperature of 45 °C, RH of 35% and wind velocity of 15 km/hr)..... 258

Figure 4.61: Relationship between the split tensile and compressive strength of silica fume cement concretes (temperature of 45 °C, a RH of 35% and wind velocity of 15 km/hr)..... 265

Figure 4.62: Relationship between the split tensile and compressive strength of plain, fly ash and Superpozz® cement concretes (temperature of 45 °C, a RH of 35% and wind velocity of 15 km/hr)..... 266

ABSTRACT (ENGLISH)

Name: Taofiq Olatunbosun Abiola
Title: Plastic Shrinkage Cracking of Blended Cement Concretes Under Hot Weather Conditions
Major Field: Civil Engineering (Structures)
Date of Degree: September 2002 (Rajab 1423)

In order to inhibit the deterioration of concrete structures in the Arabian Gulf environment, emphasis has been shifted from the requirements of concrete strength towards its durability, especially the selection of materials. Towards this end, silica fume and other types of blended cement materials are being used. However, silica fume cement concrete is also more susceptible to plastic shrinkage cracking, and under hot weather conditions, this cracking could be further aggravated. This research was conducted to investigate the effect of the type and dosage of silica fume and other blended cements on the plastic shrinkage cracking of concrete. The effect of cement type, superplasticizer type, temperature, relative humidity and wind velocity on the plastic shrinkage strains, cracking and the microstructure were conducted. Additional studies to evaluate the effect of the type of silica fume on the early age properties, such as the compressive strength; the split tensile strength and the ultrasonic pulse velocity were also conducted.

Results of this research indicated that it is the fineness of the silica fume and its state of densification that determine its plastic shrinkage strain response. The fineness of the silica fume must be evaluated in terms of not only its specific surface area, but also its average pore radius.

The plastic shrinkage strain increased with increasing temperature and wind velocity and decreasing relative humidity. The decrease in the relative humidity presented the most severe condition that promoted higher plastic shrinkage strains and cracks. A threshold value of plastic shrinkage strain was determined in plain and blended cement that will initiate plastic shrinkage cracks. This threshold value was found to be independent of the exposure conditions.

The type of superplasticizer had a significant effect on the plastic shrinkage strains in silica fume cement concretes. The effect of the fineness of the silica fume played the most important role in determining the plastic shrinkage strains in the concrete. Incompatibility between the type of superplasticizer and the silica fume cement concrete was also noted. Statistical analysis of the early age properties, such as the compressive strength, split tensile strength and pulse velocity of plain and blended cements suggested that the material variability as represented by the type and dosage of silica fume was comparable to that of plain cement concrete.

MASTER OF SCIENCE DEGREE
KING FAHD UNIVERSITY OF PETROLEUM AND MINERALS
Dhahran, Saudi Arabia

الخلاصة

ABSTRACT (ARABIC)

اسم الطالب : توفيق أولاتونبوسن أبيولا

عنوان البحث : تشققات الانكمash اللدن للخرسانة المحتوية على المواد مضافة في الأجواء الحارة

التخصص : هندسة مدنية (إنشاءات)

تاريخ منح الدرجة : رجب ١٤٢٣ هـ (سبتمبر ٢٠٠٢ م)

نظرا لحماية المنشآت الخرسانية في بيئات الخليج العربي من التدهور، فقد تم الاهتمام بنيومة الخرسانة بدلا من متطلبات القراءة، وخاصة عند اختيار المواد المستخدمة. ولهذا الغرض تم إضافة مواد غبار السيليكا وغيرها من المواد المضافة في الخرسانة. وللأسف، فإن الخرسانة المحتوية على غبار السيليكا تعتبر أكثر عرضة لتشققات الانكمash اللدن، ويمكن أن ترداد هذه التشققات تحت الظروف الجوية الحارة.

تم إجراء هذا البحث لدراسة تأثير نوع وكمية غبار السيليكا، وأنواع الأسمنت المضافة الأخرى على تشققات الانكمash اللدن في الخرسانة. ولقد تم دراسة نوع الأسمنت، ونوع الملنفات، ودرجة الحرارة، ودرجة الرطوبة النسبية، وسرعة الرياح على الانكمash اللدن والتشققات الناتجة عنه، والبنية المجهرية للخرسانة. وتم تقييم تأثير نوع غبار السيليكا على الخواص المبكرة للخرسانة مثل قوة الضغط، وقوة الانفلاق الشدي، وسرعة النبض.

وتدل نتائج هذا البحث على أن درجة نعومة غبار السيليكا ودرجة تكاثفها تحدد مدى الانكمash اللدن. ويجب تقييم نعومة غبار السيليكا ليس بتحديد مساحة سطحها فقط، بل يجب تحديد بنيتها المعمامية. كما دلت نتائج الدراسة على ازدياد انفعال الانكمash اللدن مع ارتفاع درجة الحرارة وسرعة الرياح ومع انخفاض الرطوبة النسبية. ويمثل انخفاض الرطوبة النسبية أشد الحالات تأثيراً لزيادة انفعالات الانكمash اللدن والتشققات. كما تم تحديد قيمة معينة لانفعال الانكمash اللدن في الأسمنت العادي والمخلوط تتسبب في تكوين التشققات الناتجة عن الانكمash اللدن. وقد وجد أن هذه القيمة لا تعتمد على الظروف المحيطة بالعينات الخرسانية.

وكان لنوع الملنف تأثير فعال على انفعالات الانكمash اللدن في الخرسانة المحتوية على غبار السيليكا. كما أن نعومة غبار السيليكا كان لها التأثير الأبرز في تحديد انفعالات الانكمash اللدن في الخرسانة المحتوية على ملنف.

وتحت ملاحظة عدم المواءمة بين بعض أنواع الملنفات والخرسانة المحتوية على غبار السيليكا. ودل التحليل الإحصائي لنتائج الخواص المبكرة مثل قوة الضغط، وقوة الفلق الشدي، وسرعة النبض للأسمنت العادي والأسمنت المخلوط أن قابلية الاختلاف المتمثلة بنوع وكمية غبار السيليكا مماثلة نوعاً ما لتلك التي في خرسانة الأسمنت العادي.

درجة الماجستير في العلوم

جامعة الملك فهد للتكنولوجيا والمعاهد

الطائف - المملكة العربية السعودية

CHAPTER 1

INTRODUCTION

1.1 CONCRETE DURABILITY UNDER HOT WEATHER CONDITIONS OF THE ARABIAN GULF

Concrete has been extensively used in the construction of infrastructure all over the world. As the most widely used material in the construction industry, considerable research efforts have been made to make concrete stronger while at the same time economical. High-energy, efficient and high-strength concretes were thus produced without properly addressing the durability performance of such concretes. Recent physico-chemical changes have damaged the reputation of concrete as a maintenance-free material due to the increased number of deterioration problems from all over the world.

In North America and Europe, the deterioration of highway structures is principally ascribable to the use of deicer salts. In the Arabian Gulf, deterioration is primarily caused

by the cumulative effect of severe climatic and geomorphic conditions in addition to incorrect materials specifications and defective construction practices. The ever-growing demand for infrastructure in this region has resulted in unprecedented construction activity in the last two decades. In Saudi Arabia, the construction activity is primarily concentrated in the central and coastal parts, which are characterized by hot climatic conditions. It has been observed through a growing number of case histories [1] that within a short span of time, various defects ranging from unsightly blemishes to serious failures have occurred in many types of concrete structures in this region.

Problems of concrete durability in arid and semi-arid regions, in many parts of Saudi Arabia and in other parts of the Arabian Gulf and Middle Eastern countries have been shown to be due to the following reasons [2,3]:

- (a) Severe climatic and geomorphic conditions;
- (b) Low quality of construction materials; and
- (c) Unskilled labor, lack of proper supervision, inadequate specifications and design and construction practices that is not commensurate with the local aggressive conditions.

Environmental conditions in the Arabian Gulf are typically characterized by hot, dry and

arid climatic conditions with: (1) high temperature and humidity, (2) drying winds, (3) high evaporation rates, and (4) high concentrations of chloride and sulfate salts in the soil, ground water, and atmosphere [4].

In central Saudi Arabia, it is normal to have ambient day temperatures above 45 °C and a relative humidity of less than 25% during summer months. The average temperature in the Arabian Gulf region is usually in excess of 38 °C daily, and the relative humidity may vary from 40% to 100% within the same day [4]. These sudden and continuous variations in temperature and humidity initiate cycles of expansion and contraction that damage the concrete matrix due to thermal and mechanical stresses. The damage due to these stresses is reflected by micro cracking and enhanced permeability, which results in tremendous increase in the diffusion of aggressive species such as chlorides, oxygen and carbon dioxide, to the steel surface [5].

Most of the coarse aggregates quarried in eastern Saudi Arabia are marginal, porous, absorptive, relatively soft, and excessively dusty on crushing, which in turn lead to poor durability performance of concrete using them. Fine aggregates are composed mainly of aeolian dune sands and beach sands. They are essentially fine-grained (mostly 50 to 600 µm) and have narrow grading. For typical dune sand, nearly all the material passes # 30 sieve, and the fineness modulus is less than 1.3 (which is significantly less than the

minimum 2.3 specified by ASTM C 33), and is finer than zone 4 of BS 882 [6]. The excessive fineness and its narrow grading lead to a gap-graded particle size distribution in the combined aggregate grading in nearly all the mixes made using local materials. Dune sand comprises mainly of quartz that is a sound resistant material, but coastal sands along the Arabian Gulf are mainly of carbonate origin and are absorptive, fine, poorly graded and contain certain hollow shells, and above all are heavily contaminated with chloride and sulfate salts. These characteristics make the coastal sands markedly adverse to concrete making. In addition, both the fine and coarse aggregates in the Arabian Gulf are characterized by excessive dust (material passing 75 µm sieve). Dust and excess fines cause higher water demand resulting in lower strength and greater shrinkage of concrete. Dust also forms a fine interstitial coating between the limestone coarse aggregate and the cement paste thereby weakening the bond at the aggregate-paste interface. This transition zone, being the weakest link of the concrete composite, may further lower the strength and quality of concrete [7].

The hot and arid conditions of the Arabian Gulf are conducive to the development of cracking of concrete due to plastic and drying shrinkage. This deterioration is further aided by sharp temperature gradients on the surfaces and inner portions of the concrete. The changes in diurnal and seasonal temperatures cause continuous expansion and contraction cycles, which may lead to the cracking of concrete [5]. The expansion-

contraction cycle becomes all the more damaging due to the thermal incompatibility of concrete constituents. The differential expansion and contraction movements of aggregate material and the hardened cement paste may set up tensile stresses far beyond the tensile strength of concrete resulting in micro cracking. Limestone, the predominantly used aggregate, is exactly the rock type having the widest spectrum of coefficient of thermal expansion (1 to $10 \times 10^{-6} /^{\circ}\text{C}$). The coefficient of thermal expansion of hardened cement paste is much higher (usually between 10×10^{-6} and $20 \times 10^{-6} /^{\circ}\text{C}$) [4]. With the fall in temperature, tensile and compressive stresses are set up in the cement paste and the aggregates, respectively. With a rise in temperature, the stresses are not exactly reversed but tensile stresses are set up at the aggregate-paste interface tending to cause interface bond failure and significant micro cracking in and around the transition zone [8]. It has been shown by Hsu [9] that a volume change of 0.3% is enough to generate tensile stresses of the order of 12.4 MPa (1800 psi) at the aggregate paste interface. Slate and Matheus [10] have determined the volume change of cement paste and concrete from the time of casting to an age of 7 days. This work showed that volume changes even larger than 0.35% occur during setting and hardening of concrete. The authors, on the basis of a simple mathematical model, have inferred that for a commonly occurring value of $6 \times 10^{-6} /^{\circ}\text{C}$ for limestone, tensile stresses of more than 1.72 MPa (250 psi) for every 10°C fall of temperature are set up in the concrete. These stresses are cumulatively interactive on the shrinkage and micro fissures already present due to other causes [11]. The climatic

and geomorphic factors may sometimes combine to accelerate the deterioration process. In most areas, the groundwater table is relatively shallow and close to the ground surface. The capillary rise of moisture and frequent flooding in conjunction with the high evaporation rate leave a heavy crust of salt in the upper few feet of the soil. This leaves the soil, ground water and atmosphere heavily contaminated with chloride and sulfate salts [1]. Concrete construction in the coastal areas of the Arabian Gulf is frequently exposed to ground and atmospheric conditions contaminated with salts. In the presence of high humidity, strong winds and shallow groundwater conditions, salt-contaminated ground water, moisture and dew find easy access into the concrete matrix. Other sources of salts are the numerous sabkhas, which constitute natural evaporation pans, saturated with brines and which generate chlorides, sulfates and carbonate minerals on their surface crusts. The salts have also been found to contaminate sands up to a distance of 40 km from the seashore [5].

The use of inferior materials and irrelevant specifications also contributes to the premature deterioration of concrete in the Arabian Gulf. The use of international codes and standards, such as ASTM, BS, RILEM, DIN, etc, do provide some guidelines, but the environmental conditions in the region are unique and the development of specifications suitable for these conditions is essential. The major forms of concrete deterioration in the coastal areas of the Arabian Gulf are:

- (i) Corrosion of reinforcement,
- (ii) Sulfate attack and salt weathering, and,
- (iii) Cracking due to thermal gradients, drying and plastic shrinkage.

Although reinforcement corrosion is the most common cause of concrete deterioration in the Arabian Gulf region [11], other types of defects in concrete might aid this deleterious phenomenon. Cracks due to plastic or drying shrinkage may facilitate the ingress of chlorides that ultimately lead to reinforcement corrosion. Daily and seasonal fluctuations in humidity and temperature might widen the already existing cracks or propagate new ones leading to reduction in both strength and long-term durability.

1.2 NEED FOR THIS RESEARCH

As stated in the preceding section, the environment of the Arabian Gulf presents an aggressive exposure condition to concrete, which is characterized by hot weather conditions, poor quality of construction materials and inadequate construction practices and improper specifications.

Several research studies have been carried out at the King Fahd University of Petroleum and Minerals [12-16] on the use of blended cements have indicated the superior

performance of these cements, even in the very aggressive environments of sabkha [16], in mitigating the corrosion of reinforcement. Furthermore, with the increasing use of chemical admixtures and blending materials like silica fume in concrete, recent research studies [17,18] have shown that Menzel's formula is no longer adequate for predicting the occurrence of plastic shrinkage cracking, as recommended by ACI committee 305 [19].

Silica fume and fly ash concretes require proper and extended period of curing to achieve superior durability over plain cement concretes. Under hot weather conditions, extended curing is not only difficult, but also costly. The importance of extended curing emerges from the fact that improper curing will retard the durability performance of these concretes

One of the durability aspects of silica fume and fly ash concretes that have been of predominant concern is the formation of plastic shrinkage cracks in the hot and arid environment of the Arabian Gulf. Silica fume is thought to be more susceptible to plastic shrinkage cracking than any other type of concrete, particularly in structures having large surface areas, e.g. slab, walls, etc. There is lack of sufficient data on the cumulative effect of mix design, type of silica fume and environmental conditions on the formation of plastic shrinkage cracking in silica fume concrete.

While considerable research has been conducted to evaluate the durability performance of blended cements, including silica fume and fly ash concretes [5], no data is available on the effect of type and dosage of silica fume on plastic shrinkage. Therefore, there is a need to study the effect of silica fume in view of the extensive usage of this material in Saudi Arabia and the availability of several types of silica fume to improve the durability performance of concrete materials in the Arabian Gulf region.

1.3 RESEARCH OBJECTIVES

The overall objective of this research is to evaluate the interactive effects of silica fume and environmental conditions on plastic shrinkage cracking in fresh concrete and drying shrinkage of both hardened concrete and mortar specimens. The specific objectives are:

1. To investigate the plastic and drying shrinkage of different types and dosages of silica fume cement concrete, cast and cured under hot weather conditions;
2. To assess the effect of superplasticizer type on the shrinkage characteristics of silica fume; and
3. To provide guidelines on materials selection, in relation to the type and dosage of

silica fume to be used under hot weather conditions with a view to minimize the adverse effect of plastic and drying shrinkage on the immediate and long-term durability of concrete.

CHAPTER 2

LITERATURE REVIEW

2.1 CONCRETE DURABILITY UNDER HOT WEATHER CONDITIONS OF THE ARABIAN GULF

The ACI 305 Manual on hot weather concreting [19] defines hot weather as “any combination of the following conditions that tend to impair the quality of freshly mixed or hardened concrete by accelerating the rate of moisture loss and rate of cement hydration, or otherwise resulting in detrimental results.” These factors include one or more of the following:

- High ambient temperature;
- High concrete temperature;
- Low relative humidity;
- High wind velocity; and
- High solar radiation.

Most parts of Saudi Arabia are included in the typical environment that is classified as hot weather. In this region, the summer temperature is frequently in excess of 40 °C and may exceed 45 °C during day times. Direct solar radiation may raise the temperature to as high as 70 °C on a typical summer day in this region [20]. Humidity is very low in the central parts and varies from very low to high in the coastal areas within a short span of time. Data on relative humidity and temperature, based on 20-year observation, is presented in Figures 2.1 2.2 and 2.3, respectively, for Riyadh, Dhahran and Jeddah [21] to provide an indication of the hot weather conditions in these regions.

Hot weather conditions may create several serious problems when mixing, transporting, placing, and curing concrete [4,5,8,9,22,23]. Other potential problems often noted in the freshly-mixed concrete under hot weather conditions include the following [22]:

- (i) Increased water demand;
- (ii) Increased rate of slump loss;
- (iii) Increased rate of setting;
- (iv) Increased thermal cracking and increased plastic shrinkage cracking; and
- (v) Increased difficulty in controlling air content.

The potential problems in hardened concrete placed and cured under hot weather

conditions include [22]:

- (i) Decreased ultimate compressive strength due to the following reasons.
 - a. An increase in the quantity of mixing water as a result of higher water demand;
 - b. Insufficient curing at high temperature;
 - c. Non-uniform precipitation of the products of hydration between cement grains due to comparatively rapid hydration; and
 - d. Micro cracking as a result of thermal incompatibility of concrete constituents.
- (ii) Increased drying shrinkage cracking;
- (iii) Increased permeability;
- (iv) Increased corrosion of reinforcing steel;
- (v) Decreased durability; and
- (vi) Greater variability of surface appearance.

According to ACI 305 [19], an upper limit of temperature for the placement of concrete is no longer specified or desirable. Instead, if acceptable field records are not available, concrete mix proportions may be determined by trial batches, which should be made at

temperatures anticipated in the work and mixed, following one of the procedures described in Section 2.9 of the ACI 305 manual. The following list of construction practices and measures to mitigate or avoid the potential problems of hot weather include [19]:

- (a) Use concrete materials and proportions with satisfactory records in the field under prevailing hot weather conditions;
- (b) Use cooler concrete by:
 - a. Keeping aggregates cool by shading or spraying water over them; and
 - b. Using cold water for mixing and, if necessary, using ice as part of the mixing water;
- (c) Use a concrete consistency that permits rapid placement and effective consolidation;
- (d) Transport, place, consolidate and finish the concrete with least delay;
- (e) Plan the job to avoid excessive exposure of the concrete to the adverse environment; schedule placing operations during times of day or night when the weather conditions are favorable; and
- (f) Protect the concrete against moisture loss at all times during placing and curing.

Plastic shrinkage cracking is the most important adverse impact that affects fresh

concrete, especially concrete containing silica fume (SF), which is more susceptible [17,24,25]. This is because SF concrete has a higher surface area to be wetted; hence there is very little free water left in the mixture for bleeding. Additionally, SF physically blocks the pores in fresh concrete. Thus, the rate of bleeding in SF concrete is significantly reduced thereby increasing the risk of plastic shrinkage. With the increasing use of SF in normal and high strength concrete in the Arabian Gulf, the plastic shrinkage behavior of silica fume cement concrete needs to be fully addressed. The subsequent literature review is devoted to evaluate the shrinkage characteristics of SF cement concrete under hot weather conditions.

2.2 CRACKING IN CONCRETE

At early ages, it is of utmost importance that cracks due to plastic shrinkage be avoided because these cracks will adversely affect the immediate and long-term durability of the concrete [26]. With concrete in the hardened state, it is continuously exposed to drying except in water containment or marine structures. Here, the appearance of drying shrinkage cracks during the life of the structure is inevitable and cannot be avoided. However, with good mix design and adequate precautions and procedures during the casting stage, crack width can be greatly minimized to acceptable limits. BS 8007 recommends crack width limits of 0.1 mm in locations of “critical aesthetic appearance”

and 0.2 mm elsewhere, including watertight structures [26].

Cracking is an undesirable phenomenon in concrete and several mechanisms have been identified in concrete [27]. These mechanisms may include the following:

- (a) Differential plastic shrinkage (or just plastic shrinkage);
- (b) Self-desiccation (autogenous shrinkage);
- (c) Desiccation (drying shrinkage);
- (d) Thermal gradients as the temperature difference between bulk and outside surfaces; and
- (e) Physical factors, such as excessive loads.

Although the probable mechanisms are presented here separately, practical conditions to which concrete is exposed reveal that conditions that are favorable to a particular mechanism may also be favorable to another, thus the net effect is more severe on concrete than would be expected from the individual mechanisms alone. The above mechanisms relate only to processes connected with the making and curing of concrete structures made with sound cement and aggregates and not to those due to the well known effects of mechanical vibration, the delayed hydration of CaO and other cracking-inducing processes in concrete [27].

The driving mechanisms of cracking are broadly divided into the following two classes [27]:

1. Desiccation/self-desiccation, which can be further divided into:
 - (a) Loss of water due to evaporation (plastic and drying shrinkage); and
 - (b) Fixation of liquid water as hydration water, i.e. self-desiccation or autogenous shrinkage.
2. Temperature differentials.

2.2.1 Crack Formation due to Desiccation

Plastic Shrinkage

Details of this type of cracking are elucidated in Section 2.3.

Drying Shrinkage

It has long been known that visible cracks can form in a concrete structure if it is subjected to severe drying. However, it has not been properly appreciated that long before the visible crack formation extensive micro cracking occurs even on the relatively mild drying. Powers [cited in Ref. 27] had shown that drying of a mature cement paste to 79% RH could increase its water permeability 70 times that of its pristine state, which is due to the formation of extensive micro cracking. The critical % RH below which a paste

or mortar mix starts to crack is not known [27].

Desiccation (Autogenous Shrinkage)

This mode of cracking has also been insufficiently appreciated in the concrete literature. Consider a large volume of well-compacted concrete; if the mix had a water/cement ratio higher than about 0.4, some bleeding will occur. This bleeding reduces the water/cement ratio throughout the mix during hydration and hardening. It is known that during hydration, the volume of cement-water system decreases [27]. The actual fractional decrease in volume depends on the degree of hydration and the actual water/cement ratio [28]. The continued hydration of cement after it has set will self-desiccate the structure causing the formation of water menisci on all surfaces including those in contact with the formwork. The formation of water menisci will reduce the relative humidity of the surrounding environment. No data is available on the changes of % RH inside a hardening concrete although a RH of 90% has been reported for small specimens of pure cement paste [27]. According to Powers [cited in Ref. 27], this 90% RH humidity will develop negative pressures of 13 atmospheres (1.32 MPa) at 25 °C, which is sufficient to cause cracking.

With the use of new materials, such as silica fume, to produce high-strength concrete, autogenous shrinkage has gained greater prominence because it has been found that due

to the low water/cement ratios used in these mixes, they are more susceptible to autogenous shrinkage. Further, at very early ages, autogenous shrinkage is dependent on the amount of superplasticizer and silica fume, which means that contraction (also referred to as chemical shrinkage) must be determined experimentally for every combination of binder and superplasticizer [29]

2.2.2 Crack Formation due to Temperature Gradients

It has long been observed that concrete structures, which attained high internal temperatures during setting and hardening, tended to crack during subsequent cooling [27]. Low heat Portland cement was invented to avoid this type of cracking. Freiesleben Hansen [cited in Ref. 27] has recently studied this aspect extensively. He concluded that cracking would occur whenever the temperature differences between the inner and outer surfaces of a concrete mass exceed 20°C. The general idea is as follows: on demolding a concrete structure, its surface will cool faster than its bulk. As a result of thermal contraction, the surfaces will be in tension and the bulk will be under compression. If the tensile stresses on the surfaces exceed the tensile strength of concrete, cracking will occur.

Unfortunately, however, the conditions favoring the above thermal cracking process, i.e.

high bulk temperature, high air temperature and high wind velocity and low relative humidity are also conducive to a high rate of water evaporation and subsequent shrinkage cracking. Furthermore, high bulk temperature is also conducive for self-desiccation cracking. It is desirable that the relative importance of these various crack forming processes be experimentally evaluated so that proper precautions can be taken to avoid early cracking in concrete structures.

2.3 PLASTIC SHRINKAGE CRACKING OF CONCRETE

Plastic shrinkage cracks are formed within a few hours of placing concrete, although they are often unnoticed until at least the next day. Plastic shrinkage cracks are common in structural members with a large surface area-to-volume ratio such as slabs, but they can also occur in the exposed top surfaces of walls, etc. These cracks usually take one of the following three forms [26]:

- (a) Diagonal cracks at approximately 45° to the edges of the slab, the cracks being 0.2 to 2 m apart;
- (b) A large random pattern; and
- (c) Cracks following the pattern of the reinforcement or other physical features such as change of section.

The primary cause of plastic shrinkage cracking is the drying out of the concrete surface where the menisci form between the solid particles setting up capillary tension (water) forces. This phenomenon occurs when the rate of evaporation exceeds the rate of bleeding. The ambient temperature, relative humidity, wind velocity, concrete temperature and the bleeding characteristics of concrete influence the time required for the formation of these cracks. Plastic shrinkage cracks are difficult to close once they have occurred, particularly when they are deep, and are especially undesirable in some situations as they may act as focal points for other forms of concrete deterioration (i.e., diffusion of salts, carbon dioxide or oxygen to steel reinforcement). High concrete temperature, high air temperature and high winds and low relative humidity or any combination of these can cause rapid evaporation of water, which promotes plastic shrinkage. The importance of this property has been recognized and research in recent years has attempted to advance a better understanding of the mechanisms of plastic shrinkage cracking and to determine the appropriate methods for its prevention.

According to ACI Committee 305 [19], the principal cause of plastic shrinkage cracking in Portland cement concrete is the excessive rate of evaporation of water from the surface of the concrete and the inability or lack of bleed water to replace the evaporating surface water. Above a certain limit, a higher rate of evaporation will decrease the consistency and may cause plastic shrinkage cracking and even stop the hydration of cement. Plastic

shrinkage cracks are initiated when the evaporation rate exceeds 0.2 lb/ft²-hr (1.0 kg/m²-hr), as obtained from the monograph (Fig 2.4). The ACI 305 monograph was based on Menzel's formula given by [19]:

$$W = 0.44(e_o - e_a)(0.253 + 0.096V) \quad (\text{Equation 2.1})$$

Where,

W = weight (lb) of water evaporated per square foot of surface per hour (lb/ft²-hr)

e_o = saturated vapor pressure at the temperature of the evaporating surface, psi;

e_a = vapor pressure of air, psi; and

V = average horizontal air or wind speed measured at a level about 20 in. higher than the evaporating surface, mph.

A recent study by Uno [18] established the origins and validity of the Menzel's formula above, to determine the rate of evaporation. However, the author questioned the "single figure" criterion of 0.2 lb/ft²-hr (1.0 kg/m²-hr) provided by ACI 305 [19], of 0.75 kg/m²-hr by the Canadian Code [cited in Ref. 18], and of 0.5 kg/m²-hr by the Australian Code [cited in Ref. 18] to determine a critical evaporation rate in view of some other factors, such as the fineness of cement (related to water demand), plastic state of the mix (that is, plastic, semi-plastic or wet), admixtures (primarily retarders), fibers (primarily nylon or

polypropylene), sub-base preparation (primarily sub-base membranes) and surface sprays (primarily aliphatic alcohols), which were all reported to affect plastic shrinkage of concrete but which were not taken into consideration in Menzel's formula. Uno [18] proposed an alternative approach where the critical rate of evaporation would be obtained from an equation that is related to the concrete strength (or water/cement ratio).

Uno [18] proposed 'new and easier to use formulas' as an alternative to Menzel's formula given by:

$$e_s = 0.61 * \exp \frac{17.3T}{(237.3 + T)} \quad (\text{Equation 2.2})$$

$$E = 0.313(e_{so} - r * e_{ss})(0.253 + 0.06V) \quad (\text{Equation 2.3})$$

Where,

e_s = saturation vapor pressure, kPa; and

T = temperature, °C.

E = evaporation rate, kg/m²-hr;

e_{so} = vapor pressure at concrete surface (kPa) from Equation 2.3;

e_{sa} = vapor pressure of air (kPa), from Equation 2.3;

r = (RH, percent)/100; and

V = wind velocity, km/hr.

These formulas are valid in the range of 10 to 40°C of temperature. Thus, they are not suitable for the hot weather conditions in the Arabian Gulf region where temperatures sometimes exceed 45°C during summer months.

2.3.1 Factors Affecting Plastic Shrinkage Cracking

Several factors affect plastic shrinkage cracking in concrete. These can be broadly categorized into environmental conditions and material properties. Detailed discussion of these factors is presented in the sections that follow.

Effect of Environmental Conditions

Hot and dry environments have a pronounced effect on plastic shrinkage in fresh mortar and concrete. When evaporation takes place while the concrete is still plastic, a reduction in the w/c ratio of the concrete is attained and the mortar or concrete is densified due to water evaporation. If this water loss crosses certain limits, it may cause plastic shrinkage

cracking [30-33].

Kral and Gabauer [34] investigated the cracking of concrete slabs in the first 24 hours. They were placed in a wind tunnel using varying air humidity and wind velocity as well as different mix proportions. The relationship between evaporation water, shrinkage cracking at early ages and properties of concrete was discussed on the basis of the experimental results. They concluded that shrinkage cracking at early ages occurs only if several unfavorable atmospheric conditions coincide resulting in high evaporation rates during the critical period between 2 and 4 hours after mixing and placing. Further, they indicated that shrinkage cracking of concrete can be avoided by employing mix proportions which reduce evaporation during this critical period of time, and protection and curing afterwards are required only for the purpose of hydration and strength development.

Berhane [35] investigated the effect of exposure conditions on the rate and amount of water evaporating from fresh mortar and concrete surfaces. The variables were air temperature, wind speed, relative humidity, type of cement and water content. He concluded that the measured water loss in a hot-humid environment is considerably lower than in a hot-dry climate. Due to the negligible evaporation and cooling effect in a hot and humid climate, the temperature of the mortar or concrete will rise above the already

high ambient temperature, which will adversely affect the hydration products and properties of the mortar or concrete. It was noted that in a hot-dry climate, the maximum rate of evaporation was attained 1.5 hours after casting, whereas in a hot-humid climate, the maximum rate was reached after 4 to 6 hours. It was also observed that the water loss in a hot and dry climate was about 7.5 times that lost in a hot-humid environment. These results point out the limitations of Menzel's formula [19] for estimating the evaporation rate from the surface of fresh mortar or concrete. It was shown that cracking is possible for an evaporation rate as low as $0.5 \text{ kg/m}^2\text{-hr}$ ($0.1 \text{ lb/ft}^2\text{-hr}$).

Almusallam *et al.* [36] evaluated the plastic shrinkage cracking of blended cement concretes under hot-humid and hot-dry exposure conditions using slab specimens. Fly ash, silica fume and blast furnace slag were used. It was noted that the rate of evaporation of blended cement concrete specimens was more than that in plain cement concrete. Further, it was noted that bleeding in the blended cement concretes was less than in the plain cement concrete. The cumulative effect of the two parameters, namely the rate of evaporation and bleeding, resulted in increased plastic shrinkage cracking of blended cement concretes. Finally, although cracks were observed earlier in the plain cement concrete specimens than in the blended cement concrete specimens, the total area of cracks in the latter cements was more than that in the former cements. These results also indicate that the relative humidity influences plastic shrinkage cracking of concrete

significantly in comparison with the effect of type of cement.

Role of Mix Proportions

Concrete mix design is another causal factor influencing plastic shrinkage cracking in addition to environmental conditions [30-33,37]. This is because mix design affects the magnitude of the volumetric change, rate of hydration and the development of tensile strength. Furthermore, the relationship between the decrease in volume of concrete after hydration and the released water varies considerably with age. Employing mix proportions that produce bleed water to compensate for evaporation during the early stages can reduce plastic shrinkage cracking of concrete. It has also been observed that mixes with higher paste volume possess an increased tendency to crack. Plastic shrinkage in mortar and concrete is generally observed to decrease with the increase in the volume fraction of aggregates [24,33].

Estimation of the evaporation loss from fresh concrete is most commonly done according to the ACI Committee 305 recommendations [19] that suggests that when the concrete temperature is less than or equal to the ambient temperature with a 100 percent relative humidity, then no evaporation will take place, irrespective of the wind velocity, hence the onset of plastic shrinkage cracking is predicted using the rate of evaporation. In contrast to the above, Blakey and Beresford [37] argued that the cracking is due rather to

differential settlement of the fresh concrete, caused by obstacles such as large aggregate particles or reinforcement. They found in laboratory investigations that cracking sets in about 20 minutes after casting and many cracks appear under the water surface during the period of bleeding or ponding [37]. Ravina and Shalon [33] exposed mortars to variable conditions of air temperature and humidity, wind velocity, mortar temperature, type and content of cement, and consistency. Their study suggested that plastic shrinkage cracking is not a direct function of water loss, evaporation rate or shrinkage. They found that cracking did not occur in semi-plastic mortars, but plastic and wet mortars of the same mix cracked severely. Shaeles and Hover [38] investigated plastic shrinkage cracking in simulated thin concrete slabs by testing mortar panels and emphasized the importance of mix proportions and construction operations. They observed that under a given set of test conditions, the incidence of plastic shrinkage cracking increased with the paste volume fraction. It was also observed that the origination and severity of cracks was influenced more strongly by the direction and speed of strike-off operations. Their test program did not establish a direct correlation between the severity of cracking and the rate of evaporation.

Recent studies by Almusallam *et al.* [39] investigated the effect of mix proportions on the plastic shrinkage cracking of concrete in hot environments. The cumulative effect of mixes proportions, i.e. cement content and water-cement ratio, and was assessed by

measuring the rate of bleeding, water evaporation, and time and intensity of cracks. The results indicated that cement content and water-cement ratio significantly affect the parameters controlling plastic shrinkage of concrete. Lean-stiff concrete mixes cracked earlier than the rich plastic concrete mixes. The intensity of cracks in the former was, however, less than in the latter. Plastic shrinkage cracking occurred when the rate of evaporation was in the range of 0.2 to 0.7 kg/m²-h, as against a value of 1 kg/m²-h suggested by ACI 305. The rate of evaporation and bleeding was the least in a lean-stiff concrete mix made with a cement content of 300 kg m⁻³ and a water-cement ratio of 0.40, indicating that this mix composition can be beneficially utilized in hot environments to minimize plastic shrinkage cracking.

Role of Materials Properties

Material properties such as the composition of cement and the maximum size of aggregate also play a significant role in the plastic shrinkage of concrete. Different types of cement are known to exhibit different rates of hydration and elevated temperature is known to increase the rate of hydration of cement, thus accelerating the setting of concrete. The degree of hydration depends primarily on the cement composition; therefore, the cement that gives the lowest heat of hydration is preferred particularly in mass concreting. Of the several factors that influence the magnitude of shrinkage, the important ones are sulfur trioxide (SO₃), tricalcium aluminate C₃A, and alkali (Na₂O and

K_2O) content of the cement [40]. SO_3 is normally added to cement in the form of gypsum to control the time of set. Lower shrinkage characteristics are associated with lower C_3A/SO_3 ratio and lower Na_2O and K_2O contents [40]. To control plastic shrinkage cracking, Type IV (low heat) or Type II (moderate heat) cement is usually specified rather than Type I that produces a larger amount of heat. Cement fineness also affects the rate at which heat is liberated during the hydration process as the rate of reaction increases with increasing the cement fineness thus generating more heat.

The maximum size of aggregates used has a significant effect on shrinkage as it provides a means of internal restraint that reduces the potential contraction of the paste [41]. It is the stiffness or the modulus of elasticity of the aggregate that influences its ability to restrain shrinkage [41]. In addition to the compressibility of the aggregate, the aggregate itself may exhibit a high contraction upon drying. Such aggregate should be avoided, as they will increase the likelihood of shrinkage of the concrete [42].

Role of Blended Cements

The beneficial effects of incorporating supplementary cementing materials like fly ash, blast furnace slag and silica fume in concrete on its properties are well known [43-47]. These blending materials usually develop cementitious properties at a slower rate compared to ordinary Portland cement that they replaced; hence, they require a longer

curing period. Fly ash and granulated blast furnace slag cements are recommended in hot climate for the production of durable concrete [46]. Furthermore, various proportions of fly ash, granulated blast furnace slag and silica fume are also recommended for use in the aggressive Arabian Gulf exposures [12].

Almusallam *et al.* [36] showed that concrete slab specimens made of blended cement materials such as fly ash, silica fume and blast furnace slag, and exposed to hot-humid and hot-dry environments exhibited increased plastic shrinkage cracking compared to plain cement concrete. Further details of the plastic shrinkage behavior of silica fume concrete are elucidated in subsequent sections below.

2.4 SILICA FUME CONCRETE

The subsequent sections are devoted to illustrate the characteristics of silica fume and its use in the Arabian Gulf. The physical properties of the various types of silica fume commercially available are also discussed.

2.4.1 Characteristics of Silica Fume

Silica fume (SF) is produced as a by-product from the production of silicon or ferro-silicon alloys. These alloys are produced in open furnaces with very high temperatures. During the reduction process, smoke consisting mainly of silicon oxide, (SiO_2) is discharged from the furnace. This smoke then condenses to SiO_2 (thus explaining the term condensed silica fume) when the temperature gets lower and more oxygen is found. This type of SiO_2 is produced in an amorphous form and, therefore, it is not considered dangerous to health [48]. Silica fume's main characteristics are as follows [49-51]:

- (a) It contains 85%-98% silicon dioxide, and its silica content is amorphous;
- (b) It is about 100 times finer than plain cement.
- (c) Its particles are spherical.

In view of its characteristics, SF is both a highly reactive pozzolan and a very effective filler. The pozzolanic reactivity of SF has been demonstrated in cement pastes by measuring the amount of calcium hydroxide at different times in pastes with varying amounts of SF [50]. It was found that SF reacts with calcium hydroxide (Ca(OH)_2) produced by the cement hydration process and produces calcium silicate hydrate (C-S-H), which is a product of the same hydration process. This is one reason why SF increases the concrete's compressive strength, since the voids that are filled with Ca(OH)_2 in

regular concrete mixes become filled with hardened cement paste (C-S-H). The filler effect of SF is another reason for its success in improving concrete properties. It has been found that SF in concrete essentially eliminates the pores between 0.5 and 500 μm in size [52]. A third effect of SF on concrete's compressive strength is to improve the interfacial bond between the aggregates and cement paste. The relative contribution of these three effects in increasing the compressive strength depends on the properties of the other mix constituents, and are still a subject of research [53-54].

There are two ways to use SF in producing concrete: as a replacement of cement or as an addition to it [55]. The former helps reduce the extra cost incurred by the addition of SF, by reducing the cement content. Different percentages of SF have been used in concrete, ranging from 5% to 30%. It has been reported that 24% SF as a replacement of cement is the optimum in the sense that it consumes all the $\text{Ca}(\text{OH})_2$ that is produced by the hydration of cement [53].

One of the main problems associated with use of SF is the loss of workability of fresh concrete. To correct this problem, superplasticizers are usually used in increasing amounts with increasing SF content.

2.4.2 Silica Fume in the Arabian Gulf

Some of the earliest reports on the usage of SF in the Arabian Gulf are from the years between 1982 and 1985 [48]. Early use of SF in Saudi Arabia reported problems linked to cracking of the concrete. This was observed in some testing programs carried out by Saudi-ARAMCO [cited in Ref. 48]. At the same time, SF was tested for use in the production of hollow core slabs in Bahrain. The results showed that the volume of permeable voids in the concrete was reduced by the use of SF. The major pre-cast concrete producers in Bahrain have now more than 8 years of experience in the use of SF concrete [48,56].

Research in the Arabian Gulf and elsewhere has proven that SF concrete can have superior performance in reducing the permeability of concrete, thus improving concrete durability, especially against chloride and sulfate attacks in aggressive environments [13-16]. Further, it is well known that SF can be used to produce high-strength concrete [17, 24].

2.4.3 Silica Fume Production and Delivery Forms

As mentioned previously, SF is produced as a by-product from the production of ferro-silicon or silicon alloys. These alloys are produced in open furnaces with very high

temperatures. The particles in the air stream from the furnace are collected in different types of filters, the most common today being the electrostatic filters [48].

It is of major importance to the quality of SF that collecting systems like cyclones or dropout boxes are installed as part of the filter systems. The major worldwide producers of SF are Elkem (Norway), Fesil (Norway), Pechiney (France), SKW (USA) and a number of other producers [48].

SF is collected from the filters in an undensified form. It is a unique product of almost pure SiO_2 and the particle size is about 0.2 micron. The particle size of SF is about 100 times smaller than that of the cement grains thereby allowing the SF to fill the space between cement grains. This is known as the filler effect; secondly, the SF will react with the free lime in the concrete, and transform the unbeneficial calcium hydroxide $[\text{Ca}(\text{OH})_2]$ into strong paste (C-S-H) by what is known as the pozzolanic effect.

Silica fume is delivered in the following three forms: un-densified, densified and slurry. **Undensified** SF forms some agglomerates and the bulk-density of the product is about $200\text{-}350 \text{ kg/m}^3$ as compared with $1,250 \text{ kg/m}^3$ for plain cement. The transport cost for this type of SF is very high and the producers therefore developed other delivery forms to reduce the transport costs.

The most common delivery form is the **densified** or compacted SF. Different processes are available, but the most common is the air densification. All these processes will force the SF into forming larger agglomerates. The bulk density is increased to the range of 500 to 850 kg/m³. It is of major importance to be able to break (disperse) these agglomerates in the concrete during mixing. However, results from concrete testing show that this is difficult and the problems increase with increasing bulk density [48].

Other methods of densification are roller compaction and various forms of mechanical handling. Some producers add a dispersion agent in this process.

Another way of reducing the transport costs and ease of handling of SF is to mix SF with water in a stable **slurry** of about 50% SF and 50% water. This methodology increases the bulk density to 1,400 kg/m³, of which only half is SF. The production of stable slurry needs specially designed mixers, and is normally done at the plant using undensified SF. This delivery form has several advantages to the end user; among them are no dusting and easy dosing systems. There are no problems with dispersion as for densified SF. SF slurry is available in the US and Europe, but is not very much used in the Middle East.

Various blends of SF and other chemical admixtures are also available in the market. Trade names like EMSAC, FORCE 10000; Rheobuild, TDS, Sikacem and others are

examples of formulated SF admixtures [48]. Others are EFACO, Binasilica and Bisley.

2.4.4 Plastic Shrinkage of Silica Fume Cement Concrete

Unlike other types of shrinkage such as carbonation, drying and autogenous, there is very limited information available in the literature on plastic shrinkage of silica fume cement concrete. The limited number of papers generally indicates that if the conditions are favorable for plastic shrinkage to occur, then SF concrete would be more prone to such shrinkage and cracking than ordinary Portland-cement concrete [57]. This is attributed to the fact that SF concretes exhibit little or no bleeding thus allowing very little water to rise to the surface; hence, the risk of cracking is higher in fresh SF concretes.

Shrinkage cracking of SF concrete is often observed under ambient climatic conditions of the Arabian Gulf region; allowing rapid evaporation of water from freshly-placed concretes. Therefore, to protect SF concrete from evaporation, particularly during the setting period, curing should commence directly after placement of SF concrete. Additional measures, such as covering the concrete with plastic sheeting or applying a curing compound at an early age, together with ample water curing, are highly recommended [58].

Bloom and Bentur [24] investigated the influence of SF in high-strength concrete using

low water-binder (*w/b*) ratio mixes ranging from 0.5 to 0.33. 40x40x1000 mm concrete prisms were tested for free and restrained shrinkage exposed to hot-dry environments (40 °C and 45% RH) immediately after casting. They found that the presence of SF considerably increased the free plastic shrinkage of concrete compared to referenced Portland cement with the same *w/b* ratio when subjected to drying. SF also accelerated the setting time of concrete.

Samman *et al.* [17] investigated the plastic shrinkage cracking of normal and high strength concrete incorporating SF. 600x900x300 mm specimens were placed under the following three different exposure conditions: Indoor with laboratory controlled air at 25 ± 1 °C and 55 ± 5 RH, with the wind prevented from directly blowing on the specimens, the second was outdoor with panels placed in the open air where temperature and relative humidity varied naturally. Wind barriers protected the panels from the wind but not from direct solar radiation. The third exposure condition was a combination of the second exposure condition with the addition of wind blowing on the concrete surface with the aid of electric fans. Moisture loss and plastic shrinkage cracking were monitored. It was found that the presence of silica fume in some of the high strength concretes exhibited plastic shrinkage cracking even when the rate of evaporation was less than the threshold value of $1.0 \text{ kg/m}^2\text{-hr}$ ($0.2 \text{ lb/ft}^2\text{-hr}$) recommended by the codes of practice.

Almusallam *et al.* [36] investigated plastic shrinkage cracking in blended cement

concretes of 450x450x20 mm slab specimens that included SF at dosages of 5, 10 and 15%, as well as other types of blending cement concrete materials. These specimens were exposed to hot-humid and hot-dry environments. The rate of water evaporation and bleeding was monitored in these specimens. The measurement of these two parameters indicated an increased plastic shrinkage cracking in SF and other blended cement concretes when compared to plain cement concrete.

2.4.5 Effect of Silica Fume on the Mechanism of Plastic Shrinkage Cracking

The principal cause of plastic shrinkage in Portland cement concrete is known to be the excessively rapid rate of evaporation of water from the surface of the concrete and the inability or lack of bleed water to replace the evaporating surface water [57]. Other investigators studied how the above process leads to plastic shrinkage. Wittman [59] has demonstrated experimentally that the requisite for plastic shrinkage is a build-up of capillary tension in the mixing water present in the fresh concrete after the surface becomes dry. When the surface dries, a complicated system of menisci forms at and near the concrete surface. A tensile capillary pressure within the liquid phase is developed and rises at an increasing rate until it reaches maximum that Wittman [59] called the 'break-through pressure'. Capillary pressure drops rapidly and immediately after the break-

'through pressure'. Capillary pressure drops rapidly and immediately after the break-through pressure is reached.

Plastic shrinkage begins shortly after the capillary pressure starts to develop and exerts enough negative pressure to cause horizontal (surface) and vertical (depth) contractions. Shrinkage strain rises at an increasing rate, similar to the capillary pressure, and continues to rise until the time when the break-through pressure is reached.

Based on the work of Carman [cited in Ref. 57] for fine sand, Powers [60] proposed the following equation (presented with minor modifications in Ref. 57), for determining the maximum capillary tensile pressure for a cement mixture:

$$P = 1 \times 10^{-3} * \frac{\gamma S}{w/c} \quad (\text{Equation 2.4})$$

Where,

P = capillary pressure, MN/m^2 (MPa);

γ = surface tension of water, N/m ;

S = mass specific surface area of cement, m^2/kg ; and

w/c = water-cementitious materials ratio, kg/kg .

The constant 1×10^{-3} has the dimension of density (kg/m^3).

In the development of Equation 2.4, the cement particles were assumed to be non-porous. An important point is made by this equation is that for a given γ and w/c ratio, the capillary tensile pressure (P) increases with the increase in the mass specific surface (S) of the cement.

A similar equation also for non-porous solids (spheres), but independent of w/c ratio, was developed by Pihlajavaara [61], for the maximum capillary tensile pressure and is presented with minor modifications [cited in Ref.50] as follows:

$$P = 2.6 \times 10^{-7} \gamma S \rho \quad (\text{Equation 2.5})$$

Where,

ρ = solid density of cement, kg/m^3 ;

γ and S were defined previously;

and the constant 2.6×10^{-7} is dimensionless.

Equations 2.4 and 2.5 give results that seem to agree with Wittman's experimental results of capillary pressure [59]. Taking for instance $\gamma = 7.3 \times 10^{-2} \text{ N/m}$, $S = 350 \text{ m}^2/\text{kg}$, $\rho = 3150 \text{ kg/m}^3$, and w/c = 0.35 [cited in Ref. 51], the capillary pressures calculated by Equations 2.4 and 2.5, respectively, are 0.073 MPa (10.6 psi) and 0.021 MPa (3.04 psi).

In comparison, Wittman's experiment [59] yielded 0.021 MPa (3.04 psi) as determined by extrapolation of his data. These values, especially the one from Equation 2.4 and the one obtained from the experimental work of Wittman, seem to agree very well. Even though the pressure is low, it may be high enough to generate cracks if the tensile strength of the concrete matrix is lower than the capillary pressure. Radocea [62] also experimentally measured the capillary pressures in sand; cement and silica fume slurries, the values of capillary pressures he obtained agreed well with values obtained with Equation 2.4.

If a similar capillary pressure phenomenon occurs in silica fume cement paste, it is reasonable to expect that the plastic-shrinkage mechanisms of the two systems are identical. This suggests that, maintaining the same conditions; any difference in plastic shrinkage characteristics (i.e., strain and cracking) would be due to the differences in surface area or cement particles and solid materials. Further, one may expect that, under similar drying conditions, silica fume paste will exhibit a greater degree of plastic shrinkage cracking than Portland cement paste owing to its much greater surface area [57].

2.4.6 A Model for Plastic Shrinkage

According to Radocea [62], plastic shrinkage can be defined as the volumetric

contraction of a system in which water constitutes a continuous phase and the water menisci are always located at the surface of the system. The process of plastic shrinkage involves a mass transfer from the surface to the surroundings by evaporation and a simultaneous mass transfer from inside the concrete to the surface. Since water is regarded as incompressible, the amount of water transferred to the surface is equivalent to the total deformation of the sample [62].

According to the Laplace equation, the capillary pressure P is a function of the surface tension of water (σ) and the mean curvature of the water meniscus (R):

$$P = 2\sigma/R \quad (\text{Equation 2.6})$$

For saturated granular solids exposed to drying, the time dependence of the capillary pressure must therefore be a function of the amount of evaporated water (W), the amount of water transferred to the surface (W_s), and the geometry of the spaces between the outermost particles [62]. In a well-compacted sand bed, the capillary forces are too low, relative to the friction between the sand grains, to produce a significant change in volume and to press out water from the bed, nor can the suction produced draw water to the surface without permitting its replacement by air. Thus, the water pressure will depend only on the amount of evaporated water and other related factors such as particle size and

degree of packing, which determine the spaces between the sand grains.

The capillary pressure-water evaporation (PW) curves of two materials with identical pore structures are shown in Figure 4.9. In order to produce capillary pressure P in the first material (which shrinks when exposed to drying, as shown on the right), a certain amount of water (W) must evaporate (see the PW curve on the right). This consists of an amount of water (W_s) transferred to the surface and an amount of water ($W-W_s$) that depends on the geometry of the spaces between the outermost grains. That is the (PW_E) curve in Figure 4.9 represents the second material that does not shrink. The attempt to describe the pore structure near the surface by an equivalent pore is motivated by the fact that pores, communicating with one another drying as a single pore. This means that a small pore cannot dry faster than a larger one, since water transport from adjacent larger pores will supply the smaller ones, which tend to dry faster. The dimensions of an equivalent pore can be calculated by using the PW_E curve of a material and that these dimensions depend on the particle size distribution of the material [62].

In freshly-placed cement paste, the combined effect of the dissolved layer (of water) and the electrostatic charge (of the cement grains) is such as to prevent actual contact between adjacent cement grains. During the dormant period, relatively low compressive forces are sufficient to press out a part of the mixing water, and consequently produce consolidation

of the paste. Settlement and vacuum processing of freshly-placed concrete are examples of consolidation processes involving various physical and chemical forces [62].

From the above, it can be observed that the parameters that affect the plastic shrinkage include:

1. The specific surface area of the cement paste; and
2. The geometry of the pore spaces between the outermost grains that can be obtained from the sample's pores size distribution.

2.5 SUPERPLASTICIZERS

Superplasticizers (SP) are water soluble, natural or artificial polymers sometimes used in the concrete industry as dispersing agents during the hydration of Portland cement. These types of admixtures are also known as super-fluidizers, super-water reducers or high-range water reducers. They can be used in one or more of the following three different purposes [63]:

1. To increase the workability without changing the mix composition in order to enhance the placing characteristics of concrete;

2. To reduce the mixing water and the water-cement ratio (w/c) in order to increase the strength and improve the durability at a given workability; and
3. To reduce both water and cement at a given workability in order to save cement (hence improving the economy) and reduce creep, shrinkage and thermal strains caused by heat of hydration.

In order to minimize the confusion which may arise with the use of different terms by various manufacturers, recall that superplasticizers are chemical admixtures that can be used either as high-range water reducers in the production of concrete with normal consistency or as plasticizers in the production of flowing concrete. The characteristics of these two applications are defined, respectively, in ASTM C 494 and C 1017 standard specifications. Updated guidelines for their use are presented in the ACI Manual of Concrete Practice [64].

The most widely used SPs are: (i) sulfonated melamine formaldehyde condensate, (ii) sulfonated naphthalene formaldehyde condensate. In addition to these admixtures, modified lignosulfates, sulfonic-acid esters, carbohydrate esters, etc., have also been used [65 -67].

2.5.1 Interaction of Superplasticizers and Cement Matrix

Superplasticizers are polymers that can interact physically and chemically with cement particles. Physical interaction occurs when a superplasticizer is used to disperse a non-cementitious fine powder. This type of interaction includes three modes of action: (1) adsorption of superplasticizer molecules by van der Waals and electrostatic forces on the cement grains [65,68], (2) reduction of the attractive forces between oppositely charged cement grains (deflocculation) and induction of inter-particle repulsive forces due to the high negative charge conveyed to the cement grains by the adsorbed superplasticizer (dispersion) [69,70]; and (3) steric hindrance between adsorbed polymer molecules and neighboring cement grains [70].

Superplasticizers also chemically interact with cement particles. It has been found that naphthalene-based superplasticizers can react with the most reactive sites of cement particles, particularly the C₃A, and substantially reduce the initial surface hydration rate [69,70]. According to Uchikawa *et al.* [69], naphthalene-based superplasticizers are more preferentially adsorbed by the interstitial phase and free lime than by the calcium silicate phases [70]. Superplasticizers are also reported to retard the hydration of C₃S [70]. These interactions have practical consequences because they can delay the setting time of the paste and significantly reduce the mechanical properties at early ages [69,72]. The retardation effect of superplasticizers is roughly proportional to their concentration and is

generally more pronounced with low C₃A cements [72,73].

Portland cement is a complex mixture of inorganic compounds; mainly calcium silicates, calcium aluminate, calcium ferroaluminate, and calcium sulfate, ground together at varying degrees of fineness (many of these compounds can exist in several crystalline forms). Blended cements may contain filler (limestone) or pozzolanic material (fly ash, silica fume). Some chemical admixtures are used as grinding aids during the manufacture of the cement and, therefore, remain present in the cement.

The influence of cement fineness on the amount of superplasticizer to reach a certain level of workability in the case of concretes (or fluidity in the case of grouts) has been clearly established [74]. The finer the cement, the higher will be the superplasticizer dosage required to achieve a given workability.

As mentioned previously, all types of superplasticizers react generally with the C₃A in cement. Cement-superplasticizer interaction also depends on the morphology of the C₃A phase, the alkali content [75], and the form of calcium sulfate added to clinker [76]. The role of sulfates on the rheology of Portland cement slurries has been shown: it is not the total amount of SO₃ in cement that is important, but rather the availability, or the rate of dissolution of SO₄²⁻ ions, that must be balanced with the chemical reactivity of C₃A [77].

2.5.2 Effect of Superplasticizer Dosage and Type of Cement

Research carried out by Gagne *et al* [73] in which the effect of superplasticizer dosage on the mechanical properties (permeability and freeze-thaw) of high strength concretes with and without silica fume shows that high slump (220 ± 20 mm) high-strength concretes with ordinary Type 10 (ASTM Type I) Portland cement and containing large amounts of superplasticizer can have significantly lower compressive and flexural strengths than similar concretes with usual slumps (170 ± 20 mm). Lower compressive strength was measured at all ages.

Ramachandran, *et al.* [78] investigated the behavior of ASTM Type V cement hydrated in the presence of sulfonated melamine formaldehyde. They found that at a dosage of 0.6% and 0.3%, respectively, the strength of either Type I and that of Type V cement did not affect their strength development. However, the dosage of 0.6% in Type V cement significantly reduced the 28-day strength by 17.2%. RamezanianPour and Malhorta [79] previously reported a reduction in the range of 11 to 23%.

2.5.3 Effect of Superplasticizers on Silica Fume Concrete

Silica fume has a large surface area; hence, it will increase the water demand when used in concrete. Superplasticizers are usually recommended in order to lower the water

demand to the appropriate level and allow for adequate dispersion and proper packing of the silica fume particles. It is believed that the adsorption of the molecular polymers in the superplasticizer chain on the surface of cement grains accounts for cement dispersion. This also accounts for the dispersion of silica fume in cement or concrete mixes [80].

There is disagreement as to whether the mechanisms underlying the improved mechanical properties of concrete containing both silica fume and superplasticizer are physical (as in adsorption) or pozzolanic. Rosenberg and Gaidis [81] reported chemical and physical evidence that silica fume with superplasticizers does not densify concrete in the usual sense; it enhances the paste-aggregate bond to produce a strength increase and that strength increase does appear to be related to porosity. Porosity is primarily controlled by the water-cementitious materials ratio that can be lowered with the use of superplasticizers. Data by Detwiler and Mehta [53] showed that at the age of 7 days, the influence of silica fume on compressive strength might be attributed to mainly physical effects. After 28 days, both physical and chemical effects become significant.

2.5.4 Compatibility of Silica Fume with Superplasticizers

The ACI Committee 234R-96 [80] has the following commentary statement on the interaction of silica fume and admixtures: "There is no published data describing incompatibility of silica fume with admixture combinations normally used in concrete."

However, it is advisable to conduct laboratory testing using the proposed admixtures to assure that all materials are compatible." It has been reported in the literature that for a given superplasticizer type, there exists a saturation point after which any addition of superplasticizer will not significantly improve the workability of the paste [74,82]. Excessive dosages of superplasticizer will result in segregating the aggregates and cement. Saturation concentration is usually expressed as the ratio between the mass of solid fraction of superplasticizer and the mass of cementitious materials [73]. The saturation concentration of most cement-superplasticizer combinations usually range between 0.8 and 1.2 percent and is basically affected by the type and quality of superplasticizer, fineness of cement, C₃A content, type and content of sulfates, and type of mixer (speed, shear action) in addition to the SF content and type [77].

Yogendran *et al.* [83] have shown that when the silica fume replaces 5% (w/b = 0.34) of Portland cement in cement paste without superplasticizer, constant flowability is ensured without any increase in w/b. However, for replacement of over 10%, the water requirement varies linearly with the SF content. The results of the influence of SF on the water requirement with SP are less clear. Up to 15% SF, the consistency does not vary as compared to the control mix, but the stiffness increases considerably when the SF content is increased to 25% [84]. Pastes with lower than optimal SP content exhibit thixotropy after the addition of SF. The thixotropy increases with increasing the SF content and

decreases with decreasing SP content below the optimum [85]. According to Mangialardi *et al.* [cited in Ref. 85], the addition of microsilica to Portland cement pastes causes a marked increase in the adsorption of SP. This increase is directly related not to the greater specific surface area of microsilica but to its ability to interact with the lime produced from the cement hydration. The results of tests [cited in Ref. 85] on cement pastes with the addition of SF from 0 to 15% of cement mass indicate that their rheological properties depend on the fractions of the components, which can be ordered as follows: SF>SP>w/c> %C₃A> %SO₃ in cement. This was based on statistical analysis expressed as the coefficients in regression analysis. The influence of SF on the response variables (yield stress and plastic viscosity) used in the regression analysis was more than double that of the other factors. This means that the addition of SF exerts the most significant influence on the rheological characteristics of cement paste.

2.5.5 Superplastcizers, Silica Fume and Hot Weather

Hot weather plays a very important role on the properties of fresh concrete. Fresh concrete mixes stiffen with time, particularly when continuously mixed. The stiffening effect is reflected in reduced slump and, accordingly, is referred to as 'slump loss' [86]. Under moderate weather conditions, the stiffening of fresh concrete, and its associated slump loss present no real problems in practice because the concrete remains workable enough to allow its handling, namely, its transporting, placing, compacting and finishing,

without any appreciable difficulties. Under hot weather conditions, however, this may not be the case because the rate of stiffening and the associated slump loss are both increased [87-89], and the initial and final setting times are both decreased [90,91] with the rise in temperature.

The results presented by Pinto and Hover [92,93] on the behavior of silica fume and superplasticizer addition on the setting behavior of high-strength concrete mixes show that the addition of superplasticizer alone up to a dosage of 1.6% by weight of cement retarded the setting time of the mortar, while the separate addition of silica fume up to 10% by weight had an accelerating effect on the setting time of cement mortar. The combined effect of SP and SF displayed significant interaction with the delayed set for a certain superplasticizer dosage. This effect decreased with increasing the silica fume content. Temperature was also found to have a significant effect on the setting time, with the initial set time and time difference the between initial and final set decreasing nonlinearly when the temperature increased from 0 °C to 40 °C.

2.5.6 Characterization of the Interaction between Superplasticizers and Plain and Blended Cement Concretes

In view of the above-cited literature review, and in order to understand the effect of superplasticizers on the plastic shrinkage strain in plain and blended cement concretes,

the characteristics of superplasticizers that affect cement paste are outlined and discussed below; a schematic diagram of this interaction is shown in Figure 2.6 [94].

1. Dispersion mechanisms;
2. Effect on the hydration of cement paste (hydration products and reaction kinetics); and
3. Effect on the microstructure.

These factors are elucidated in the subsequent sections.

2.5.7 Modified Lignosulfate Polymer (MLP)

Lignin is a complex material that forms approximately 20% of the composition of wood. During the production of papermaking pulp from wood, waste liquor is formed as a by-product containing a complex mixture of substances, including decomposition products of lignin and cellulose, sulfonation products of lignin, various carbohydrates (sugars) and free sulfuric acid or sulfates. Subsequent neutralization, precipitation and fermentation processes produce a range of lignosulfates of varying purity and composition depending on a number of factors, such as neutralizing alkali, the pulping process used, the degree of fermentation and even the age of the wood used as pulp feedstock [95].

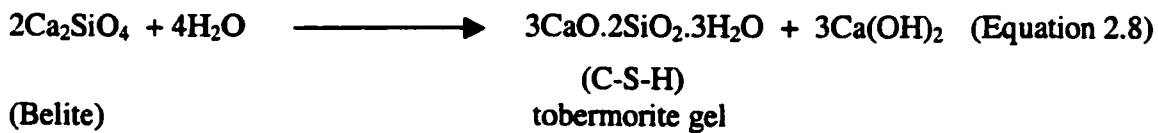
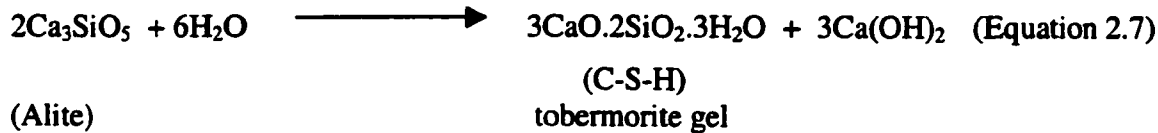
Commercial lignosulfates used in admixture formulations are predominantly calcium or sodium based with sugar contents of 1 to 30%. The lignosulphate molecule is a substituted phenyl propane unit containing hydroxyl, carboxyl, methoxy and sulphonic acid groups. The polymer could typically have any average molecular weight of about 20 to 30, 000 with a range varying from a few hundred to 100,000. The range of molecular weight present in the lignosulphate is dependent on the manner and condition under which refinement was done. Three such methods are used, namely ultra-filtration, heat treatment at a specific pH and fermentation [95].

Dispersion mechanisms

Most organic admixtures exhibit an affinity towards the surface of cement particles, or cement hydration products, resulting in significant adsorption. Precluding chemical reactions between the cement phases and the added lignosulfate, the adsorbed molecules will alter the surface properties by conveying a negative charge to the particle surfaces, i.e. negative zeta potential. This will induce repulsion between neighboring cement particles and thus contribute to increased dispersion. In the case of high molecular weight polymers, physical interference (steric) will lead to additional short-range repulsive forces [95].

Effect on the Hydration of Cement Paste

Research carried out by Mollah *et al.* [96] indicated that in the presence of lignosulfate, the formation of portlandite $\text{[Ca(OH)}_2]$ is drastically reduced, and there is a decrease in the level of orthosilicate (SiO_4^{4-}) polymerization in the hydration of cement paste. When Portland cement is allowed to react with water, the principal products are tobermorite gel (C-S-H) (60-70%), Ca(OH)_2 (20-25%) and about 5-15% of other minor phases [96]. The principal reactions involved may be represented by the following two idealized equations [95]:



With the formation of the C-S-H phase, Ca^{2+} ions are released into the pore solution. It is thought that the negatively-charged lignosulfate ions will concentrate against the layer

formed by the Ca^{2+} ions, and since the negative surface charge is compensated for by Ca^{2+} ions that form an electrical bi-layer, the next zone in the solution is the tri-layer diffusion ions that consist of lignosulfate ions. This layer may be termed as "The Diffusion ion Swarm"[96]. The diffusion ion swarm will be dominated by lignosulfate ions. It is therefore reasonable to assume that the Ca^{2+} ions released from the system will not be available for reactions leading to the formation of $\text{Ca}(\text{OH})_2$ which in effect will reduce the pH of the medium. Removal of Ca^{2+} ions from the solution will also prevent them from entering into setting and curing reactions of the hydrating cement systems thereby leading to retardation in the setting time [96].

Effects on the Microstructure of Cement Paste

See Section 2.5.9 for details.

2.5.8 Sulfonated Naphthalene Polymer/Formaldehyde (SNP/SNF)

SNP and SNF are part of a family of superplasticizers of the salts of naphthalene formaldehyde sulphonic acids and are referred to collectively as polynaphthalene sulfonated superplasticizer (PNS). This material is produced from naphthalene by oleum or sulphur trioxide sulphonation. Subsequent reaction with formaldehyde leads to polymerization and the sulphonic acid is normally neutralized with sodium hydroxide

[95]. The commercial available materials of low polymerization tend to reduce the surface tension of the aqueous phase in the concrete, which can lead to air entrapment. In view of this, air-detaining agents, such as tributyl phosphate and dibutyl phthalate are added. Materials based on higher molecular weights are said to be more effective and as they do not affect the surface tension, will not cause air entrapment.

Dispersion Mechanisms

The dispersion mechanism of PNS (SNP/SNF) superplasticizers is similar to that of lignosulfates. However, the improved fluidity in the addition of SNP to cement paste is related to the adsorption of the superplasticizer on the cement particles, and its removal from the pore solution is of special interest [97]. Results from the literature [97] suggested that the uptake rate of PNS from the pore solution is parallel to the degree of hydration and can be interpreted as an effective removal of it by the hydrated phases. It was also noted that the degree of PNS uptake is related to the degree of polymerization. Monomer (single-polymer), dimer (two-polymer) and probably other lower molecular weight polymers are more likely to remain differentially in the pore solution, while higher molecular weight polymers are absorbed on the cement particles. Information on the molecular structure and dispersion mechanisms of various types of superplasticizer is given in Ref. 98.

Effect on the Hydration of Cement Paste

PNS have been shown to react specifically with the aluminates (C_3A , C_4AF and SO_3) phases of cement paste competing for SO_4^{2-} ions. This preferential absorption of polymer molecules into the C_3A -gypsum system leaves only small amounts of polymer for dispersion of the C_3S and C_2S phases that leads to delays in the dormant period of cement paste. It has been shown that the higher the molecular weight of the sodium salts of polynaphthalene sulfonated superplasticizer, the longer the dormant period and the later occurrence of the main peak of heat evolution. In other words, the higher the molecular weight, the greater is the retardation. The lower the monomer content, the higher is the fluidity [97].

Effect on the Microstructure of Cement Paste

See Section 2.5.9 for details.

2.5.9 Polycarboxylic Ether (PCE)

Polycarboxylic ether (PCE) is part of a new group of superplasticizers known as acrylic polymers (AP) that include copolymers of carboxylic acids (CAE), PCE and cross-linked acrylic polymers (CLAP) [98]. Unlike PNS (SNP/SNF) superplasticizers that have numerous sulfonated groups that form a layer with a negative electrostatic charge around

the cement particles on which the polymer is adsorbed, PCEs possess a different chemical structure [98]. It consists of a carboxylic ether polymer with long side chains (e.g. of ethylene oxide-malic acid or ethylene oxide-acrylic acid copolymers) [98]. These side chains can easily be modified to obtain specific performance in terms of dispersibility, set retardation and slump retention, by varying the size of the groups, their composition, and molecular weight of the main chain, as well as that of the pendant (attached) groups [98].

Dispersion Mechanisms

At the beginning of the mixing process, PCE imitates the same electrostatic dispersion mechanism as the traditional high-range water reducing action such as SNF/SNP, but the side chains linked to the polymer backbone generate a steric hindrance which stabilizes the particles ability to separate and disperse. Research has shown steric hindrance is the predominant dispersion mechanism [99].

Effect on the Hydration of Cement Paste/Mortar

Research carried out by Guadong and Beaudoin [100] using AC impedance spectroscopy and other techniques indicated that PCE retarded the hydration of cement mortar for a period of up to 1 day compared to mortars containing PNS (and PMS, polymelamine sulfonate) with dosages up to 1.5% for the same W/C. The effects of PCE on the various phases of the products of hydration were not elaborated upon. The interaction of PCE and

cement paste is yet to be fully understood [101].

Effect on the Microstructure of Cement Paste/Mortar

In a recent study [101] using SNP, SM (PMS) and PCE and other types of superplasticizers (not considered here), cement paste and mortar incorporating these superplasticizers were characterized using such techniques as NMR imaging, XRD analysis, SEM microscopy and mercury intrusion porosimetry (MIP). However, none of the superplasticized cement paste/mortars incorporated silica fume, although a separate paste incorporated silica fume was made for comparison, in addition to the reference cement paste. Some of the following conclusions were drawn from this research:

1. The effect of the superplasticizer on the hydration process is closely related to its dispersing action in the fresh state. The superplasticizers studied led to a lower amount of polymerized silicates (C_3S and C_2S), which is indicative of the formation of a lower amount of C-S-H gel*

*Other effects of the various superplasticizers on the hydration of cement outlined in the preceding sections were more or less confirmed.

2. The incorporation of superplasticizers also led to a decrease of the total porosity

(as determined by the total volume of mercury intruded), at the ages considered, as a result of the dispersing action of the admixtures. The decrease in the total porosity varied with the type of superplasticizer (the superplasticizers were incorporated at their saturation not optimal dosages).

2.6 MICROSTRUCTURE OF CONCRETE

A cement-based engineering material, such as mortar or concrete, is a composite of a binding matrix, primarily containing hydrated Portland cement, sand and aggregate. Different length scales can characterize each phase, which corresponds to a typical pore diameter, the size of which spans from nanometers to millimeters. First, considering the cement paste, at the smallest scale, cement paste is largely composed of calcium silicate hydrate (C-S-H) gel, which is comprised of nanometer size particles and pores. At the micrometer scale, the cement paste appears as a composite of hydrated products, unhydrated products and space previously occupied by mixing water (referred to as capillary pores). At the millimeter scale and larger, the cement paste and aggregate (sands and stones) form a composite material that may contain air voids (at the millimeter scale). Another feature that may be present in concrete is the interfacial zone [102,103]. The interfacial zone is a region of order 10 to 40 micrometers near the cement-paste/aggregate boundary where there is an increase of porosity. The increase of porosity is probably a

result of the inability of cement particles to densely pack near the paste/aggregate boundary. The interfacial zone can dramatically enhance the transport properties of concrete. Although the quantity of pores is great in cement-based materials, the permeability of these systems is dependent on the amount, porosity and connectivity of the pores. The amount of pores and their connectivity strongly influence the materials properties, particularly the strength and permeability, which affect the resistance to harmful penetrants. Figure 2.5 shows the dimensional range of solids and pores in hydrated cement paste [104].

Because of the complexity of the pore structure of these materials, measuring the total porosity and size distribution is difficult. The methods typically used, which are mercury intrusion porosity (MIP), water-vapor adsorption and nitrogen adsorption, assume that the geometry of the pores is regular, that the pores are interconnected and that the size distribution is not affected by the loss of water in the pores upon drying. A single technique is not able to characterize the whole range of pore sizes found in cement materials. MIP can measure larger capillary pores (0.005 to 10 μm), whereas the adsorption techniques can describe C-S-H gel porosity ($<0.03 \mu\text{m}$) [102].

Figure 2.6 shows a typical pore size distribution for the binder paste in high-strength concrete [105]. The following four different pores can be identified:

- Gel pores;
- Capillary pores;
- Mesopores; and
- Air pores.

The average radius of each pore group differs from the nearest group by at least an order of magnitude. Each group can, therefore, be considered to consist of voids having nearly equal radius. The continuous curve in Figure 2.6 was obtained from nitrogen adsorption tests of cement paste. The dashed and dotted curve is calculated from MIP data. Data on the largest pores can be obtained from optical microscopy [105].

Nitrogen adsorption is usually carried out on amorphous hydrated cement paste while MIP normally uses hardened concrete or paste samples [102]. Concrete porosities can be transformed into binder porosities by chemical analysis that includes volumetric calculations, and determining the amount of chemically bound water by thermogravimetric means [105]. Typical porosities using nitrogen adsorption are shown in Figure 2.7 for various types of concrete.

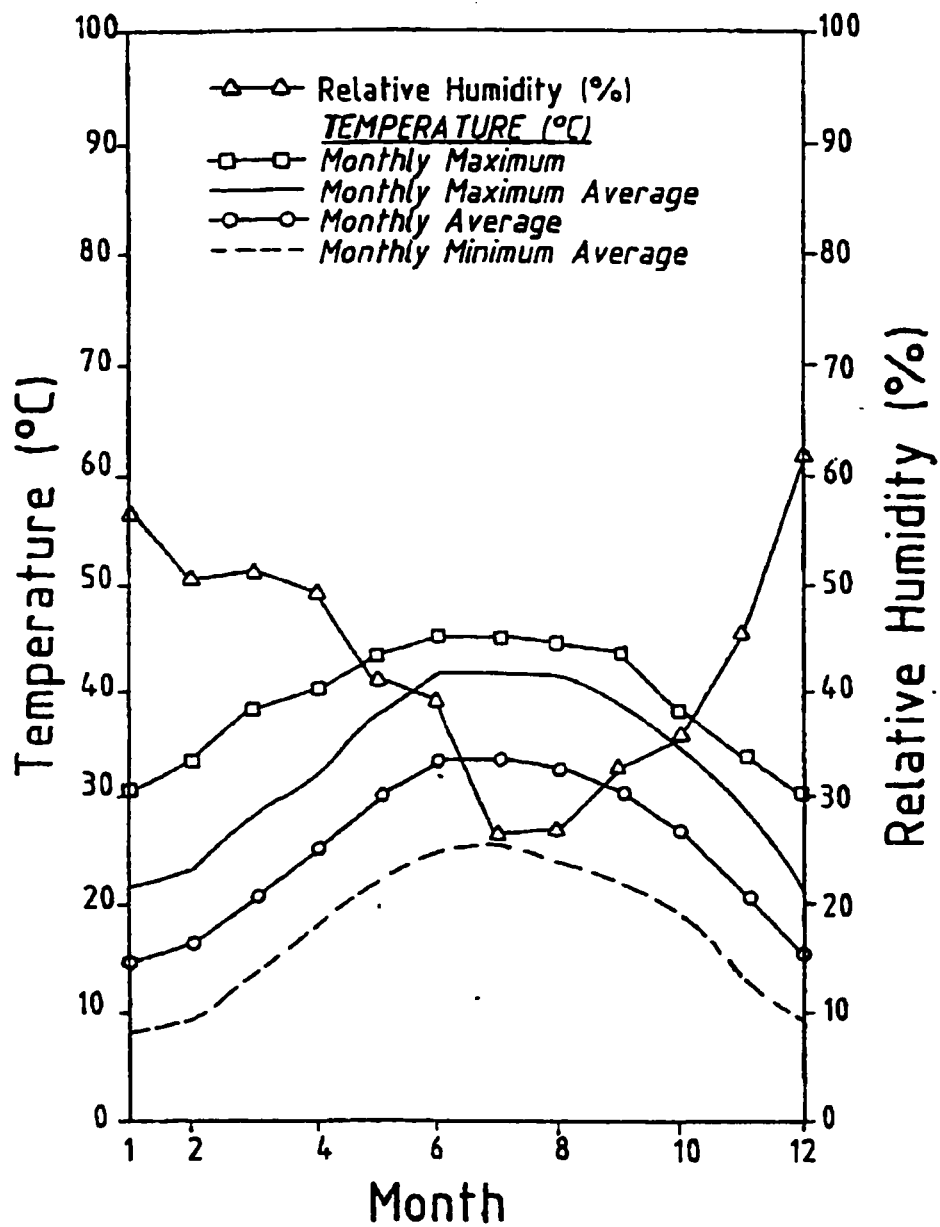


Figure 2.1: Variation of temperature and relative humidity in Riyadh [21].

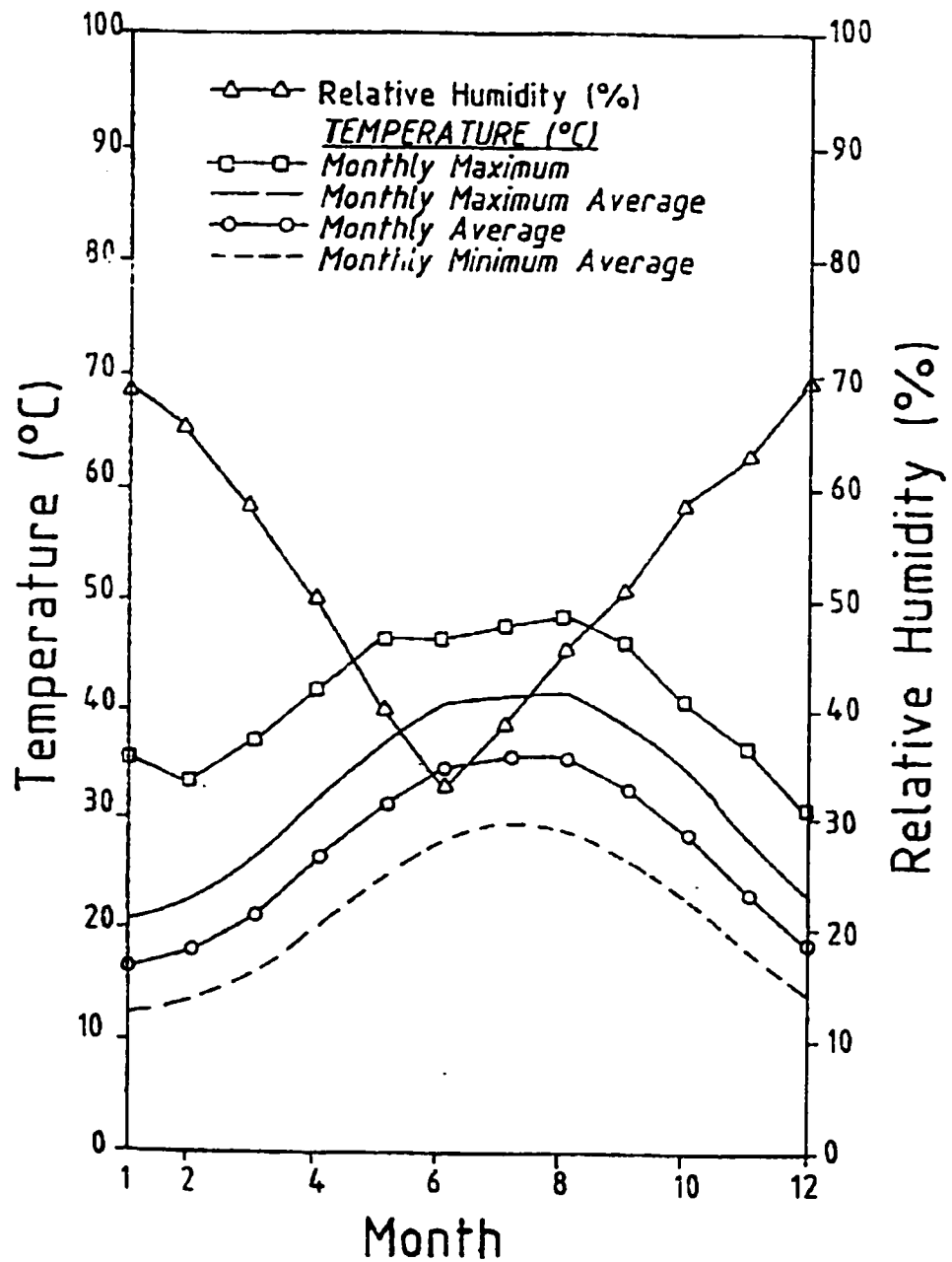


Figure 2.2: Variation of temperature and relative humidity in Damman [21].

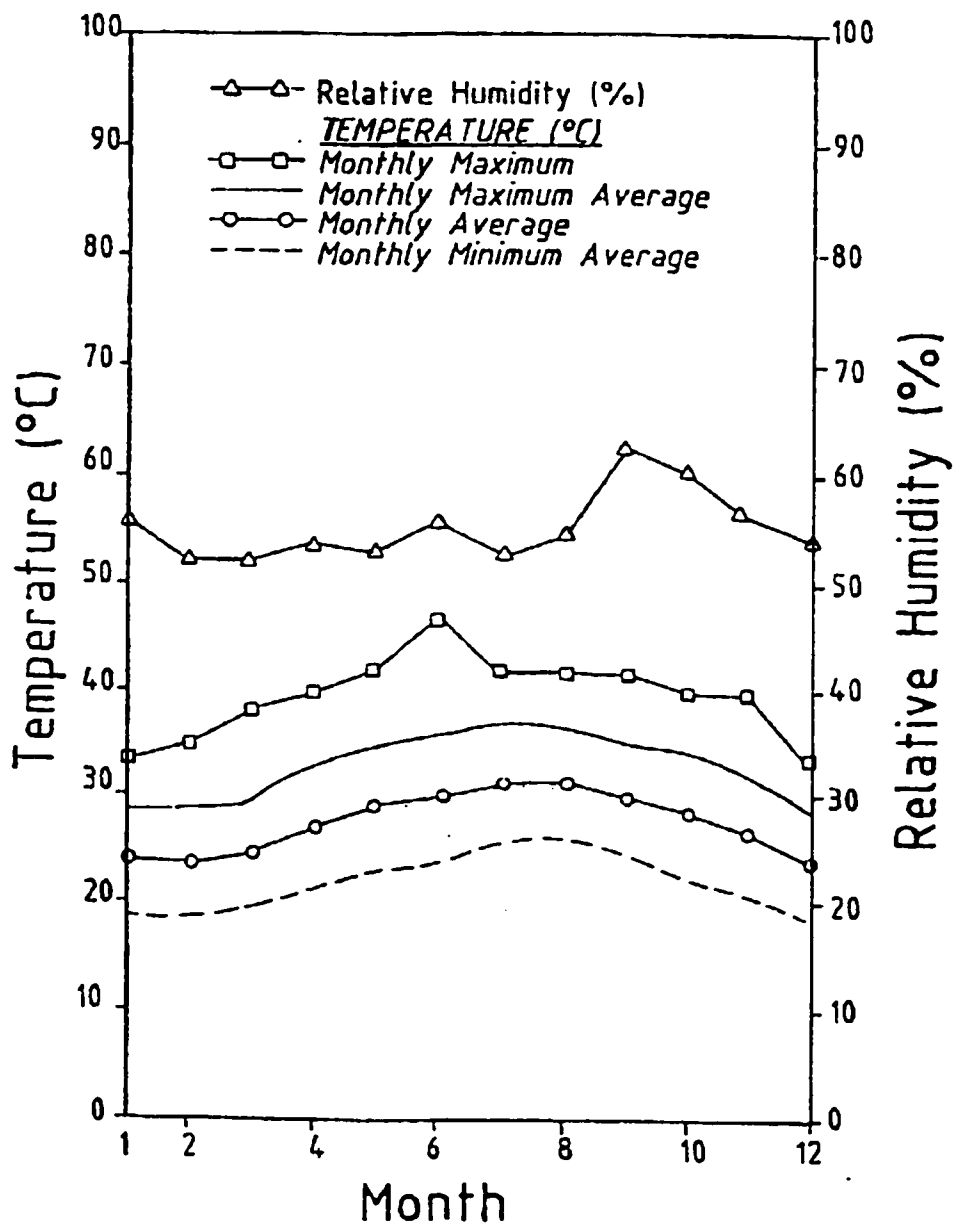


Figure 2.3: Variation of temperature and relative humidity in Jeddah [21].

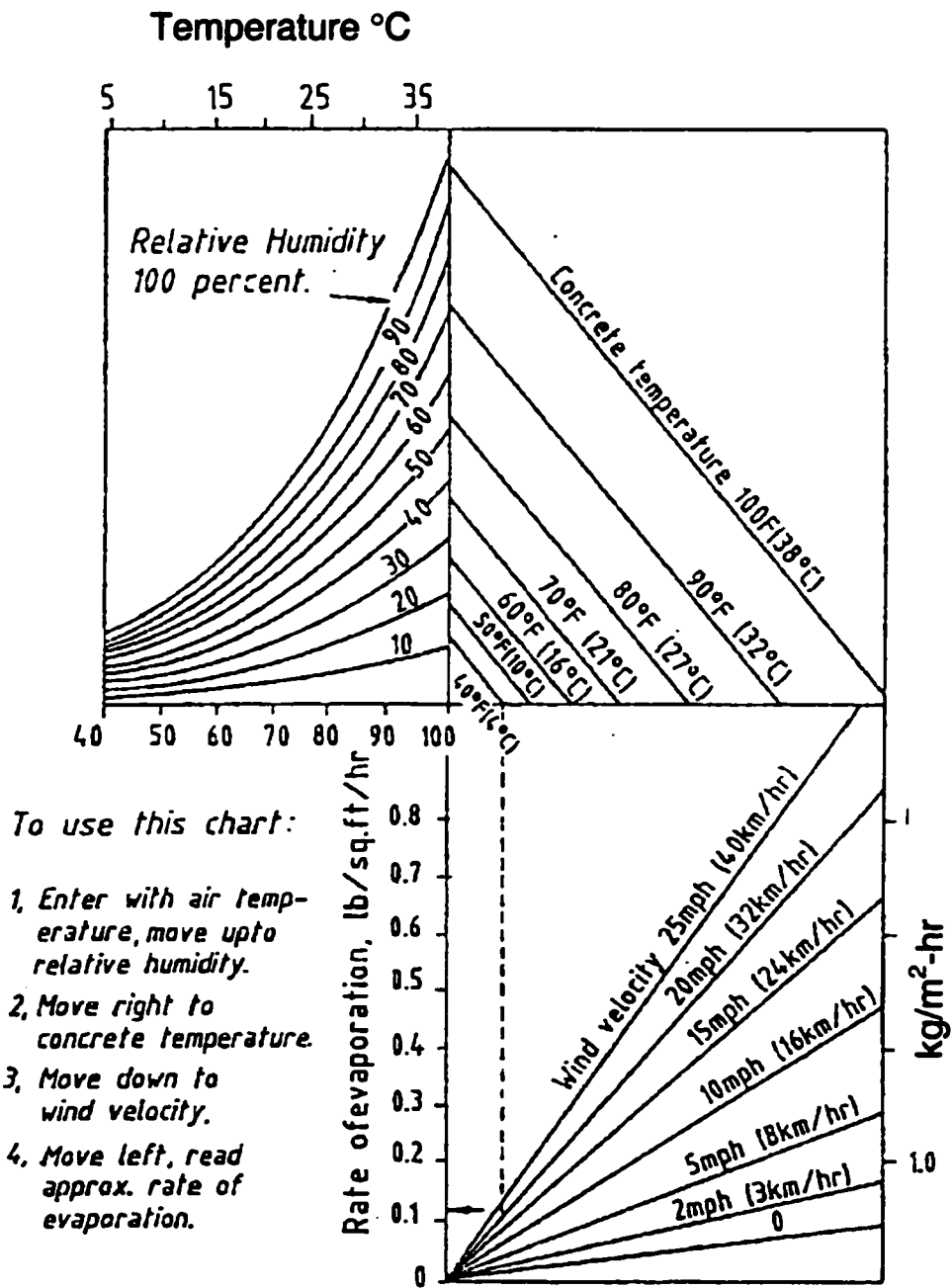


Figure 2.4: Effect of ambient conditions on the rate of water evaporation [19].

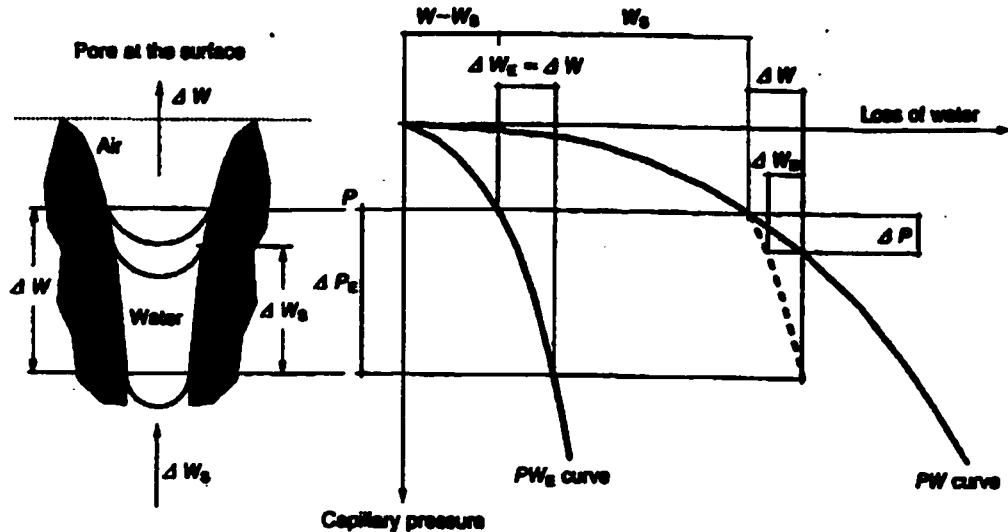


Figure 2.5: PW curve, PW_E and the change in DWs [62].

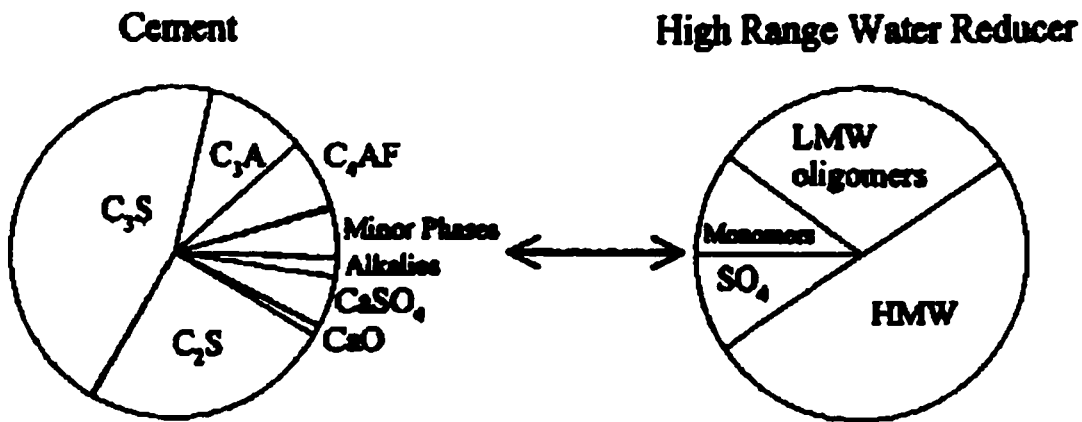


Figure 2.6: Schematic illustration of the interaction between a cement (multi-phase mineral system) and a chemical admixture (multi-component organic system) [94].

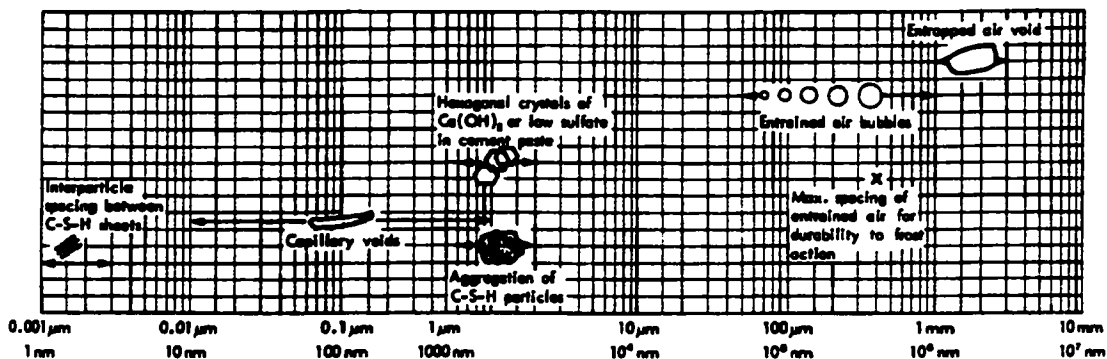


Figure 2.7: Dimensional range of solids and pores in hydrated cement paste [104].

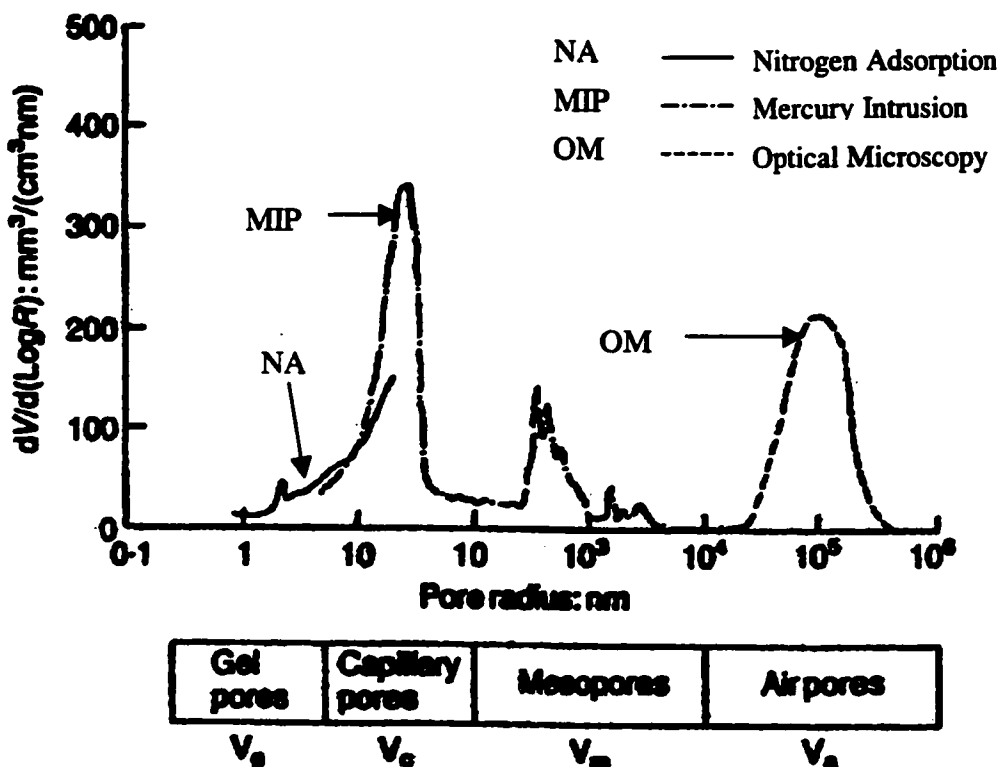


Figure 2.8: Typical pore size distribution for paste in a high-strength concrete [105].

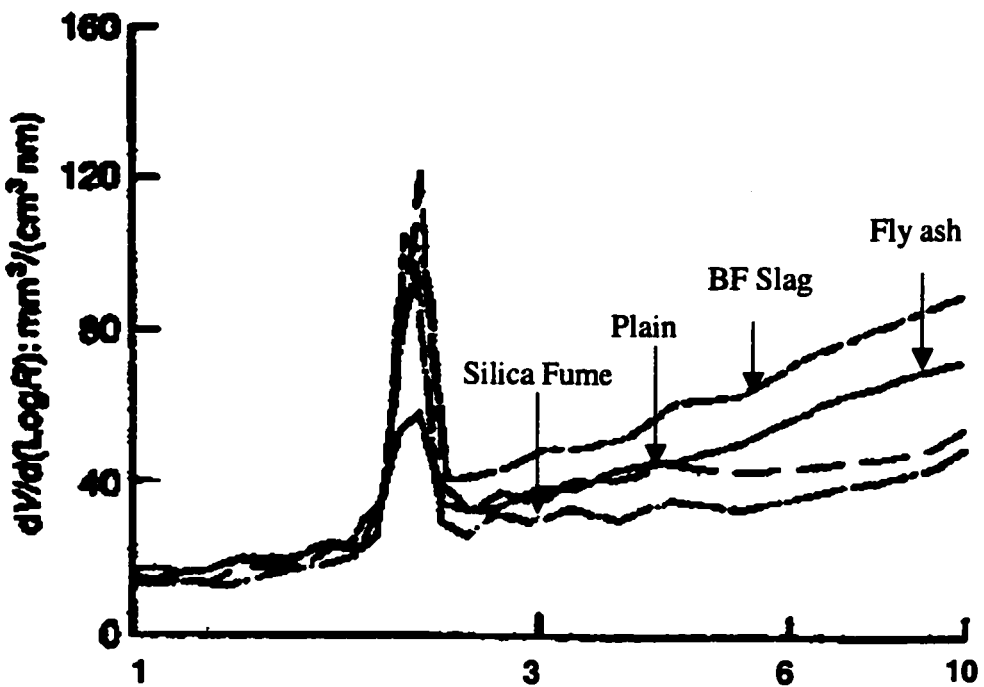


Figure 2.9: Typical porosities using nitrogen adsorption method for various types of concretes at the age of 28 days [105].

CHAPTER 3

EXPERIMENTAL PROGRAM

This research work is concerned with evaluating the plastic shrinkage cracking of fresh concrete using silica fume from five sources and their interaction with four types of superplasticizer. The effect of temperature, relative humidity and wind velocity on the plastic shrinkage cracking, plastic shrinkage strain, concrete temperature, crack length, time to cracking and crack intensity were evaluated. The exposure conditions were selected to represent severe media such as those prevailing on summer days in the Eastern Province of Saudi Arabia. The experimental program is broadly divided into the following four series:

In Series I (a), the effect of SF, temperature, wind velocity and humidity on plastic shrinkage cracking and plastic shrinkage strain in concrete prepared with SF from five sources was studied. Drying shrinkage was also monitored for a period of 90 days for these slab specimens. In Series I (b), the effect of varying temperature, wind velocity and

humidity on plastic shrinkage cracking, shrinkage strain and time to cracking on concrete prepared using one type and dosage of SF was carried out.

In Series II, the compressive strength and pulse velocity tests on specimens stored under the same controlled exposure conditions as in Series I (a) specimens were conducted at specified time intervals from the time of casting up to a period of 28 days.

In Series III, the split tensile strength of concrete exposed to similar conditions as in Series II was determined from the time of casting up to a period of 28 days.

In Series IV, the effect of type and dosage of superplasticizers on plastic shrinkage cracking and strain of plain and blended cement concretes was studied. The blended cements incorporated in this Series included three types of silica fume at a constant dosage and four types of superplasticizers at the optimum dosage. Details of the experimental program are shown in Figures 3.1 through 3.7

3.1 MATERIALS

3.1.1 Coarse Aggregates

The coarse aggregate used in this study was brought from Abu-Hadriya and Riyadh

Road. Three aggregate sizes of 3/8 inch (9.5 mm), 3/16 inch (4.76 mm) and 3/32 inch (2.38 mm) were used in all the concrete mixes except in the drying shrinkage prisms where mortar specimens were used. The 9.5 mm and 4.76 mm sizes were brought from Abu-Hadriya while the 2.38 mm sizes were brought from Riyadh road. Abu-Hadriyah aggregates were of crushed limestone with a specific gravity of 2.42 and absorption of 2.5%. Grading of the coarse aggregate was chosen so that it falls within size number 8 of ASTM C 33 limits so as to provide optimum workability. The adopted grading and the corresponding ASTM limits are shown in Table 3.1 and Figure 3.8

3.1.2 Fine Aggregates

Dune sand was used as the fine aggregate with water absorption of 2.5% and a specific gravity of 2.64.

3.1.3 Cement

ASTM C 150 Type I cement was used in all the concrete mixes. The chemical composition of the cement is shown in Table 3.2

3.1.4 Silica Fume

Silica fume, from five different sources, as well as fly ash and Superpozz® were used.

The chemical and physical properties of the supplementary cementing materials are presented in Tables 3.3 through 3.10. All the concrete mixtures were designed to give sufficient workability of 50 to 75 mm slump. For Series I (a) mixes, the superplasticizer used was sulfonated naphthalene polymer, SNP (Conplast M432 MS). The dosages were 0.75%, 1.0% and 1.25% (by weight of binder content) for silica fume dosages of 5%, 7.5% and 10%, respectively. A constant dosage of 0.5% was used for 30% fly ash, 10% Superpozz® and plain cement concrete mixes.

3.1.5 Superplasticizer

In the second part of the experiment (Series IV), trial mixes were prepared by varying the superplasticizer content to obtain sufficient workability in the range of 50 to 75 mm. This was conducted for each of the five types of silica fume and then repeated for the other types of superplasticizer. The following four types of superplasticizer were used:

- (i) Conplast M432MS (SNP)
- (ii) Sika 520 (MLP)
- (iii) Glenium 51 (PCE)
- (iv) EUCON 537 MS (SNF)

3.2 MIX DESIGN

The mix design variables are shown in Figures 3.1 to 3.5 and are summarized below:

- Silica fume procured from five different sources at three dosages of 5.0, 7.5 and 10%
- 10% Superpozz® and 30% fly ash, ASTM C 618 Type F
- For Series I (a) mixes, one type of superplasticizer was used, the water/binder ratio was 0.45
- For Series IV mixes, four types of superplasticizer were used with a constant dosage of silica fume (7.5%) using three different types of silica fume. The water/binder ratio was 0.5.

3.3 CURING CONDITIONS

Test specimens were exposed to the selected environmental conditions immediately after casting to investigate the effect of hot weather conditions on the shrinkage characteristics of plain and blended cement concretes.

3.4 EXPERIMENTAL PROCEDURE

The experimental procedure was based on the methodology of a previous research carried

out at this university [5]. The specimens were cast and placed in a controlled temperature and humidity chamber, as shown in schematically in Figure 3.10. The required temperature was maintained using electric heaters and wind velocity was maintained using an electric wind blower. The other important feature of the chamber was the control of the humidity using commercially available humidifier that was refurbished for the purposes of this experiment. Humidity measurements were taken using a dial gauge and an electronic gauge because the electronic gauge was more sensitive to changes of temperature. Details of the experimental setup are shown in Figures 3.6 and 3.7 and in Figures 3.10 through 3.20.

3.4.1 Preparation of Materials and Moulds

Materials preparation included the washing and sieving of aggregates, weighing the aggregates in order to give the required proportions, etc. Details are presented below.

All the materials were proportioned by weight. Trial mixes were also conducted on the various mixes to determine the optimum superplasticizer content to produce the required workability. Aggregates were initially sieved to obtain the required sizes and, thereafter, washed and dried to remove dust and fine particles.

To cast the concrete slab specimens, steel angles and plexi-glass were used to fabricate

the moulds. These moulds prohibit the absorption of moisture from the concrete mix. Therefore, uniform conditions amongst all tests were assured, thereby forcing a one-dimensional movement of mix water. Simulating the cast of a slab over a plastic barrier provided a worst-case scenario for plastic shrinkage cracking. The molds were also sufficiently rigid thus minimizing any settlement or bending stresses.

Casting was aligned under the wind blower in such a way that the whole area of the slab was covered uniformly and the direction of air movements was parallel to the surface.

3.4.2 Mixing Process

The concrete constituents were mixed in an electrically operated concrete mixer of 1.7 m^3 capacity. Mixing was done in accordance with ASTM C 192. The materials were put into the mixer in the following sequence: first the coarse aggregate was placed in the mixer, and then the sand after which the cement and silica fume were added. The silica fume was added and mixed with the cement separately before being transferred to the mixer. Some of the mixing water was added and mixing continued for 2 minutes. Thereafter, the remaining mixing water was added and mixing continued for another 2 to 3 minutes until the mix became homogeneous. The concrete was then discharged into a container and transported to the chamber where it was cast into the moulds. A straight aluminum angle was used to consolidate and level the concrete surface. The concrete surface was leveled

in one direction.

3.5 MONITORING AND DATA ANALYSIS

Data was obtained by continuous monitoring via automatic recordings at regular time intervals by the data acquisition system as well as visual observations. Details of the monitoring process are illustrated below.

3.5.1 Plastic Shrinkage Cracking

The effect of exposure conditions and mix composition on plastic shrinkage was evaluated through visual inspection by monitoring the time to cracking and the intensity of cracks. Both the length and average width of the cracks were recorded. Photographs were sometimes taken to manifest the surface conditions and plastic shrinkage cracks of the slabs.

3.5.2 Plastic Shrinkage Strain and Temperature Measurements

Temperature was measured at two locations on adjacent sides of the slabs at three points through the depth of the samples using embedded thermocouple wires. These wires were connected to a data acquisition system that automatically recorded the temperature at

regular intervals of time.

The shrinkage strain was measured using light-steel angles placed at the top surface of the concrete but anchored to a depth of 10 mm, as shown in Figure 3.7. These angles were placed at the mid-section of the four sides of the moulds. The movements of the angles were monitored using LVDTs connected to a data acquisition system for a period of 24 hours. Shrinkage displacements were recorded every 30 minutes continuously up to a period of 24 hours after casting. Controlled exposure conditions were maintained for the first 6 hours after casting. Thereafter, the specimens were returned to the ambient conditions.

3.5.3 Drying Shrinkage Strain

Drying shrinkage readings on slabs were carried out using DEMEC gauge studs that were glued to the top surface of the slabs using an epoxy resin. The specified gauge length and the initial gauge readings were recorded. Further drying shrinkage readings were taken after 3, 7, 14, 28, 56 and 90 days of exposure.

For the mortar specimens 25x 25x285mm prisms were cast with the desired mix using the various types and dosages of silica fume. After demolding, the specimens were cured in sweet water in the laboratory for 14 days. The initial length readings were determined on

removal of the specimens from water after which they were stored in the laboratory. Drying shrinkage values were determined at time intervals of 3, 7 14, 28 56 and 90 days of exposure to the ambient laboratory conditions.

3.5.4 Compressive and Split Tensile Strengths

76.2 x 52.4 mm cylindrical specimens were cast and immediately transferred to the exposure chamber, and kept under controlled conditions for 6 hours. Compressive strength values were then determined in accordance with ASTM C 39 after 6, 12 and 24 hours and 28 days. Three specimens were tested for each exposure condition and time. The split tensile strength was determined using three cylindrical specimens in accordance with ASTM C 496 after 6, 12, 24 hours and 3, 7, and 28 days.

3.5.5 Ultrasonic Pulse Velocity

The ultrasonic pulse velocity measurements were conducted using the commercially available Pundit machine. Pulse velocity was carried out on both the slab specimens and the cylinders. For the slabs the indirect method was used to measure the pulse velocity in accordance with ASTM C 597. Lines were drawn in both directions; 100 mm apart on the surface of the slab and readings were then taken at each of the intersection of these grid lines. Care was taken to avoid the plastic shrinkage cracks on those slab specimens that

exhibited cracking. Lubricating grease was applied to keep out air pockets and to provide good coupling between transducers and the concrete surface. An average of eight values was used to represent the value for each slab.

For the cylindrical specimens, the pulse velocity was measured prior to testing them for compressive strength.

3.5.6 Pore Size Distribution and Specific Surface Area

A piece of about 200 grams of cement paste was used in the determination of the pore size distribution and specific surface area of samples with a water-cement ratio of 0.34, using the nitrogen adsorption method. This water/cement ratio was chosen so that the workability of the cement paste was similar to that of the corresponding concrete. Specimens were cast and stored in the humidity chamber under similar conditions to that of the concrete slabs. Storage in the exposure chamber lasted for 6 hours under controlled conditions, followed by ambient conditions within the chamber up to a period of 24 hours. The hardened specimens were then cured in water for one day, and then transferred into the open air for 56 days. Finally, the hardened cement pastes were pulverized into powder and passed through a $150 \mu\text{m}$ (ASTM No. 100) sieve to obtain homogeneous mixtures.

Theoretical Background

Solid particles exposed to a gas under pressure will adsorb molecules of that gas onto its particle surfaces. The quantity of gas adsorbed is dependent on the applied pressure and temperature and the amount and size of pores present in the solid. This is the basis of gas adsorption of which the nitrogen adsorption method is the standard (ASTM C 1069) for amorphous (powdered) materials that are both mesoporous (solids with non-porous molecules) and microporous (solids with porous molecules) [106].

Current techniques using nitrogen adsorption are based on the Brunauer-Emmett-Teller (BET) multi-layer adsorption theory that developed standard models for the determination of the surface area of various solids for use in industry. These standard models are referred to as adsorption isotherms [107]. This method employs a special apparatus called the BET machine that uses nitrogen gas at a constant temperature of 77°K (-196.3 °C).

An adsorption isotherm is the quantitative relationship at a constant temperature between the amount of gas adsorbed, n , by unit mass of solid (the adsorbent) and the equilibrium pressure, p , or relative pressure, $p-p^0$, of the gas (the adsorptive). The material in the adsorbed state is known as the adsorbate. Physical adsorption (referred to as physisorption, adsorption without any chemical reactions) isotherms are usually

displayed in graphical forms, as typically shown in Figure 3.9 [107].

The pore size distribution and specific surface area of the solid material is determined according to ASTM C 1069 [108] as follows:

- (i) The Samples are pre-treated (heated under a vacuum) at 90°C for one hour then at 350°C for another two hours to achieve the necessary cleanliness and dryness from water, and other substances on the surface of the material (also called degassing).
- (ii) The process of nitrogen adsorption then follows where adsorption isotherms are obtained for the material. In practice, the full isotherm of Figure 3.9 is obtained using single-point (a single point on the sample) or multi-point values (more than one point on the sample), depending on what is desired and the capabilities of the machine.
- (iii) The adsorption isotherms obtained are then compared with standard adsorption isotherms known as the BDDT classification, parts of which are shown in Figure 3.9.
- (iv) The pore size distribution and specific surface areas are then calculated (all steps are done automatically by the Quantachrome Nova-1200 BET Surface Area Analyzer machine).

Table 3.1: Grading of coarse aggregates used in all mixes.

Sieve Opening (mm)	Percent Passing	ASTM C 33 Limits
12.5	100	100
9.5	100	85 - 100
4.75	60	10 - 30
2.4	20	0 - 10
1.2	5	0 - 5

Table 3.2: Chemical analysis of Type I Portland cement used in all mixes.

Property	Weight (%)
SiO ₂	20.96
Fe ₂ O ₃	3.56
Al ₂ O ₃	5.25
CaO	63.67
MgO	1.35
SO ₃	2.58
K ₂ O	--
Na ₂ O	--
LOI	1.67
C ₃ S	50.0
C ₂ S	22.0
C ₃ A	8.0
C ₄ AF	10.5

Table 3.3: Sources of silica fume and fly ash selected for evaluation in this study.

Type of silica fume/fly ash	Brand name of silica fume/fly ash	Source	Salient properties
Type I	Pechiney	Ludun, France	Densified silica fume
Type II	EFACO	Egypt	Undensified silica fume
Type III	Elkem	Norway	Densified silica fume
Type IV	Binasilica	SABAYEC, Jubail	Densified silica fume
Type V	BISLEY	South Africa	Densified silica fume
Fly ash	Lethabo fly ash	South Africa	ASTM C 618 Class F fly ash
Superpozz®	Superpozz®	South Africa	Highly pulverized alumino-silicate fly ash

Table 3.4: Properties of Pechiney® (Ludun, France) silica fume.

Property	Test results	ASTM C 1240 requirements
Moisture content, %	1.19	3.0 max.
Loss on ignition, %	2.21	6.0 max.
SiO ₂ , %	91.5	85 min.
Fe ₂ O ₃ , %	1.76	--
Al ₂ O ₃ , %	0.56	--
CaO, %	0.76	--
MgO, %	1.30	--
Na ₂ O, %	0.43	--
K ₂ O, %	0.78	--
SO ₃ , %	0.55	--
Material retained on # 325 sieve, %	1.54	10 max.
Accelerated pozzolanic activity index, % (7 days)	91.0	85% (7 days)
Shrinkage (Type I cement after 28 days), %	0.069	--
Shrinkage (Type I + silica fume cement after 28 days), %	0.084	--
Increase over control, %	0.015	0.1 max.
Sulfate-resistance expansion (6 months), %	0.028	0.05 max. (High resistance)

Table 3.5: Properties of EFACO® (Egypt) silica fume.

Property	Test results	ASTM C 1240 requirements
Moisture content, %	1.35	3.0 max.
Loss on ignition, %	1.62	6.0 max.
SiO ₂ , %	98.0	85 min.
Fe ₂ O ₃ , %	2.73	--
Al ₂ O ₃ , %	0.70	--
CaO, %	0.12	--
MgO, %	0.67	--
Na ₂ O, %	0.39	--
K ₂ O, %	0.90	--
Material retained on # 325 sieve, %	2.01	10 max.
Specific surface area, m ² /g	16.7	15 min.
Accelerated pozzolanic activity index, % (7 days)	98	85% (7 days)
Shrinkage (Type I cement after 28 days), %	0.069	--
Shrinkage (Type I + silica fume cement after 28 days), %	0.099	--
Increase over control, %	0.030	0.1 max.
Sulfate-resistance expansion (6 months), %	0.048	0.05 max. (High resistance)

Table 3.6: Properties of ELKEM® (Norway) silica fume.

Property	Test results	ASTM C 1240 requirements
Loss on ignition, %	1.61	6.0 max.
SiO ₂ , %	91.9	85 min.
Fe ₂ O ₃ , %	1.85	--
Al ₂ O ₃ , %	0.73	--
CaO, %	0.43	--
MgO, %	0.89	--
Na ₂ O, %	0.33	--
K ₂ O, %	1.23	--
SO ₃ , %	0.26	--
Material retained on # 325 sieve, %	1.38	10 max.
Specific surface area, m ² /g	27.7	15 min.
Accelerated pozzolanic activity index, % (7 days)	88	85% (7 days)
Shrinkage (Type I cement after 28 days), %	0.069	--
Shrinkage (Type I + silica fume cement after 28 days), %	0.071	--
Increase over control, %	0.002	0.1 max.
Sulfate-resistance expansion (6 months), %	0.025	0.05 max. (High resistance)

Table 3.7: Properties of BINASILICA® (SABAYEC, Jubail) silica fume.

Property	Value	ASTM C 1240 requirements
Moisture content, %	0.98	3.0 max.
Loss on ignition, %	5.14	6.0 max.
SiO ₂ , %	93.7	85 min.
Fe ₂ O ₃ , %	0.12	--
Al ₂ O ₃ , %	0.16	--
CaO, %	0.65	--
MgO, %	0.39	--
Na ₂ O, %	0.20	--
K ₂ O, %	0.20	--
SO ₃ , %	0.23	--
Cl, %	0.07	--
Material retained on # 325 sieve, %	3.25	10 max.
Specific surface area, m ² /g	20.3	15 min.
Accelerated pozzolanic activity index, % (7 days)	87	85% (7 days)
Shrinkage (Type I cement after 28 days), %	0.069	--
Shrinkage (Type I + silica fume cement after 28 days), %	0.070	--
Increase over control, %	0.001	0.1 max.
Sulfate-resistance expansion (6 months), %	0.024	0.05 max. (High resistance)

Table 3.8: Properties of BISLEY® (South Africa) silica fume.

Property	Value	ASTM C 1240 requirements
Moisture content, %	0.95	3.0 max.
Loss on ignition, %	1.76	6.0 max.
SiO ₂ , %	89.4	85 min.
Fe ₂ O ₃ , %	2.90	--
Al ₂ O ₃ , %	1.20	--
CaO, %	1.20	--
MgO, %	0.07	--
Na ₂ O, %	0.12	--
K ₂ O, %	0.034	--
SO ₃ , %	0.30	--
Material retained on # 325 sieve, %	0.50	10 max.
Specific surface area, m ² /g	18.06	15 min.
Accelerated pozzolanic activity index, % (7 days)	86	85% (7 days)
Shrinkage (Type I cement after 28 days), %	0.069	--
Shrinkage (Type I + silica fume cement after 28 days), %	0.071	--
Increase over control, %	0.002	0.1 max.
Sulfate-resistance expansion (6 months), %	0.045	0.05 max. (High resistance)

Table 3.9: Properties of Lethabo® fly ash from South Africa.

Property	Value
Moisture content, %	< 0.1
Loss on ignition, %	0.8
SiO ₂ , %	52.8
Fe ₂ O ₃ , %	3.5
Al ₂ O ₃ , %	34.3
CaO, %	4.4
MgO, %	1.1
Na ₂ O, %	0.4
K ₂ O, %	0.5
P ₂ O ₅ , %	0.3
SO ₃ , %	0.1
Material retained on # 325 sieve, %	9.5
Water requirement, % of control	90
Reactivity, MPa	10.0

Table 3.10: Properties of Superpozz® from South Africa.

Property	Value
Moisture content, %	<0.2
Loss on ignition, %	0.4
SiO ₂ , %	53.5
Fe ₂ O ₃ , %	3.6
Al ₂ O ₃ , %	34.3
CaO, %	4.4
MgO, %	1.0
Relative density	2.25
Theoretical surface area (m ² /kg)	1,300
pH, in water	11-12
Color	Light gray
Particle shape	Spherical
Top cut (90% passing)	11 µm
Top cut (99% passing)	25 µm

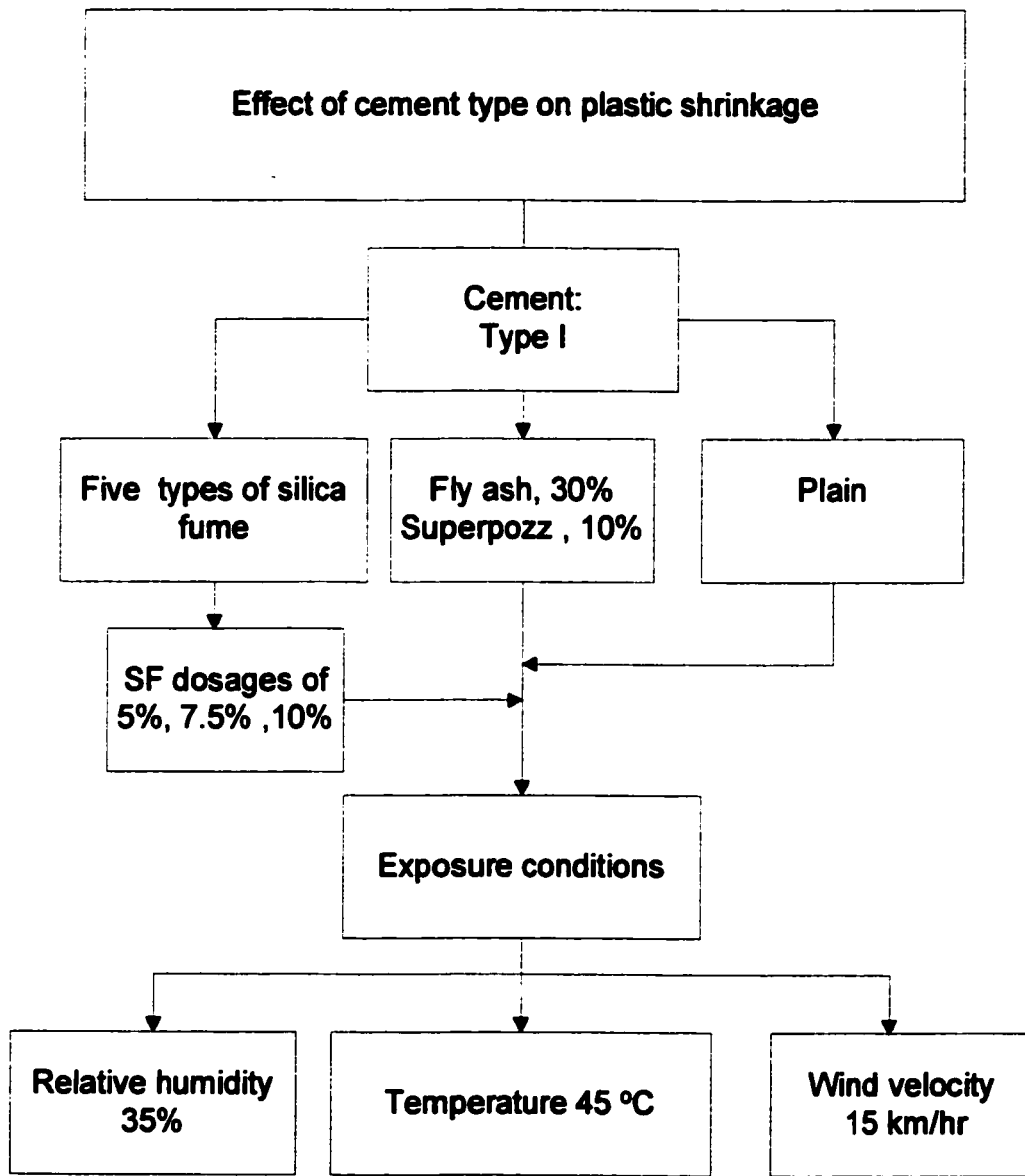


Figure 3.1: Effect of cement type on plastic shrinkage strain and cracking.

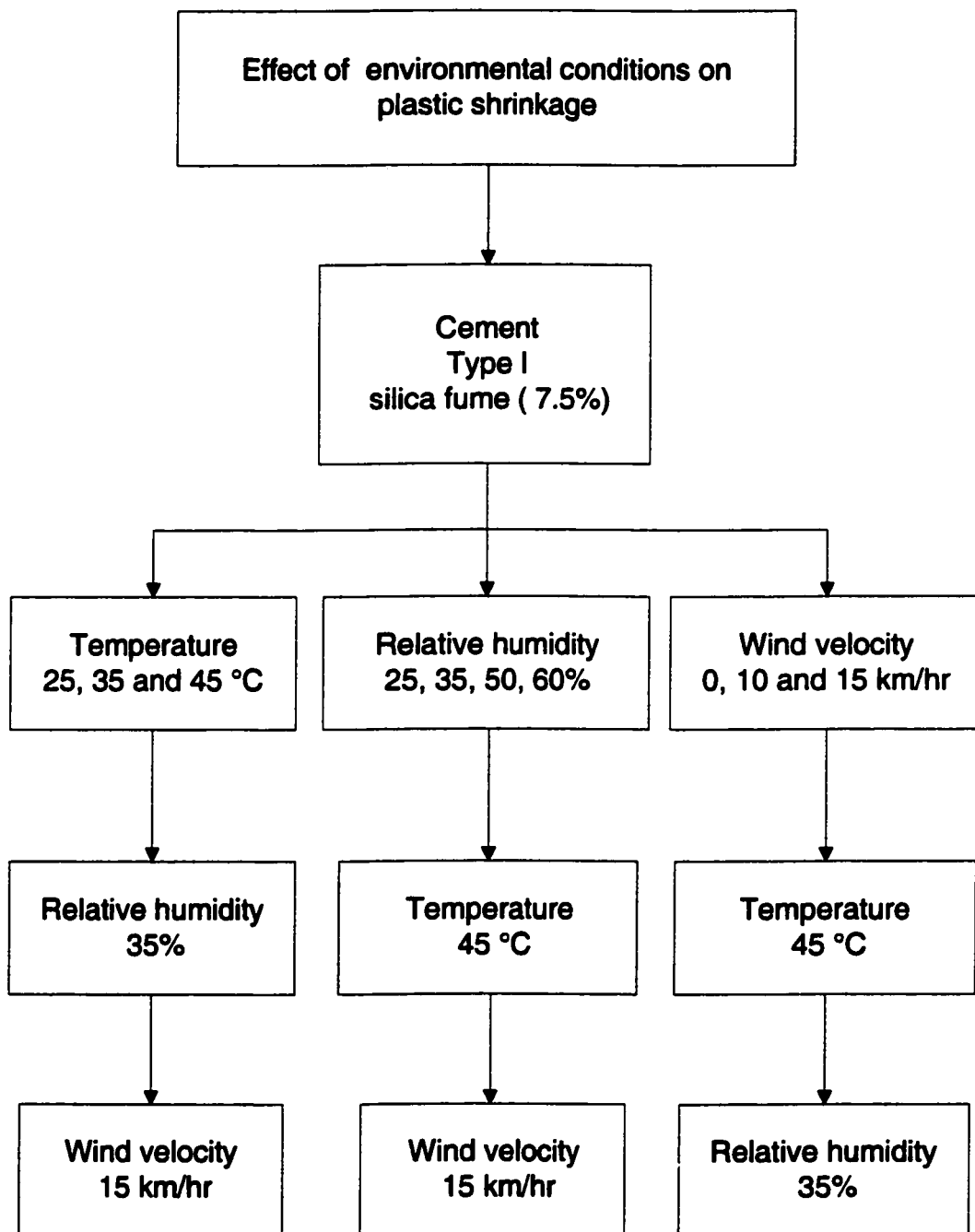


Figure 3.2: Effect of environmental conditions on plastic shrinkage strain and cracking.

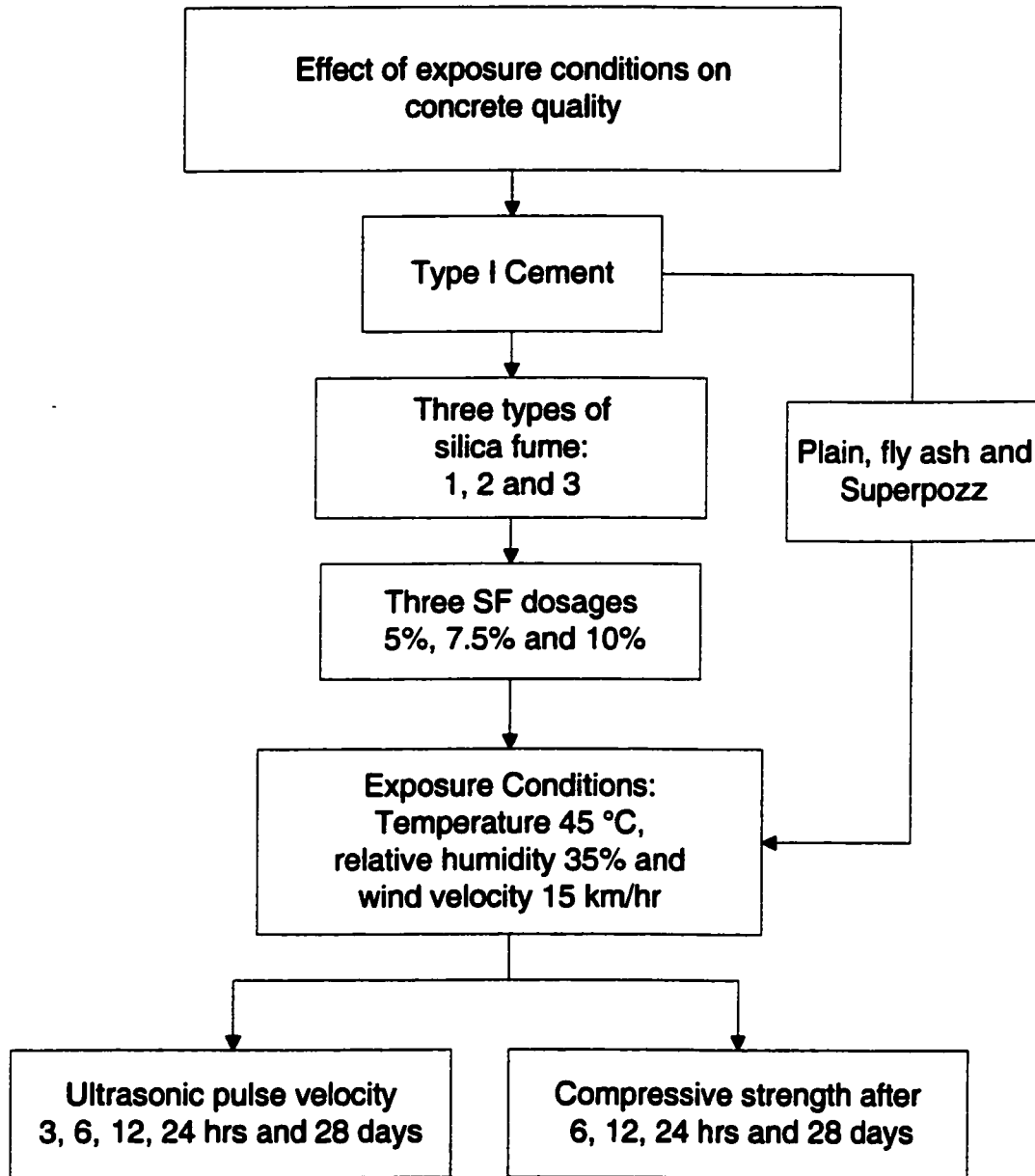


Figure 3.3: Effect of exposure conditions on concrete quality.

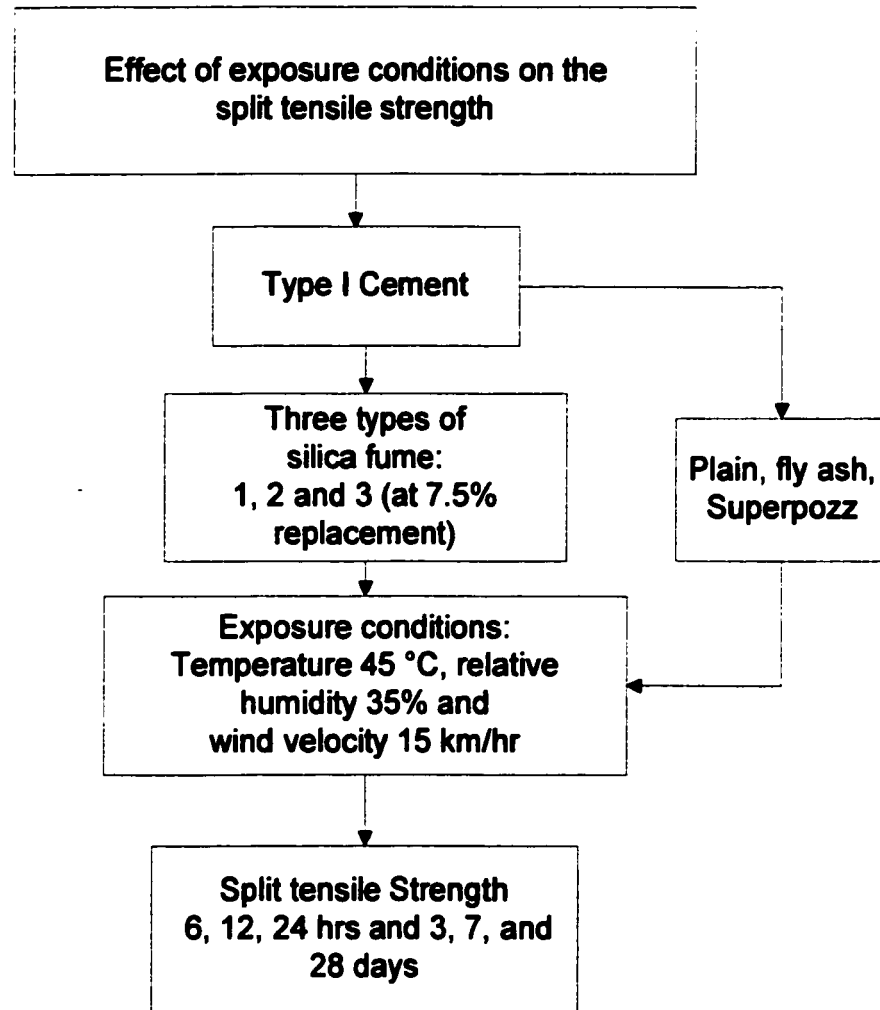


Figure 3.4: Effect of exposure conditions on split tensile strength.

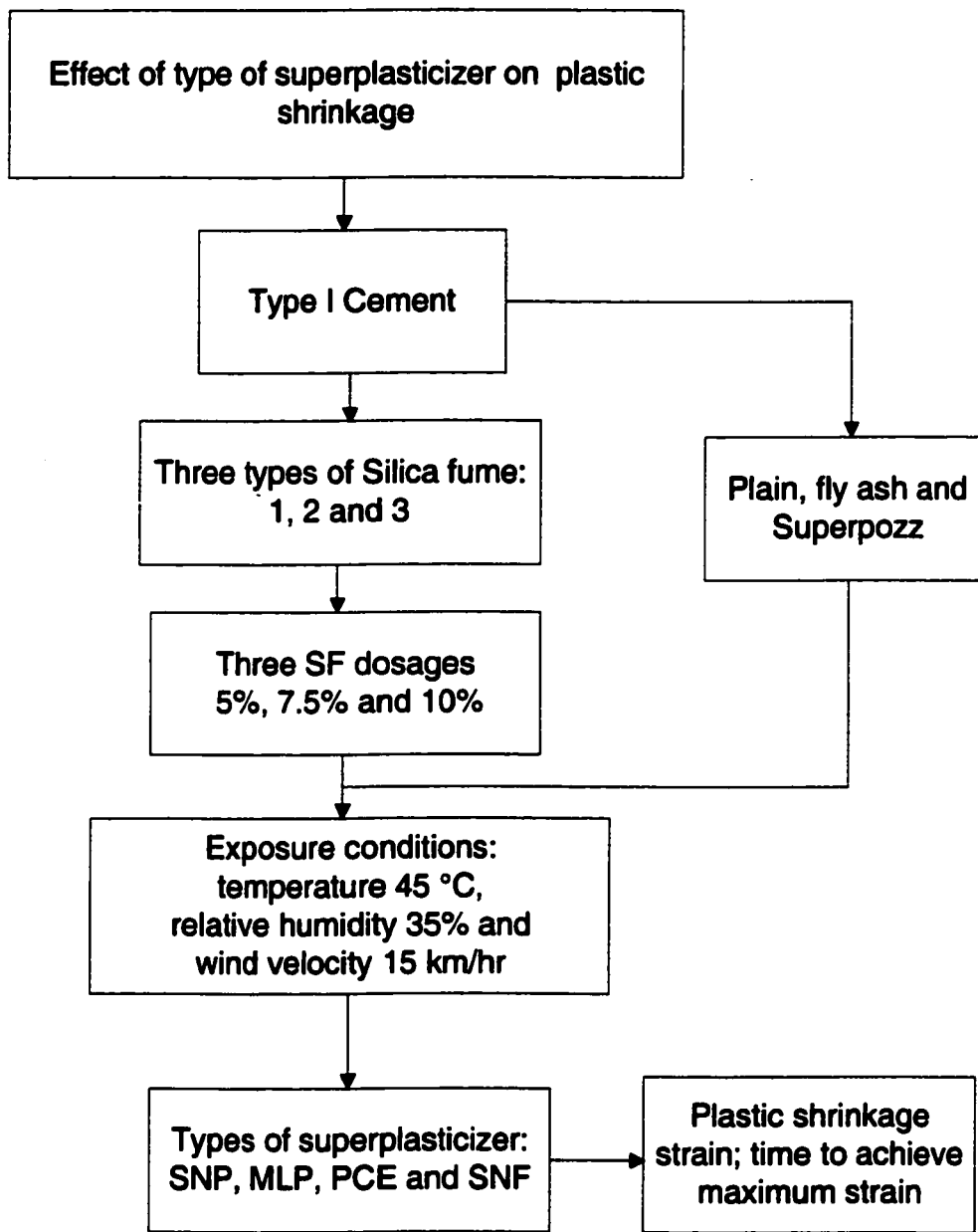


Figure 3.5: Effect of superplasticizer on plastic shrinkage strain.

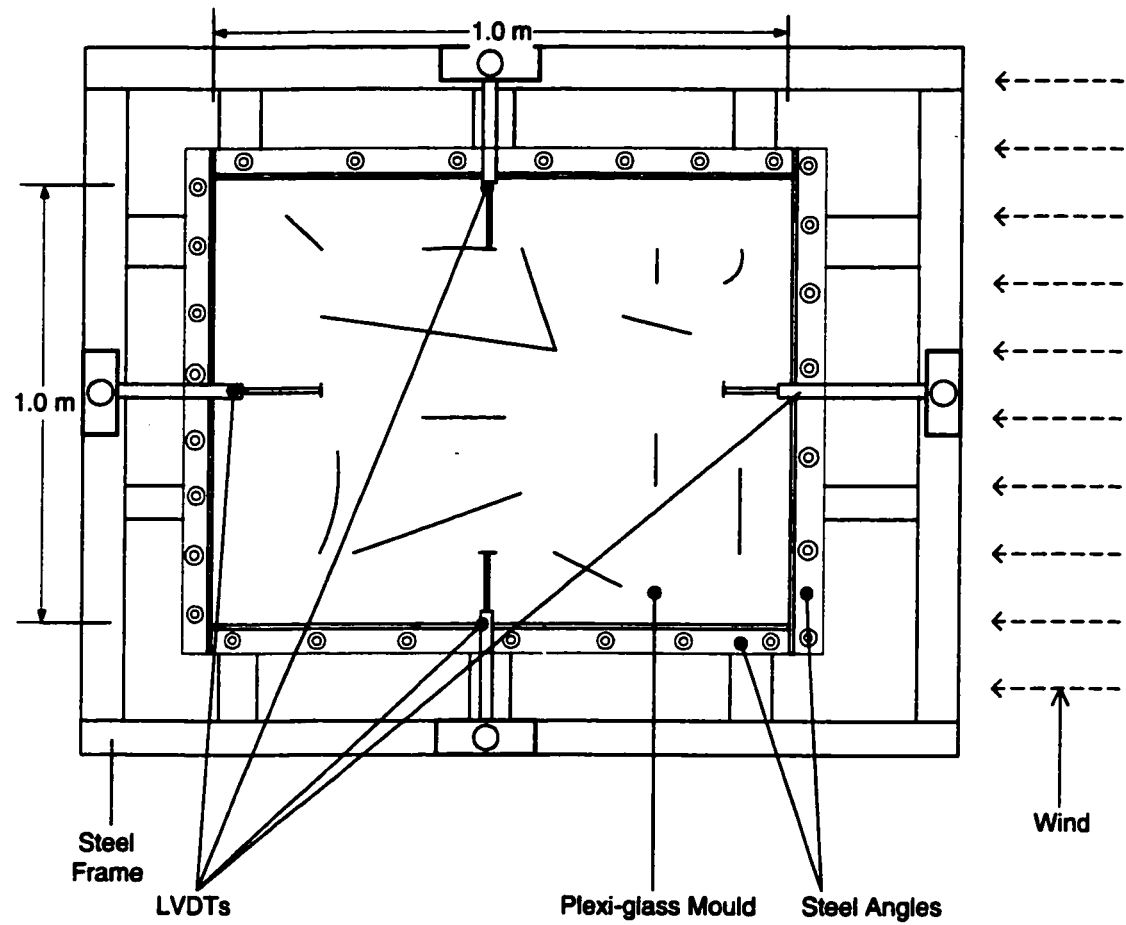


Figure 3.6: Plan view of setup.

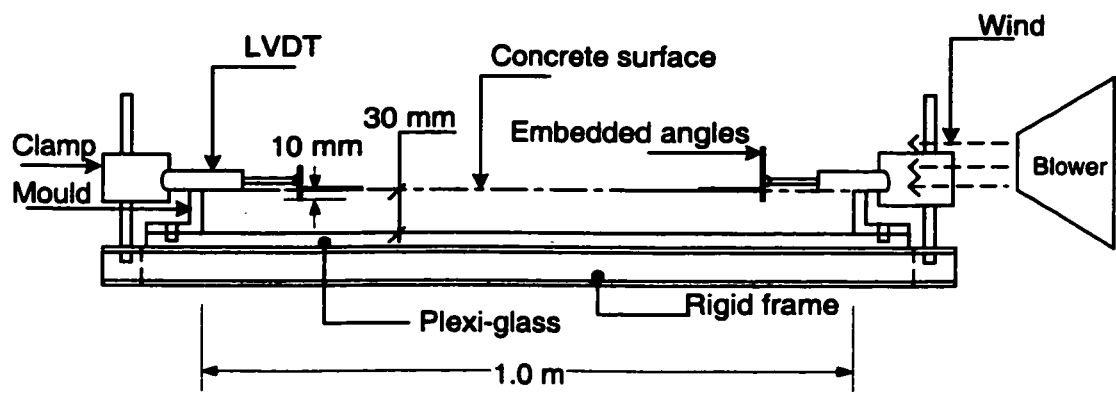


Figure 3.7: Elevation view of setup.

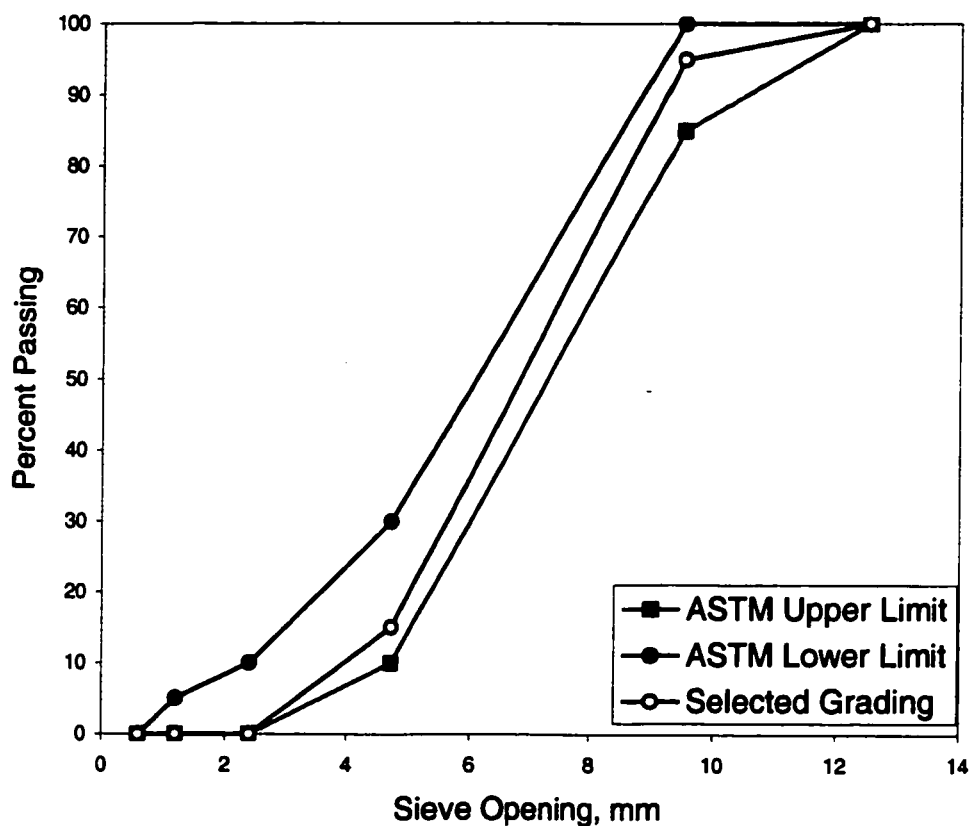


Figure 3.8: Grading of coarse aggregates used in all mixes.

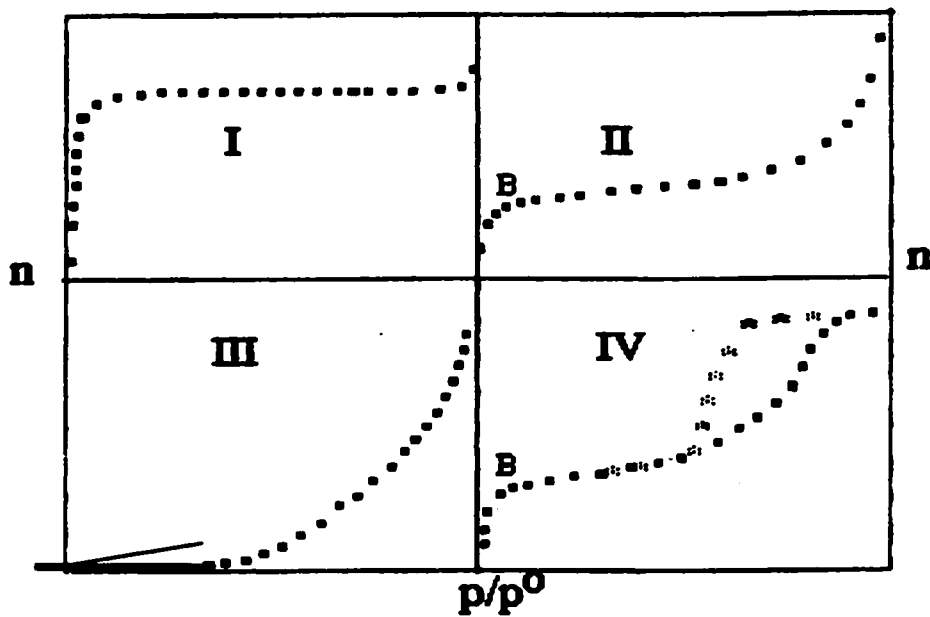


Figure 3.9: Types of physosorption isotherms used in the BDDT classification [107].



Figure 3.10: Photographic documentation of the exposure chamber.

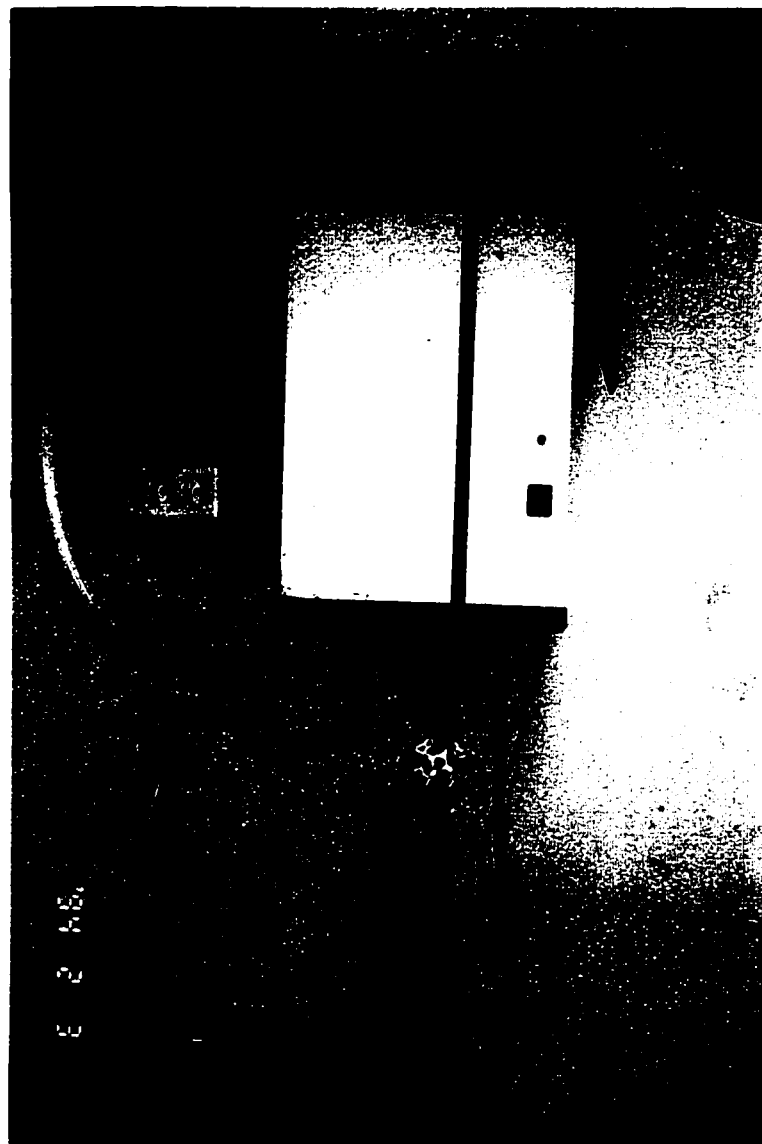


Figure 3.11: Photographic documentation of the humidifier.

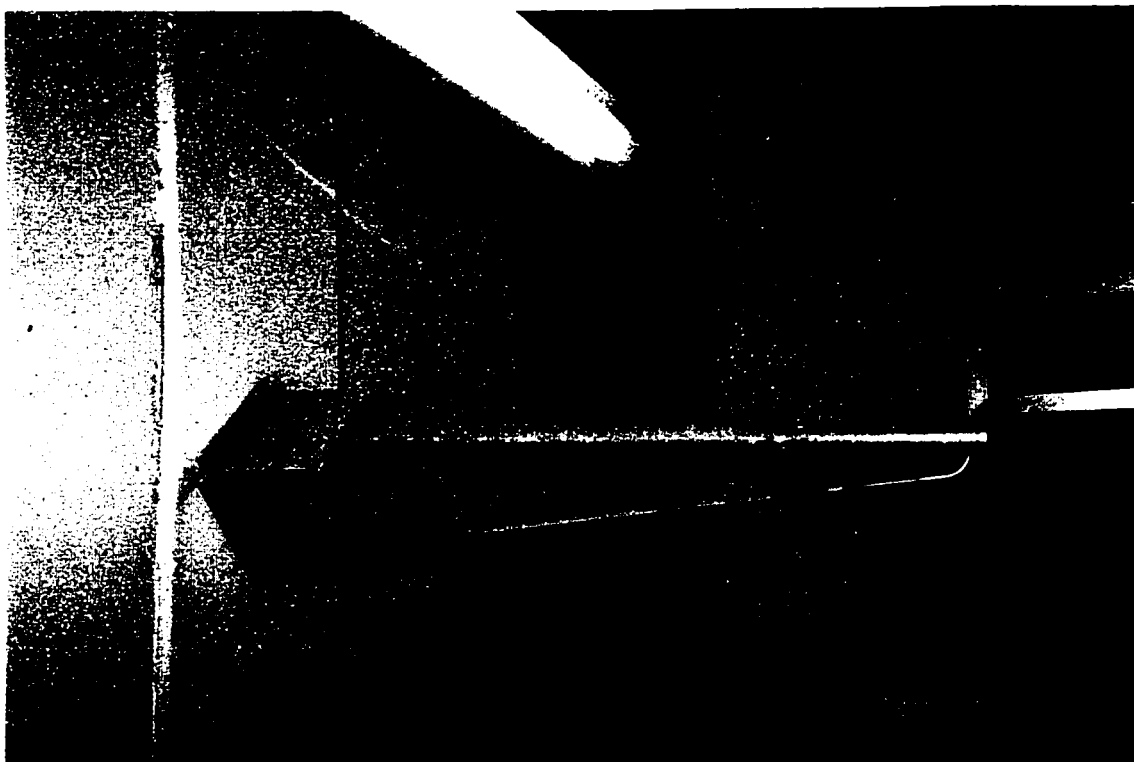


Figure 3.12: Humidifier outlet.

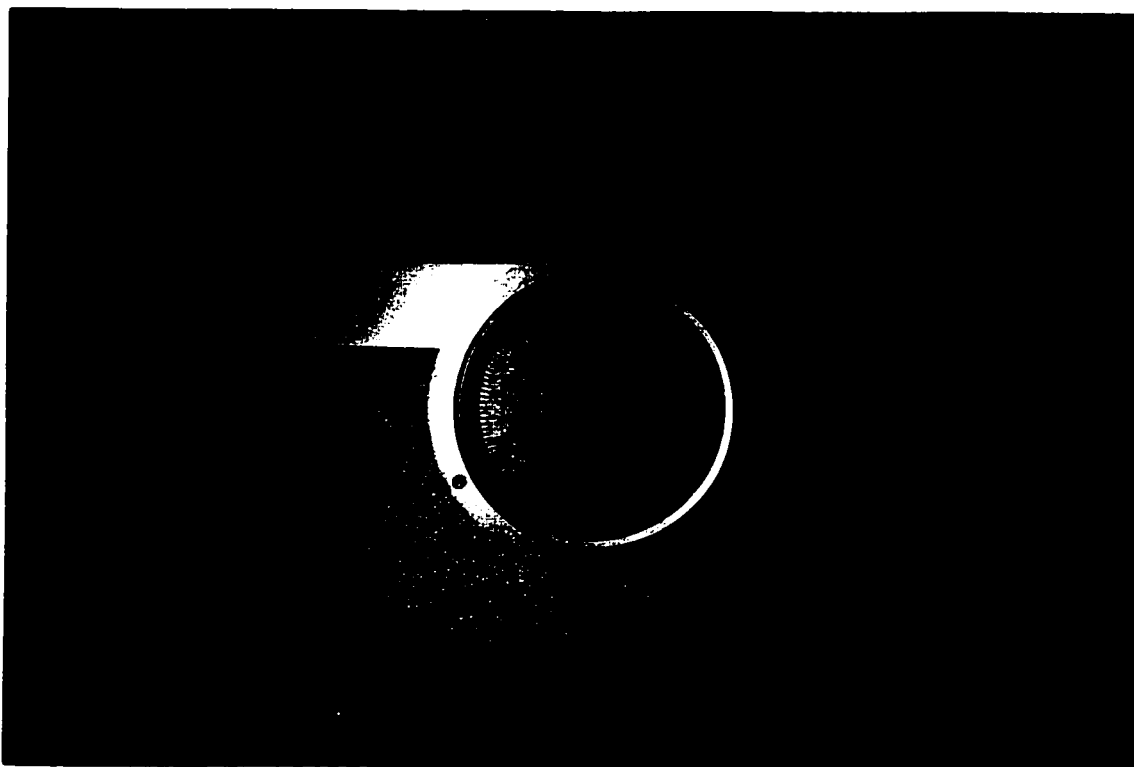


Figure 3.13: Mechanical humidity gauge.



Figure 3.14: Electronic humidity gauge.

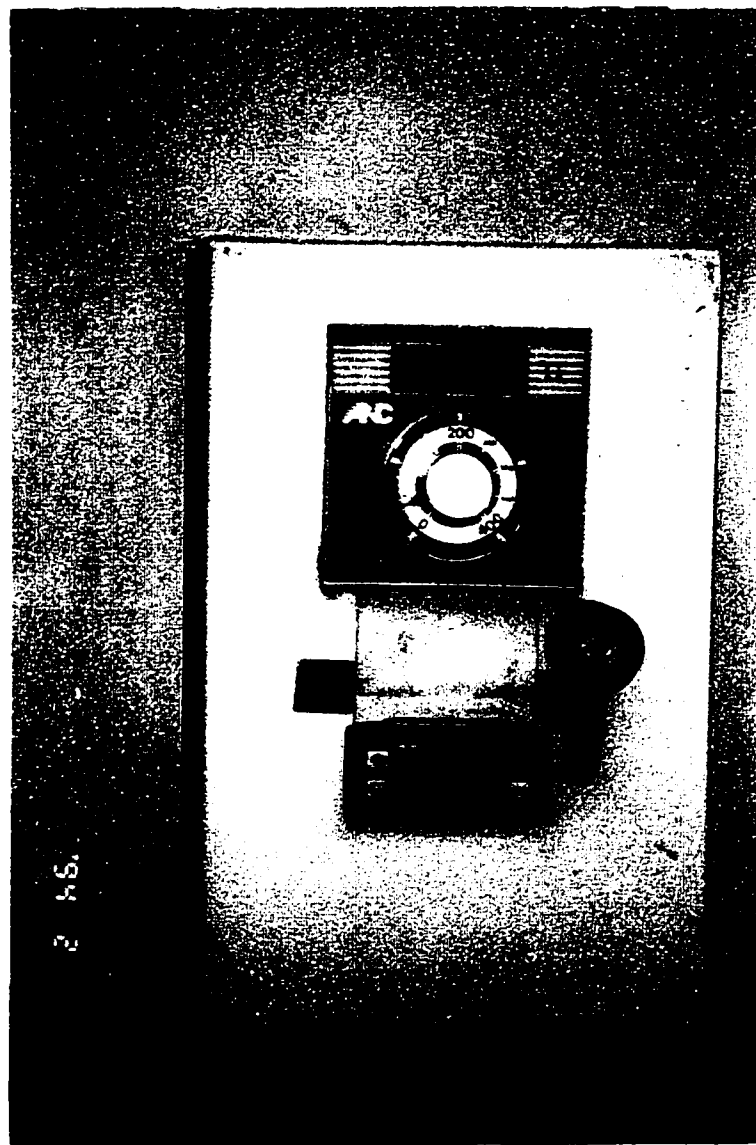


Figure 3.15: Temperature and relative humidity controllers.



Figure 3.16: Experimental setup showing the LVDTs, thermocouple wires and wind blower.

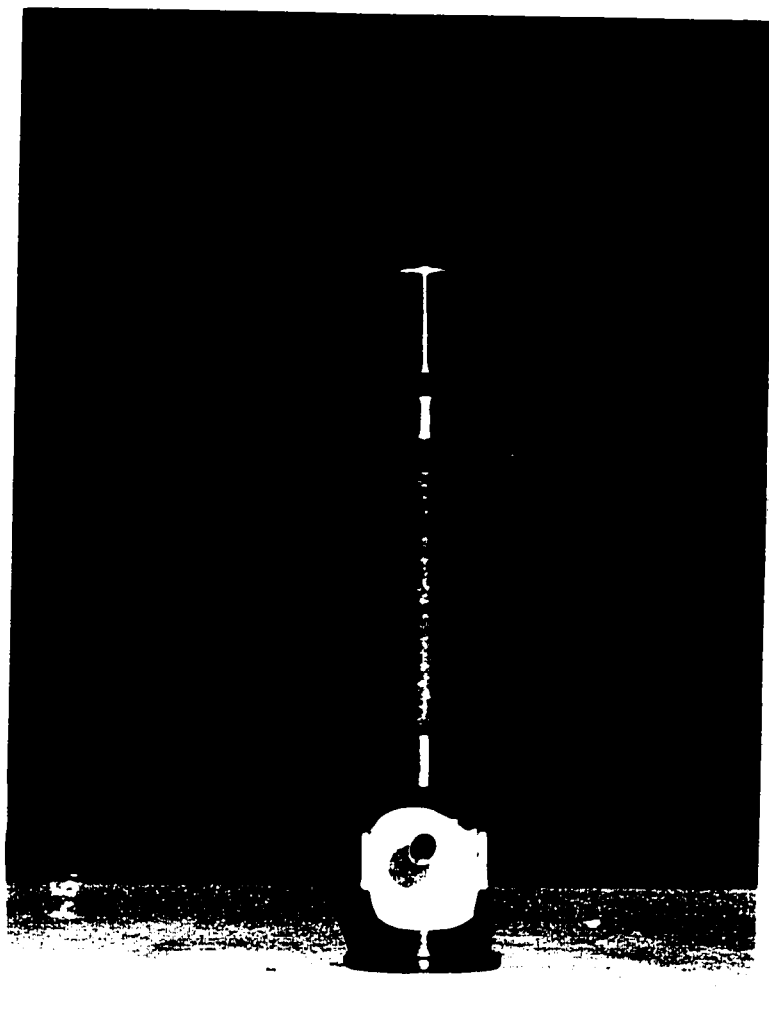


Figure 3.17: Crack microscope

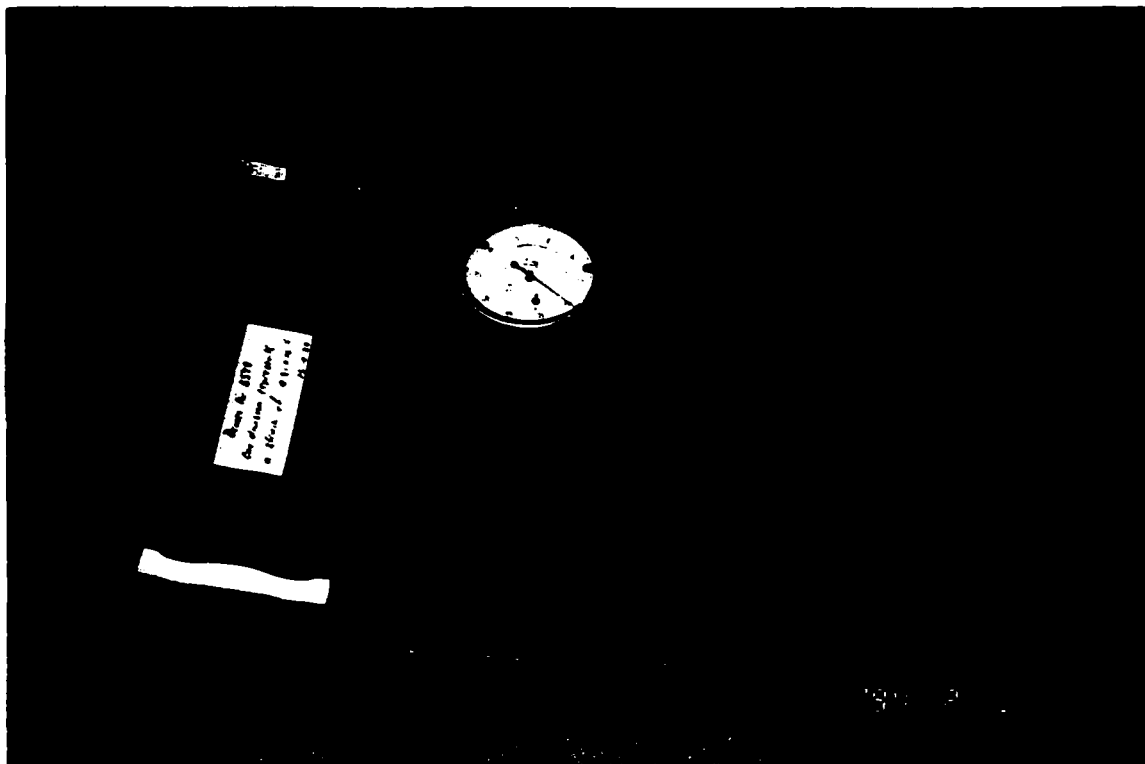


Figure 3.18: DEMEC gauge and gauge stud bar.

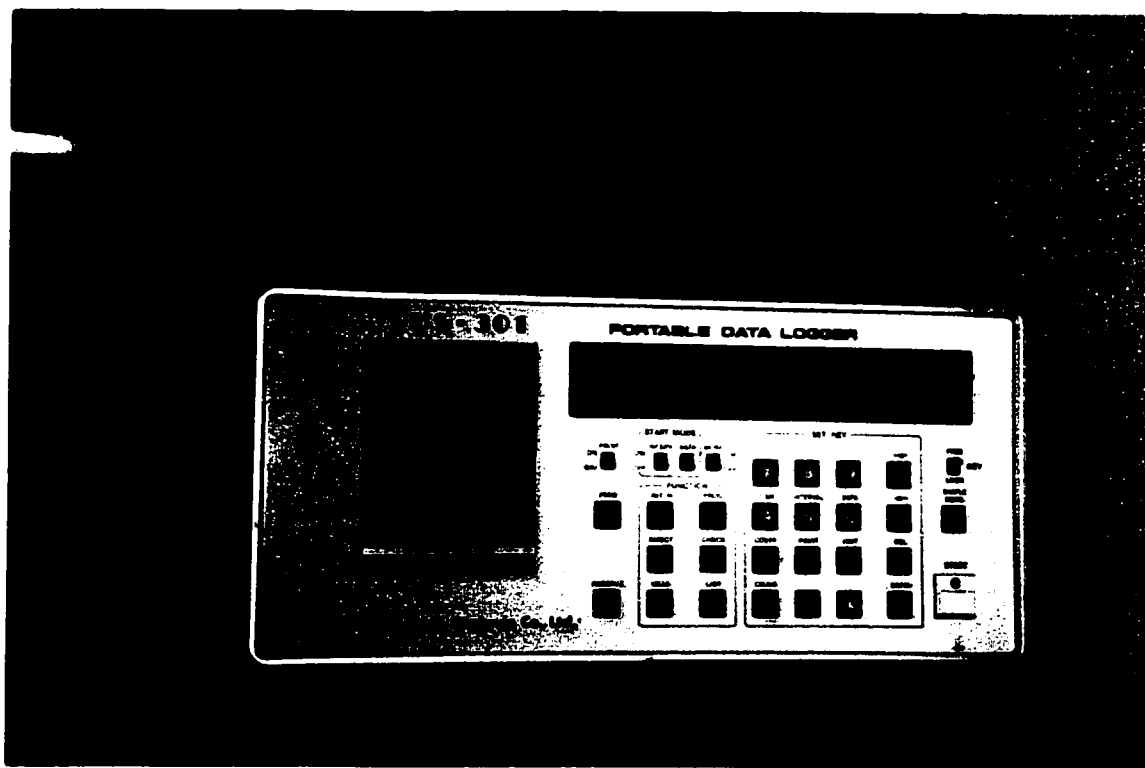


Figure 3.19: Data logger.

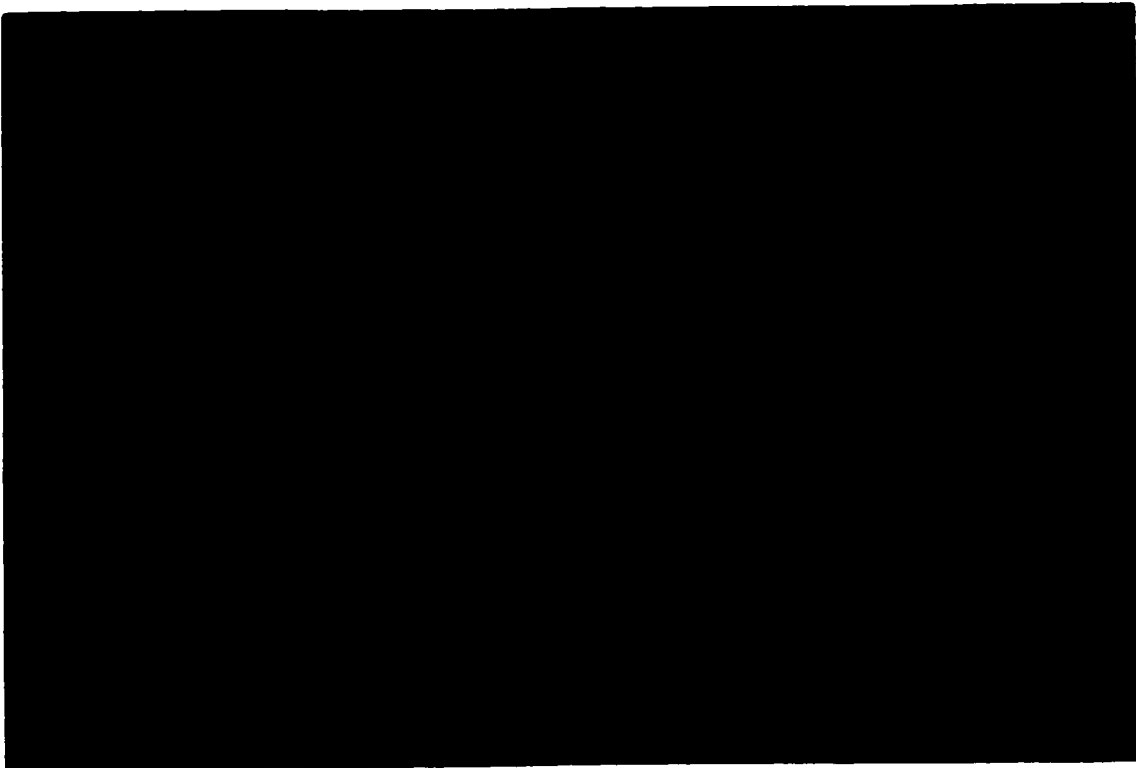


Figure 3.20: Slab surface showing drying shrinkage studs and a nearby crack.

CHAPTER 4

RESULTS AND DISCUSSIONS

The test procedures for all the four series were mentioned in Chapter 3. To simplify the discussion, the results are divided primarily into plastic shrinkage strain, drying shrinkage strain, and tensile and compressive strengths. The results are presented in the following sections.

4.1 PLASTIC SHRINKAGE STRAIN

Plastic shrinkage strain values are presented showing their variation over time from the time of casting up to a period of 24 hours, for the various types and dosages of silica fume.

4.1.1 Effect of Cement Type on Plastic Shrinkage Strain

Figure 4.1 shows the variation of plastic shrinkage strain over a period of 24 hours for Type 1 silica fume cement concrete specimens at various dosages of silica fume. The plastic shrinkage strain increased from the time of placement and then stabilized at a constant value after about 6 hours of exposure to a temperature of 45°C, RH of 35% and wind velocity of 15 km/hr. The plastic shrinkage strain in the silica fume cement concretes was more than that in the plain cement concrete, the strain increasing with the dosage of silica fume. The trend of the data in Figure 4.1 agreed well with that previously reported by other researchers [5,47]. They also indicated that the shrinkage strains in the silica fume cement concrete specimens were more than that in the plain cement concrete at all exposure durations. Figures 4.2 through 4.5 show the variation of plastic shrinkage strains with time for Type 2, Type 3, Type 4 and Type 5 silica fume cement concretes. The plastic shrinkage strains in these types of silica fume cement concretes also exhibited a trend similar to that of Type 1 silica fume cement concrete.

The variation of plastic shrinkage strain in the fly ash, Superpozz® and plain cement concretes is shown in Figure 4.6. The plastic shrinkage strain in the fly ash and Superpozz® cement concretes was more than that in the plain cement concrete. The plastic shrinkage strain in the fly ash cement concrete being more than that in the Superpozz® cement concrete. Moreover, the plastic shrinkage strains in the cement

concrete specimens prepared with both fly ash and Superpozz® were lower than those in all the five types of silica fume at the three dosages, as summarized in Table 4.1.

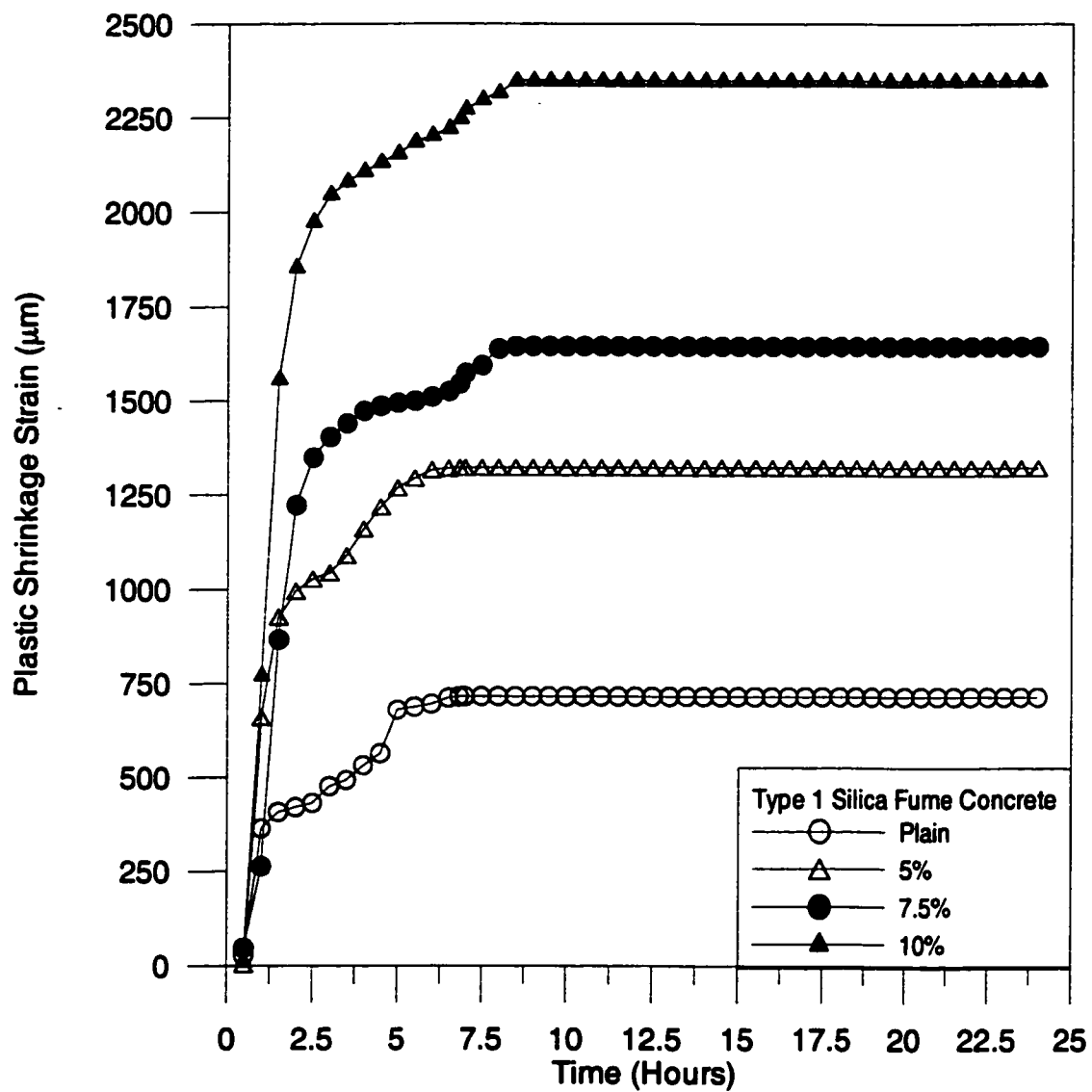


Figure 4.1: Plastic shrinkage strain in Type 1 silica fume cement concrete exposed to a temperature of 45°C, RH of 35% and wind velocity of 15 km/hr.

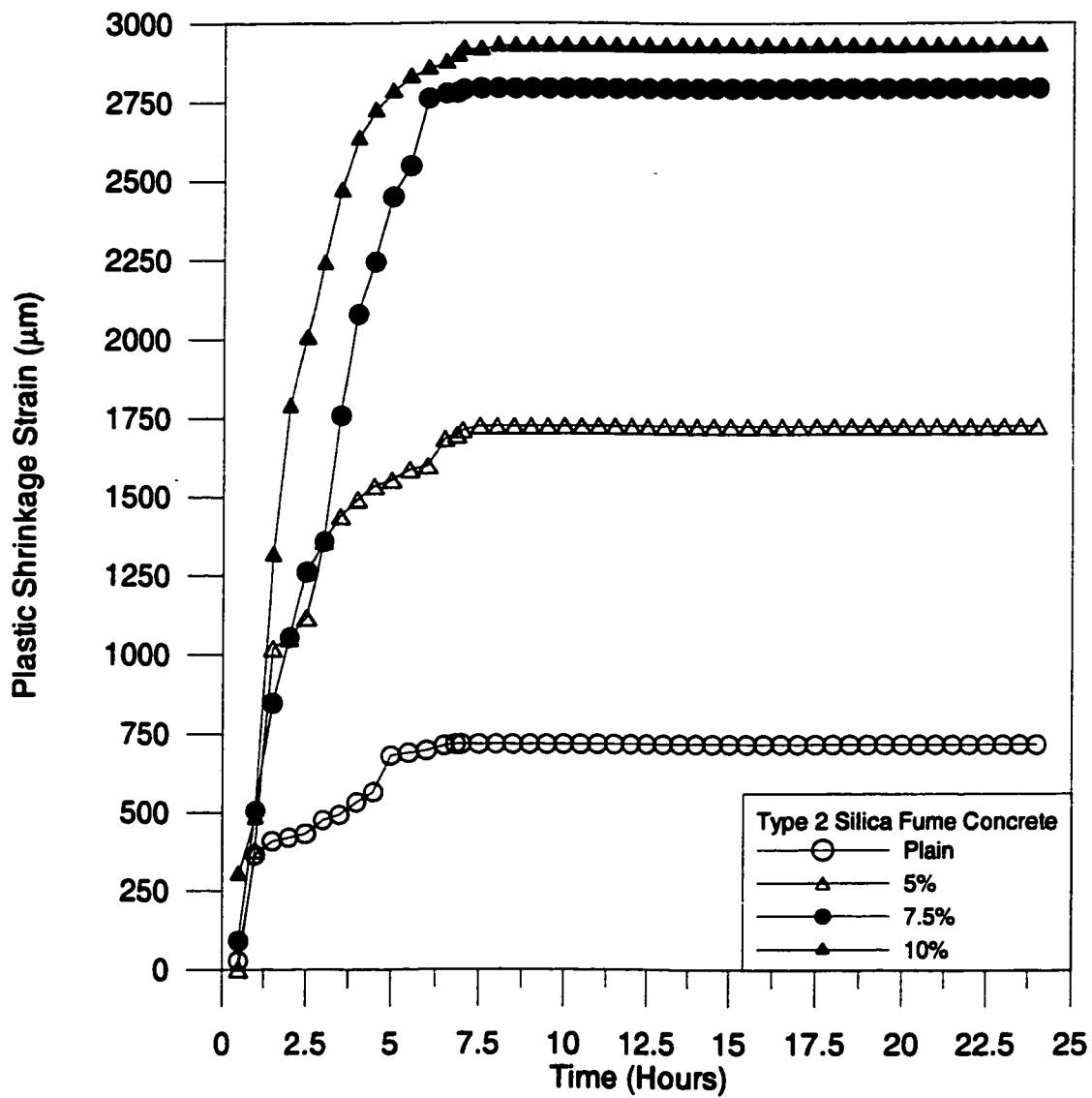


Figure 4.2: Plastic shrinkage strain in Type 2 silica fume cement concrete exposed to a temperature of 45°C, RH of 35% and wind velocity of 15 km/hr.

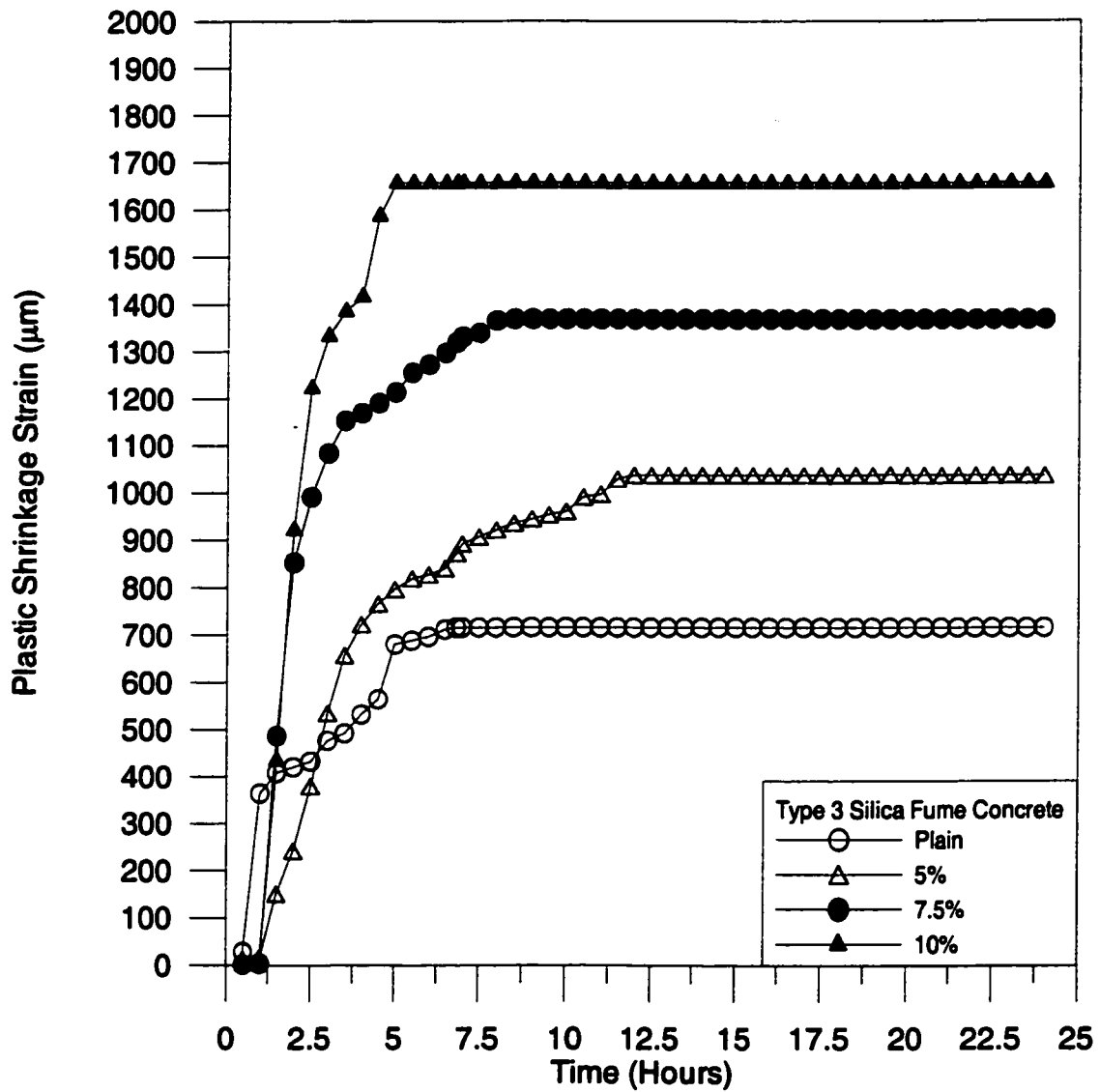


Figure 4.3: Plastic shrinkage strain in Type 3 silica fume cement concrete exposed to a temperature of 45°C, RH of 35% and wind velocity of 15 km/hr.

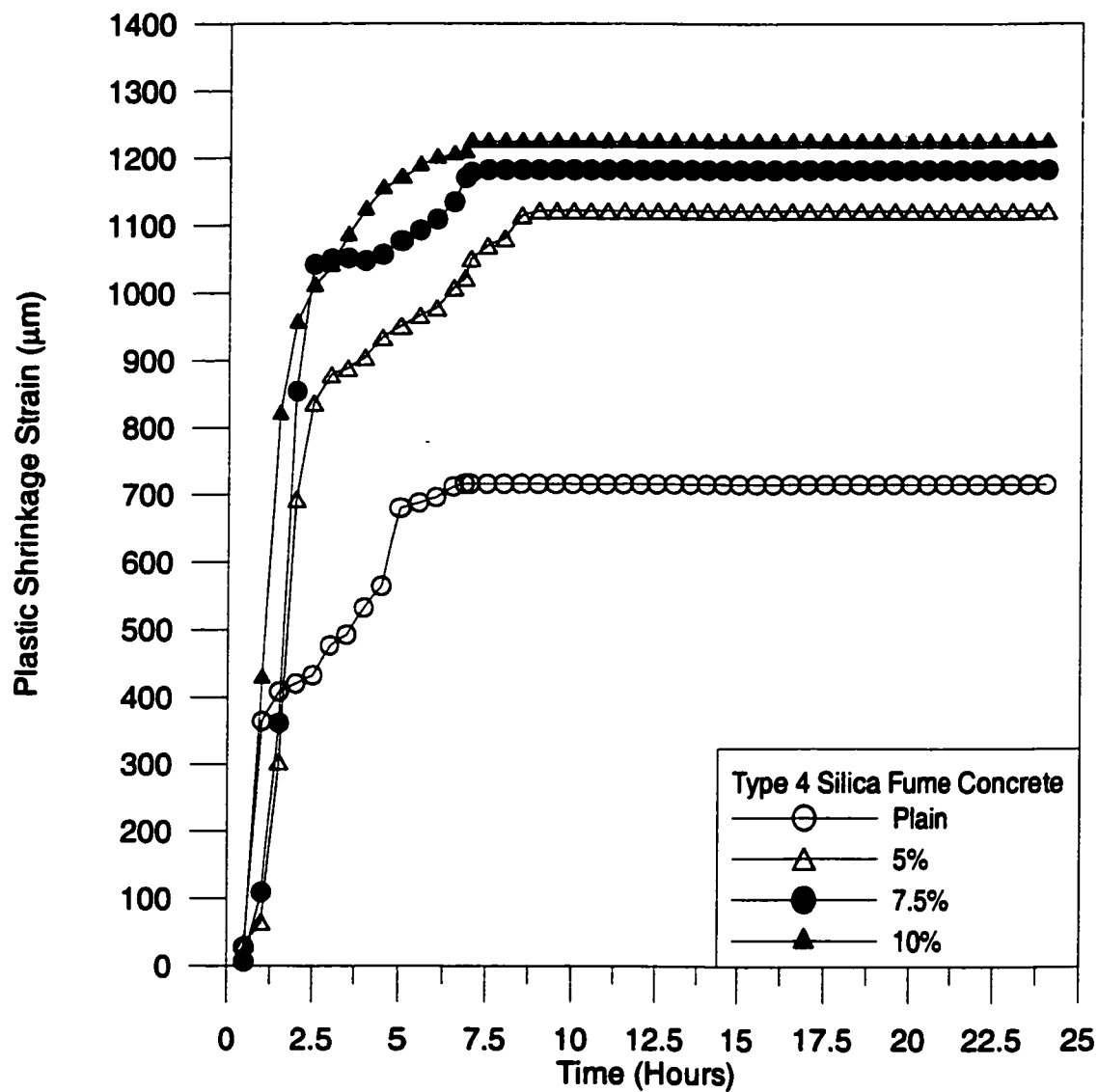


Figure 4.4: Plastic shrinkage strain in Type 4 silica fume cement concrete exposed to a temperature of 45°C, RH of 35% and wind velocity of 15 km/hr.

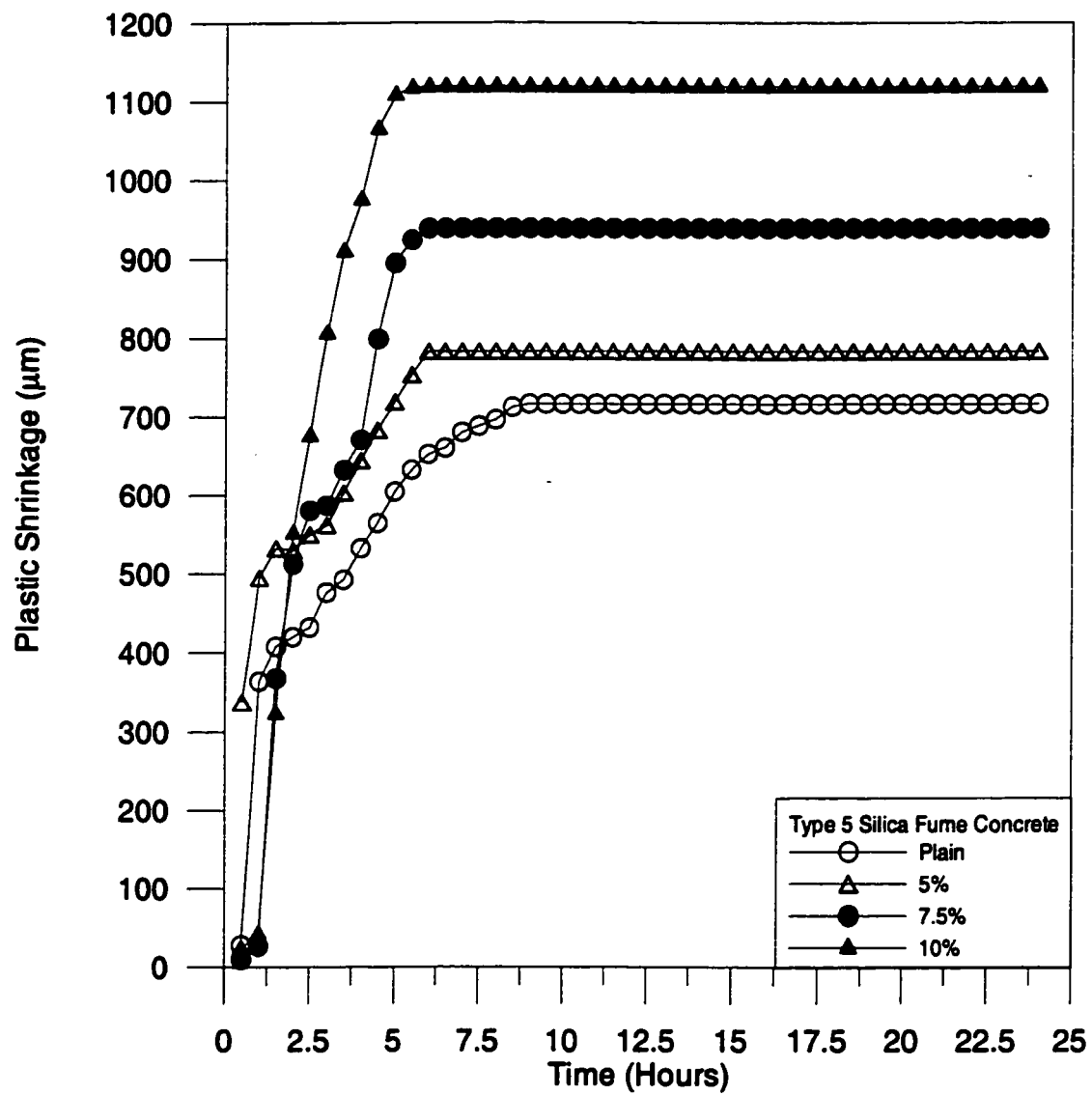


Figure 4.5: Plastic shrinkage strain in Type 5 silica fume cement concrete exposed to a temperature of 45°C, RH of 35% and wind velocity of 15 km/hr.

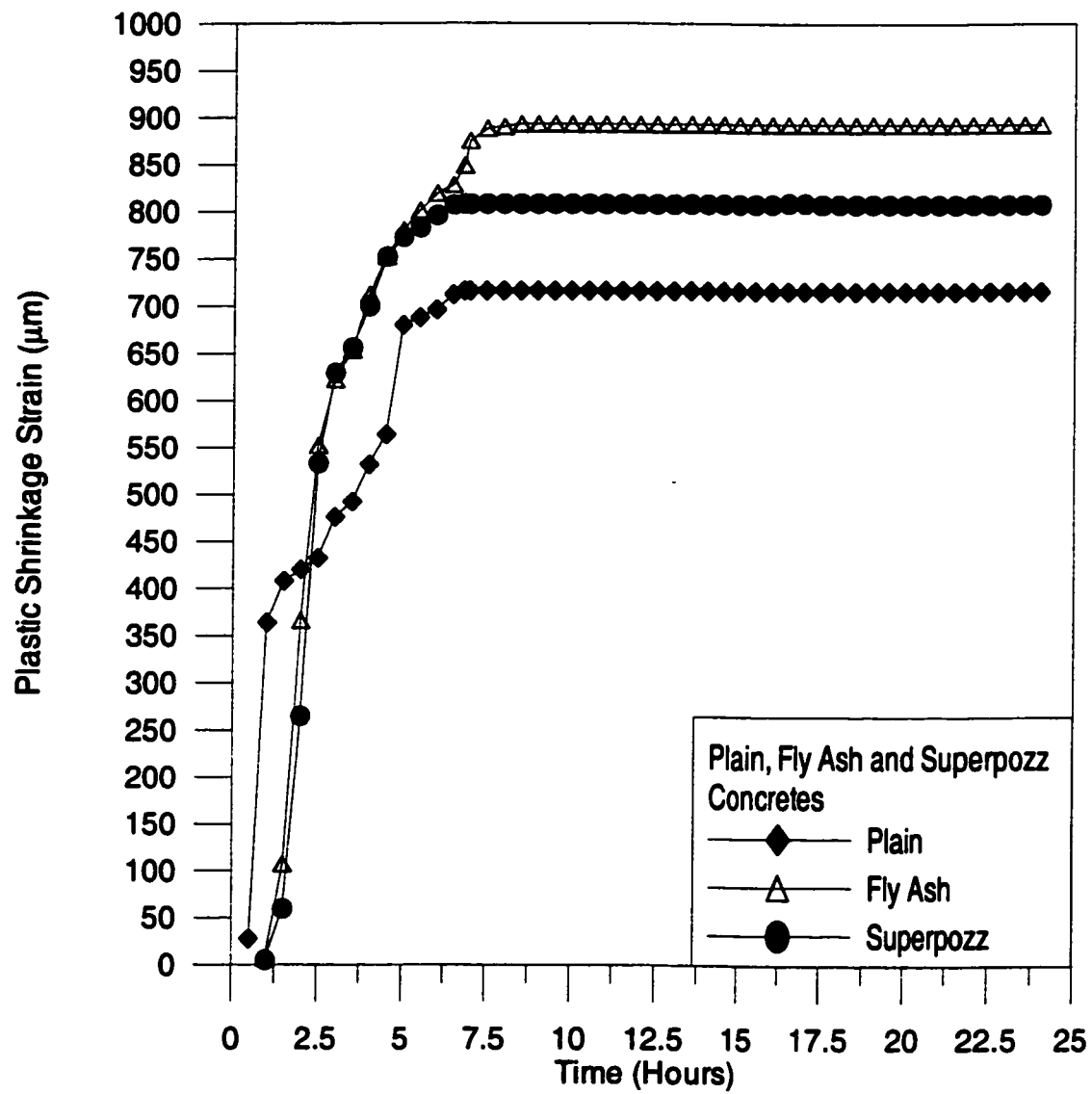


Figure 4.6: Plastic shrinkage strains in plain, fly-ash and Superpozz® cement concretes, exposed to a temperature of 45°C, RH of 35% and wind velocity of 15 km/hr.

Table 4.1: Maximum plastic shrinkage strain in the blended cement concretes at different dosages, exposed to a wind velocity of 15 km/hr, temperature of 45 °C and RH of 35%.

Type of Silica Fume	% Replacement	Maximum plastic shrinkage strain (μm)
Type 1	5	1322
	7.5	1645
	10	2348
Type 2	5	1724
	7.5	2794
	10	2924
Type 3	5	1038
	7.5	1370
	10	1656
Type 4	5	1122
	7.5	1183
	10	1224
Type 5	5	783
	7.5	939
	10	1119
Plain	0	716
Fly Ash	30	893
Superpozz®	10	808

4.1.2 Discussion on the Plastic Shrinkage Strain

Plastic shrinkage strain values are presented showing their variation over time from the time of casting up to a period of 24 hours, for the various types and dosages of silica fume cement concretes.

Effect of Cement Type on Plastic Shrinkage Strain

In this investigation, the rate of evaporation is assumed to be constant since all the cement types were exposed to the same conditions. The water/binder ratio was constant throughout all the mixes, no air entrainment was used, the same type and dosage of superplasticizer was used in all mixes and the slabs were of the same thickness. Thus, the variables that are considered to influence the plastic shrinkage of the plain and blended cement concretes are reduced to the following:

1. The specific surface area of the blended cement pastes, its state of densification, and its bulk density, and
2. The geometry of the pores between the outmost cement grains (as represented by the average pore radius and the total pore volume).

These variables were selected in accordance with the work carried out by Cohen *et al.*

[57] and Radocea [62], who found out that the main parameters that influence plastic shrinkage strains in blended cements are:

1. The surface area of agglomerated silica fume particles in the cement paste, either densified or undensified is used;
2. The geometry of the pores between the outmost cement grains as represented by the pore size distribution of the cement paste; and
3. The rate of water evaporation and bleeding.

Effect of Cement Type on Plastic Shrinkage Strain: Relationship between the Specific Surface Area and the Plastic Shrinkage Strain

Comparing the plastic shrinkage strains in the cement concrete made with the five types of silica fume; it is obvious that Type 2 silica fume, which is the only type of silica fume that is undensified, produced the highest amount of plastic shrinkage strain as depicted in Table 4.1. This trend was maintained at all dosages when this type of silica fume is compared with the other types.

Table 4.2 summarizes the specific surface area and bulk density data for the various types of blended cement materials and the parent cement concrete. The data is plotted in Figure 4.7. An inverse relationship exists between the bulk density and the plastic shrinkage

strain and, as expected, those blended cements that had the higher bulk density also had the lower plastic shrinkage strain. This is attributed to the fact that the larger particle sizes formed by agglomerates due to densification increased the density. A comparison of the bulk densities and the plastic shrinkage strains in Tables 4.1 and 4.2 shows that the behavior of the blended cements in terms of plastic shrinkage strain can be correlated with the physical properties of the blending materials (i.e., specific surface area and bulk density, shown in Figure 4.7). For example, Type 2 silica fume cement concrete that produced the highest plastic shrinkage strain also had the lowest bulk density, the only type of silica fume that is undensified. Next in succession were Type 1, Type 3, Type 4 and Type 5 silica fume. A direct relationship existed between the specific surface area and the plastic shrinkage strain. As the specific surface area increased, the plastic shrinkage strain also increased. This is expected and generally agrees with what has been reported in the literature [57]. The specific surface area of the blended cements is one of the most important properties that determine their fineness and, as the specific surface area increases the fineness of the pores increases leading to an increase in the area from which water can evaporate, thus increasing the plastic shrinkage strain.

The results of this study indicate that the fineness of the cement as represented by its specific state of densification, i.e., the specific surface area, and the bulk density, are good indicators of the potential for plastic shrinkage under hot weather conditions.

Relationship between Average Pore Radius and the Plastic Shrinkage Strain of Plain and Blended Cement Concretes

Tables 4.3 and 4.4 and Figures 4.8 and 4.9 depict the average pore radius (APR) and the total pore volume (TPV), respectively, for the plain and blended cements. In Figure 4.8 APR values are plotted against plastic shrinkage values for the 7.5% dosage of silica fume. The APR increased with the plastic shrinkage up to a maximum value before decreasing. No definite relationship could be observed in the data relating the APR to the plastic shrinkage strains.

Effect of Cement Type on Plastic Shrinkage Strain: Relationship between the Total Pore Volume and the Plastic Shrinkage Strain

Table 4.4 and Figure 4.9 depict the relationship between the total pore volume and the plastic shrinkage strain in plain and blended cement concretes. No definite relationship could be observed between the two. The APR and TPV values of the various types of blended cement concretes are presented in Table 4.4. From these data it could be observed that the rate of increase of the TPV is not the same in all the blended cement concretes. With the exception of Type 3 silica fume cement, the APR was about constant despite a steady increase in the TPV as the plastic shrinkage strains increased. Thus, the increase in the reactivity with age is indicated by an increase in the TPV, due to the fact

that as the hydration process progresses, its products fill the available pores [101]. Plain cement concrete exhibited the least reactivity, while fly ash cement concrete exhibited the best reactivity.

Based on previous research [46], parameters such as the average pore radius (APR) and the total porosity (TPV) usually serve as better indicators of cement/concrete properties, rather than the pore size distribution that is also obtained using nitrogen adsorption and MIP techniques. Therefore, only these values were used to compare the various types of blended cement concretes.

Table 4.2: Specific surface area and bulk density of silica fume cement concrete.

Type of Cement Replacement	Specific Surface Area (m ² /g)	Bulk density (kg/m ³)	Particle Densification
Type 1	23.5	627	Densified
Type 2	16.7	328	Undensified
Type 3	27.7	711	Densified
Type 4	20.3	797	Densified
Type 5	18.06	790	Densified
Fly Ash	0.30	1099	N/A
Superpozz®	1.30	1034	N/A
Plain	0.25	1287	N/A

Table 4.3: TPV, APR and plastic shrinkage strain (7.5% silica fume dosage).

Type of Cement Replacement	Total Pore Volume (mm ³ /g)	Average Pore Radius (nm)	Plastic Shrinkage Strain (μm)
Superpozz®	22.5	5.63	808
Type 5-7.5%	20.3	6.04	939
Type 4-7.5%	30.8	6.16	1183
Type 2-7.5%	32.5	6.93	2794
Plain	18.8	7.14	716
Fly Ash	33.8	7.26	893
Type 1-7.5%	28.5	7.65	1645
Type 3-7.5%	31.1	12.6	1370

Table 4.4: TPV, APR and plastic shrinkage strain (7.5% silica fume dosage).

Type of Cement Replacement	Total Pore Volume (mm ³ /g)	Average Pore Radius (nm)	Plastic Shrinkage Strain (μm)
Plain	18.8	7.14	716
Superpozz®	22.5	5.63	808
Type 5-7.5%	20.3	6.04	939
Type 1-7.5%	28.5	7.65	1645
Type 4-7.5%	30.8	6.16	1183
Type 3-7.5%	31.1	12.6	1370
Type 2-7.5%	32.5	6.93	2794
Fly Ash	33.8	7.26	893

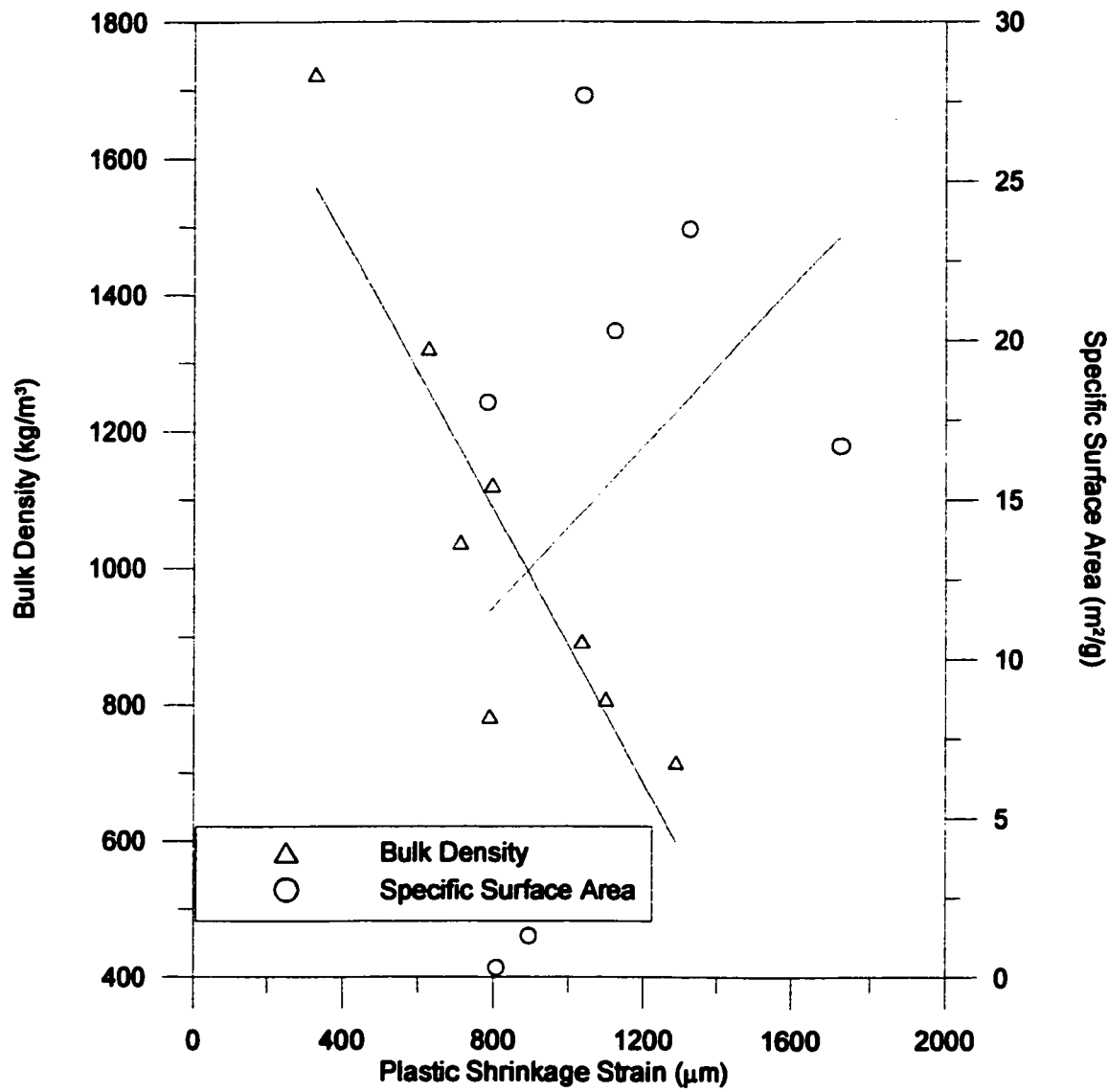


Figure 4.7: Variation of the plastic shrinkage with bulk density and specific surface area of blended cement concretes for 7.5% silica fume cement concrete.

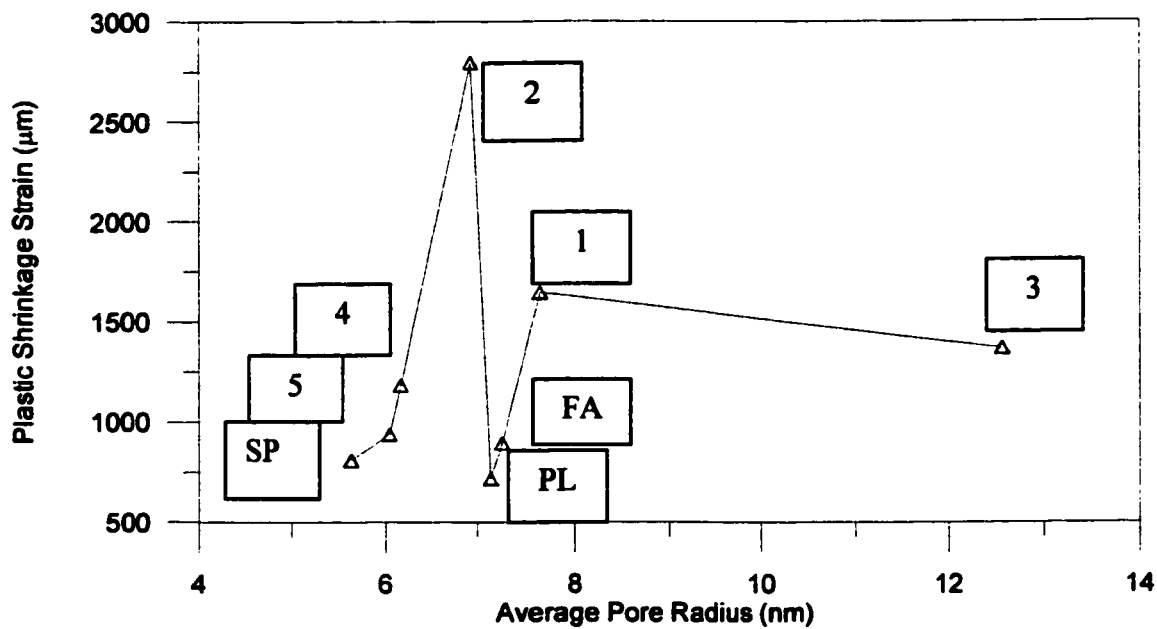


Figure 4.8: Variation of the plastic shrinkage strain with the average pore radius for plain and blended cements.

1	2	3	4	5	- Types 1, 2, 3, 4, 5 silica fume cements
PL					- plain
FA					- fly ash
SP					- Superpozz®

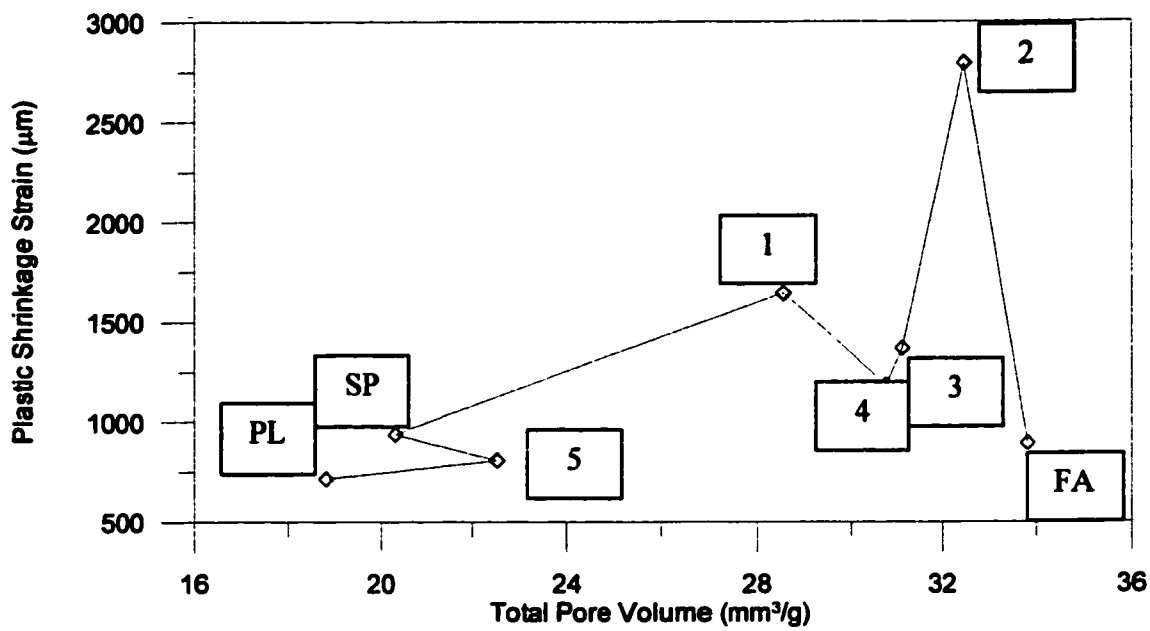


Figure 4.9: Variation of the plastic shrinkage strain with the total pore volume for plain and blended cements.

4.2 EFFECT OF EXPOSURE CONDITIONS ON PLASTIC SHRINKAGE STRAIN

Tables 4.5 through 4.7 summarize the data on the effect of exposure conditions on plastic shrinkage strain in Type 1 silica fume at a dosage of 7.5%. (Series I (b)). The results of this phase are presented below.

4.2.1 Effect of Temperature on Plastic Shrinkage Strain

Table 4.5 and Figure 4.10 show the effect of temperature variation on the plastic shrinkage strain at a constant relative humidity of 50% and a wind velocity of 15 km/hr. At 25°C, the plastic shrinkage strain was 1073 μm , and at 35°C it increased to 1137 μm while at 45°C the shrinkage strain was 1327 μm . These data indicate that as the exposure temperature increased the plastic shrinkage strain also increased. Furthermore, the increase in the plastic shrinkage strain with temperature appears to be more influential at temperatures higher than 35°C, as shown in Figure 4.10.

4.2.2 Effect of Relative Humidity on Plastic Shrinkage Strain

The effect of relative humidity on the plastic shrinkage strain, with the temperature and wind velocity being constant at 45°C and 15 km/hr, respectively, is presented in Table 4.6 and Figure 4.11. At a RH humidity of 25%, the plastic shrinkage strain was 2036 μm .

At 35% RH, the plastic shrinkage strain decreased to 1708 μm and increasing the relative humidity to 50% decreased the plastic shrinkage strain to 1327 μm while a RH humidity of 60% further decreased the shrinkage strain to 1218 μm . As shown in Figure 4.11, the plastic shrinkage strain decreased almost linearly with the relative humidity.

4.2.3 Effect of Wind Velocity on the Plastic Shrinkage Strain

Table 4.7 and Figure 4.12 show the effect of wind velocity on the plastic shrinkage strain at a constant temperature of 45°C and a relative humidity of 50%. In the specimens exposed to no wind, the plastic shrinkage strain was 1135 μm . At a wind velocity of 10 km/hr, the plastic shrinkage strain increased to 1252 μm and at a wind velocity of 15 km/hr, a plastic shrinkage strain of 1708 μm was recorded. In Figure 4.12, it can be observed that as the wind velocity tended to increase, the plastic shrinkage strain also increased. The increase in the plastic shrinkage strain with wind velocity appears to be more influential when the wind velocity was more than 9 km/hr.

4.2.4 Discussion on the Effect of Exposure Conditions on Plastic Shrinkage Strain

From the data depicted in Figures 4.10 through 4.12, it can be observed that the variation of relative humidity produced the most severe variation in the plastic shrinkage strains

keeping all other parameters constant. This finding agrees well with the results of previous researchers [35,36,39]. They emphasized the importance of preventing the loss of moisture in fresh concrete, especially in blended cement concretes from the time of placement to a period of about 24 hours. This can be achieved by properly curing the concrete with wet burlap or frequent water sprays or the use of effective curing compounds. Therefore, it is imperative that proper and extended curing of concrete is carried out in order to prevent the adverse effect of hot weather conditions.

The effect of high exposure temperatures on plastic shrinkage strain is also quite detrimental, resulting in higher plastic shrinkage strains and higher potential to cracking. This may be attributed to the fact that a high exposure temperature increases the rate of hydration of the cement paste and the hydration products do not have sufficient time to diffuse throughout the cement matrix. Consequently, the hydration products remains near the cement grains, leaving the interstitial space relatively open. Results of a previous research [5] has shown that temperature has a greater effect on the finer pores, leading to higher pore volumes, higher potential to plastic shrinkage cracks and ultimately detrimental to the properties of the fresh and hardened concrete. Another consequence of elevated temperature is the enhanced evaporation of mix water that accelerates the shrinkage of concrete.

The effect of high exposure temperatures on plastic shrinkage strain and cracking can be

minimized if adequate precautions are taken. Casting should be undertaken later in the afternoon when the temperature gets lower and with an extended cool period, and large volume pores should be avoided during the summer months in the Arabian Gulf region. It might also be important to keep the mixing water and the aggregates cool and shaded so as to reduce the mix temperature.

High wind velocities increase both the plastic shrinkage strain and the cracking potential due an increase in the rate of evaporation of water from the concrete surface. Should the rate of evaporation exceed the rate of bleeding in the concrete then plastic shrinkage cracks will occur. The effect of high wind velocity is more pronounced at higher exposure temperatures as can be observed from Table 4.5. If casting is to be undertaken at cooler times of the day when the temperature is, say, 25°C, then wind velocities exceeding 15 km/hr must be avoided. When the temperature is 35°C, it is expected that windbreakers and barriers will be used to protect the concrete from the potential of plastic shrinkage cracking.

Table 4.5: Variation of plastic shrinkage strain with temperature in the concrete specimens exposed to a wind velocity of 15 km/hr and relative humidity of 50%.

Temperature (°C)	Plastic Shrinkage Strain (μm)
25	1073
35	1137
45	1327

Table 4.6: Variation of plastic shrinkage strain with relative humidity in the concrete specimens exposed to a wind velocity of 15 km/hr and temperature of 45 °C.

Relative humidity (%)	Plastic Shrinkage Strain (μm)
25	2036
35	1708
50	1327
60	1218

Table 4.7: Variation of plastic shrinkage strain with wind velocity in the concrete specimens exposed to a relative humidity of 50 % and temperature of 45 °C.

Wind Velocity (km/hr)	Plastic Shrinkage Strain (μm)
0	1135
10	1252
15	1327

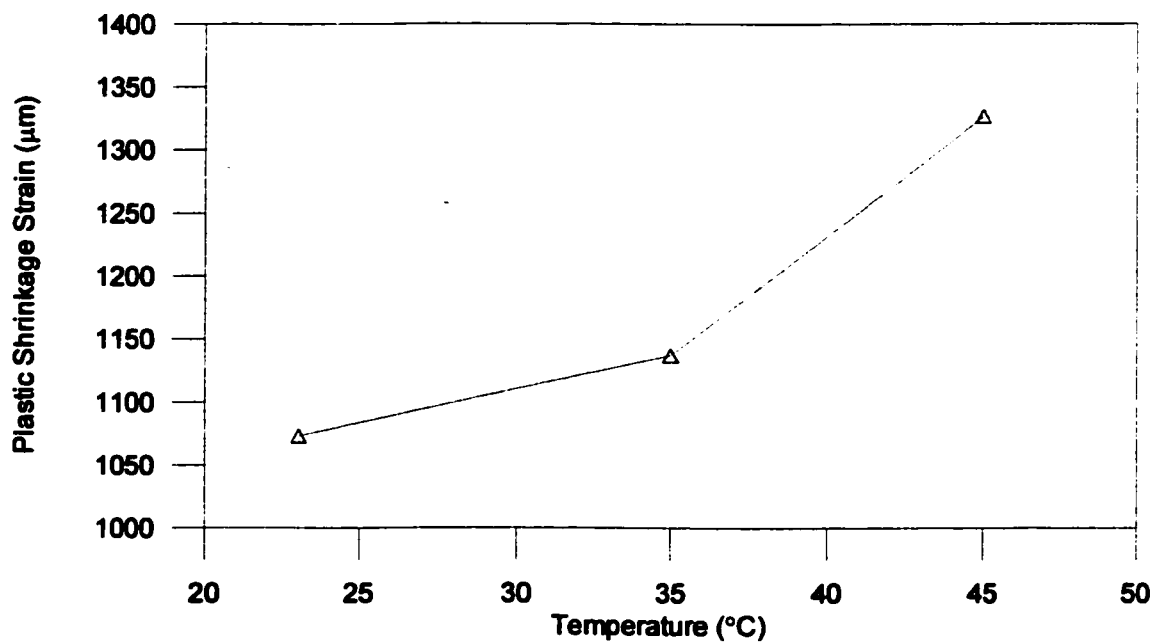


Figure 4.10: Variation of the plastic shrinkage strain with temperature in Type 1 silica fume cement concrete (7.5%), exposed to a RH of 50% and wind velocity of 15 km/hr.

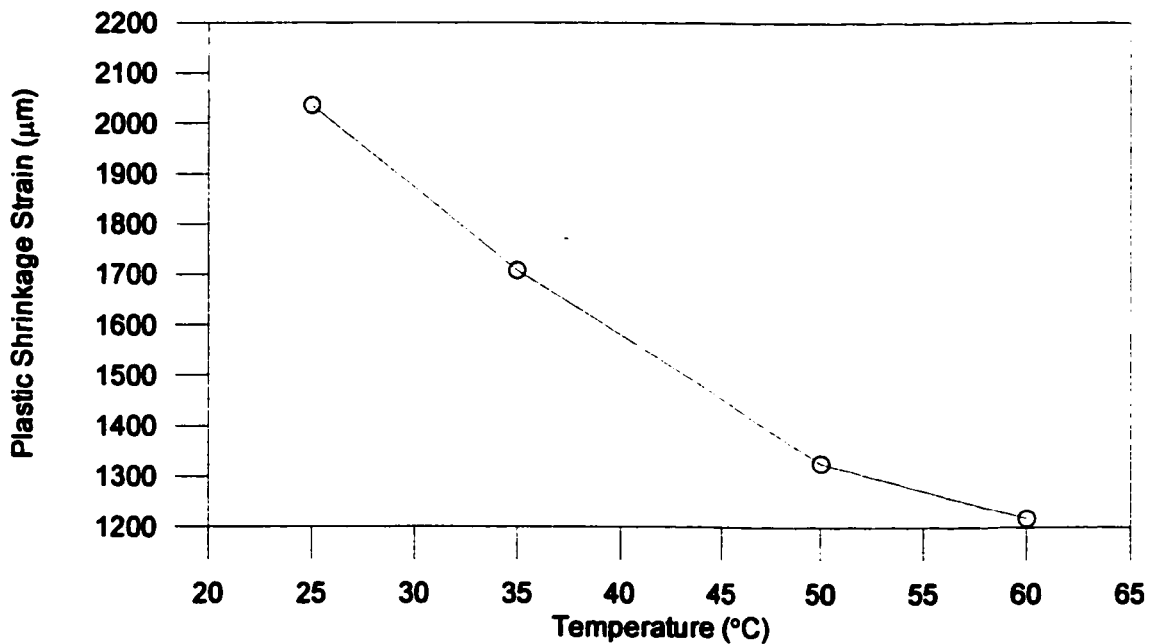


Figure 4.11: Variation of the plastic shrinkage strain with the relative humidity in Type 1 silica fume cement concrete (7.5%), exposed to a temperature of 45°C and wind velocity of 15 km/hr.

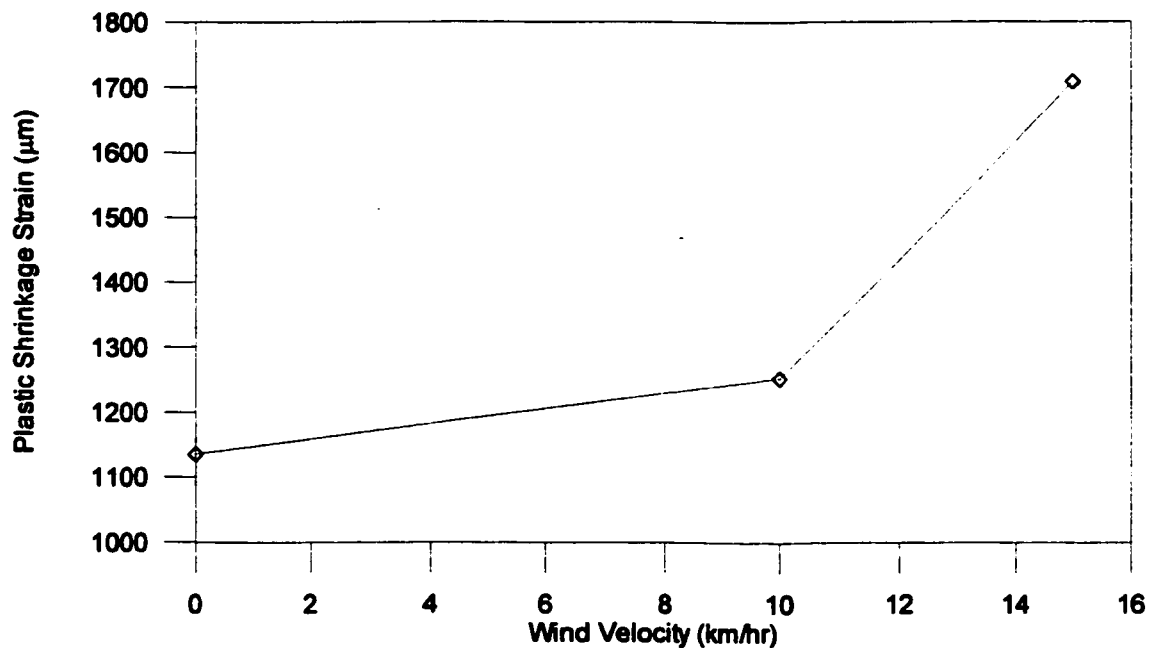


Figure 4.12: Variation of the plastic shrinkage strain with the wind velocity in Type 1 silica fume cement concrete (7.5%), exposed to a temperature of 45°C and a RH of 50%.

4.3 PLASTIC SHRINKAGE CRACKING

Plastic shrinkage cracks were observed in only three of the five types of silica fume cement concretes. In almost all the slabs that exhibited cracking, the cracks consisted of a single diagonal crack that propagated through the entire depth, at the center of the slab. The cracks propagated very fast (within 30 minutes from the time of casting). In Type 1 silica fume cement concrete that cracked at all dosages of silica fume, as the area of the cracks increased their depths decreased.

4.3.1 Effect of Blended Cement Type on Plastic Shrinkage Cracking

From the data presented in Table 4.8, it can be observed that only Types 1, 2 and 4 silica fume cement concretes exhibited plastic shrinkage cracking. Type 1 silica fume concrete specimens cracked at all dosages while Types 2 and 4 cracked at 10% dosage only. In Type 1 silica fume mix, the time to cracking decreased with increasing the dosage of silica fume from 5% to 10%. The total area of cracks increased with increasing the dosage of silica fume. Typical modes or cracks are shown in Fig 4.13 through 4.15 for various types of concrete.

4.3.2 Effect of Exposure Conditions on Plastic Shrinkage Cracking

Effect of Temperature

Table 4.9 shows the effect of ambient temperature on plastic shrinkage cracking in the specimen exposed to a wind velocity of 15 km/hr and a relative humidity of 50%. Cracks were observed only in the concrete specimens exposed to a temperature of 45°C. The cracks appeared after 2 hours of exposure covering an area of 0.0902 % of the slab.

Effect of Relative Humidity

The effect of relative humidity on plastic shrinkage cracking in the specimens exposed to a wind velocity of 15 km/hr and temperature of 45 °C is presented in Table 4.10. At a relative humidity of 25%, cracks appeared after 1.5 hours of exposure covering an area of 0.222% of the slab. At a RH of 35%, cracks appeared after 2 hours covering an area of 0.10 % of the slab and at a RH of 50% cracks also appeared after 2 hours but covered an area of 0.0902% of the slab. No plastic shrinkage cracks were noted in the specimen exposed to a RH of 60%.

Effect of Wind Velocity

Table 4.11 depicts the effect of wind on the plastic shrinkage cracks in the specimens exposed to a relative humidity of 50% and temperature of 45 °C. With a wind velocity of

15 km/hr, cracks appeared after 2 hours covering an area of 0.09% of the total slab area. No cracks were observed in the specimens exposed to a wind velocity of 0 and 10 km/hr.

4.3.3 Discussion on Plastic Shrinkage Cracking

Effect of Plain and Blended Cement Type on Plastic Shrinkage Cracking

With reference to the data in Table 4.8, it can be observed that Type 1 silica fume cement concrete cracked at a dosage of 5%, Types 2 and 4 silica fumes cement concrete cracked at a dosage of 10%. In order to observe the effect of the fineness of the silica fume on the likelihood of cracking, the ratio of the specific surface area (SSA) to the average pore radius (APR) is used. These data are presented in Table 4.12 and Figure 4.16. A definite relationship could not be observed between the SSA/APR ratio and the plastic shrinkage strain. However, cracking was noted in the concrete specimens with plastic shrinkage strains of more than 1100 μm . For the types of blended cement concrete that did not exhibit cracking, namely Types 3 and 5 silica fume, plain, fly ash and Superpozz[®] cement concretes, their plastic shrinkage strain values were all lower than a threshold value of 1122 μm . In the case of Type 3 silica fume that had the highest specific surface area, no cracks were observed because it also had the highest APR. This finding verifies the use of the ratio of the SSA/APR rather than just the SSA alone. From Figure 4.16, it can be observed that the critical SSA/APR ratio is 2.5.

Effect of Exposure Conditions on Plastic Shrinkage Cracking

From the data presented in Tables 4.9 through 4.11, it could be observed that under severe exposure conditions such as a wind velocity of 15 km/hr and a temperature of 45 °C, a minimum relative humidity of 60% is required to avoid plastic shrinkage cracking.

As mentioned in Chapter 2, plastic shrinkage cracking is a result of the drying out of the concrete surface where the menisci form between the solid particles setting up capillary tension (water) forces. With the inclusion of silica fume, the phenomenon of cracking could be further aggravated due to its fineness and the refinement of the pores of the concrete. Further, there is a reduction in the rate of bleeding of the concrete and if the rate of evaporation exceeds the rate of bleeding, cracking would occur. The effects of hot weather on concrete serves to increase the rate of cement hydration, thereby producing concrete with much coarser pores than would otherwise be produced [5].

Recent research by Bentz *et al.* [111] has demonstrated that the initial cement-particle size distribution of fresh cement paste had a significant effect on the early properties of sealed specimens at identical w/c ratios. The larger pores present in the coarser cement paste reduced the rate of RH decay with increasing hydration, concurrently reducing the associated capillary stresses within the cement paste pore solution. In turn, both the potential to shrinkage and the eigenstress (the stresses associated with microcracking)

were reduced [111].

In this study, the concrete specimens were exposed under similar weather conditions using the same water-cement ratios. Based on Bentz *et al.*'s study, it is expected that those silica fume cement concretes with larger pores present in the coarser cement paste would reduce the rate of RH decay with increasing hydration; higher rates of bleeding would also result in these concretes, and if the rate of bleeding exceeds the rate of evaporation, the potential of plastic shrinkage cracks would reduce. Hence, under similar conditions, coarser silica fume-cement concretes are expected to perform better than finer ones in reducing plastic shrinkage cracking under prevailing weather conditions. Thus, the initial particle size distribution of the concrete was determined by the fineness and dosage of the various types of silica fumes. A measure of the fineness (or coarseness) of the silica fume cement concretes is the SSA/APV ratio presented in Table 4.12 and Figure 4.16. Here it can be observed that the finer silica fumes (those having above the threshold value in Figure 4.16) exhibited cracking while the coarser ones did not. Bentz *et al.* carried out their study under laboratory conditions while the results presented in Table 4.12 and Figure 4.16 were conducted under hot weather conditions. Therefore, it is reasonable to conclude that the effect of cement fineness on plastic shrinkage cracking is independent of exposure conditions.

Table 4.8: Plastic shrinkage cracking in blended cement concretes exposed to a temperature of 45 °C, wind velocity of 15 km/hr and relative humidity of 35%.

Type of Silica Fume	% Replacement	Plastic Shrinkage Cracks			
		Time to Cracking	Crack Length (mm)	Average Crack width (mm)	Average Crack Area (%)
Type 1	5	2.5	63	1.5	0.0378
	7.5	2	74.5	1.6	0.04768
	10	1.5	140.5	1.075	0.06041
Type 2	5	No cracks observed			
	7.5	No cracks observed			
	10	1.5	24.5	1.1	0.01078
Type 3	5	No cracks observed			
	7.5	No cracks observed			
	10	No cracks observed			
Type 4	5	No cracks observed			
	7.5	No cracks observed			
	10	1.5	45.5	2.77	0.05014
Type 5	5	No cracks observed			
	7.5	No cracks observed			
	10	No cracks observed			
Plain		No cracks observed			
Fly Ash		No cracks observed			
Superpozz®		No cracks observed			

Table 4.9: Variation of plastic shrinkage cracks with temperature in the concrete specimens exposed to a wind velocity of 15 km/hr and relative humidity of 50%.

Temperature (°C)	Time To Crack (hours)	Crack Length (mm)	Average Crack Width (mm)	Average Crack Area (%)
25	No cracks	No cracks	No cracks	None
35	No cracks	No cracks	No cracks	None
45	2.0	96	2.35	0.09024

Table 4.10: Variation of plastic shrinkage cracks with relative humidity in the concrete specimens exposed to a wind velocity of 15 km/hr and temperature of 45 °C.

Relative humidity (%)	Time To Crack (hours)	Crack Length (mm)	Average Crack Width (mm)	Average Crack Area (%)
25	1.5	210	2.65	0.2226
35	2.0	97	2.58	0.10
50	2.0	96	2.35	0.09024
60	No cracks	No cracks	No cracks	None

Table 4.11: Variation of plastic shrinkage cracks with wind in the concrete specimens exposed to a relative humidity of 50 % and temperature of 45 °C.

Wind (km/hr)	Time To Crack (hours)	Crack Length (mm)	Average Crack Width (mm)	Average Crack Area (%)
0	No Cracks	No cracks	No cracks	None
10	No Cracks	No cracks	No cracks	None
15	2.0	96	2.35	0.09024

Table 4.12: Relationship between SSA, APR and plastic shrinkage cracking.

Type of Cement Replacement	Specific Surface Area (m ² /g)	Average Pore Radius (nm)	SSA/APV Ratio (mm ² /gnm)	Threshold Plastic Shrinkage Strain (μm)*	Cracking	Densification
Type 1-5%	23.5	7.65	3.07	1322	Cracked	Densified
Type 2-10%	16.7	6.93	2.41	2924	Cracked	Undensified
Type 4-10%	20.3	6.16	3.29	1224	Cracked	Densified
Type 3	27.7	12.6	2.20	1038	No cracks	Densified
Type 5	18.1	6.04	2.99	783	No cracks	Densified
Plain	0.25	7.14	0.035	716	No cracks	N/A
Fly Ash	0.3	7.26	0.041	893	No cracks	N/A
Superpozz®	1.3	5.63	0.231	808	No cracks	N/A

* The threshold plastic shrinkage strain value is 1,122 μm.



Figure 4.13: Plastic shrinkage cracks in Type 4 silica fume cement concrete (10% replacement) exposed to a temperature 45 °C, wind velocity of 15 km/hr and RH of 35%.

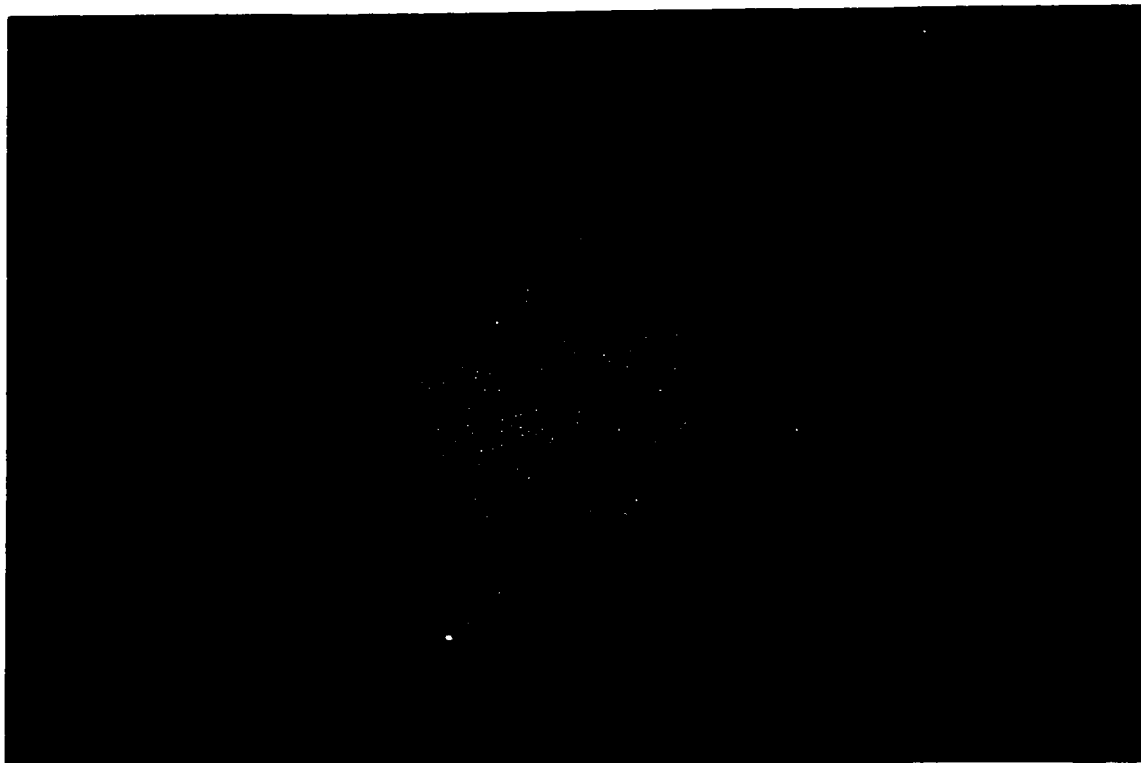


Figure 4.14: Plastic shrinkage crack in Type 1 silica fume cement concrete (10% replacement) exposed to a temperature 45 °C, wind velocity of 15 km/hr and RH of 35%.



Figure 4.15: Plastic shrinkage crack in Type 1 silica fume cement concrete (5% replacement) exposed to a temperature 45 °C, wind velocity of 15 km/hr and RH of 35%.

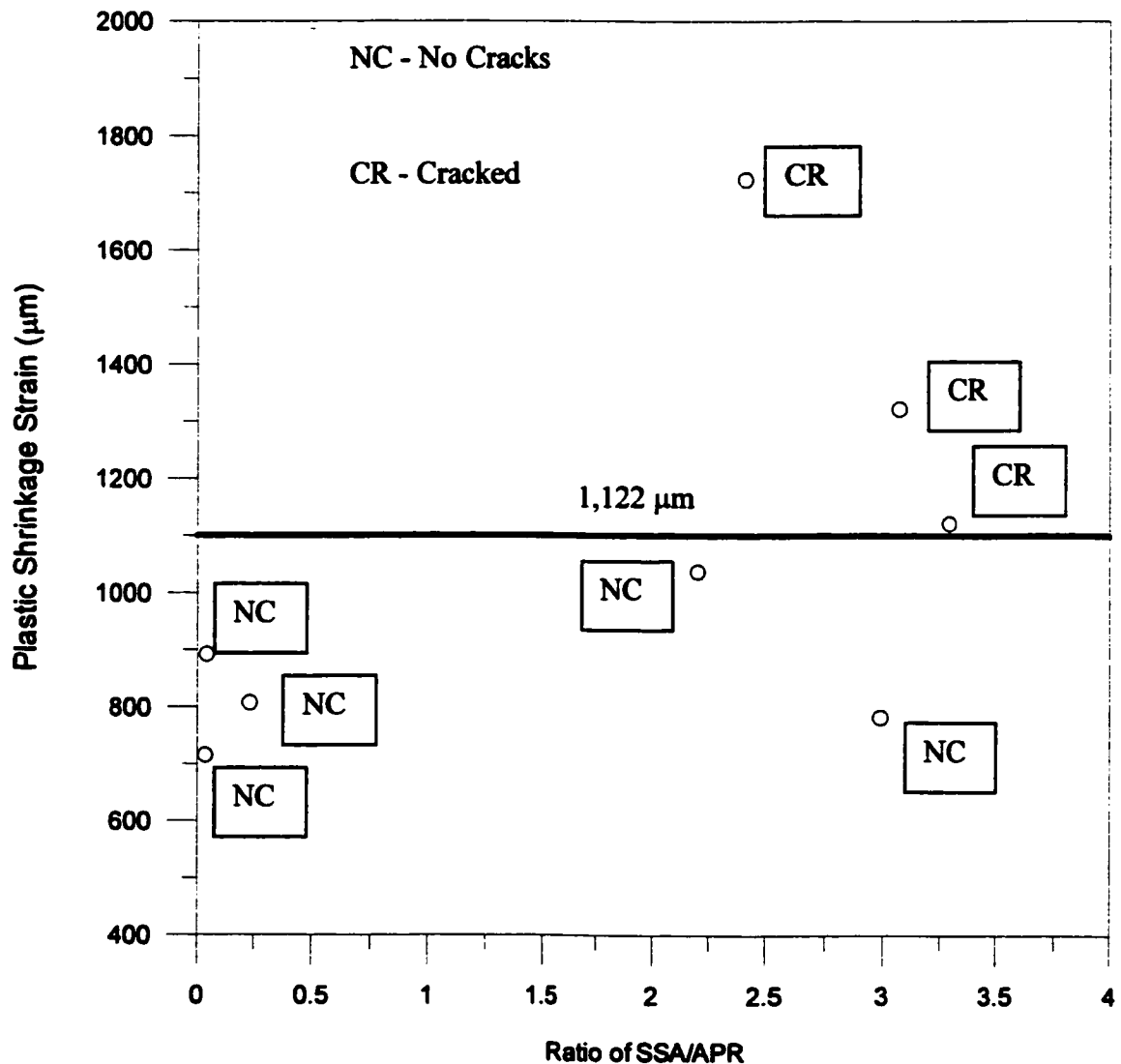


Figure 4.16: Threshold value of plastic shrinkage strain where cracking may occur for plain and blended cement concretes under hot weather conditions.

4.4 TIME TO ACHIEVE MAXIMUM STRAIN

The data in Figures 4.1 through 4.6 show that the time to achieve maximum strain varied with the type of blended cement. In the silica fume cement concretes, the maximum strain also varied with the dosage of silica fume. Table 4.13 summarizes the times to achieve maximum strain for the various types and dosages of blended cement concretes. The time to achieve maximum strain of Type 1 silica fume cement concrete increased with the dosage of silica fume. The maximum strain was achieved after 6.5, 8.75 and 8.81 hours, respectively, in 5, 7.5 and 10% silica fume. Type 2 silica fume cement concrete exhibited a similar trend, with 5% achieving the maximum strain after 7.94 hours, followed by 8.0 and 8.25 hours, respectively, at silica fume dosages of 7.5% and 10%. However, the trend was reversed in Type 3 silica fume cement concrete. The maximum strain was achieved after 12.2, 9.0 and 4.25 hours, respectively, at silica fume dosages of 5%, 7.5% and 10%. Type 4 silica fume cement concrete showed a similar trend to that of Type 3, the maximum strain occurred after 9.08, 7.88 and 7.5 hours, respectively, for silica fume dosages of 5, 7.5 and 10%. Type 5 silica fume exhibited a similar trend to Types 3 and 4. The maximum strain was achieved after 6.63, 5.25 and 5.17 hours, respectively, for silica fume dosages of 5, 7.5 and 10%.

Types 1 and 2 silica fume cement concrete specimens showed a trend of increasing the

time to achieve the maximum strain with an increase in the dosage of silica fume, while Types 3, 4 and 5 silica fume cement concrete specimens exhibited an opposite trend of decreasing time to achieve maximum strain with increasing dosage of silica fume.

The time to achieve maximum strain in the plain and Superozz® cement concretes was 6.42 and 6.13, respectively, while it was 8.25 hours in fly ash cement concrete.

4.4.1 Discussion on the Time to Achieve Maximum Strain

One type of superplasticizer was used in all silica fumes for Series (Ia) and (Ib) experiments. The dosage of superplasticizer was kept constant for each dosage of silica fume regardless of its type. At a silica fume dosage of 5%, a 0.75% dosage of superplasticizer was used. At a silica fume dosage of 7.5%, a superplasticizer dosage of 1.0% was used, and at a silica fume dosage of 10%, a superplasticizer dosage of 1.25% was used. The use of a constant dosage of superplasticizer for a similar dosage of silica fume produced mixes of slightly differing workabilities in the different types of silica fume cement concretes, but within the slump range of 50 to 75 mm. This ensured that the effect of the type of silica fume (and dosage) with respect to the time to achieve maximum strain can be compared among the various types of silica fume, with little or no effect from the addition of the superplasticizer. Thus, any shortening or retardation of the

time to achieve maximum strain is due solely to the type and dosage of the silica fume and not due to the influence of the superplasticizer.

From the data in Table 4.13, it can be observed that the time to achieve maximum strain of blended cement concretes was influenced by the type as well as dosage of the silica fume. In general, the addition of silica fume at dosages of 5 and 7.5% increased the time to achieve maximum strain of the blended cement concretes when compared to that of plain cement. An increase of the silica fume dosage to 10% had both an acceleration or retardation effect on the time to achieve maximum strain, depending on the type of silica fume. Fly ash had a retardation effect to that of the silica fumes on the time to achieve maximum strain, while Superpozz® did not significantly affect the time to achieve maximum strain.

The increase in the time to achieve maximum strains could be attributed to the slow development of the tensile strength of the silica fume cement concretes. As the tensile strength of the concrete increases with time, the plastic shrinkage strain also increases, continuing until the concrete hardens. However, owing to the different types and dosages of the silica fume, the plastic shrinkage strain would increase faster in those types of silica fume whose tensile strength develops slower.

In the case of Types 3, 4 and 5 silica fume cement concretes, the time to achieve

maximum strain decreased with increasing the dosage of silica fume. This indicated that these types of silica fume cement concretes were able to develop sufficient tensile strength at earlier times so as to be able to resist the plastic shrinkage strains. For these types of silica fume cement concretes, as the dosage of silica fume was increased, the pozzolanic reaction proceeded faster leading to a faster increase in both the capillary pressure which led to higher plastic shrinkage strains and also the tensile strength. The increase in the tensile strength proceeded faster, leading to shorter times for the maximum plastic shrinkage strain to be achieved.

In the case of Types 1 and 2 silica fume cement concretes the time to achieve maximum strain increased with increasing the dosage of silica fume. These types of silica fume cement concretes did not develop sufficient tensile strength to mitigate the increase in the plastic shrinkage strain with time. Owing to the larger pores and specific surface areas in these types of silica fume cements, as the dosage of silica fume was increased more water was lost due to evaporation leading to a lack of completion of the pozzolanic reaction. This, in turn, led to lower gains in the tensile strength with time, thereby increasing the time to achieve maximum strain. No relationship could be observed between the time to achieve maximum strain and the magnitude of the plastic shrinkage strain.

Table 4.13: Time to achieve maximum plastic shrinkage strain in plain and blended cement concretes.

Type of Cement Replacement	% Replacement	Time to Achieve Maximum Plastic Shrinkage Strain (Hours)
Type 1	5	6.50
	7.5	8.75
	10	8.81
Type 2	5	7.94
	7.5	8.00
	10	8.25
Type 3	5	12.2
	7.5	9.00
	10	4.25
Type 4	5	9.08
	7.5	7.88
	10	7.50
Type 5	5	6.63
	7.5	5.25
	10	5.17
Plain	0%	6.42
FlyAsh	30%	8.25
Superpozz®	10%	6.13

4.5 DRYING SHRINKAGE

Drying shrinkage of silica fume cement concrete was monitored on mortar bar specimens in accordance with ASTM C 157. The mortar bars were stored under laboratory conditions and the measurements were conducted for 90 days. Concrete slab specimens were also monitored for drying shrinkage by fixing DEMEC gauges, as described in Chapter 3. After plastic shrinkage tests, the slabs were cured using wet burlap and left under the prevailing weather conditions for monitoring the drying shrinkage for 90 days.

4.5.1 Drying Shrinkage of Mortar Bars

Figures 4.17 through 4.22 depict the drying shrinkage of plain, silica fume, fly ash and Superpozz® cement mortars. These data are summarized in Table 4.14. As expected, the drying shrinkage increased with the increase in the period of exposure. There was almost linear increase in the shrinkage up to about 28 days. Thereafter, the increase in the shrinkage was not that significant. Furthermore, the drying shrinkage in all the silica fume cement mortar specimens was more than that in the plain cement mortar. Moreover, the drying shrinkage increased with the silica fume dosage in the cement.

Maximum drying shrinkage occurred in Type 2 silica fume cement mortar specimens

with values of 1203, 1635 and 1713 μm at silica fume dosages of 5, 7.5, and 10%. Next in succession comes Type 1 silica fume cement mortar with maximum drying shrinkage values of 1157, 1251 and 1537 μm at dosages of 5, 7.5 and 10%. Type 4 silica fume cement mortar exhibited drying shrinkage values of 1093, 1185 and 1480 μm at silica fume dosages of 5, 7.5 and 10%, while Type 3 exhibited shrinkage values of 1087, 1193 and 1483 μm at 5, 7.5 and 10% silica fume dosages, respectively. The lowest shrinkage values of 1079, 1106, and 1197 μm at dosages of 5, 7.5 and 10%, respectively, were noted in Type 5 silica fume cement mortar.

The drying shrinkage strains in plain, fly ash and Superpozz[®] cement mortars are depicted in Figure 4.22. After 90 days, the maximum strain was noted in the Superpozz[®] cement mortar while the value in the fly ash cement mortar was almost similar to that in the plain cement concrete (see Table 4.14).

4.5.2 Discussion on Drying Shrinkage of Mortar Bars

The mortar bars were cured under similar laboratory conditions for all blended cement mixes using the same water-binder ratio. As the silica fume dosage was increased, the specific surface area of silica fume in the cement paste increased, which consequently increased the water demand necessary to complete the pozzolanic reaction between the silica fume and cement paste. However, because the water/cement ratio remained

constant, differences in the extent in refinement of the pores in the mortar bars took place at different rates, leading to denser pores in some silica fumes and coarser pores in others. The extent of the refinement of the pores varied with the type as well as dosage of the silica fume. This refinement of pores was also influenced by the initial pore size distribution, which favored more space for free-water diffusion and reduced rigidity of the solid matrix as a result of the inclusion of finer material, namely the silica fume. Differences in the drying shrinkage strain in the type and dosage of blended cement mortars could therefore be attributed to differences in the fineness of silica fume in terms of its content and specific surface area.

According to El-Hindy *et al.* [113], an increase in the water-binder ratio increased the drying shrinkage of the cement paste and accelerated its development, providing more space for free water diffusion and reducing the rigidity of the solid matrix to resist deformation. On the other hand, silica fume densifies the hydrated cementitious paste, thereby slowing down the water evaporation and hence the drying shrinkage. Research carried out by Whiting *et al.* [114] showed that curing had a significant effect on drying shrinkage in silica fume cement concrete. When cured for less than 7 days, an increase in the dosage of silica fume resulted in an increase in the drying shrinkage of the concrete. However, when the concrete cured for more than 7 days, the silica fume content did not have a significant effect on the drying shrinkage. The results of this study indicate that in

addition to the water/binder ratio and the extent of curing, the type and dosage of silica fume have a significant effect on the drying shrinkage of mortar bars.

Table 4.14: Maximum drying shrinkage in plain and blended cement mortars.

Type of Cement Replacement	% Replacement	Drying Shrinkage (μm)
Type 1	5	1157
	7.5	1251
	10	1537
Type 2	5	1203
	7.5	1635
	10	1713
Type 3	5	1087
	7.5	1193
	10	1483
Type 4	5	1093
	7.5	1185
	10	1480
Type 5	5	1079
	7.5	1106
	10	1197
Plain	0	1072
FlyAsh	30	1093
Superpozz®	10	1176

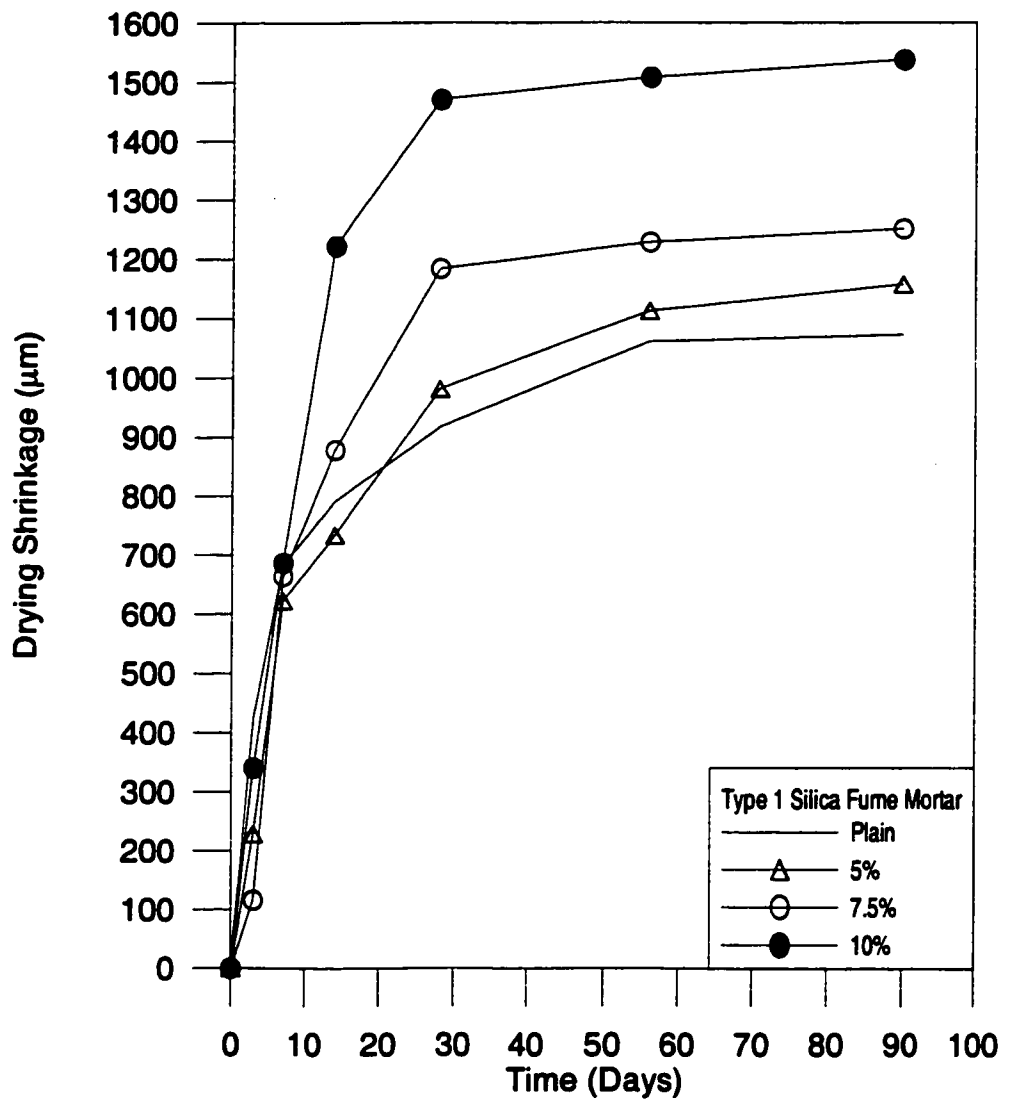


Figure 4.17: Drying shrinkage of Type 1 silica fume cement mortars.

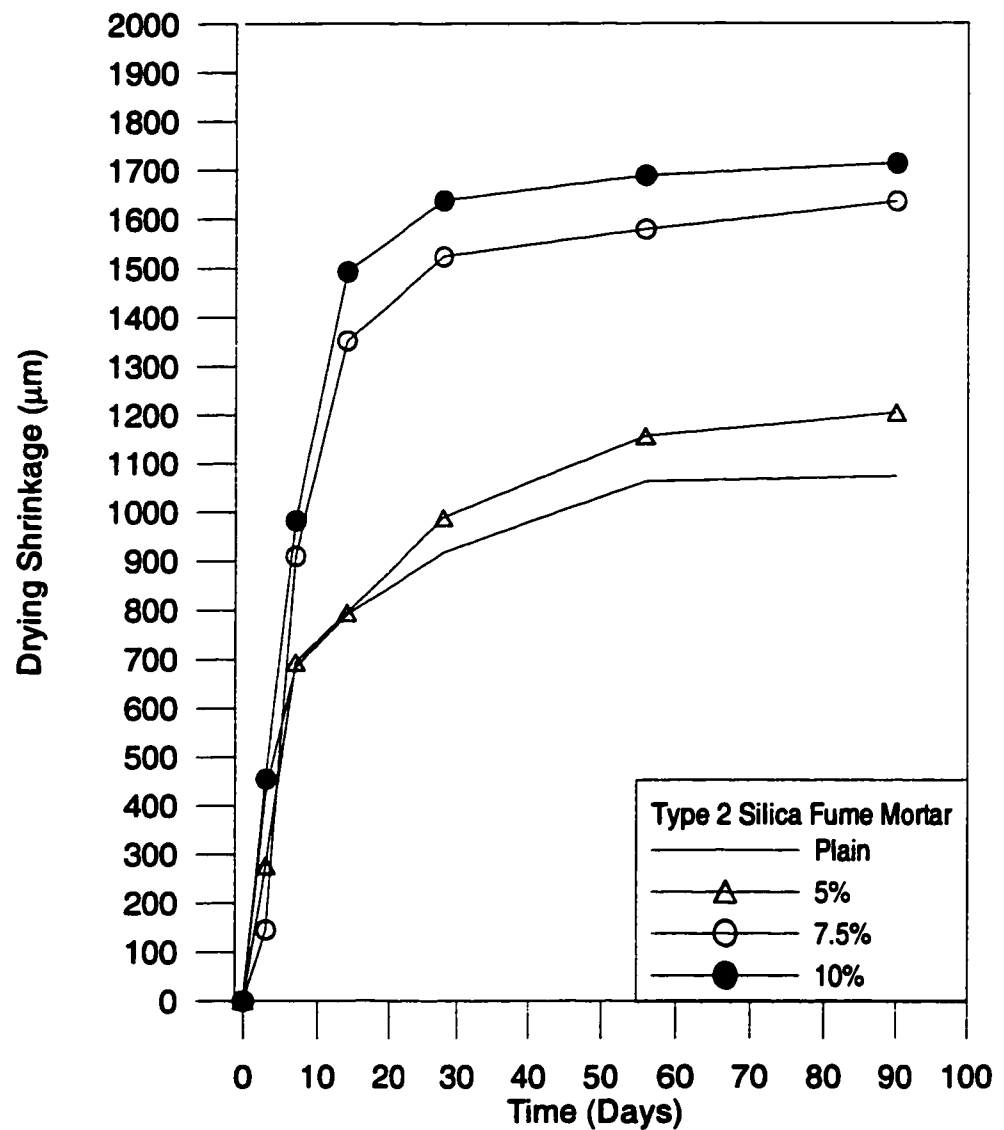


Figure 4.18: Drying shrinkage of Type 2 silica fume cement mortars.

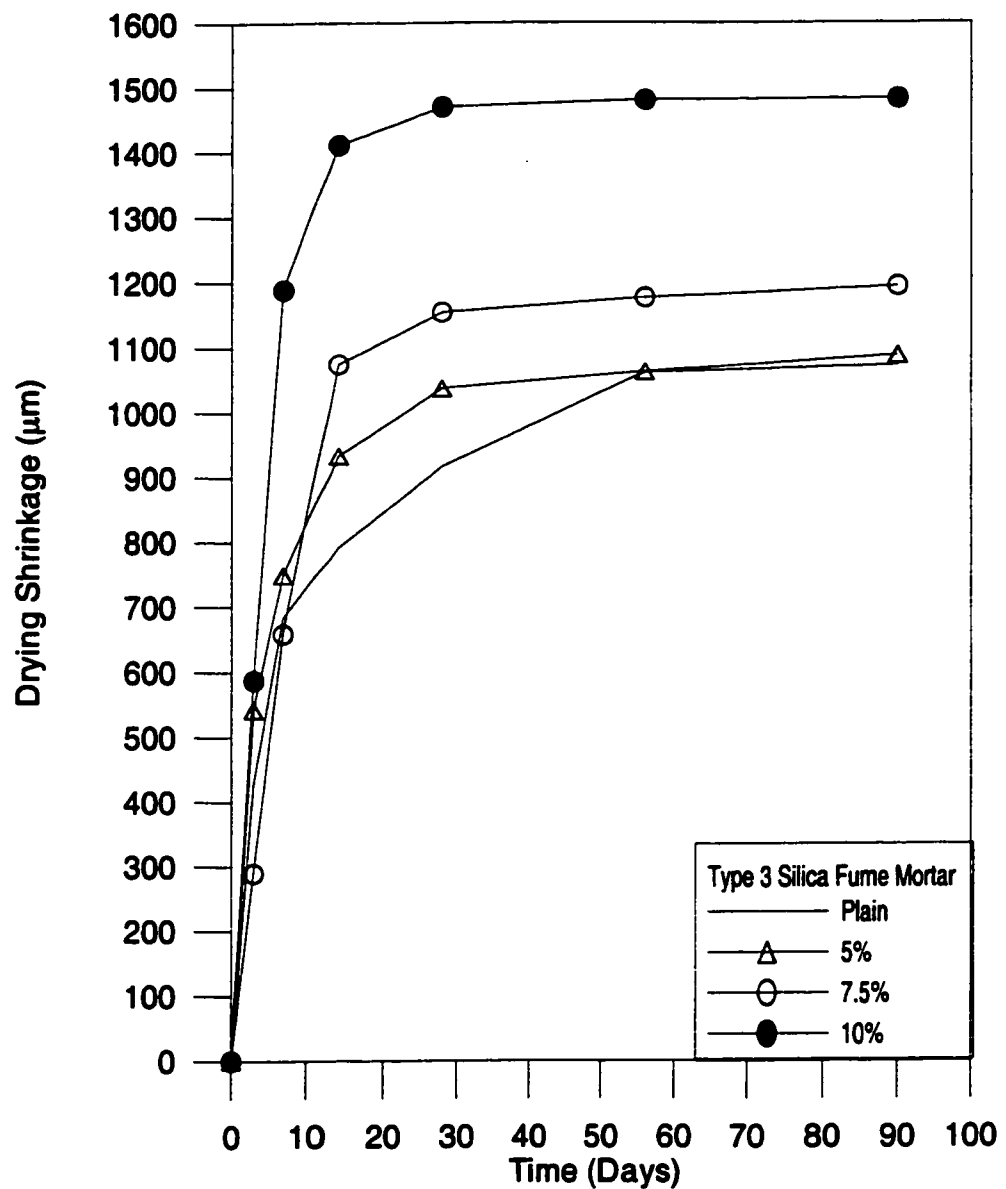


Figure 4.19: Drying shrinkage of Type 3 silica fume cement mortars.

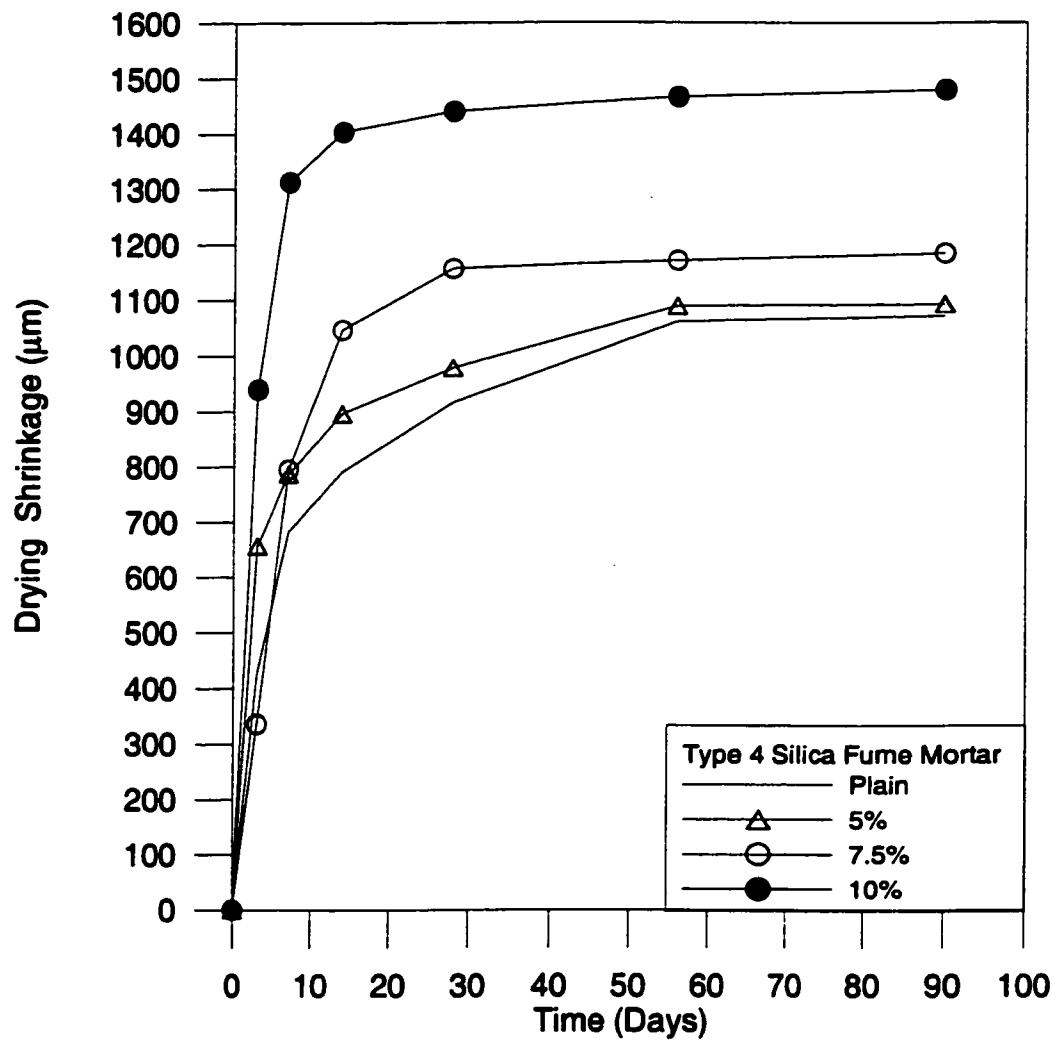


Figure 4.20: Drying shrinkage of Type 4 silica fume cement mortars.

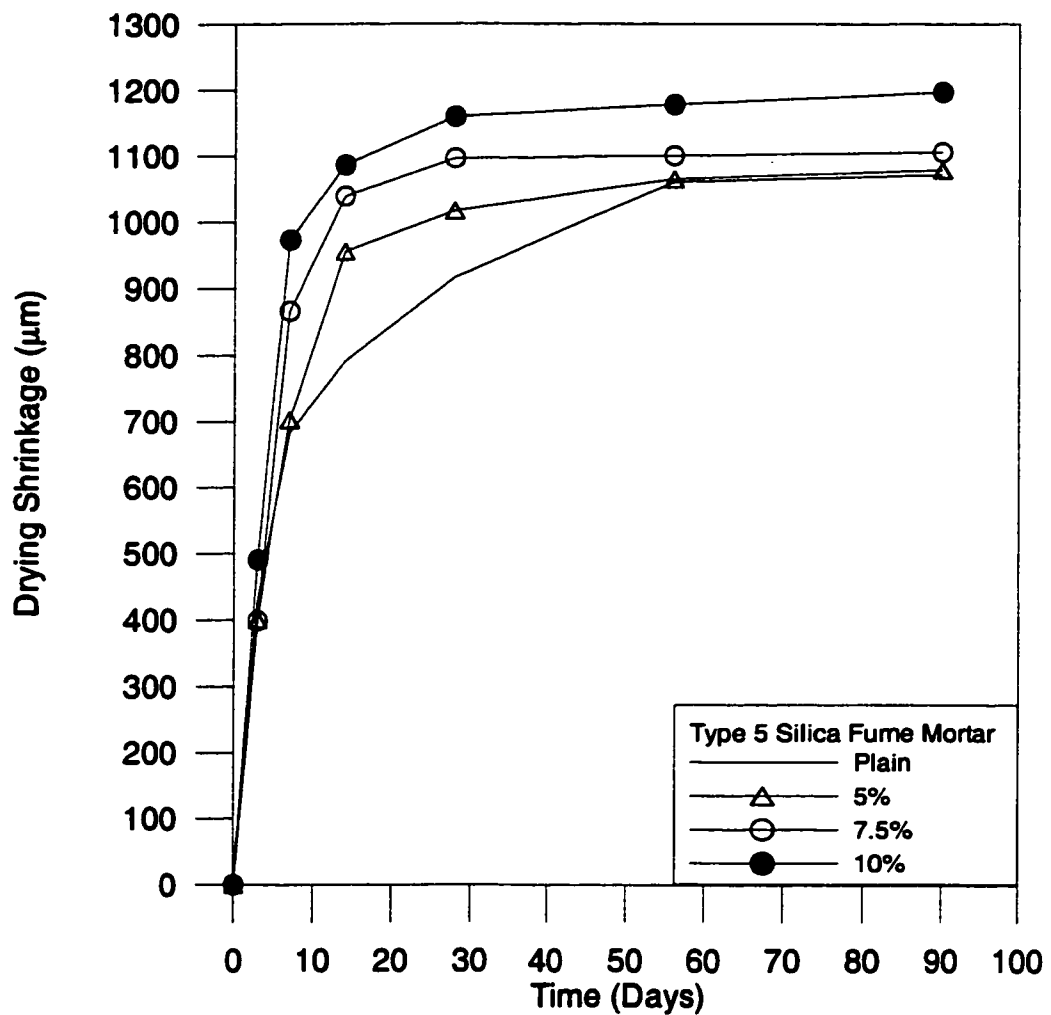


Figure 4.21: Drying shrinkage of Type 5 silica fume cement mortars.

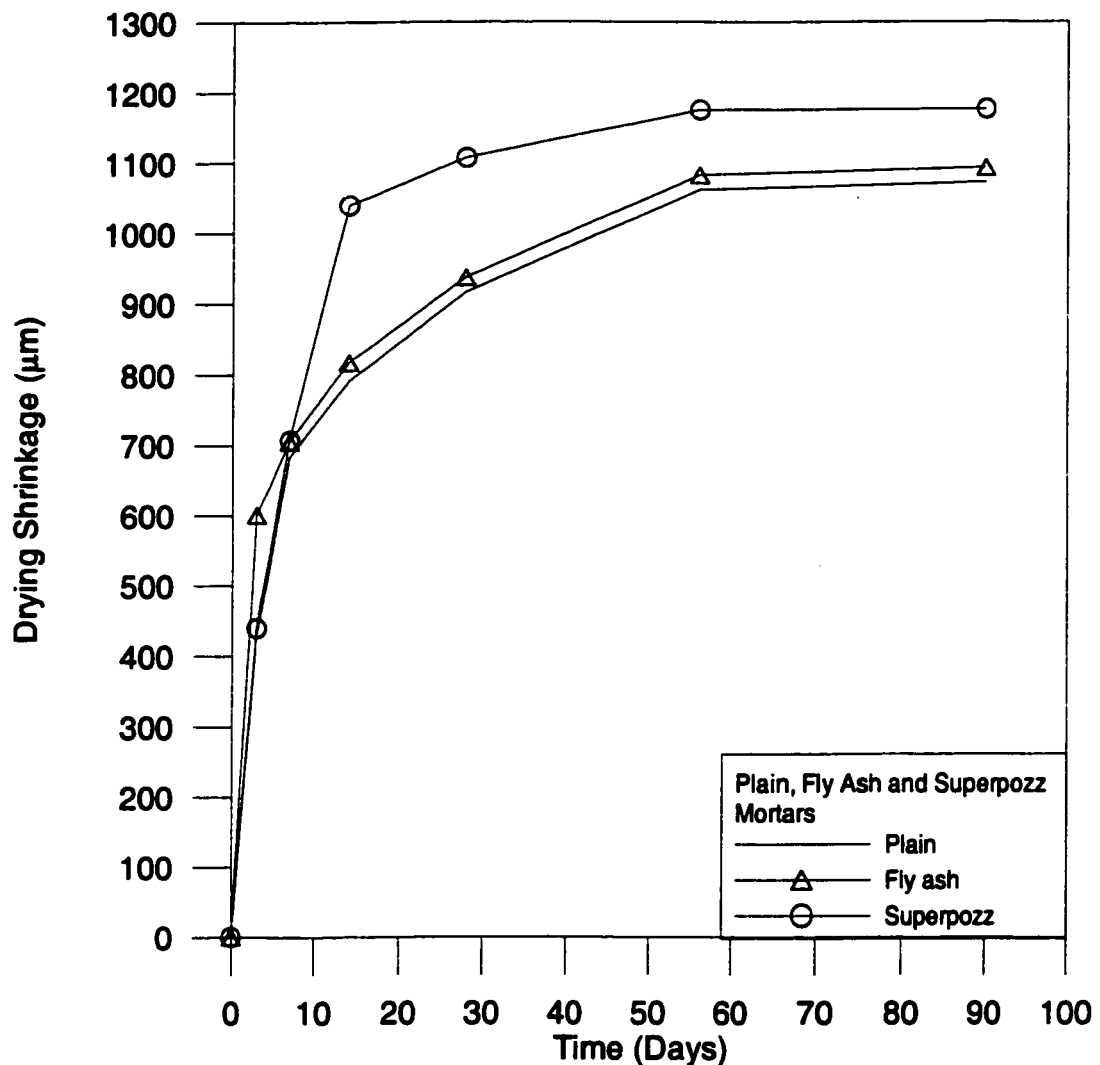


Figure 4.22: Drying shrinkage of Superpozz[®] and fly ash cement mortars.

4.5.3 Drying Shrinkage of Concrete Slabs

Figures 4.23 through 4.27 depict the drying shrinkage strain in slab specimens for various types of silica fume at various dosages. The drying shrinkage strain increased with the exposure period in all the concrete specimens. The shrinkage strains after 90 days of curing are summarized in Table 4.15.

Maximum strains of 831, 1219, and 1226 μm were measured in Type 1 silica fume cement concrete at 5%, 7.5% and 10% dosages, respectively, while a maximum strain of 723 μm was noted in plain cement concrete. Maximum strains of 614 and 664 μm in Type 2 silica fume occurred at dosages of 5 and 7.5% respectively, while a maximum strain of 1304 μm occurred at a dosage of 10%. Also, a maximum strain of 569 μm occurred in Type 3 silica fume cement concrete at a dosage of 5% while the maximum strains of 962 and 1010 μm occurred at dosages of 7.5 and 10%, respectively. Thus Types 1, 2 and 3 silica fume showed an increase in the drying shrinkage strains with increasing the dosage of silica fume. In contrast to the above, Types 4 and 5 silica fume cement concretes showed a decrease in the drying shrinkage strain when the dosage of silica fume was increased. A maximum strain of 1083 μm was noted at a dosage of 5% in Type 4 silica fume cement concrete, while the maximum strains were 829 μm and 629 μm , respectively, at dosages of 7.5 and 10%. Maximum strains of 752, 502 and 487 μm were noted in Type 5 silica fume at dosages of 5, 7.5 and 10%, respectively.

Figure 4.28 depicts the drying shrinkage in plain, fly ash and Superpozz® cement concrete slabs. The drying shrinkage of fly ash and Superpozz® were both higher than that of plain cement concrete. The highest strain of 898 μm was measured in the Superpozz® cement concrete.

4.5.4 Discussion on the Drying Shrinkage of Concrete Slabs

There appears to be some controversy in the literature about the effect of silica fume on the drying shrinkage properties of concrete. Several authors [115,116] have reported that silica fume mitigated drying shrinkage in concrete, while other authors [117,118] have reported that it aggravated it. Others presented results that drying shrinkage in silica fume cement concrete is about the same as that of ordinary cement concrete [119,120]. Al-Sugair [49] is of the opinion that there was no conflict in the results presented by the various authors as such. He was of the opinion that both effects of silica fume on the drying shrinkage of concrete were possible. He demonstrated that the extent to which silica fume addition increased or decreased drying shrinkage in concrete was dependent on:

1. Curing and exposure conditions; and
2. Water-binder ratio.

In this study, the curing and exposure conditions and the water-binder ratio were similar

for all the concrete mixes, yet different drying shrinkage strains were noted in the various types and dosages of blended cement concrete. Therefore, other parameters must exist that affect the drying shrinkage strains in blended cement concretes. From the information available in the literature, the other parameters to consider as influencing the drying shrinkage in concrete are:

1. The fineness of the blended cement material [121]; and
2. The presence of coarse aggregates [122].

In concrete, the fineness of the blending material (and the cement also) has two important properties that play a vital role in determining the pore structure of the concrete:

- a. The specific surface area of the blending material [57]; and
- b. The initial particle size distribution of the cement [110].

The specific surface area is an intrinsic property, while the initial cement-particle size distribution is dependent on the former as well as the other factors, such as adequate dispersion of the cement particles, curing conditions and the water-cement ratio [110].

Increase in the coarse aggregates reduces the total volume of cement paste; thereby

reducing the drying shrinkage, while a larger maximum size of the aggregates also reduces the drying shrinkage by reducing the available surface area to be coated by the cement paste [122].

In this study, the maximum size of the coarse aggregates and the fine-to-coarse aggregate ratio were kept invariant in all mixes, thus ensuring that the drying shrinkage strains could be compared between types and dosages of blended cement concretes. It follows, therefore, that the fineness of the blended cement material remains the only other parameter that would affect the drying shrinkage strains.

Based on the information available from the literature and the results of this study, the following mechanisms are proposed to explain the effect of silica fume on drying shrinkage in concrete.

The first mechanism proposed by a previous research [49] is that silica fume reduces the permeability and pore size in concrete, which could reduce the rate of drying shrinkage, since it will take more time for water to find its way out of the specimens.

In the second mechanism, the increase in the surface area of the silica fume increases the densification of the microstructure of the concrete and reduces the size of the capillary

pores both in the matrix and in the paste-aggregate interface, thus increasing the capillary pressure. Accordingly, the rate of drying shrinkage will be larger and the magnitude of shrinkage to be greater. This second mechanism has been proposed by Bentur and Cohen [117] and has been used by Cohen *et al.* [118] to explain the increased drying shrinkage of expansive-cement containing silica fume. As explained in Chapter 2, a direct relationship exists between the specific surface areas of the silica fume and the capillary pore pressure. In this study, the differences in the specific surface area of the various types of silica fume were not that significant. Furthermore, this could not explain the decrease/increase of the drying shrinkage strains with increasing the dosage of silica fume that varied with the different types of silica fume cement concretes. In those silica fume cement concretes that utilized densified silica fume, the specific surface area of agglomerated silica fume particles could play a significant role, a situation that will lead to the effect of the third mechanism.

In the third mechanism, as a result of the severe exposure and curing conditions, and the dispersion of agglomerated particles, the initial particle size distribution of the cement paste influences the movement of free water within the cement paste and at the aggregate-paste interface. Increasing the dosage of silica fume has the effect of increasing the rate of pozzolanic reaction which, depending on the availability of water (and the other factors mentioned earlier), proceeds to completion or remains incomplete. In the

silica fume cement concretes with high reactivity, the pozzolanic reaction proceeds to completion producing concrete matrices having denser pores that prevent the evaporation of free water, thereby reducing drying shrinkage strains. In those silica fume cement concretes that exhibit lower reactivity, increasing the dosage of silica fume probably increases the amount of unhydrated cement paste, leading to coarser pores, higher rates of evaporation of free water and, consequently, higher drying shrinkage strains.

Figures 4.29 through 4.31 depict the drying shrinkage strains vs. the APR in the silica fume cement concretes for different dosages of silica fume. The APR is used as an indicator of the denseness of the silica fume cement concrete. Types 4 and 5 silica fume cement concretes had the lowest APRs indicating denser pores, while the APRs of Types 1, 2 and 3 silica fume cement concretes were higher, indicating coarser pores in these silica fume cement concretes. The APR increases in the order of Type 2, 1 and 3 silica fume cement concretes. From these Figures, it can be observed that the maximum drying shrinkage values increased with the dosage of silica fume, ranging from 1083 μm at 5% replacement of Type 4 silica fume to 1304 μm at 10% replacement of Type 2 silica fume, the corresponding APRs are 6.16 nm and 6.93 nm. In Types 4 and 5 silica fume cement concretes, a reduction in the drying shrinkage strains was noted as the dosage of silica fume was increased. In the case of Types 1, 2 and 3 silica fume cement concretes, the drying shrinkage strains increased as the dosage of silica fume was increased. In Figure

4.31, a maximum value of the drying shrinkage strain is clearly shown, after which the drying shrinkage strains decreased. From these results and the information previously presented from the literature, it can be observed that the various mechanisms that affect the drying shrinkage strains in silica fume cement concretes occur concurrently.

In order to reduce drying shrinkage under hot weather conditions, it is recommended to use the type and dosage of silica fume that would prevent the evaporation of free water by increasing the refinement of the pores of the concrete, having an APR as low as possible.

The specific surface area of plain, fly ash and Superpozz® cement pastes is significantly lower than that of the silica fume cement pastes. Therefore, the mechanisms that affect the drying shrinkage strains in these concretes would differ from those that affect the drying shrinkage strains in the silica fume cement concretes. With APRs of 7.16 and 7.26 nm, respectively, plain and fly ash cement concretes have pores that are very coarse (relative to their surface areas). The initial pore size distribution retains very little free water, therefore, after the exposure and curing periods, little free water is available within the pores of the concrete to evaporate, thus the drying shrinkage in these types of cement concretes are generally lower than those of the silica fume cement concretes. With an APR of 5.63 nm, Superpozz® cement concrete has the smallest APR value compared to

all the other types of cement pastes. However, Superpozz® cement concrete did not have the lowest value of drying shrinkage strain. This could be attributed to its very low specific surface area of 1.3 m²/g. The denseness of the pores without a concomitant increase in the specific surface area permits an increase in the capillary pore pressure, loss of free water and hence a lower drying shrinkage strain.

Table 4.15: Maximum drying shrinkage in plain and blended cement concrete slab specimens.

Type of Silica Fume	% Replacement	Drying Shrinkage after 90 Days (μm)
Type 1	5	831
	7.5	1219
	10	1226
Type 2	5	614
	7.5	664
	10	1304
Type 3	5	569
	7.5	962
	10	1010
Type 4	5	1083
	7.5	829
	10	629
Type 5	5	752
	7.5	503
	10	487
Plain	0%	723
FlyAsh	30%	792
Superpozz®	10%	898

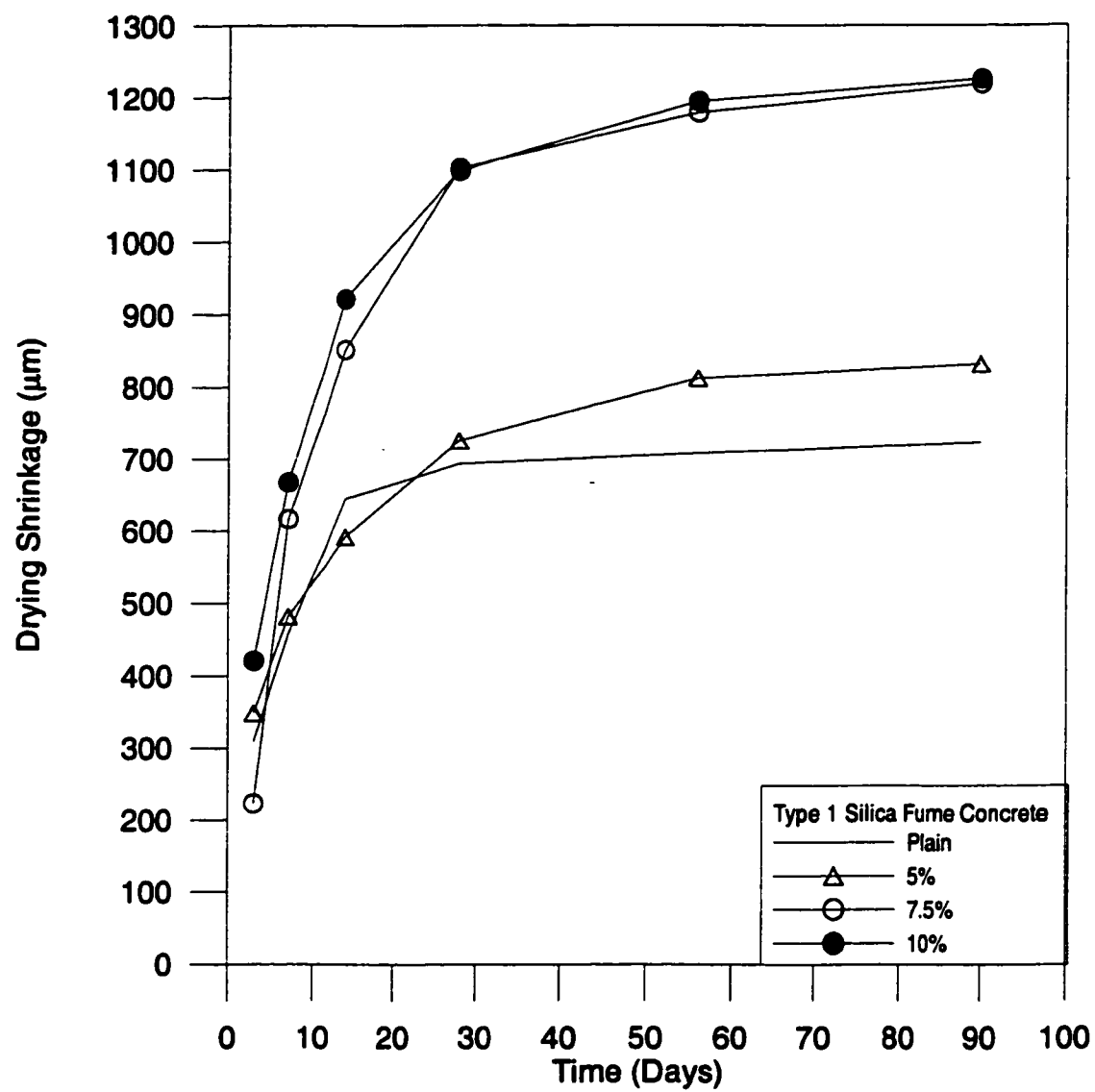


Figure 4.23: Drying shrinkage of Type 1 silica fume concrete slabs.

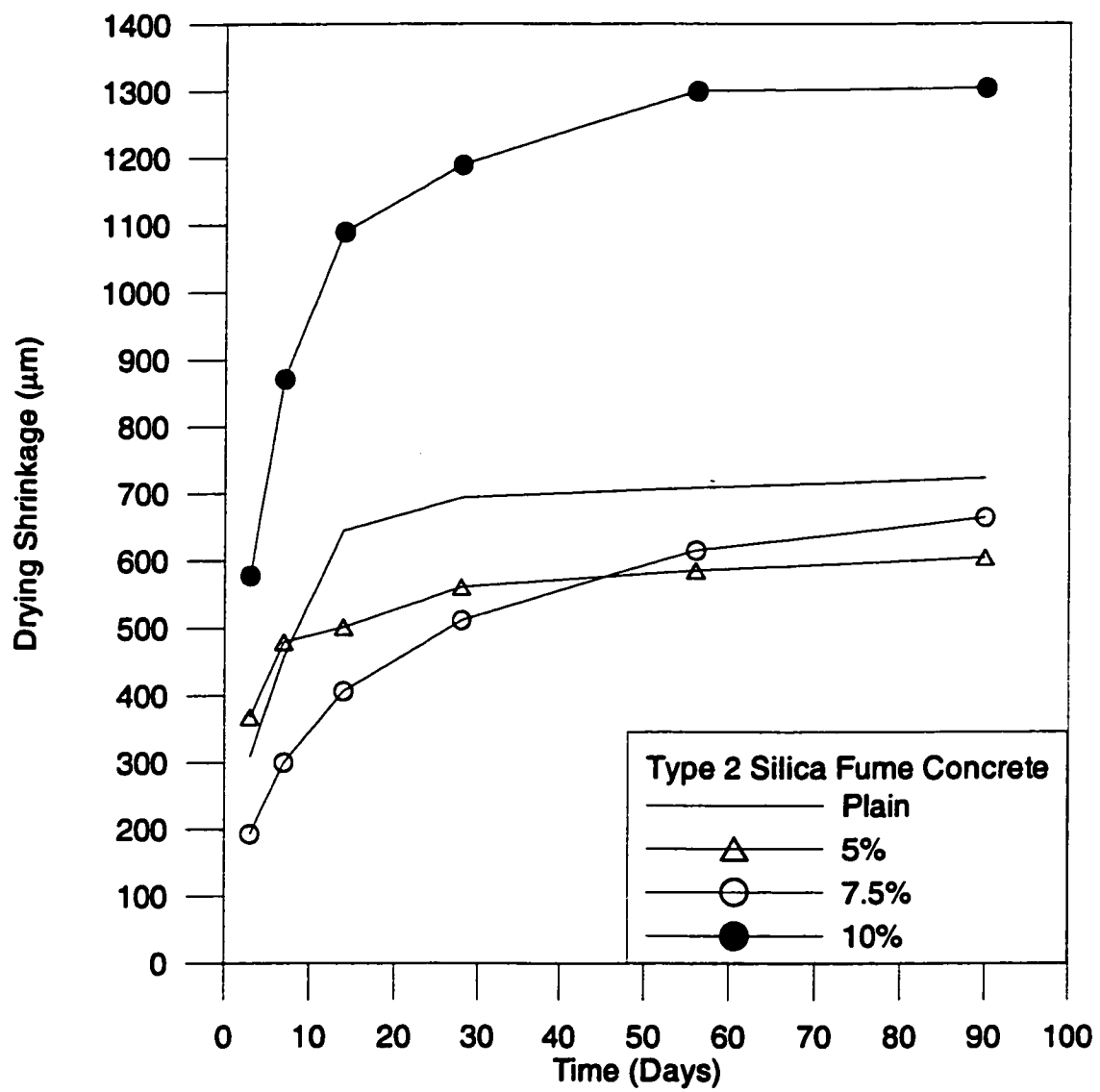


Figure 4.24: Drying shrinkage of Type 2 silica fume concrete slabs.

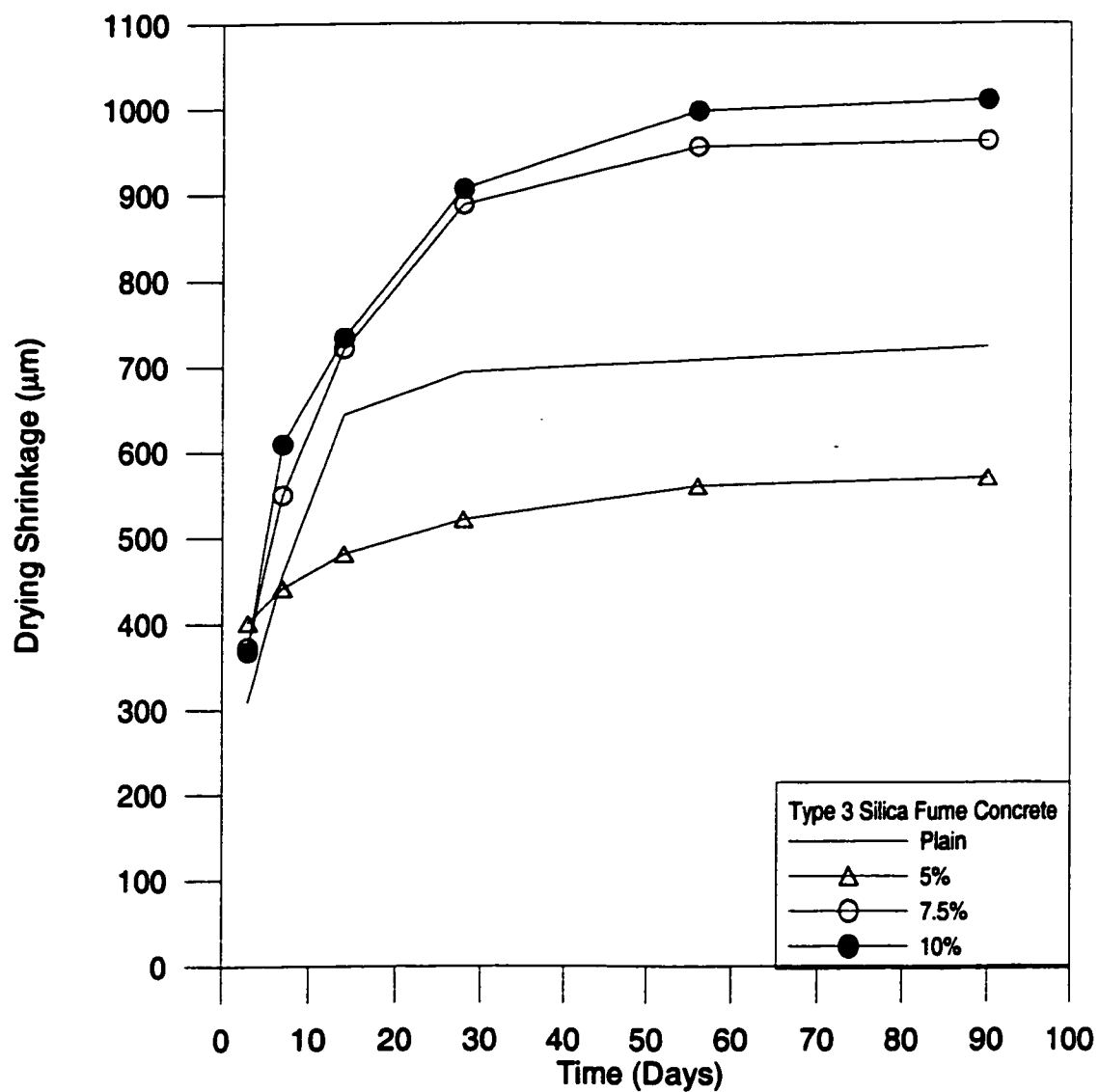


Figure 4.25: Drying shrinkage of Type 3 silica fume concrete slabs.

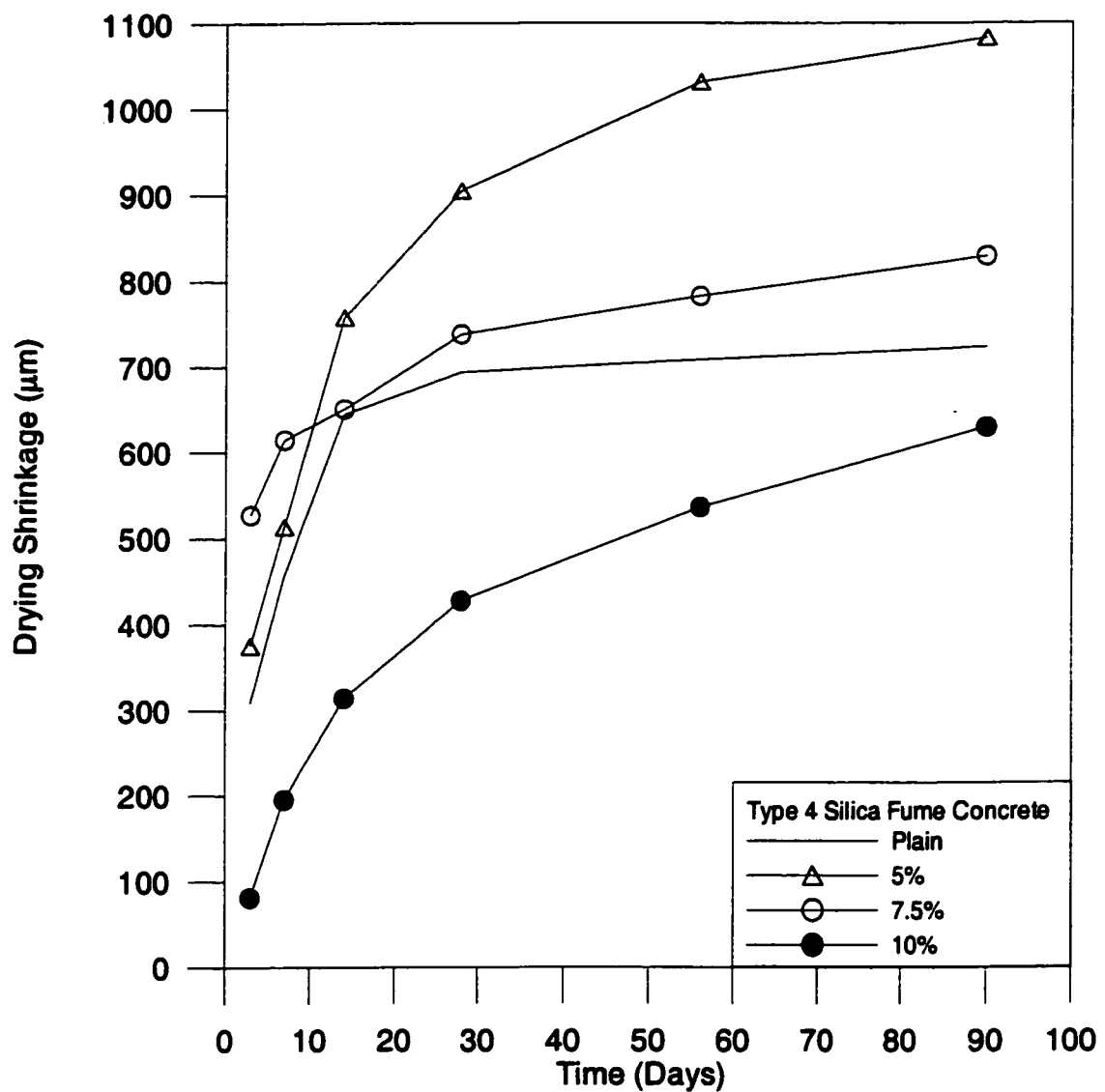


Figure 4.26: Drying shrinkage of Type 4 silica fume concrete slabs.

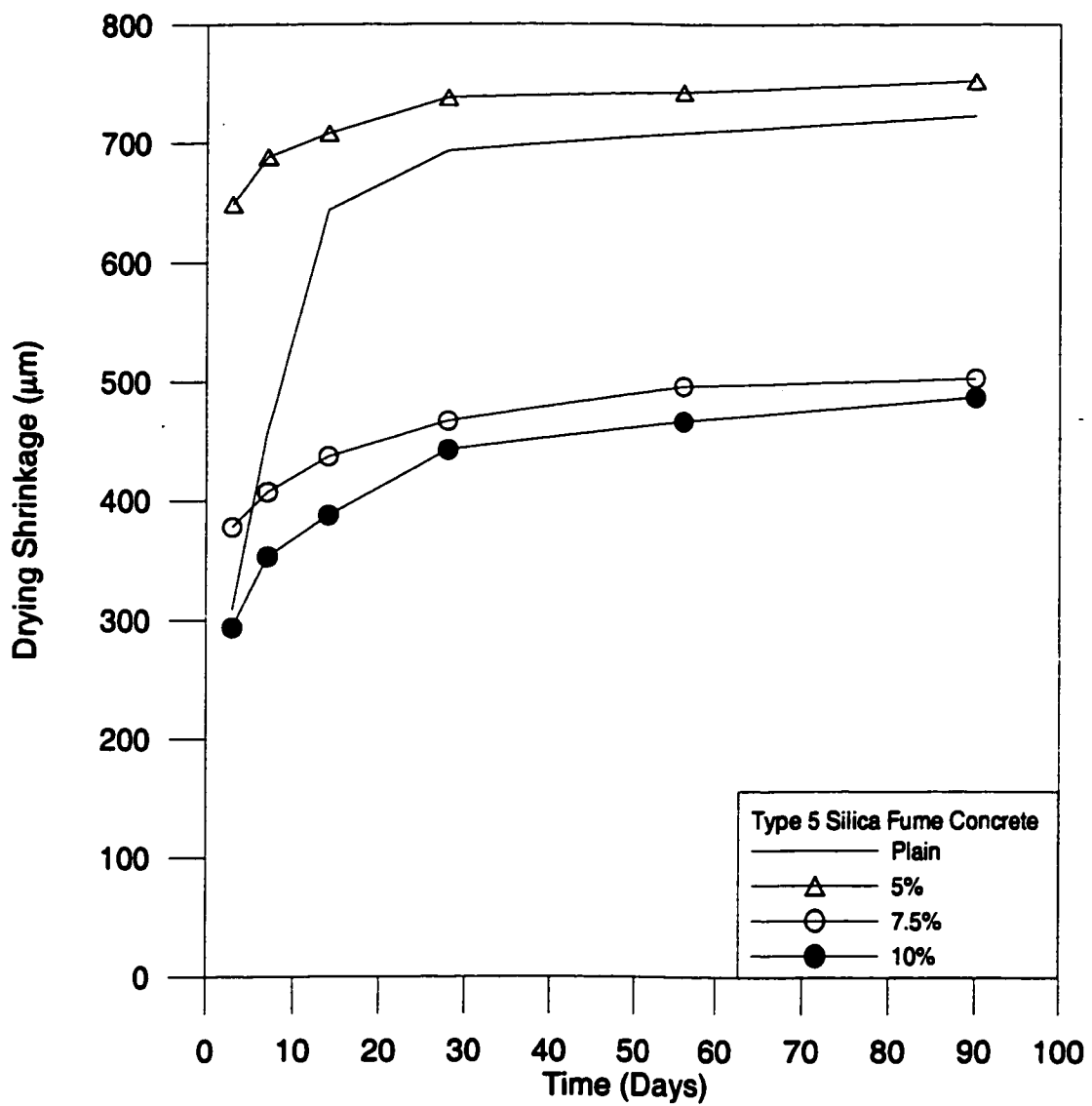


Figure 4.27: Drying shrinkage of Type 5 silica fume concrete slabs.

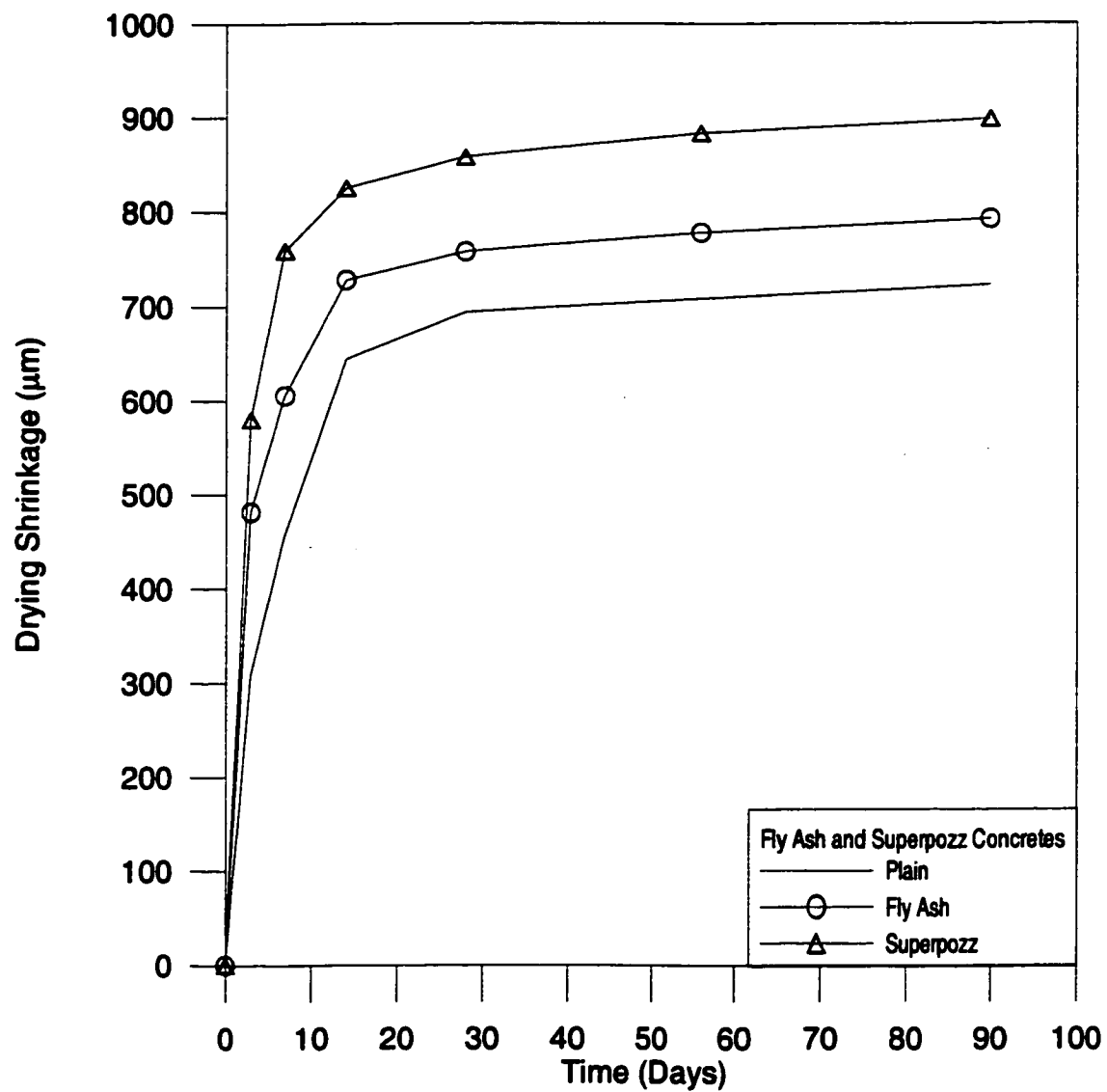


Figure 4.28: Drying shrinkage of plain, fly ash and Superpozz® concrete slabs.

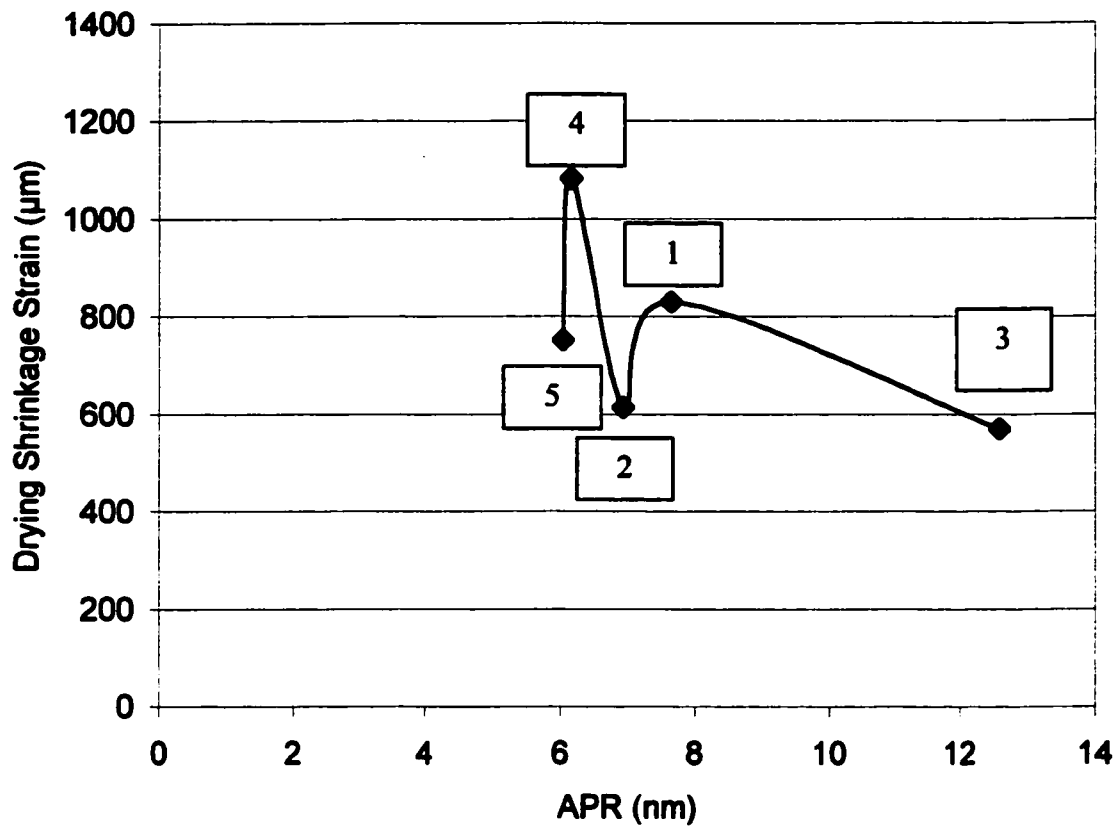


Figure 4.29: Drying shrinkage strains vs. APR for silica fume dosages of 5%.

1	2	3	4	5	- Types 1, 2, 3, 4, 5 silica fume cements
PL					- plain
FA					- fly ash
SP					- Superpozz®

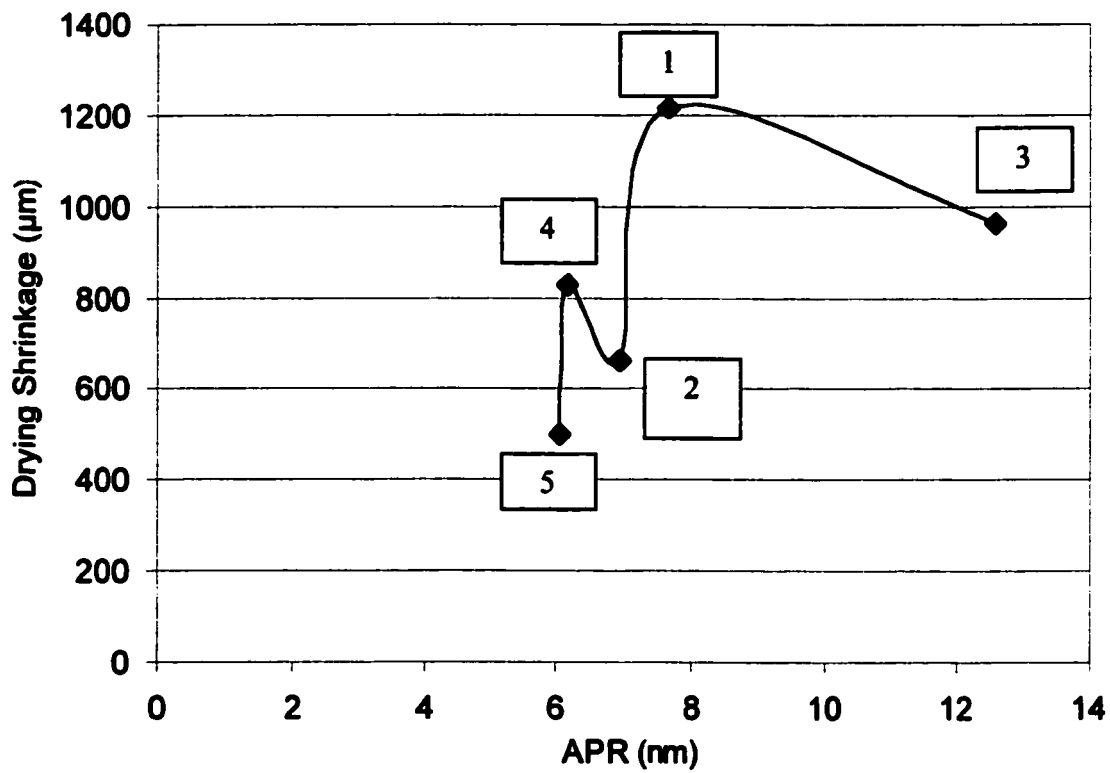


Figure 4.30: Drying shrinkage strains vs. APR for silica fume dosages of 7.5%.

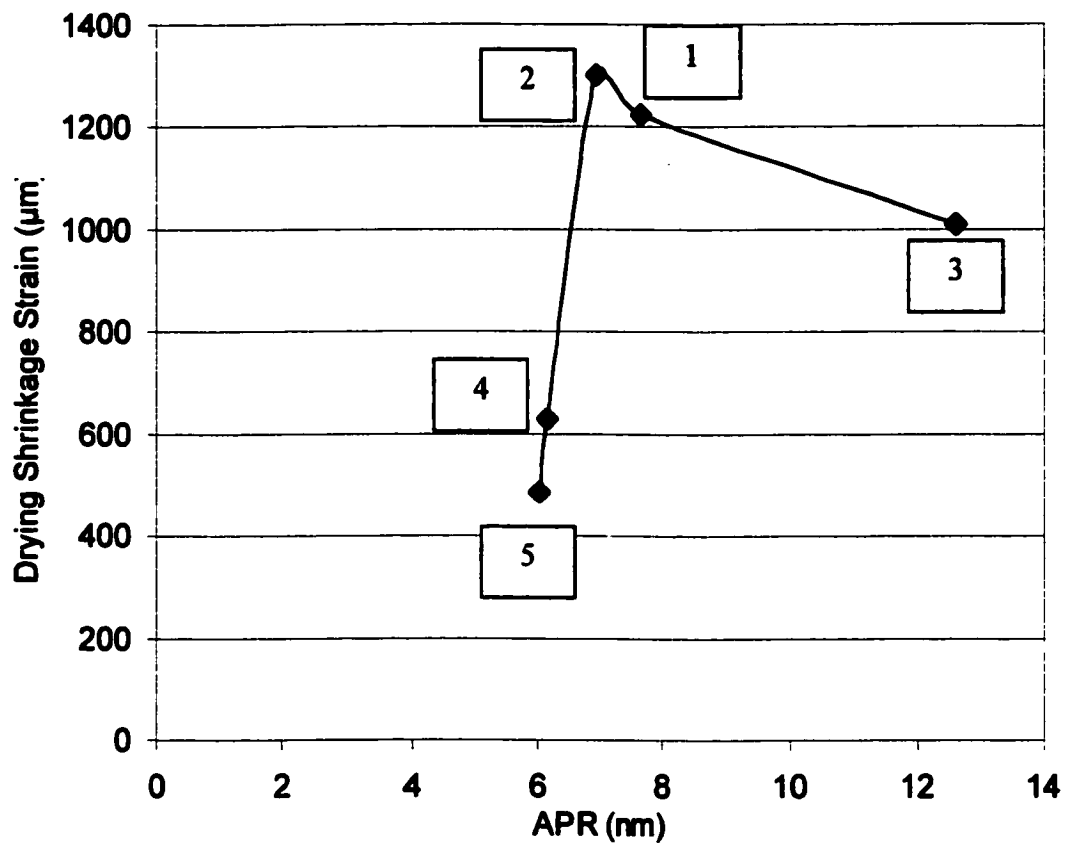


Figure 4.31: Drying shrinkage strains vs. APR for silica fume dosages of 10%.

4.5.5 Comparison of Drying Shrinkage values

Drying shrinkage in concrete is influenced by several parameters that include composition of ingredient materials and exposure conditions, namely relative humidity, temperature and wind velocity [123].

The material effect includes the following:

- Water/cement ratio [124];
- Mix design [125];
- Presence of admixtures, such as superplasticizers and silica fume [113,114]; and
- Specimen size [126].

Exposure conditions include:

- Curing [123]; and,
- Relative humidity [123].

Almudaiheem [123] provided an excellent compendium of drying shrinkage values from literature showing the effects of specimen size, relative humidity and ultimate drying shrinkage values. For 152 x 457 mm cylinders exposed at 20% and 50% RH, the ultimate shrinkage values were 1138 μm and 1092 μm , respectively, which are comparable to

what was obtained in this research which are 1072 μm for plain mortar specimens and 722 μm for concrete slab specimens, respectively, after 90 days of exposure.

Swamy and Lambert [127] also provided an excellent compendium of drying shrinkage values with 500 days being considered as ultimate for fly ash cement concrete. Again, the values of 792 μm and 893 μm obtained for fly ash and Superpozz[®] cement concretes, respectively, compared well to the values reported by them.

According to the manufacturer of Superpozz,[®] the special characteristic that make it a super-pozzolan, (and as a substitute for silica fume) is its very fine surface area of 1300 m^2/kg and that it is fine enough to achieve 99% passing an ASTM 25 μm sieve. This property along with those stated in Table 3.10 (it satisfies ASTM requirements for a Class F pozzolan) made it possible to classify Superpozz[®] as a very fine fly ash (FFA) according to the terminology used by Haque and Kayali [121], which is somewhat similar to the fly ash that was used in their study. With a mix design of 400 kg/m^3 of cement and 10% replacement with FFA, a maximum strain of 425 μm was reported at 56 days for 100 mm cubes. The cubes were initially cured in a fog room at $21 \pm 2^\circ\text{C}$ for 7 days at a RH of $95\% \pm 3\%$ before being transferred to a control room at $23 \pm 2^\circ\text{C}$ and RH of $40 \pm 5\%$ for the duration of the test. This contrasted with values of 1175 and 885 μm obtained for Superpozz[®] mortar and concrete, respectively. This difference could be attributed

mainly to the water-binder ratio of 0.35 used by the authors as opposed to the 0.5 used for the mortar bars and 0.45 for the concrete used in this study.

4.6 TEMPERATURE DISTRIBUTION IN CONCRETE SLABS

The temperature distribution in the concrete slabs was obtained from about 30 minutes after the addition of mixing water up to 24 hours thereafter.

4.6.1 Effect of Cement Type

Figures 4.32 through 4.36 display the temperature distribution in the silica fume cement concrete slabs at various dosages of silica fume from the time of placement to about 24 hours. The specimens were exposed to a temperature of 45°C, RH of 35% and a wind velocity of 15 km/hr. The initial temperature of placement varied between 28°C and 35°C as could be seen from initial data points on the graphs after approximately 30 minutes after the addition of mixing water to the concrete. As shown in Figure 4.32, for Type 1 silica fume cement concrete at a dosage of 5%, the temperature increased from 32.6°C (at placement) up to a peak value of about 45°C after 6 hours. Thereafter, the temperature decreased gradually. All the other types of silica fume exhibited a similar trend at all dosages. Furthermore, no significant variation was noted between the temperature of

plain and blended cement concretes. Brull *et al.* [128] reported almost a similar trend as observed in this investigation.

The variation in the peak temperature, in terms of dosage and type of silica fume, was not very substantial ranging between 44.5°C and 45.8°C for all the types of silica fume cement concretes investigated.

Figure 4.37 depicts the temperature distribution in plain, fly ash and Superpozz® cement concretes. There were very little differences in the maximum temperature values for these cement concretes, a trend similar to those noted in the silica fume cement concretes.

Table 4.16 shows the time when the peak temperature was achieved. This time ranged between 4 and 7 hours for all types and dosages of blended cements, with the exception of Types 4 and 5 silica fume cement concrete that exhibited peak times of about 9 hours.

4.6.2 Discussion on the Effect of Cement Type

The exposure temperature as well as the hydration of cement influenced the temperature of the concrete slabs. An increase in the exposure temperature increased the rate of hydration reaction between the cement particles and water as well as the pozzolanic reaction between the silica fume and calcium hydroxide. An increase in heat of hydration

has been observed when the dosage of silica fume is increased in the cement paste [92].

Table 4.16 depicts the data on the time to achieve peak temperature rounded to the nearest 0.5 hour. It can be observed that the external exposure temperature played a dominant role in determining the temperature of the concrete slabs as compared to the internal temperature due to the heat of hydration. The temperature distribution in the concrete slabs was neither sensitive to the type of blended cement, nor to the dosage of silica fume.

Table 4.16: Summary of time to peak temperatures for plain and blended cement concretes.

Type of cement	Time for Peak Temperature (Hours)		
	5%	7.5%	10%
Type 1	6.0	6.0	5.0
Type 2	4.5	5.5	5.0
Type 3	5.5	6.0	7.5
Type 4	6.5	9.0	7.0
Type 5	4.5	9.5	4.5
Plain (0%)	6.0	--	--
Fly ash (30%)	4.5	--	--
Superpozz® (10%)	6.0	--	--

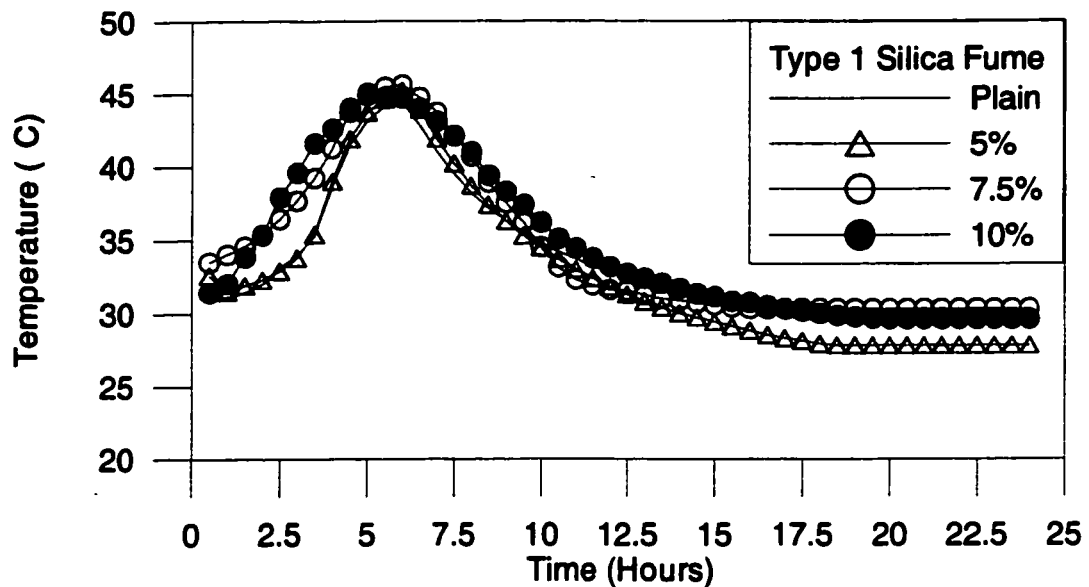


Figure 4.32: Temperature variation in Type 1 silica fume cement concretes with time.

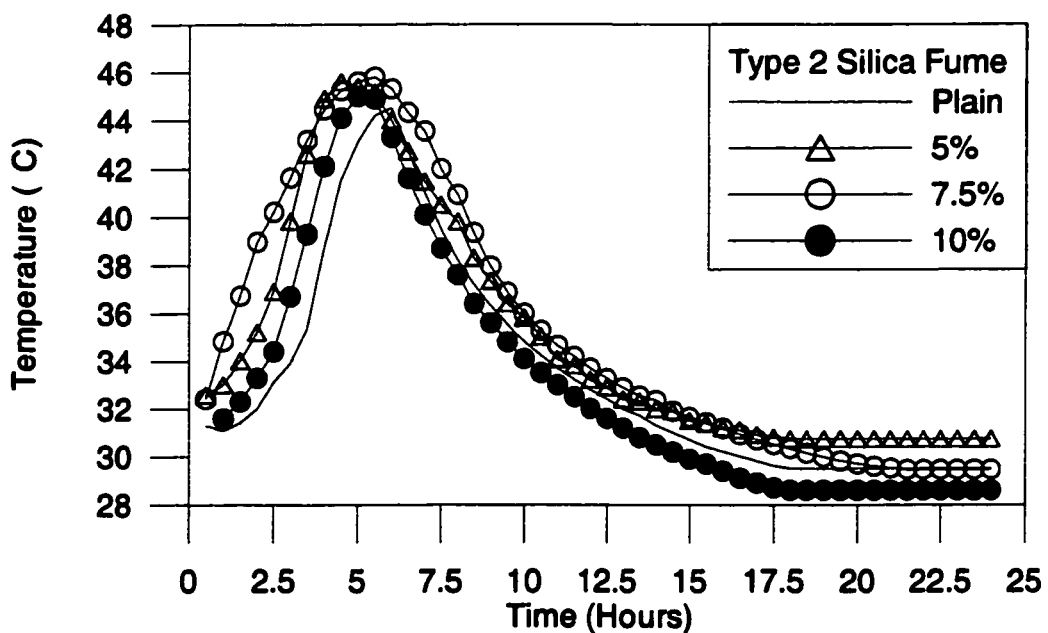


Figure 4.33: Temperature variation in Type 2 silica fume cement concretes with time.

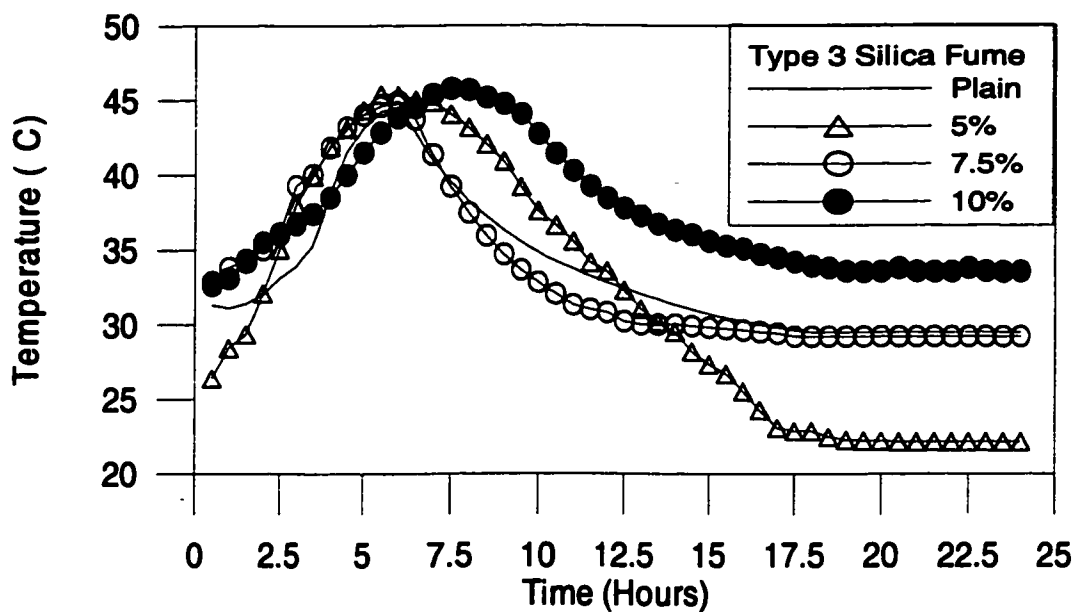


Figure 4.34: Temperature variation in Type 3 silica fume cement concretes with time.

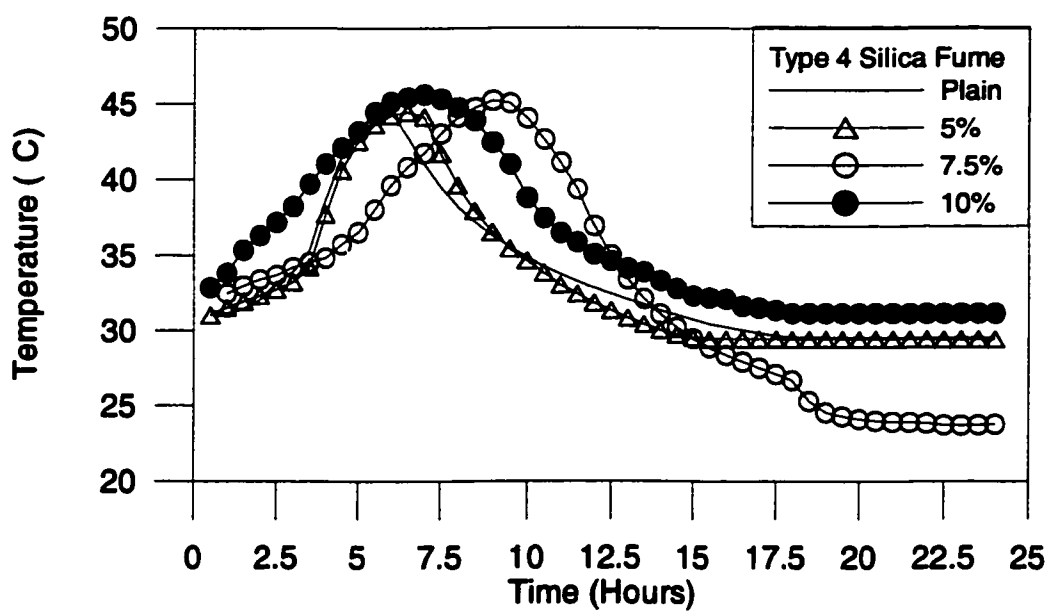


Figure 4.35: Temperature variation in Type 4 silica fume cement concretes with time.

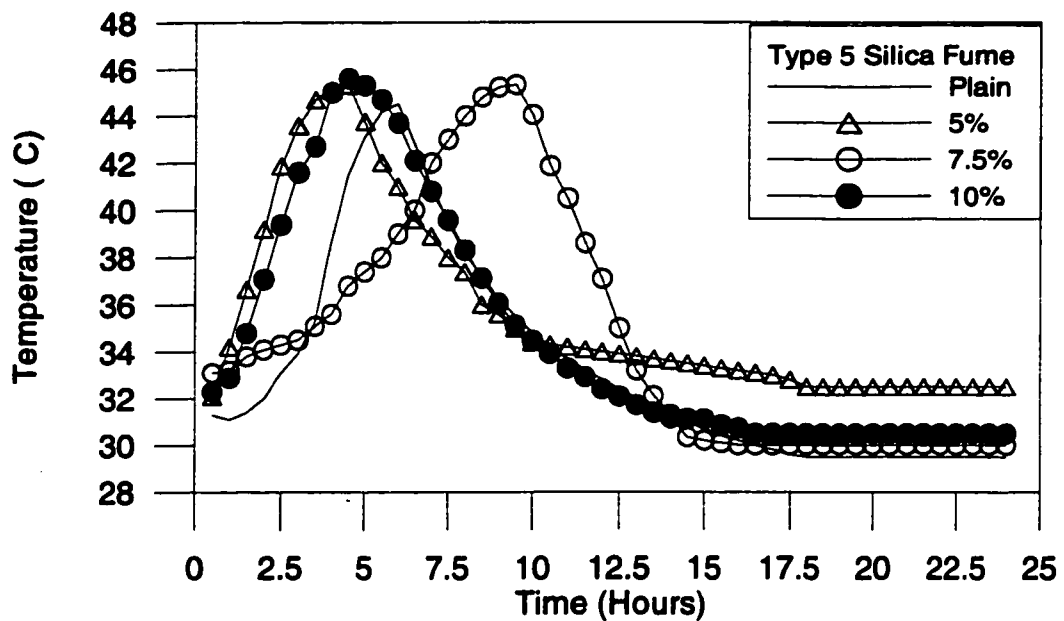


Figure 4.36: Temperature variation in Type 5 silica fume cement concretes with time.

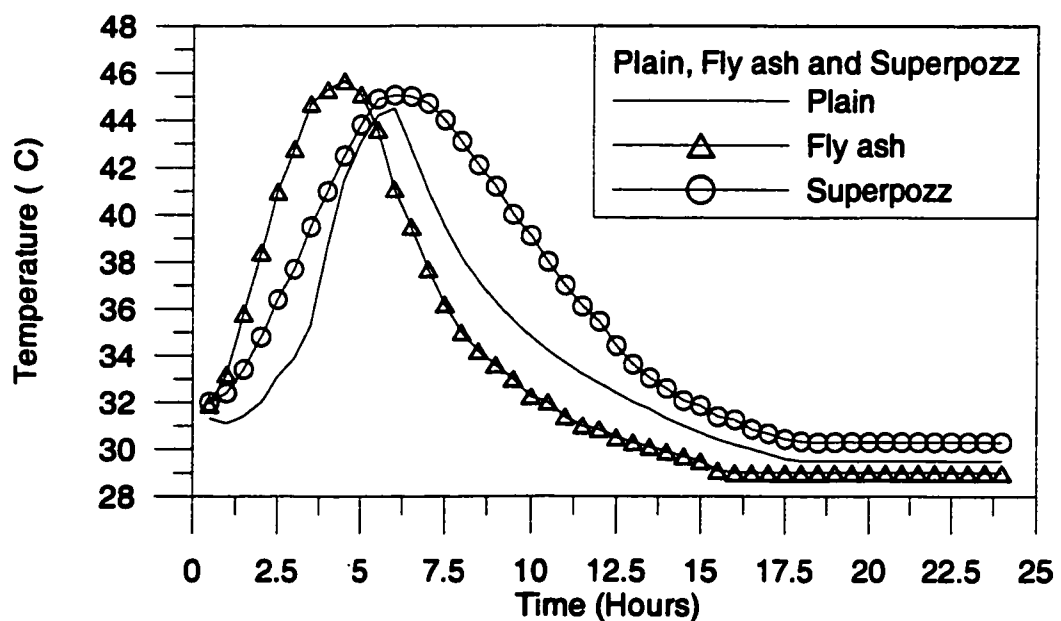


Figure 4.37: Temperature variation in plain, fly ash and Superpozz[®] cement concretes with time.

4.6.3 Effect of Exposure Conditions on the Temperature Variation

Effect of Exposure Temperature

Figure 4.38 shows the effect of exposure temperature in Type 1 silica fume cement concrete at a constant dosage of 7.5%. The placement temperature is shown as the first point on the curve.

At an exposure temperature of 25°C, the concrete temperature had a peak value of 26.7°C. At an exposure temperature of 35°C, the concrete temperature had a peak value of 32.3 °C that was just a little higher than that at 25°C. At an exposure temperature of 45°C, the peak concrete temperature was 40.0°C.

Table 4.17 shows the time to achieve the maximum peak temperature at various exposure temperatures. The increase of the exposure temperature from 25°C to 35°C accelerated the peak time by reducing it from 3 to 1.5 hours in addition to increasing the peak temperature from 26.9 °C to 32.3 °C. However, when the exposure temperature was increased to 45°C, the peak time increased to 4.5 hours.

Effect of Relative Humidity on Concrete Temperature

Figure 4.39 depicts the variation of the concrete temperature in the specimens exposed to

varying relative humidities and a constant wind velocity of 15 km/hr and a temperature of 45°C. There was little variation in the peak temperature, which ranged from 44.1 to 44.9°C when the relative humidity was increased from 25 to 60%.

As shown in Table 4.18 the time to achieve the maximum temperature also did not change appreciably with changes in the relative humidity. Thus, changes in the relative humidity had a negligible effect on the time to achieve peak concrete temperature.

Effect of Wind Velocity on Concrete Temperature

Figure 4.40 shows the effect of wind velocity on the concrete temperature. Again, no appreciable change was noted in the peak concrete temperature due to the variation in wind velocity. Peak temperatures of 44.2, 45.0 and 44.1°C occurred at wind velocities of 0, 10 and 15 km/hr, respectively. As the wind velocity was increased from 0 to 10 km/hr the time to achieve peak concrete temperature increased, while it decreased when the wind velocity was increased from 10 to 15 km/hr.

As shown in Table 4.19, there was no appreciable change in the time to achieve peak temperature with varying wind velocity. However, comparing the values in Tables 4.18 and 4.19, it can be noted that there was an increase in the peak times when the wind velocity was varied compared to the case when the relative humidity was varied. This is

expected, as the introduction of wind reduces the concrete temperature thereby increasing the time it will take to achieve peak temperature.

4.6.4 Discussion on the Effect of Exposure Conditions on Peak Concrete Temperature

Increasing the exposure temperature from 25 to 35°C reduced the time to achieve the peak concrete temperature from 3 to 1.5 hours, with a similar initial placement temperature at both exposure temperatures. At an exposure temperature of 25 °C the peak concrete temperature was 26.7 °C, while at an exposure temperature of 35 °C the peak concrete temperature was 32.3 °C. Therefore, increasing the temperature from 25 to 35°C increased the rate of reaction. At lower temperatures of 25 and 35 °C, the concrete was not very much affected by the exposure temperature; therefore, the pozzolanic reaction took place at a slower rate, in the presence of available water. When the temperature was increased to 45 °C, the pozzolanic reaction proceeded at a much faster rate and although the rate of evaporation of water would be higher than at 25 or 35 °C, there was still enough water available to enable the pozzolanic reaction last longer. This could be a result of the reaction starting at an earlier time, rather than at a later one due to the increased exposure temperature.

Varying the relative humidity did not significantly affect the peak temperature in the

concrete specimens. This could be attributed to the fact that the exposure conditions were quite severe; therefore, changes in the internal concrete temperature remained unchanged.

Varying the wind velocity had the effect of increasing the peak times by comparing the values in Table 4.18 and 4.19. This is attributed to the fact that increasing the wind velocity increases the rate of evaporation that lowers the concrete surface temperature as well as the peak temperature.

Table 4.17: Effect of exposure temperature on the time to achieve peak concrete temperature.

Exposure Temperature (°C)	Time to Achieve Peak Temperature (Hours)
25	3.0
35	1.5
45	4.5

Table 4.18: Effect of exposure relative humidity on the time to achieve peak concrete temperature.

Exposure Humidity (%)	Time to Achieve Peak Temperature (Hours)
25	4.0
35	4.5
45	5.0
60	4.5

Table 4.19: Effect of exposure wind velocity on the time to achieve peak concrete temperature.

Wind Velocity (km/hr)	Time to Achieve Peak Temperature (Hours)
0	5.5
10	6.5
15	5.0

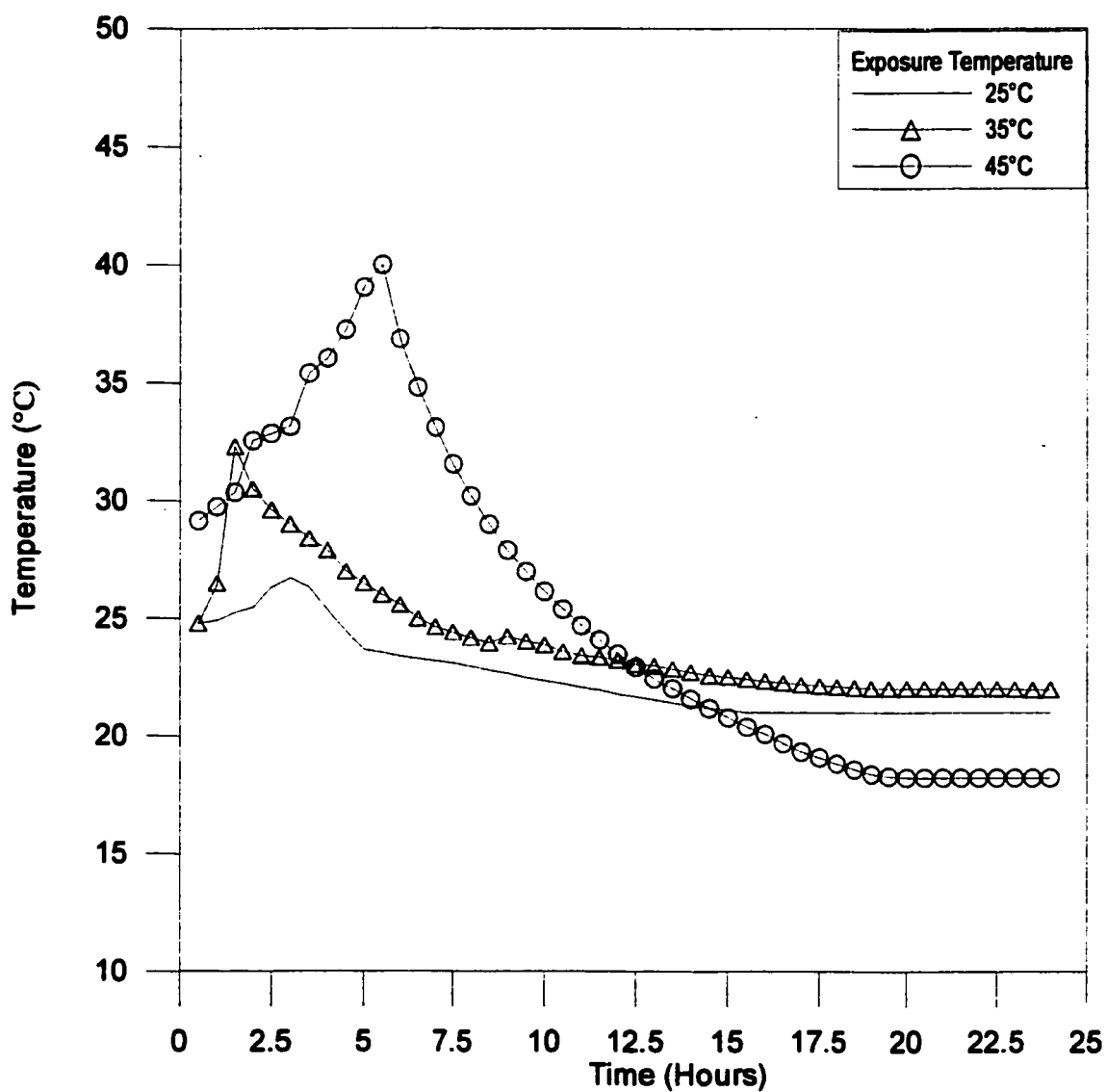


Figure 4.38: Effect of exposure temperature on concrete temperature in the concretes exposed to a RH of 50% and wind velocity of 15 km/hr (Type 1 silica fume at a dosage of 7.5%).

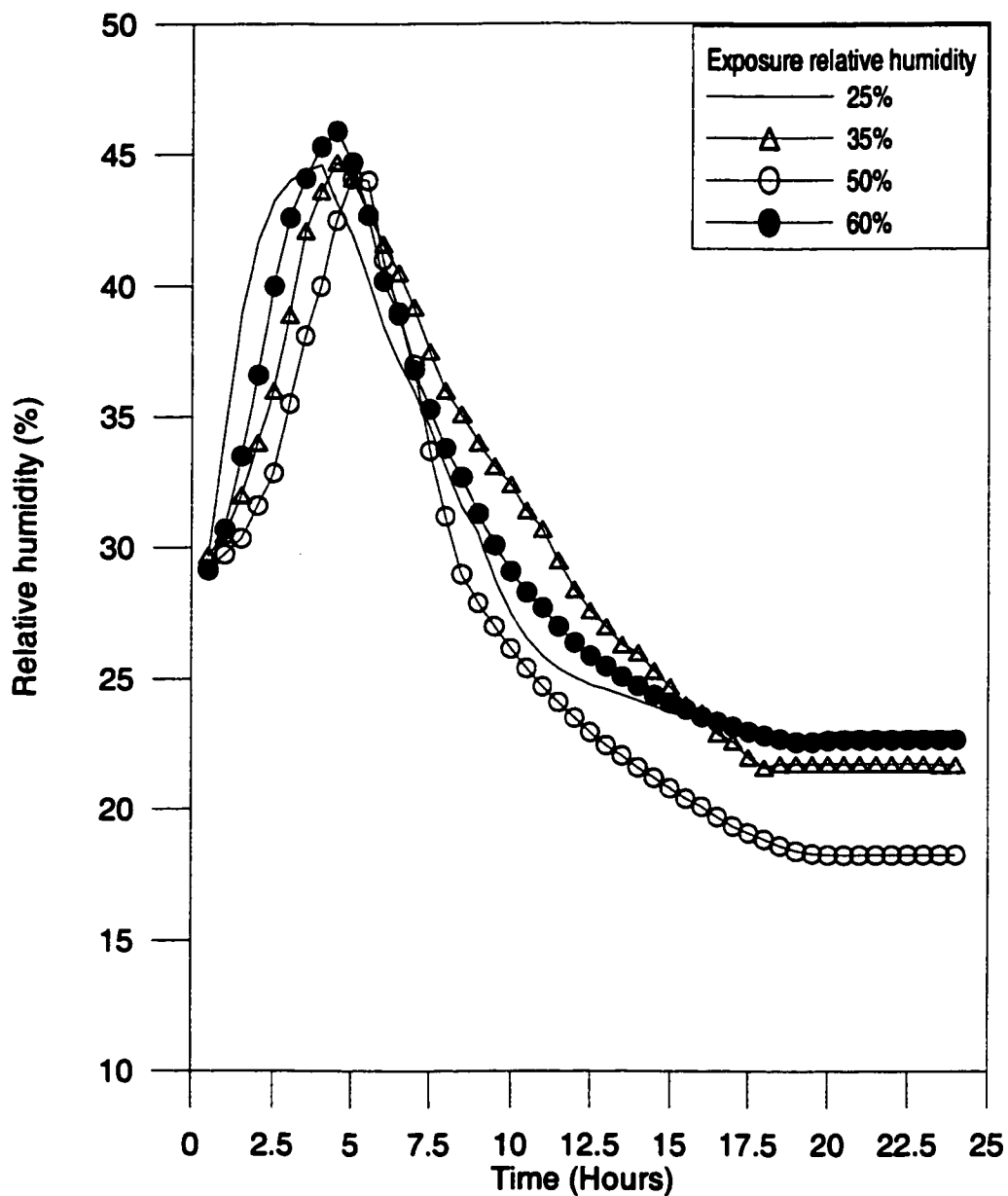


Figure 4.39: Effect of relative humidity on the concrete temperature, in the concretes exposed to a temperature of 45°C and wind velocity of 15 km/hr (Type 1 silica fume at a dosage of 7.5%).

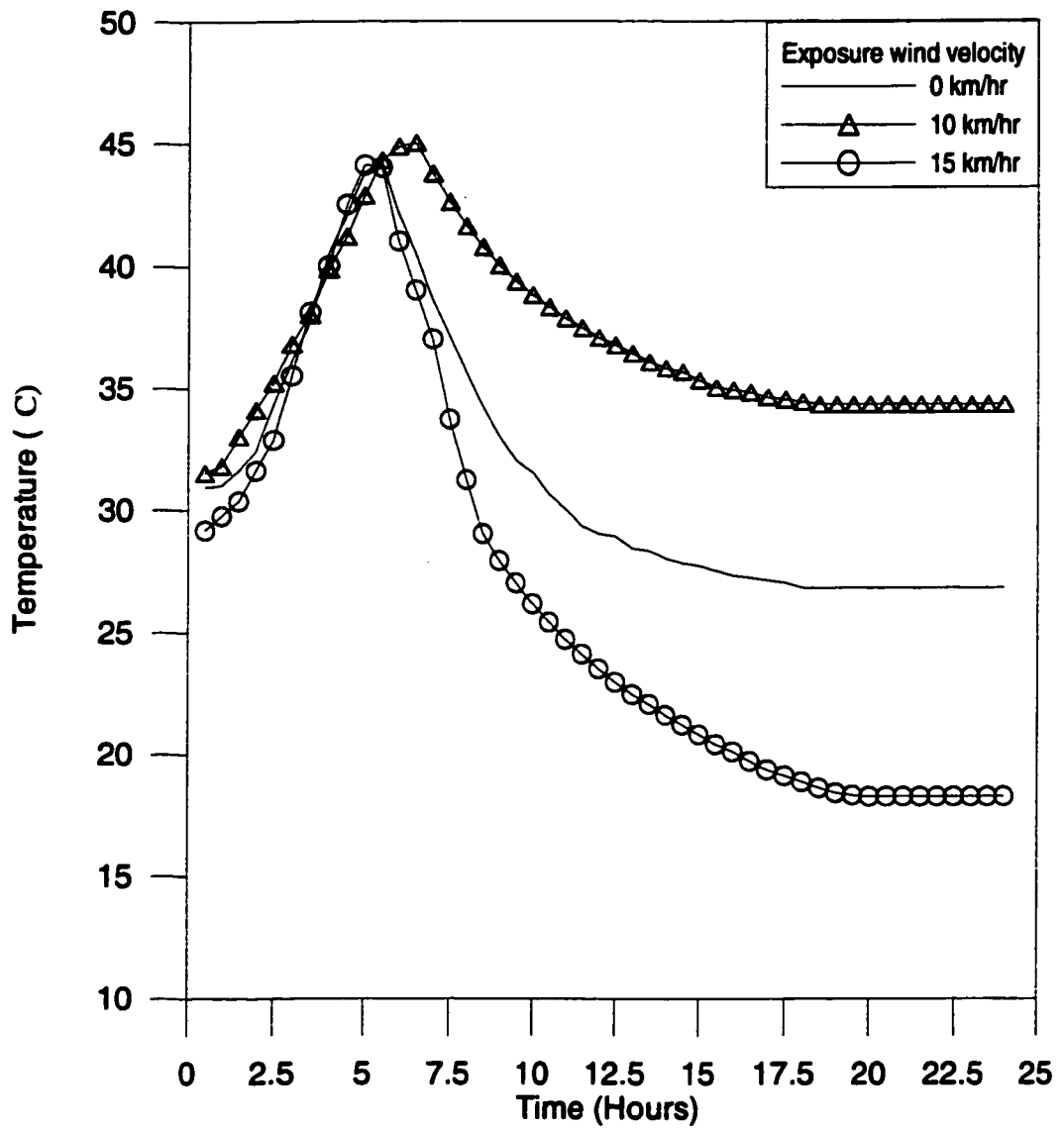


Figure 4.40: Effect of wind velocity on the concrete temperature in the concretes exposed to a temperature of 45°C and a RH of 35% (Type 1 silica fume at a dosage of 7.5%).

4.7 ULTRASONIC PULSE VELOCITY IN CONCRETE SLABS

Table 4.20 summarizes the pulse velocity after 90 days in the concrete slabs. The data in this table indicate that the pulse velocity in Types 1, 4 and 5 silica fume cement concretes decreased marginally with an increase in the dosage of silica fume from 5 to 10%. This means that the concrete specimens with 5% silica fume were denser than those with 7.5 and 10% silica fume. On the other hand, the concrete slabs made with Types 2 and 3 silica fumes exhibited a different trend; the pulse velocity increased with increasing the dosage of silica fume. Plain cement concrete with a pulse velocity of 2.92 km/s appeared to be denser than all the types of cement concretes, with the exception of Types 1, 4 and 5 silica fume cement concretes at 5% dosage. The pulse velocity in the fly ash and Superpozz® cement concretes was vividly more than that in the plain and silica fume cement concretes. Further, the pulse velocity in fly ash cement concrete was more than that of Superpozz® cement concrete.

4.7.1 Discussion on the Pulse Velocity in the Concrete Slabs

It was expected that blended cement concretes would perform better than plain cement concrete in terms of the general quality (pore refinement) of the concrete matrix as measured by the pulse velocity. The results reported in this investigation indicated

otherwise. This may be attributed to the effects of the aggressive conditions in hindering the hydration process in these types of silica fume cement concretes. Specifically, it must be noted that all the concrete slabs were cured with wet burlap for only one day after the removal from the humidity chamber and kept outside the chamber in the open air thereafter.

It can be observed that the pulse velocity results reported in Table 4.20 varied marginally for the concrete specimens prepared with the various types and dosages of silica fume.

As reported in Section 4.5, Type 1 silica fume concrete produced visible surface cracks at all dosages (see Table 4.8). The drying shrinkage of the concrete specimens prepared with this type of silica fume also increased with increasing the silica fume dosage. Thus, the presence of micro-cracks in this type of silica fume concrete probably led to an increase in the pulse velocity in this silica fume cement concrete. However, it is to be noted that micro-cracks are not distributed in the same way as surface cracks (macro-cracks) [109, 129-131]. For Types 2 and 3 silica fume cement concretes, the increase in the pulse velocity (densemess) with the silica fume dosage may be ascribed to the fact that the hydration reactions in the cement paste commenced at an earlier time. Further, with an increased exposure temperature at 45°C per se, the rate of hydration reaction was increased. Also, water necessary for the hydration process is still available at this time.

On the other hand, Types 4 and 5 silica fume cement concretes that exhibited a reduction in the pulse velocity with increasing the dosage of silica fume completed hydration at a later time, when most of the water required for hydration would have evaporated due to the aggressive exposure conditions, and therefore the water needed to complete the hydration process was not available, resulting in less dense matrix. Type 4 silica fume concrete cracked at a dosage of 10% replacement, and the results of the plastic shrinkage as well as drying shrinkage strain values suggest that micro-cracks might be present at this dosage as well.

Both fly ash and Superpozz® cement concretes had a higher pulse velocity compared to that of plain and silica fume cement concretes. Fly ash cement concretes are well known for their slow strength development especially during the first 28 days after casting [58]. While this may be considered a disadvantage in the removal of forms during construction, this could actually be an advantage under hot weather conditions. This is because this delay in the hydration is not usually affected by the severe exposure conditions, particularly at the early age when the concrete specimens are weak, as reported by a number of authors [127,132]. The higher pulse velocities noted in these types of blended cement concretes may be attributed to their lower specific surface areas. The rate of evaporation is similar in fly ash and Superpozz® cement concretes and the silica fume cement concretes, due to similar exposure conditions. A lower specific

surface area would lead to higher rates of bleeding in both fly ash and Superpozz® cement concretes, but lower capillary pore pressures. The net affect appeared to be lower rates of water loss, with more water being retained within the cement matrix of fly ash and Superpozz® cement concretes. Although the rates of hydration in these cements are lower, water was still available and retained with the cement matrix for a longer time, leading to a continuation of the pozzolanic reaction, denser matrix and, consequently, higher pulse velocities.

Table 4.20: Summary of the ultrasonic pulse velocity test results after 90 days on the concrete slab specimens.

Silica Fume	Pulse Velocity (km/s)		
	5%	7.5%	10%
Type 1	2.96	2.89	2.82
Type 2	2.81	2.84	2.85
Type 3	2.82	2.84	2.93
Type 4	3.01	2.92	2.83
Type 5	3.03	2.86	2.84
Plain (0%)	2.92	---	---
Superpozz® (10%)	3.70	---	---
Fly ash (30%)	4.40	---	---

4.8 EFFECT OF SUPERPLASTICIZERS ON THE PLASTIC SHRINKAGE STRAIN

The following types of superplasticizers were used to prepare the silica fume cement concrete mixes in order to investigate their effect on the plastic shrinkage strain and the time to achieve maximum strain:

SNP = sulfonated naphthalene polymer (Conplast M432 MS)

MLP = modified lignosulfate polymer (Sikament-520)

PCE = polycarboxylic ether (Glenium-51)

SNF = sulfonated naphthalene formaldehyde (EUCON M537 MS)

4.8.1 Maximum Strain

Figure 4.41 shows the maximum strain values in three types of silica fume at a constant dosage of 7.5% and exposed to a temperature of 45°C, wind velocity of 15 km/hr and RH humidity of 35%. This information is summarized in Table 4.21. Tables 4.22 through 4.25 depict the optimum dosages of superplasticizers used to achieve the desired workability of 50-75mm in the silica fume cement concretes.

Comparison of the effect of superplasticizers on the plastic shrinkage strain as

schematically depicted in Figure 4.41 and numerically summarized in Table 4.21 indicates that the highest plastic shrinkage strains were noted in the concrete admixed with SNP followed by SNF, PCE then MLP. It is to be noted that SNP and SNF are generically of the same family of chemical compounds, namely sulfonated naphthalene formaldehyde. Type 2 silica fume cement concrete had the highest plastic shrinkage strains in all the types of superplasticizers used in this investigation. These results are in agreement with the results of Series (Ia) experiments because Type 2 silica fume was the only type that was undensified. Plain cement concrete specimens had markedly lower strain values compared to all the other types of silica fume irrespective of the type of superplasticizer used. None of the concrete slabs with the optimum dosage of superplasticizer to achieve the necessary workability in series IV mixes exhibited cracks.

4.8.2 Discussion on the Maximum Shrinkage Strains

From the above data, it can be observed that the types of silica fume as well as the type of superplasticizer play a significant role in determining the plastic shrinkage strains in plain and blended cement concretes. In Section 4.4, a threshold value of plastic shrinkage strain that could result in cracking was reported to be $1100 \mu\text{m}$. As shown in Table 4.21, Type 2 silica fume cement concrete exhibited plastic shrinkage strains of 1251 and $1195 \mu\text{m}$, respectively, with the use of SNP and PCE types of superplasticizers. Type 3 silica fume cement concrete with SNP superplasticizer also exhibited plastic shrinkage strains of 1118

μm . Therefore, it is expected that plastic shrinkage cracks could result in these types of silica fume-superplasticizer combination.

4.8.3 Time to Achieve Maximum Strain Values

Figure 4.42 shows the time to achieve maximum strains. If we consider about 5 to 6 hours as the normal time to achieve maximum strain values from Figure 4.42, PCE generally demonstrated the highest time values indicating a strong retardation effect on plain and densified silica fume cement concretes. In the case of the undensified silica fume, Type 2, the time to achieve maximum strain was noted to be the highest with SNF.

4.8.4 Compatibility of Superplasticizer with Silica Fume

There is no widely accepted definition of incompatibility of silica fume and superplasticizers. However, based on the information available in the literature, incompatibility may be defined in this study as “any undesirable effect that may be produced in the properties of the concrete due to the combination of silica fume, cement and superplasticizer under the intended exposure conditions.” Incompatibility would be regarded as excessive retardation in the setting time, leading to a reduction in the early-age strength, and poor pore structure development due to air entraining effects of the superplasticizer, flash set, false set, etc [95].

From the data in Figure 4.42, the various accelerating and retardation effects can be detected with the use of the four types of superplasticizers with the three types of silica fume and plain cement concretes. PCE showed the strongest retardation effect in three of the four types of silica fumes considered; several authors have reported similar results [98,101,133]. PCE showed the highest incompatibility in terms of its excessive retardation. However, the 28-day compressive strength of the silica fume cement concrete incorporating PCE in fact exceeded that of the other types of superplasticizers used in one study [133]. Other studies carried out by a number of authors have shown that PCE usually performed better in refining the pore size distribution in the cement paste than the other types of superplasticizers [101]. This occurred in ordinary cement paste [101], as well as in the presence of silica fume [134]. This refinement is attributed to PCE's better dispersion mechanism compared to the other types of superplasticizer [101]. PCE exhibited the highest time to achieve maximum strain in plain and silica fume cement concretes with the exception of Type 2 silica fume cement concrete. No relationship has been reported in the literature between the state of hydration of cement and its setting time [101]. Thus, the plastic shrinkage strains of PCE can only be attributed to the fineness of the silica fume in the cement paste.

4.8.5 Effect of Superplasticizers on Plastic Shrinkage Cracking

In Series IV experiments, where the different types of superplasticizers were used with a

constant dosage of Type 1 silica fume, no plastic shrinkage cracks were observed in the concrete. As previously reported, plastic shrinkage cracks were noted in Series I experiments under similar exposure conditions to that of Series IV experiments. The lack of plastic shrinkage cracks in Series IV experiments could be attributed to a variety of reasons, namely:

1. Difference in the water-to-binder ratio of 0.45 for Series I experiments and 0.5 for Series IV experiments.
2. In the case of Series IV experiments, there were no differences in the specific surface areas of the mixes.

As mentioned in Chapter 2, the water-to-binder ratio plays a significant role in determining the plastic shrinkage potential of the resulting concrete. Although the mixes in Series I and IV were planned to achieve the same workability, the increased water-binder ratio in Series IV mixes makes it probable that more water was available in these mixes. The rate of water evaporation would be higher producing concrete having coarser pores (larger APR) that would reduce the potential for plastic shrinkage cracking.

In Series IV experiments, the specific surface area of the silica fume was similar in all the mixes. Thus, the fineness of cement binders could only be influenced by the dispersion

mechanisms of the superplasticizers and the concurrent chemical superplasticizer-cement interactions. Differences in plastic shrinkage strains were noted in the mixes, but no plastic shrinkage cracks occurred. It would appear that the APR of the silica fume in the concretes is more influential in determining the potential of plastic shrinkage cracking than the effect of pore refinement as represented by the SSA.

Table 4.21: Maximum plastic shrinkage strains in Series IV mixes (temperature of 45 °C, RH of 35% and wind velocity of 15 km/hr).

Material	Maximum Plastic Shrinkage Strain (μm)			
	SNP	MLP	PCE	SNF
Plain	620	444	521	670
Type 1	956	728	678	787
Type 2	1251	865	1195	944
Type 3	1118	668	796	730

Table 4.22: Optimum dosage of SNP (Conplast M432 MS) superplasticizer used in Series IV mixes (temperature of 45°C, RH of 35% and wind velocity of 15 km/hr).

Pozzolan	Dosage %	Required dosage of SP, %
Plain	0	2.0
Type 1 silica fume	7.5	2.4
Type 2 silica fume	7.5	2.2
Type 3 silica fume	7.5	2.3

Table 4.23: Optimum dosage of MLP (Sika-520) superplasticizer used in Series IV mixes (temperature of 45°C, RH of 35% and wind velocity of 15 km/hr).

Pozzolan	Dosage %	Required dosage of SP, %
Plain	0	1.6
Type 1 silica fume	7.5	2.0
Type 2 silica fume	7.5	1.8
Type 3 silica fume	7.5	1.9

Table 4.24: Optimum dosage of PCE (Glenium-51) superplasticizer used in Series IV mixes (temperature of 45°C, RH of 35% and wind velocity of 15 km/hr).

Pozzolan	Dosage (%)	Required dosage of SP (%)
Plain	0	0.40
Type 1 silica fume	7.5	0.70
Type 2 silica fume	7.5	0.60
Type 3 silica fume	7.5	0.66

Table 4.25: Optimum dosage of SNF (EUCON 537 MS) superplasticizer used in Series IV mixes (temperature of 45°C, RH of 35% and wind velocity of 15 km/hr).

Pozzolan	Dosage %	Required dosage of SP, %
Plain	0	0.375
Type 1 silica fume	7.5	0.775
Type 2 silica fume	7.5	0.700
Type 3 silica fume	7.5	0.750

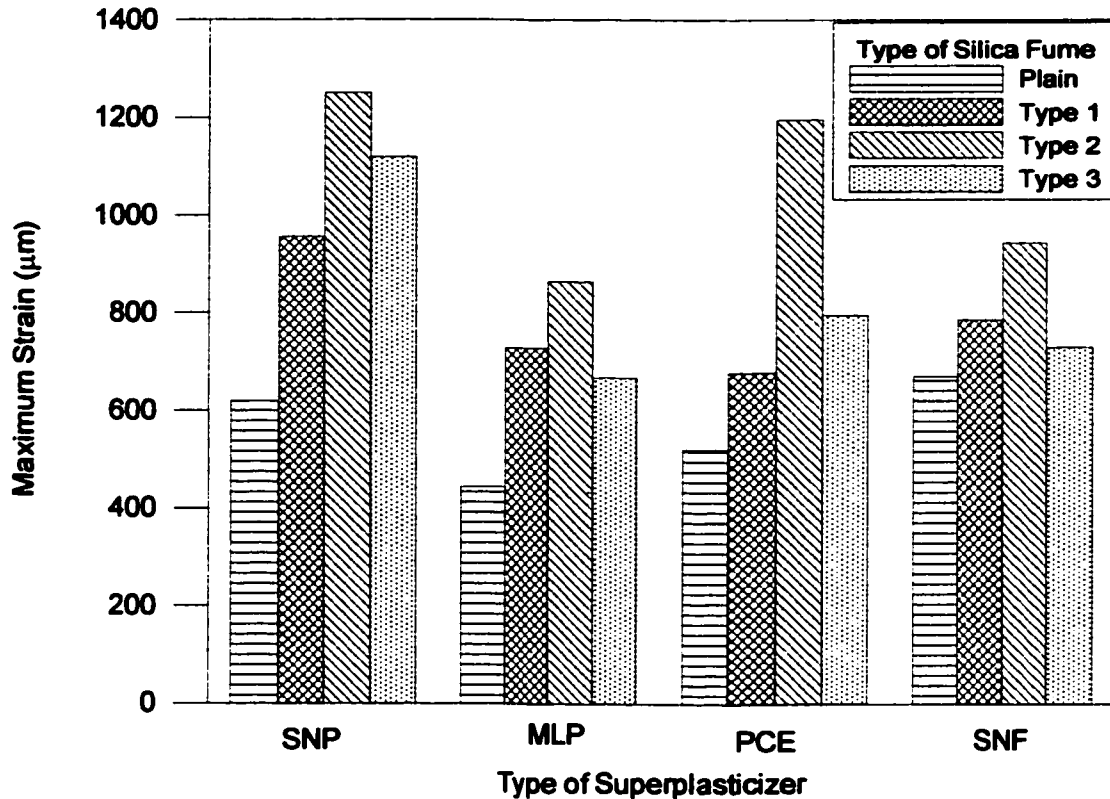


Figure 4.41: Maximum strain values in Series IV mixes (three types of silica fume at a constant dosage of 7.5% using four different types of superplasticizers).

SNP = sulfonated naphthalene polymer (Conplast M432 MS)

MLP = modified lignosulfate polymer (Sikament-520)

PCE = polycarboxylic ether (Glenium-51)

SNF = sulfonated naphthalene formaldehyde (EUCON M537 M)

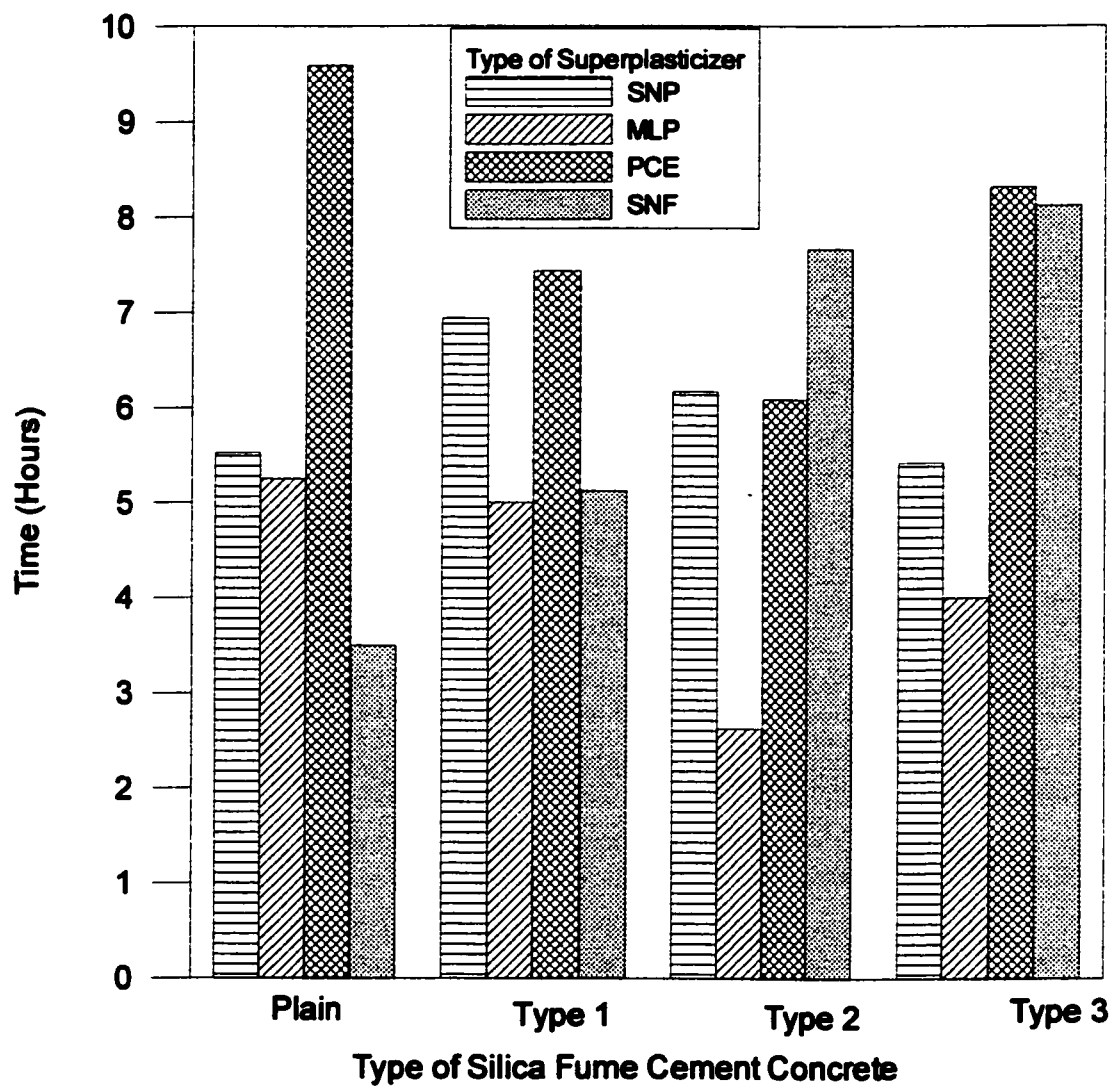


Figure 4.42: Time to achieve maximum strain values in three types of silica fume at a constant dosage of 7.5% and plain cement concrete using four different types of superplasticizers.

4.9 PORE SIZE DISTRIBUTION AND SPECIFIC SURFACE AREA OF PLAIN AND BLENDED CEMENT CONCRETES

Figures 4.43 and 4.44 depict the variation in the pore volume with the pore radius in plain and silica fume cements using the nitrogen adsorption method. For the sake of clarity, Figure 4.43 shows only the pore volume radius distribution for plain and Type 1 silica fume cement pastes. The pore volume increased with increasing the pore radius. At a pore radius of about 2 nm, perturbations can be observed in the graphs. A similar observation has been reported by a number of authors [105,135]. According to Pentala [105], at approximately this pore radius, the gel porosity is not actually the measured value; rather it is merely the pore radius where the pressure in the adsorption device has so low a value that the adsorbed nitrogen molecules in fact evaporate.

4.9.1 Variation of Pore Volume with Pore Radius for Silica Fume Cements

Figure 4.44 depicts the variation of the pore volume with the pore radius for all the types of silica fume and plain cements. There is some scatter in the data for the different types of silica fume cements. This variation is a property of the respective silica fume cement pastes [105]. Up to a pore volume of about $10 \text{ mm}^3/\text{g}$, plain cement had smallest pore radii compared to the silica fume cements. Plain cement paste did not have pore radii less than 1.9 nm (the first point for plain cement paste in Figure 4.44), while all types of silica

fumes had pore radii (and the corresponding pore volumes) smaller than this size up to 0.8 nm. Between pore volumes of 5 and 10 mm³/g, Type 4 silica fume cement paste possessed the largest pore radius, next in succession came Types 3, 2, 1, 5 silica fumes and plain cement paste; the pore volumes being between 15 and 20 mm³/g, the order from the largest to the smallest radii is: Type 3, 2, 4, 1, plain and Type 5; from pore volumes of 20 mm³/g and above the order is: Type 3, 2, 1, plain, 4 and Type 5.

4.9.2 Variation of Pore Volume with Pore Radius for Plain, Fly Ash and Superpozz® Cements

Figure 4.45 depicts the data of the pore volume with pore radius for fly ash, plain and Superpozz® cement pastes. Up to a pore volume of about 15 mm³/g, plain cement paste had the smallest pore radii compared to fly ash and Superpozz® cements. For pore volumes of more than 15 mm³/g, the order shifted to Superpozz®, plain and fly ash. Fly ash had the largest pore radii and also the largest volume of pores compared to plain and Superpozz® cements.

Table 4.26 summarizes the values of the specific surface area (SSA), the average pore radius (APR) and the total pore volume (TPV) in hydrated plain and blended cement pastes. The types of silica fume cements are ordered in terms of their specific surface area. Type 3 silica fume cement had the highest SSA, while plain cement had the lowest

SSA. The TPV shown in column three is a measure of the reactivity of the various blended cements. This is because at the pozzolanic reaction progresses, its products fill the pores the concrete, increasing the pore volume [46]. Fly ash cement had the highest TPV, while it was the least in Type 5 silica fume cement. The APR indicates the denseness of the pores within the cements; Superpozz® cement was the densest, having the smallest APR, while Type 3 silica fume cement was the coarsest, having the largest APR.

Table 4.26: Specific surface area, total pore volume and average pore radius of plain and blended cements after 56 days.

Material	Specific Surface Area (m ² /g)	Total Pore Volume (mm ³ /g)	Average Pore Radius (nm)
Type 3-7.5	27.7	31.12	12.57
Type 1-7.5	23.5	28.54	7.65
Type 4-7.5	20.3	30.76	6.16
Type 5-7.5	18.06	20.32	6.04
Type 2-7.5	16.70	32.47	6.93
Superpozz®	1.30	22.52	5.63
Fly ash	0.30	33.81	7.26
Plain	0.25	18.82	7.14

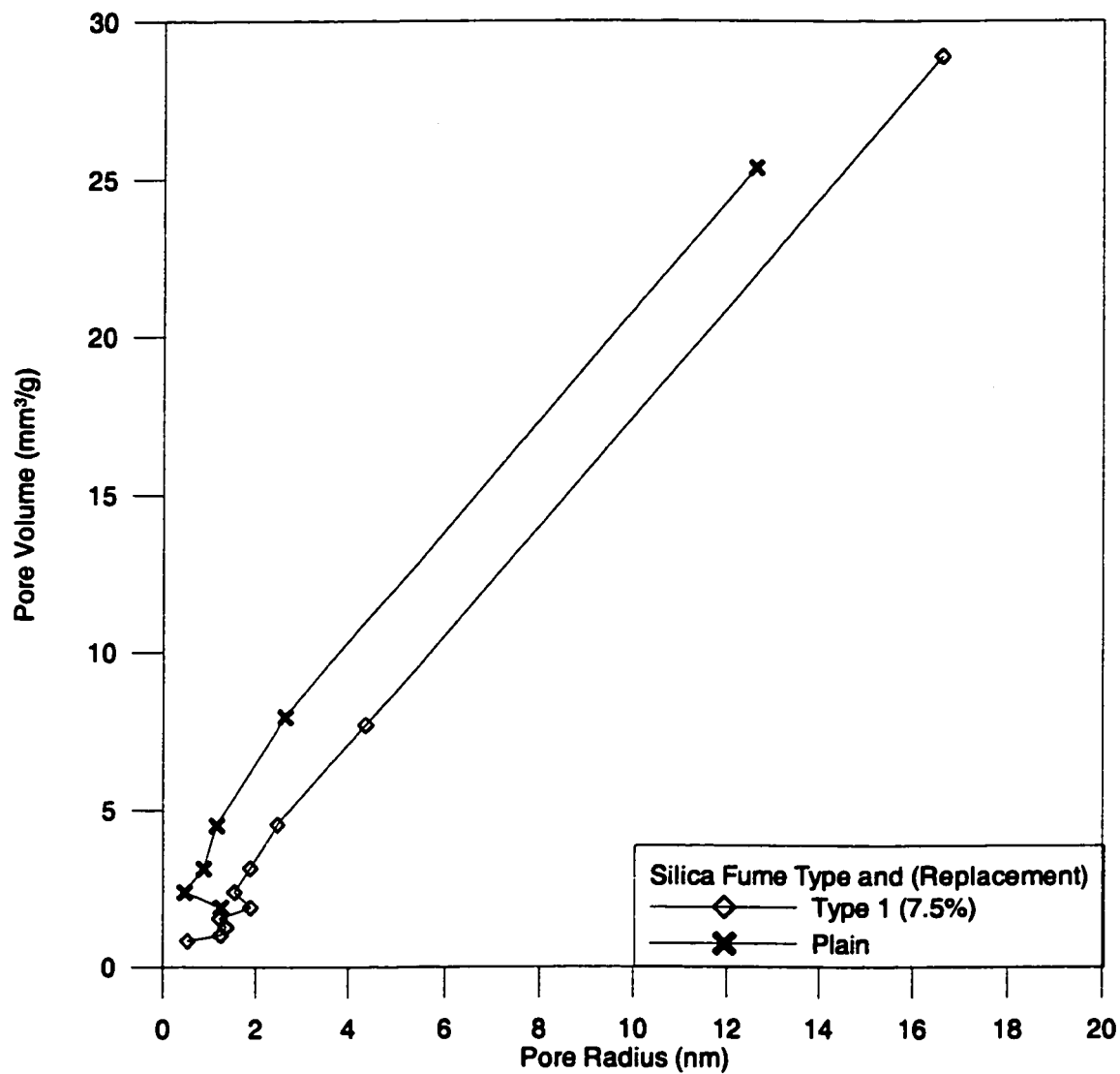


Figure 4.43: Typical plot of pore volume versus pore radius for plain and Type 1 silica fume cement pastes.

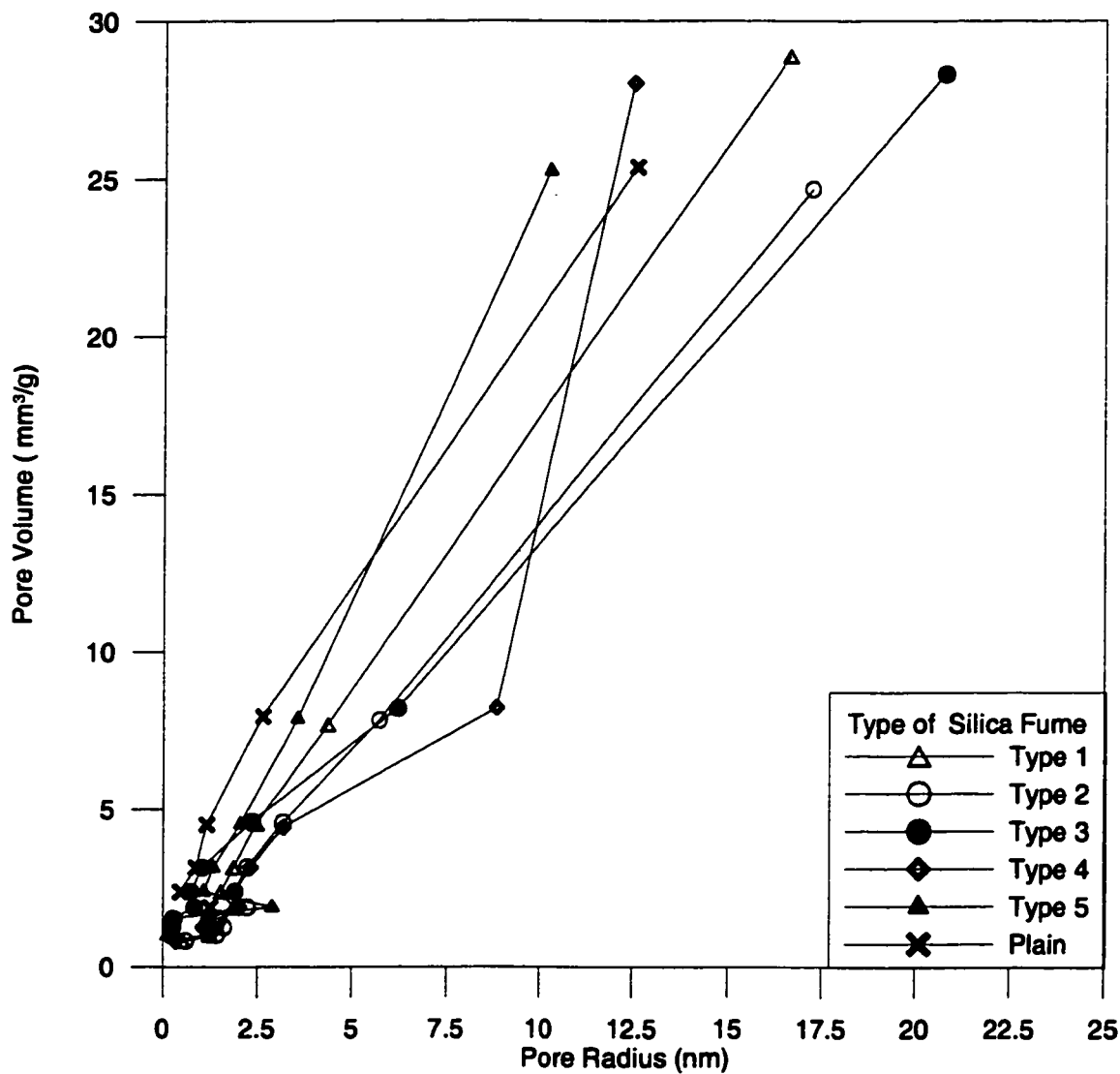


Figure 4.44: Variation of the pore volume with the pore radius for the various types of silica fume cement pastes at a constant dosage of 7.5%.

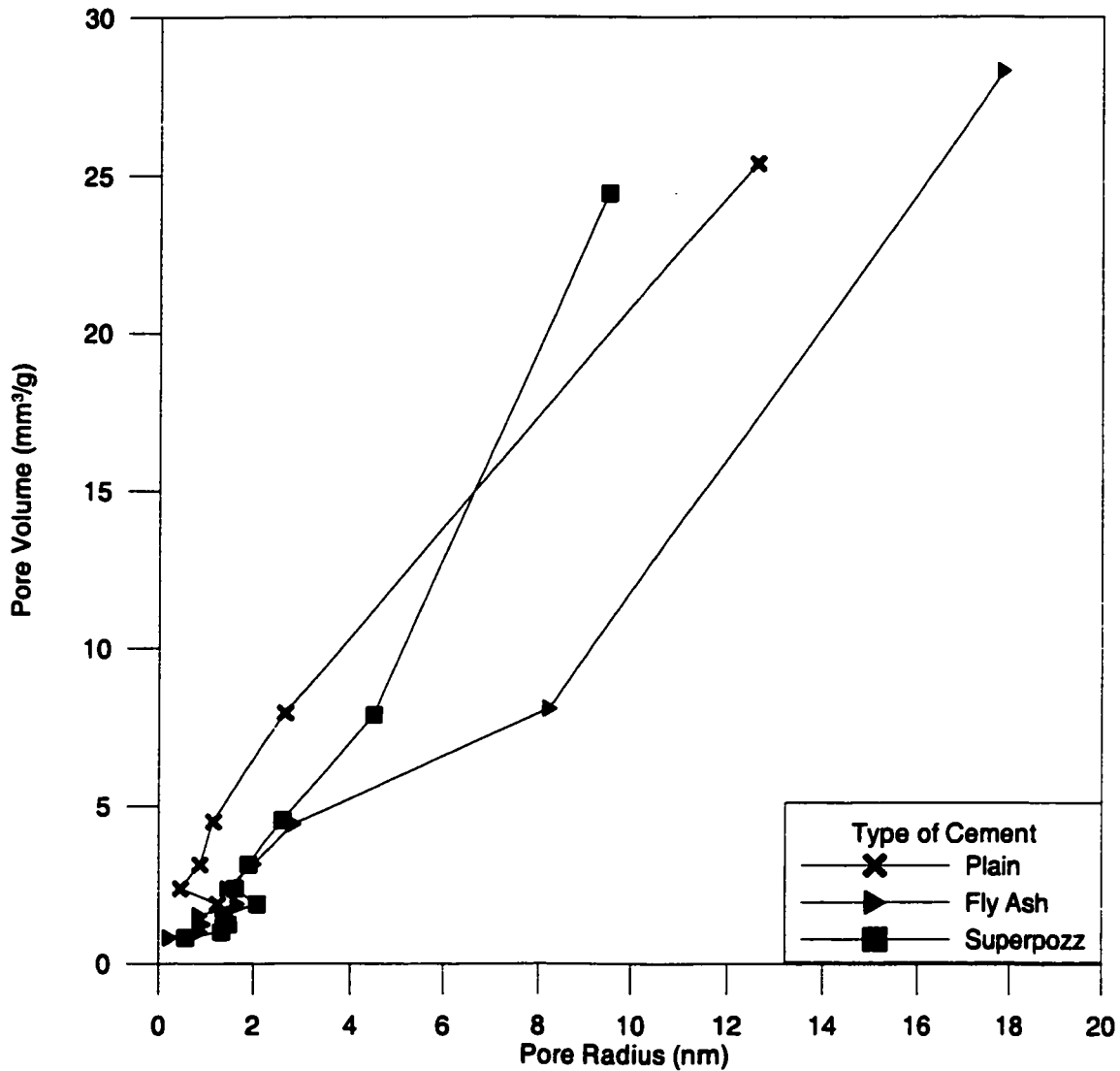


Figure 4.45: Variation of the pore volume with the pore radius for the plain, fly ash and Superpozz® cement pastes.

4.10 PROPERTIES OF SILICA FUME CONCRETE AT EARLY AGES

The properties of silica fume cement concrete at early ages was evaluated in terms of compressive strength, split tensile strength and ultrasonic pulse velocity that were measured on cylindrical specimens cast and stored under the desired exposure conditions prior to testing.

4.10.1 Ultrasonic Pulse Velocity

The ultrasonic pulse velocity was measured after 6, 12 and 24 hours and 28 days of casting. These specimens were stored in the exposure chamber at a temperature of 45°C, RH of 35% and wind velocity of 15 km/hr.

Figures 4.46 through 4.48 show the variation of the pulse velocity with exposure period for Types 1, 2 and 3 silica fume cement concretes at dosages of 5, 7.5 and 10%. The pulse velocity at early ages in the plain, fly ash and Superpozz® cement concrete is depicted in Figure 4.49. The pulse velocity increased with time, and then stabilized after about 12 hours.

The pulse velocity also decreased with increasing the dosage of silica fume going from 5

to 10% for all types of silica fume. Increasing the silica fume content meant that the cement content within the paste was correspondingly reduced. As the cement fraction was reduced, there would be no binder available, thereby producing concrete of greater coarseness at the early age of hydration. This also implied that the pozzolanic reaction of the silica fume did not contribute significantly to the binding capacity of the binder paste.

Superpozz® cement concrete had comparable pulse velocity values to those of plain cement concrete, while fly ash cement concrete had the lowest values of pulse velocity. This implies that fly ash cement concrete was not as dense as either Superpozz® or plain cement concrete. Unlike the silica fume cement concretes; the coarseness of the fly ash cement concrete may be attributed to its slow strength development, especially after the first 24 hours after casting.

4.10.2 Discussion of Pulse Velocity Results

The following points may summarize the pulse velocity behavior of silica fume cement concrete.

1. The fact that Type 2 silica fume cement concrete is undensified and Types 1 and 3 are not densified did not affect the pulse velocity of the resulting concretes.
2. There was little or no difference in the pulse velocity data of plain cement concrete and that of the silica fume cement concretes under hot weather

conditions.

3. Pulse velocity and compressive strength (discussed in the next section) results for plain cement concretes obtained here were similar to those obtained by Elvery and Ibrahim at early ages [136].

4.10.3 Compressive Strength

Figures 4.50 through 4.52 depict the variation in compressive strength with time for plain and blended cement concretes. The compressive increased with time up to a time of about 24 hours. In Type 3 silica fume cement concrete, the 28-day compressive strength was about twice that of the 1-day compressive strength at all dosages. For Types 1 and 2 silica fume cement concretes, the 28-day compressive strength was about 1.5 times that of the 1-day compressive strength at all dosages. Type 2 silica fume cement concrete is the only type of silica fume that was undensified and produced the highest 28-day compressive strength at all dosages of silica fume and during all exposure periods. A general reduction in the 28-day compressive strength was noted as the dosages of the silica fumes were increased in all the types of silica fume cement concretes.

The variation in the compressive strength with the exposure period for plain, fly ash and Superpozz® is shown in Figure 4.53. The compressive strength of the Superpozz® cement concrete was higher than that of the plain and fly ash cement concretes at all exposure

periods, while the compressive strength of the fly ash cement concrete was comparable to that of plain cement concrete.

4.10.4 Discussion on Compressive Strength Results

The compressive strength increased with the exposure period. There were some differences in the rate of strength development for silica fume and plain cement concretes, especially within the first 24-hour period. The rate of increase in the strength of the three different types of silica fume cement concretes increased at a higher rate than that of plain cement concrete. Also, the different dosages produced differing compressive strengths, the range of variation falls within a narrow limit for all the types of silica fume cement concrete. Based on the compressive strength data, the optimum dosage of silica fume would be in the range of 5% to 7.5%. Moreover, undensified silica fume should be preferred over densified silica fume in order to achieve higher compressive strengths.

Fly ash cement concrete produced a much lower compressive strength compared to that of all the other types of blended cement concretes. Several authors [129,139] have reported lower initial compressive strength of the fly ash cement concrete especially during the first 28 days after casting.

The compressive strength of Superpozz® cement concrete was superior to that of plain

cement concrete, as evidenced in Figure 4.53. In this regard, the behavior of Superpozz® cement was more or less similar to that of the silica fume cement concretes rather than that of fly ash. Also, the rate of strength gain of both Superpozz® and fly ash were similar to that of plain cement concrete, as shown by the shape of the graphs.

The maturity method was recommended by the ACI Committee 306 to predict the compressive strength of concrete at early age as an alternative to laboratory or field-cured cylinders where such cylinders are not available [104]. In a recent study carried out by Wen *et al* [137], the strength development of silica fume cement concrete at early ages under varying temperature conditions was predicted using the maturity function based on Arrhenius equation given by:

$$t_{20} = \sum \exp \left\{ \frac{E}{R} \left[\frac{1}{293} - \frac{1}{273 + T} \right] \right\} \Delta t \quad (\text{Equation 4.1})$$

Where,

E = Empirical activation energy (kJ/mol);

R = Gas constant ($R = 0.008314 \text{ kJ/ K mol}^{-1}$);

T = Mean concrete temperature in °C in time increment Δt ; and

t_{20} = equivalent age at 20°C.

A number of authors have expressed that, in order to give reliable results, the following

limitations about the maturity method must be taken into consideration [136,138]:

- The influence of relative humidity during curing is not taken into consideration;
- The heat of hydration and variable cement composition are also not considered;
- The effect of curing temperature during the first 24 hours is not considered as well; and,
- Some authors [138] are of the opinion that the maturity rule can only be applied fairly if the initial temperature of the concrete is between 16 and 27°C and no loss of moisture takes place during the period considered.

Because of these limitations, it is not possible to use the maturity technique to predict the concrete compressive strength in this study (Figures 4.50 through 4.53). However, what is worthy of observation in the study carried out by Wen *et al* was their conclusion that the compressive strength of silica fume cement concrete followed a two-stage process (over temperature) in contrast to that of plain cement concrete. This was demonstrated by the empirical activation energy E (see Equation 4.1), which was derived experimentally as [137]:

$$E = 38.5 \quad \text{when } T \leq 40^\circ\text{C}$$

$$E = 38.5 + 0.2(T - 40) \quad \text{when } T > 40^\circ\text{C}$$

The above values of E are valid in the range of 0 to 60°C [137]

For plain cement concrete, the values of E are as follows [137]:

$$E = 33.5 \quad \text{when } T \geq 20^\circ\text{C}$$

$$E = 33.5 + 1.47(20 - T) \quad \text{when } T < 20^\circ\text{C}$$

These values of E will be translated into different rates of hydration reactions from Equation 4.1 for plain and silica fume cement concretes. Thus, it is possible to explain the difference in the curves in Figures 4.50 through 4.53 of the silica fume and plain cement concretes in terms of the differences in the rate of strength gain of these concretes.

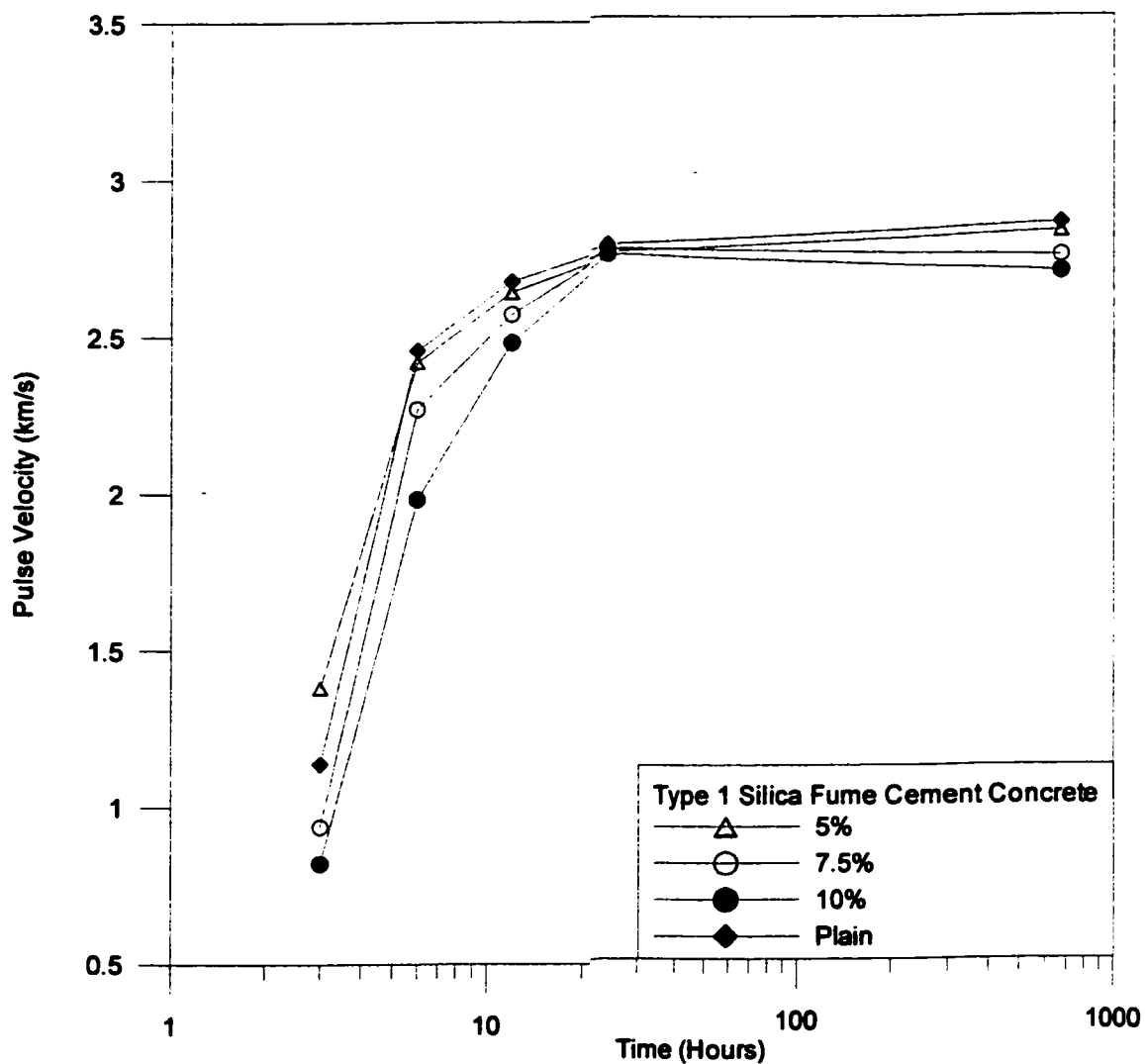


Figure 4.46: Variation of pulse velocity with time in Type 1 silica fume cement concrete.

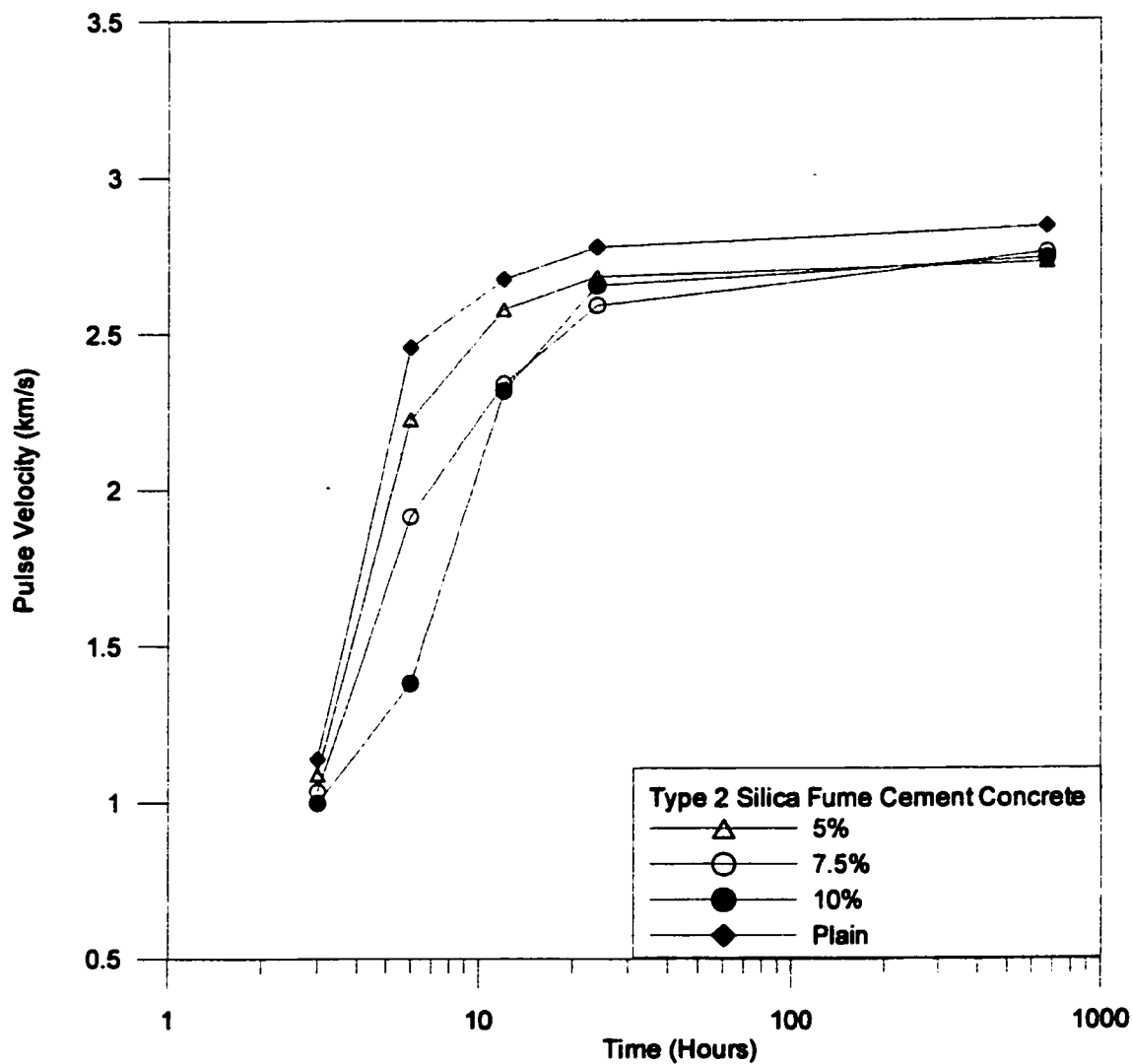


Figure 4.47: Variation of pulse velocity with time in type 2 silica fume cement concrete.

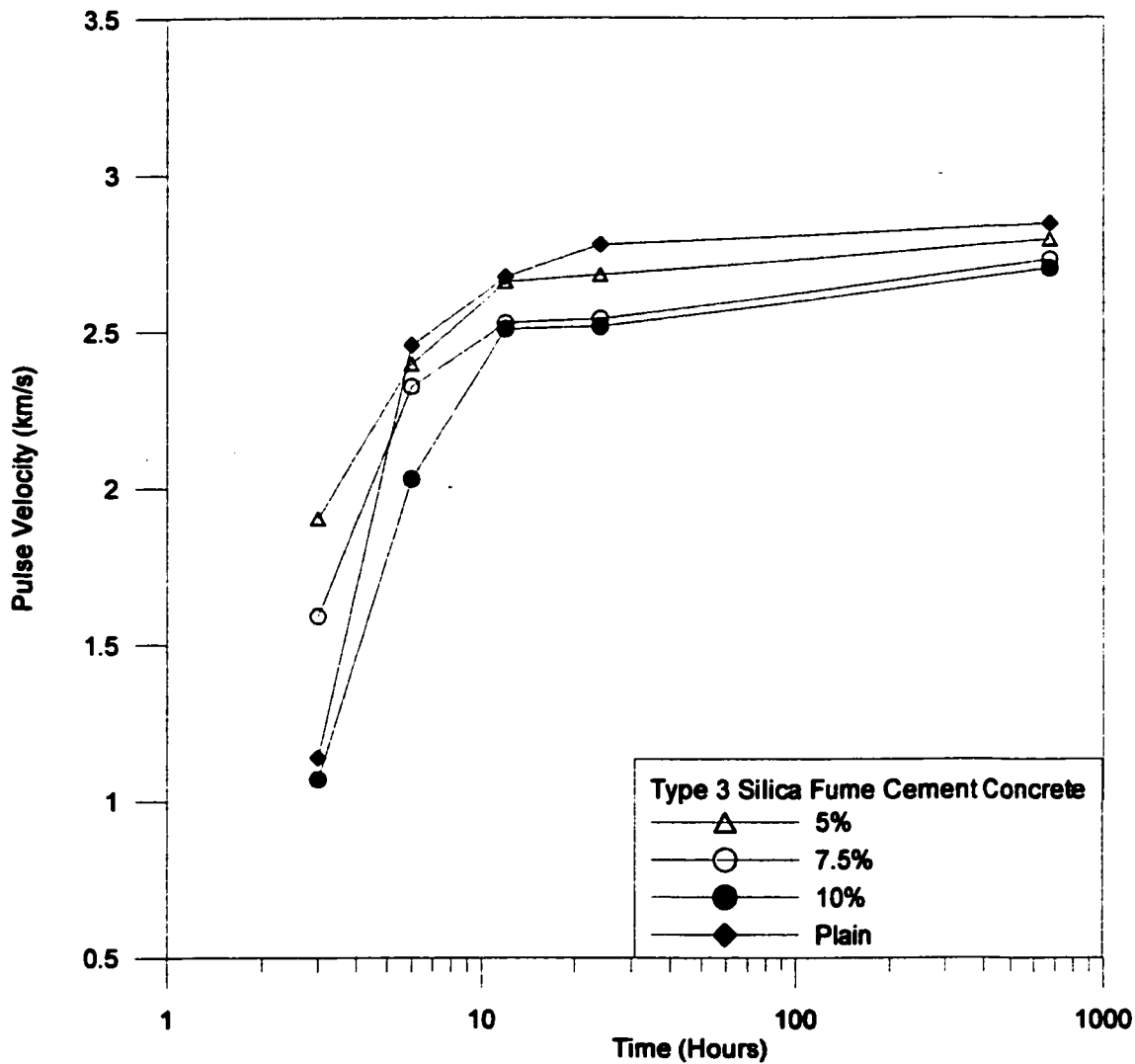


Figure 4.48: Variation of pulse velocity with time in Type 3 silica fume cement concrete.

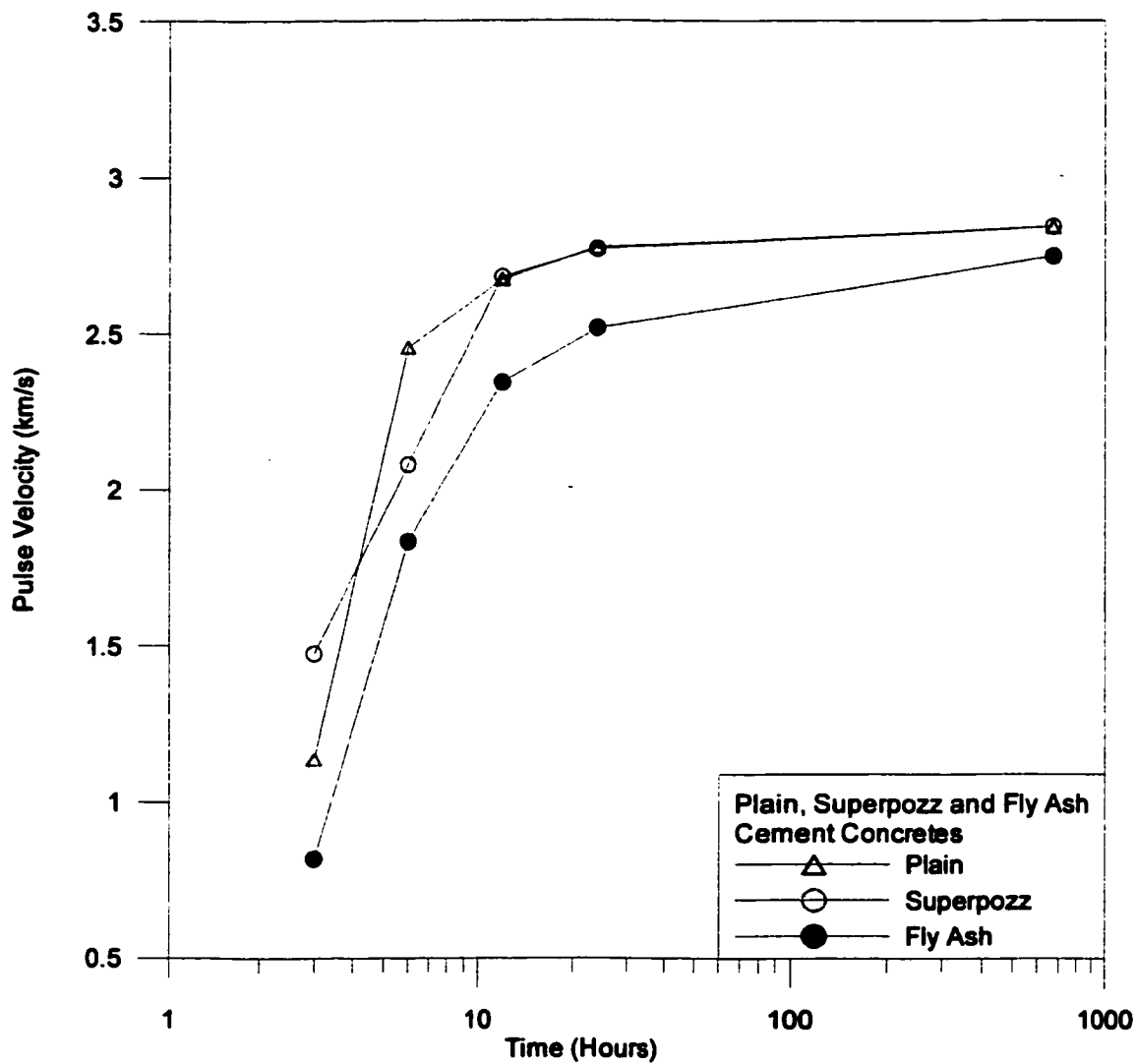


Figure 4.49: Variation of pulse velocity with time in plain, fly ash and Superpozz[®] cement concretes.

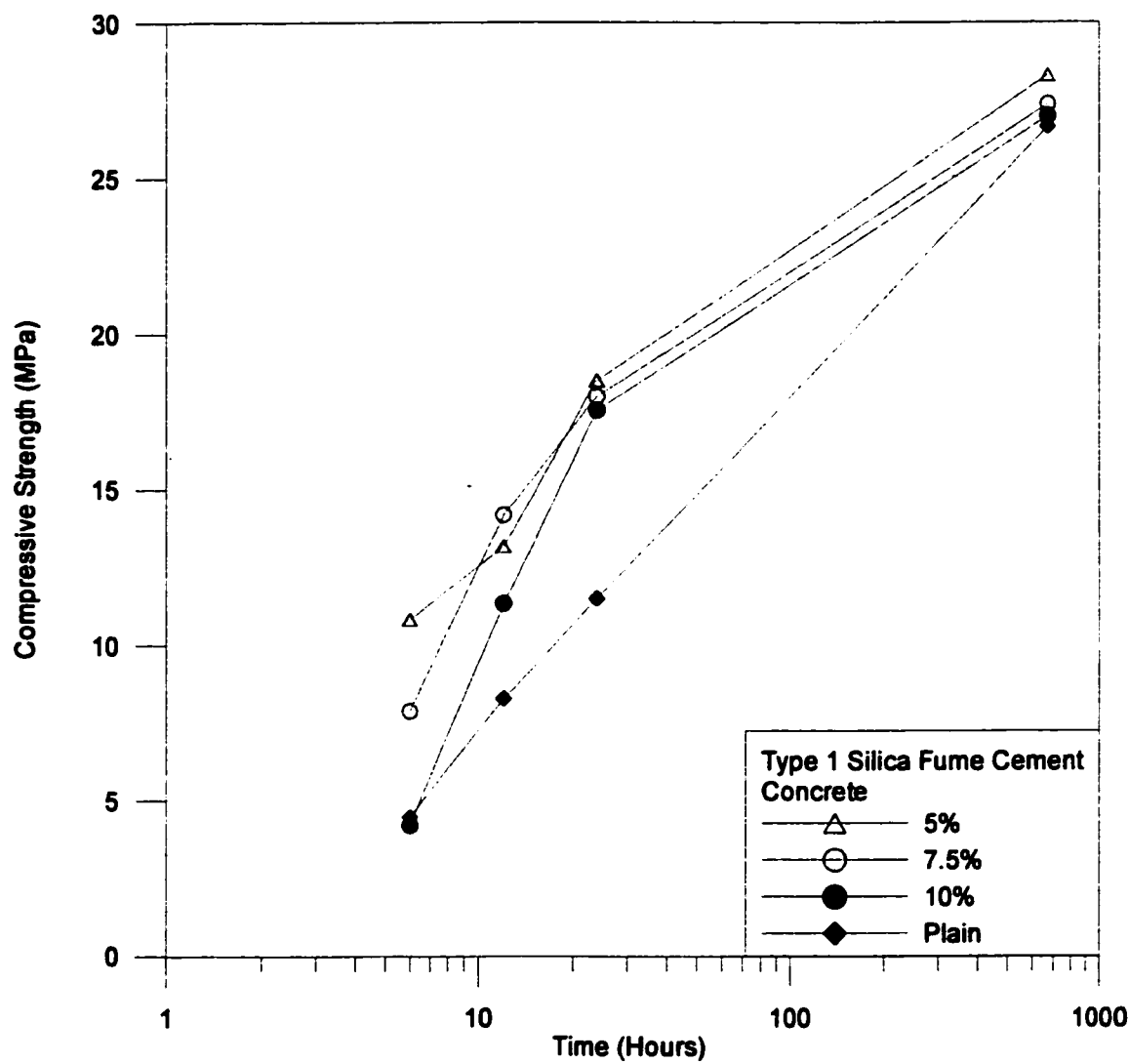


Figure 4.50: Variation of compressive strength with time in Type 1 silica fume cement concrete.

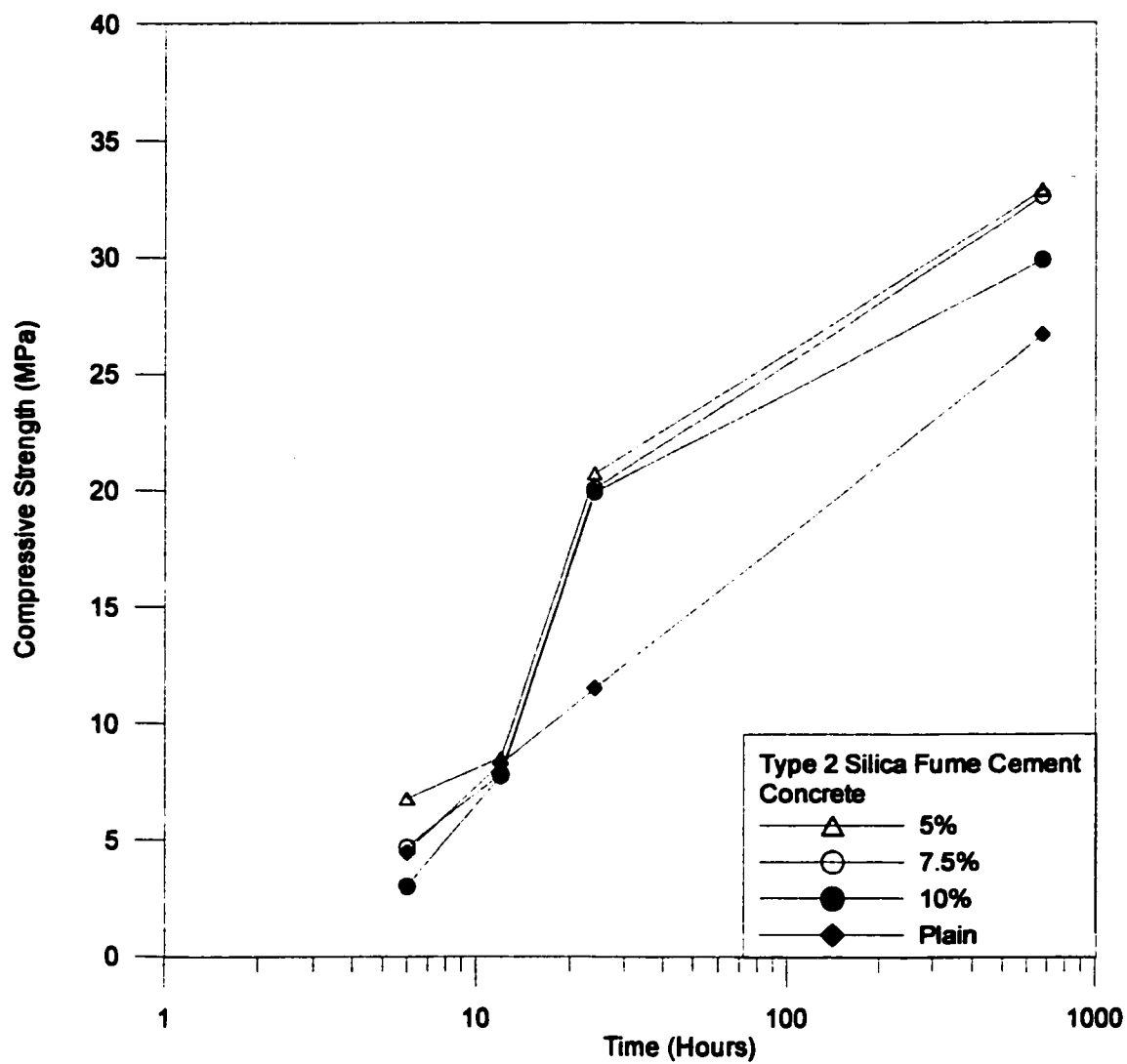


Figure 4.51: Variation of compressive strength with time in Type 2 silica fume cement concrete.

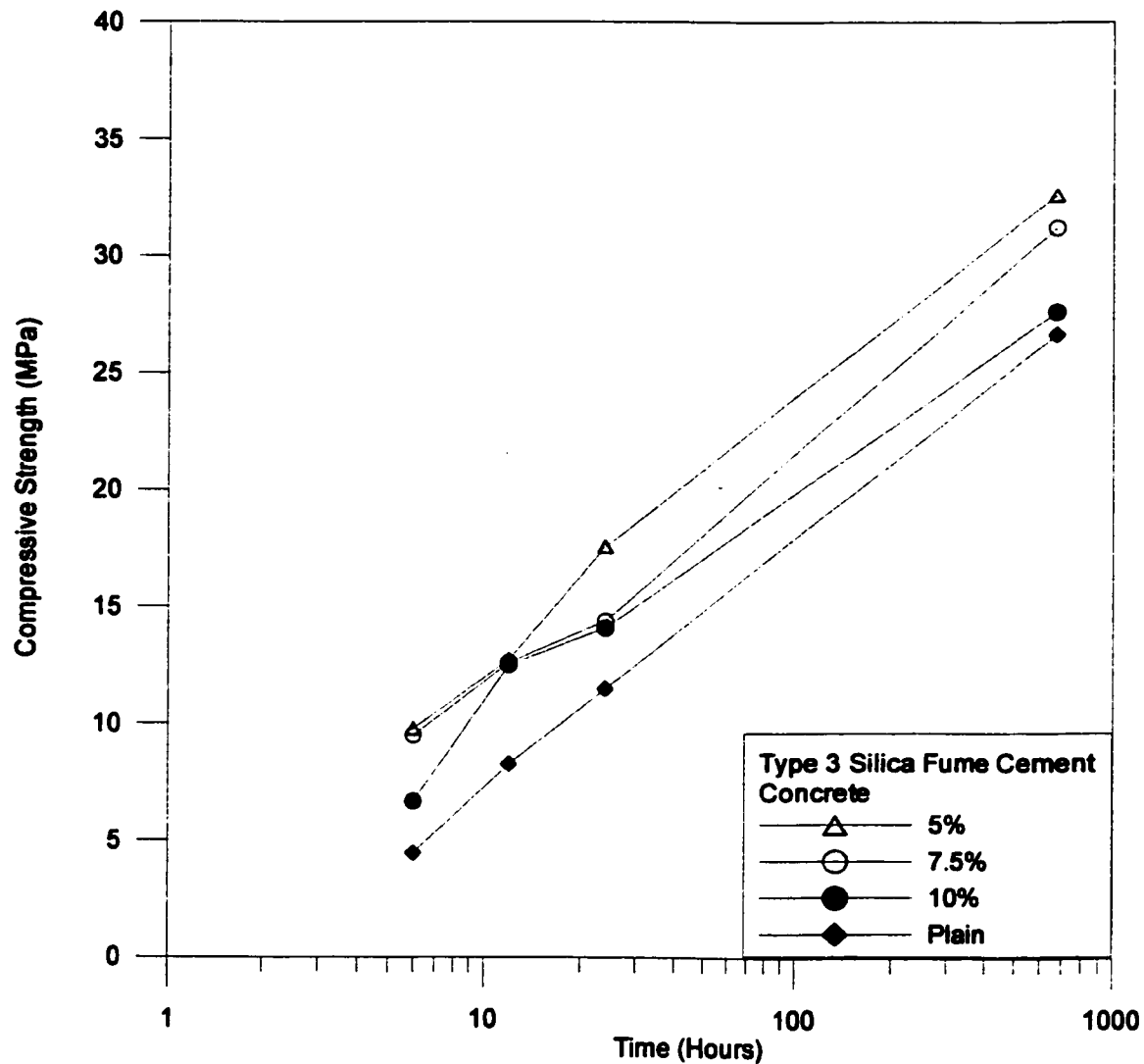


Figure 4.52: Variation of compressive strength with time in Type 3 silica fume concrete.

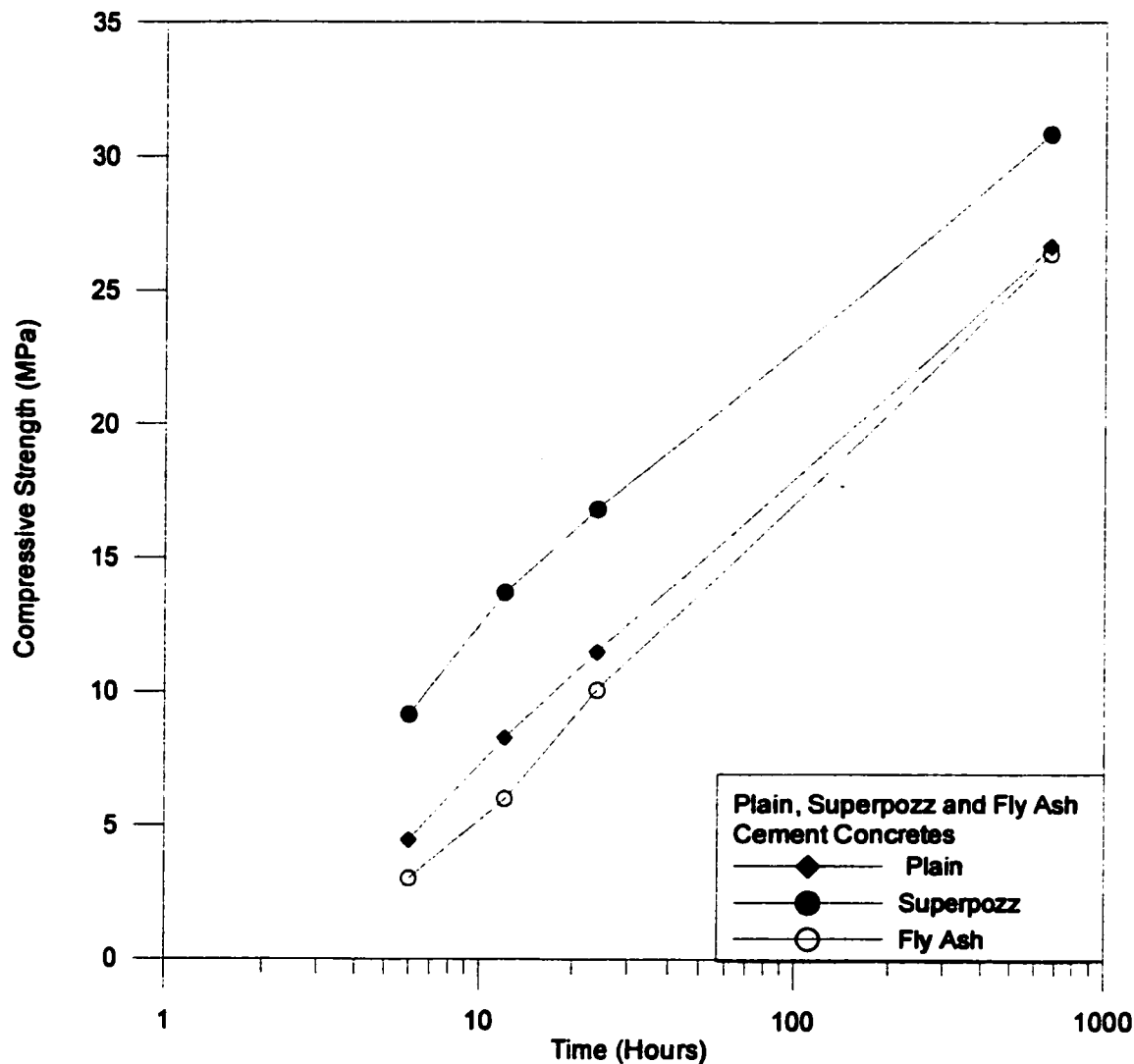


Figure 4.53: Variation of compressive strength with time in plain, fly ash and Superpozz® cement concretes.

4.10.5 Correlation between Compressive Strength and Pulse Velocity

Linear regression analysis was carried out to investigate the relation between the ultrasonic pulse velocity and the compressive strength of plain and blended cement concretes. A two-line (i.e., bi-linear) best-fit model was statistically chosen in agreement with what was presented by previous authors [136,140]. The lines were of the general form:

$$Y_1 = A_1 * X + B_1 \quad \text{and} \quad Y_2 = A_2 * X + B_2 \quad (\text{Equation 4.2})$$

Where,

A_1, A_2 and B_1, B_2 are constants;

Y = compressive strength, MPa; and

X = pulse velocity, km/s.

A bi-linear model was used because previous researchers had used it and the fact that a linear model was found to be inadequate [140-141].

Relationship between Compressive Strength and Pulse Velocity of Silica Fume Cement Concretes

Figures 4.54 through 4.60 depict the correlation between the compressive strength and

the ultrasonic pulse velocity for the various types of blended cement concretes. Each of the bi-linear relations shown in these figures consists of two lines, the first line fitted through the data points corresponded to the times of up to 24 hours, while the second line corresponded to the time from 1 day to 28 days. These time periods were chosen because the data values within these periods gave the best fit and provided the highest value of the coefficient of correlation.

Tables 4.27 through 4.31 depict the correlation coefficients for the plotted values of Figures 4.54 through 4.58. In Table 4.27, a 5% dosage of Type 1 silica fume (shown in Figure 4.54) showed the highest variability in the correlation by producing the least value of R^2 of 0.84. A similar trend can be observed with Types 2 and 3 silica fume cement concrete at this dosage, as shown in Tables 4.28 and 4.29, respectively. Also in Table 4.27, the correlation coefficients (R^2) values shown in the "All (Type 1)" row depict the effect of including all the silica fumes when fitting the data points. Comparing the value of R^2 on this row with that of, say, 7.5% or 10% dosage in the same table, a reduction in the R^2 can be observed, implying that the magnitude of the error has increased. However, when compared to the R^2 value at a dosage of 5%, the value improved. A similar trend can be observed in the data in Tables 4.28 and 4.29 for Types 2 and 3 silica fume cement concretes, respectively. Table 4.30 compares all the three types of silica fume cement concrete when the effect of the dosage of the silica fume was discarded.

Relationship between Compressive Strength and Pulse Velocity for Plain, Fly Ash and Superpozz® Cement Concretes

Table 4.31 summarizes the correlation coefficient values for plain, fly ash and Superpozz® cement concretes. The two lines for plain cement concrete had slopes similar to that reported by the 42-CEA Committee [140] and that reported by Elvery and Ibrahim [136], although neither authors reported the values of the correlation coefficients.

For fly ash cement concrete, the coefficients for Line 1 (at a time of 0 to 24 hours) had the lowest value of R^2 compared to that of plain and Superpozz® cement concretes, but was higher than that of Types 2 and 3 silica fume cement concretes. The correlation coefficient was 0.98 and 0.91 for plain and Superpozz® cement concretes, respectively.

Figure 4.58 shows the relation between pulse velocity and compressive strength for all the silica fume cement concretes irrespective of the type and dosage of silica fume. The corresponding correlation coefficients are shown in Table 4.30. The correlation coefficients are 0.767 and 0.446, for Lines 1 and 2, respectively.

4.10.6 Discussion on the Relationship between Compressive Strength and Pulse Velocity

Relationship between Compressive Strength and Pulse Velocity for Silica Fume Cement Concretes

Comparing the values in Tables 4.27 through 4.29 to that in Table 4.30 indicates that the statistical error in correlating the data is due to two components as follows:

- Error due to materials variability
- Normal statistical error due to curve fitting

Tables 4.27 through 4.29 provide an estimate of normal statistical error due to curve fitting, while Table 4.30 provides an estimate of the error due to materials variability due to the type and dosage of silica fume. Especially in the case of Line 2 in Tables 4.27 through 4.29, only two points were available to fit values. Increasing the number fitted values and replicating others, could significantly reduce the total amount of sampling error, thus improving the fit.

Type 2 silica fume cement concrete produced the worst fit with an R^2 value of 0.70 for Line 1 (Table 4.28) while Types 2 and 3 silica fume cement concretes had R^2 values of 0.96 and 0.83, respectively. In the case of Line 2 (Table 4.28), however, Type 2 silica

fume cement concrete produced the best fit with an R^2 of 0.76, while R^2 values for Types 1 and 3 silica fume cement concretes were 0.52 and 0.65, respectively.

From the above it can be observed that the relationship between pulse velocity and the compressive strength varies with time (Lines 1 and 2 produced differing R^2 values) as well as with the Type and dosage of the silica fume. The correlation improved with increasing the dosage of silica fume in all the three types of silica fume cement concretes. This could be attributed mainly to the increase in the compressive strength as a result of increasing in the pozzolanic reaction as the silica fume in the paste was increased. It was noted in the previous section that the pulse velocity decreased with increasing dosage of silica fume.

Correlation of Compressive Strength and Pulse Velocity for Plain, Fly Ash and Superpozz® Cement Concretes

From the data presented in Table 4.31, it can be observed that plain cement concrete had the highest R^2 value for Line 1 of 0.98, indicating that there was little or no error due to materials variability. Superpozz® had an R^2 value of 0.91, indicating lower materials variability than fly ash cement concrete that had a value R^2 of 0.87. Comparing the TPV data in Table 4.26 with the R^2 values in Tables 4.30 for Types 1, 2 and 3 silica fume cement concretes, a trend could be observed: the highest TPV of 32.5 mm³/g

corresponded with the lowest value of R^2 of 0.70, for Type 2 silica fume cement concrete. Other values of TPV: R^2 are $31.1\text{mm}^3/\text{g}$: 0.83 for Type 3 and $28.5\text{mm}^3/\text{g}$: 0.96 for Type 1 silica fume cement concretes. A similar trend was noted for plain, fly ash and Superpozz® cement concretes. Thus, the lower the R^2 value indicates the higher reactivity of the silica fume, which in turn leads to higher pozzolanic products of hydration.

From the data presented in Tables 4.27 through 4.31 it can be surmised that in order to achieve the desired quality control in producing silica fume cement concrete and other types of blended cement concrete in, say, pre-cast concrete members in the laboratory or in the field, the use of the ultrasonic pulse velocity in predicting the compressive strength must take into cognizance both the type as well as the dosage of the silica fume employed in producing the concrete. The relation between the correlation coefficient R^2 and the TPV values would not hold for Line 2 however, because it has been shown by previous research that after 24 hours the pulse velocity is less accurate in predicting the compressive strength of concrete [136].

Table 4.27: Correlation coefficients for the relationship between pulse velocity and compressive strength for Type 1 silica fume cement concrete.

Silica Fume Type 1	Line 1			Line 2		
	A ₁	B ₁	R ₁ ²	A ₂	B ₂	R ₂ ²
All	18.1	32.8	0.96	91.3	228.3	0.52
5%	21.36	41.12	0.84	152.9	402.6	1*
7.5%	21.4	40.8	0.99	367.4	988.7	1*
10%	18.1	32.1	0.96	159.6	411.6	1*

* Only two values were used to fit the line.

Table 4.28: Correlation coefficients for the relationship between pulse velocity and compressive strength for Type 2 silica fume cement concrete.

Silica Fume Type 2	Line 1			Line 2		
	A ₁	B ₁	R ₁ ²	A ₂	B ₂	R ₂ ²
All	15.0	-23.8	0.70	88.2	-211.6	0.76
5%	24.0	-48.0	0.57	254.7	-662.4	1*
7.5%	21.1	-37.4	0.79	74.2	-172.3	1*
10%	14.1	-20.6	0.85	114.0	-282.8	1*

* Only two values were used to fit the line.

Table 4.29: Correlation coefficients for the relationship between pulse velocity and compressive strength for Type 3 silica fume cement concrete.

Silica Fume Type 3	Line 1			Line 2		
	A ₁	B ₁	R ₁ ²	A ₂	B ₂	R ₂ ²
All	14.4	-23.4	0.83	85.1	-205.8	0.65
5%	20.5	-39.6	0.69	134.1	-341.9	1*
7.5%	19.4	-35.5	0.91	89.5	-212.9	1*
10%	13.8	-21.3	0.96	73.2	-170.1	1*

*Only two values were used to fit the line.

Table 4.30: Correlation coefficients for the relationship between pulse velocity and compressive strength for all types of silica fume cement concretes.

Silica Fume Type	Line 1			Line 2		
	A ₁	B ₁	R ₁ ²	A ₂	B ₂	R ₂ ²
Type 1	18.14	-32.77	0.955	91.24	-228.29	0.522
Type 2	14.99	-23.77	0.699	88.20	-211.58	0.762
Type 3	14.44	-23.38	0.826	85.14	-205.83	0.655
All	15.13	-24.79	0.767	65.75	-154.34	0.446

Table 4.31: Correlation coefficients for the relationship between pulse velocity and compressive strength for plain, fly ash and Superpozz® cement concretes.

Cement Type	Line 1			Line 2		
	A ₁	B ₁	R ₁ ²	A ₂	B ₂	R ₂ ²
Plain	21.27	47.99	0.976	231.13	-630.56	1*
Fly Ash	9.278	14.36	0.871	70.876	-168.51	1*
Superpozz®	9.824	11.45	0.914	196.97	-529.3	1*

*Only two values were used to fit the line.

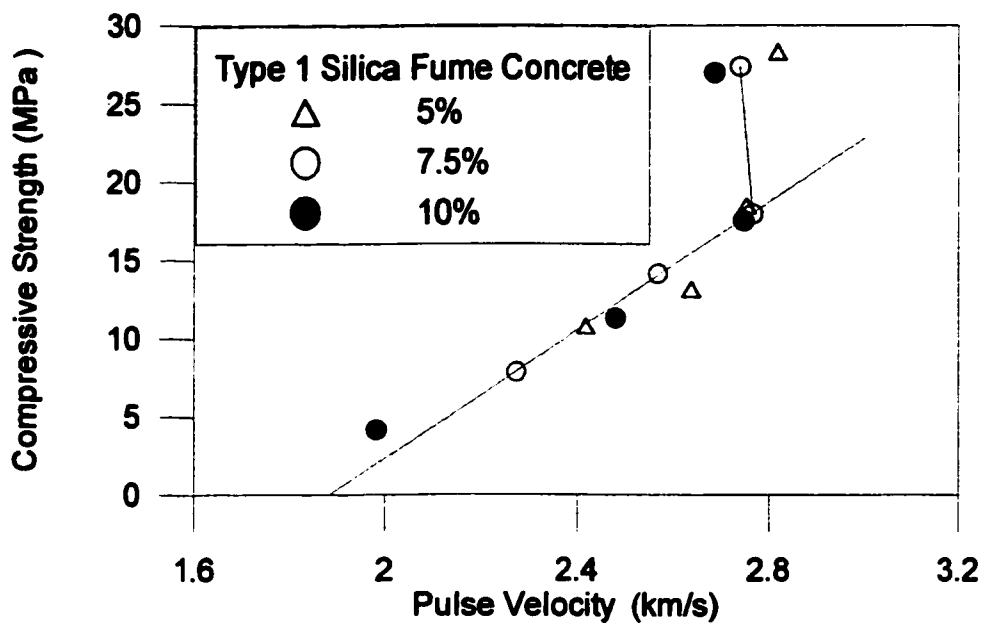


Figure 4.54: Relationship between compressive strength and pulse velocity for Type 1 silica fume cement concrete (temperature of 45 °C, RH of 35% and wind velocity of 15 km/hr).

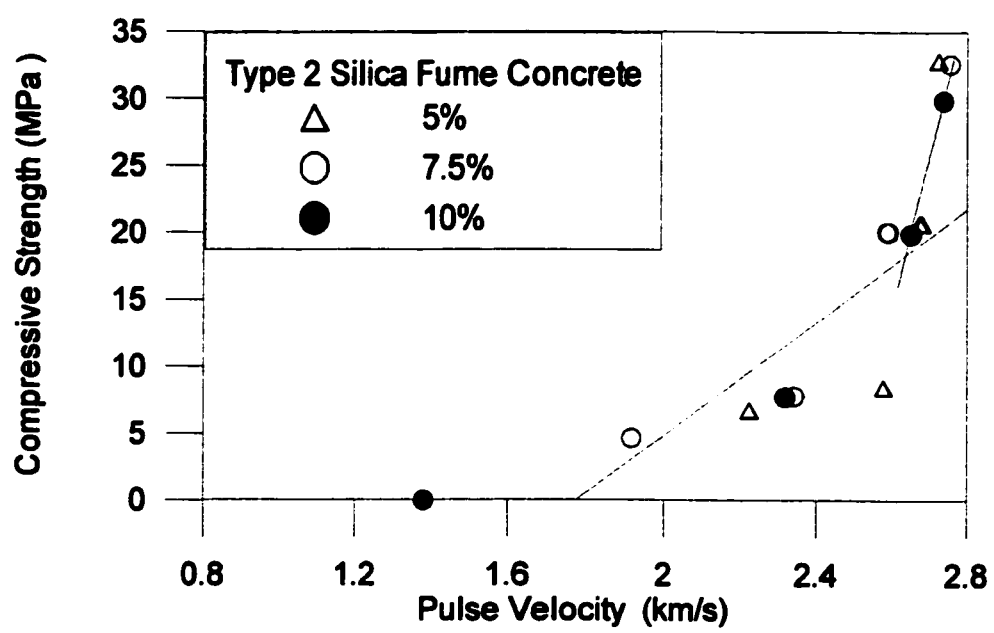


Figure 4.55: Relationship between compressive strength and pulse velocity for Type 2 silica fume cement concrete (temperature of 45 °C, RH of 35% and wind velocity of 15 km/hr).

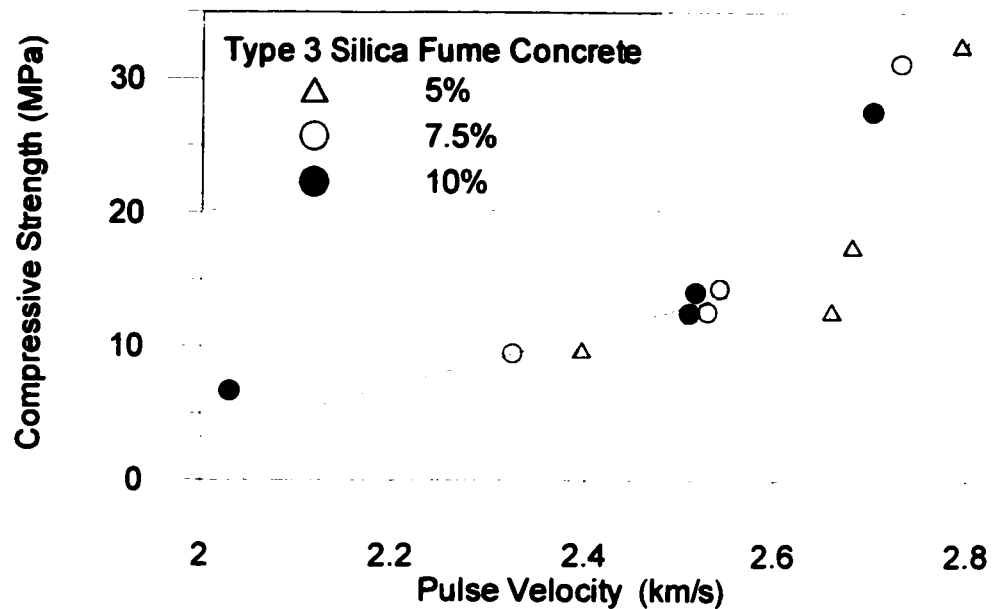


Figure 4.56: Relationship between compressive strength and pulse velocity for Type 3 silica fume cement concrete (temperature of 45 °C, RH of 35% and wind velocity of 15 km/hr).

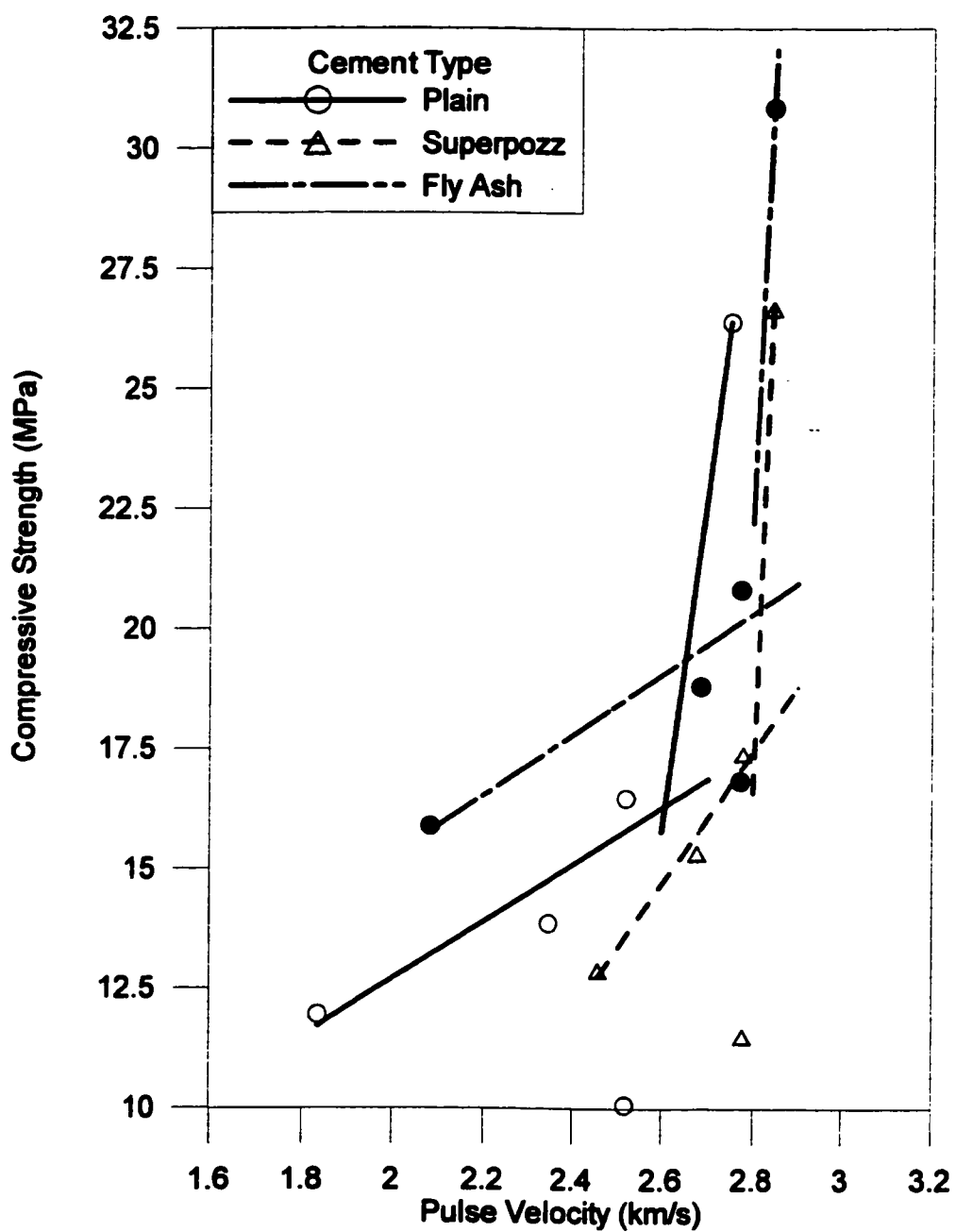


Figure 4.57: Relationship between compressive strength and pulse velocity for plain, fly ash and Superpozz® cement concrete (temperature of 45 °C, RH of 35% and wind velocity of 15 km/hr).

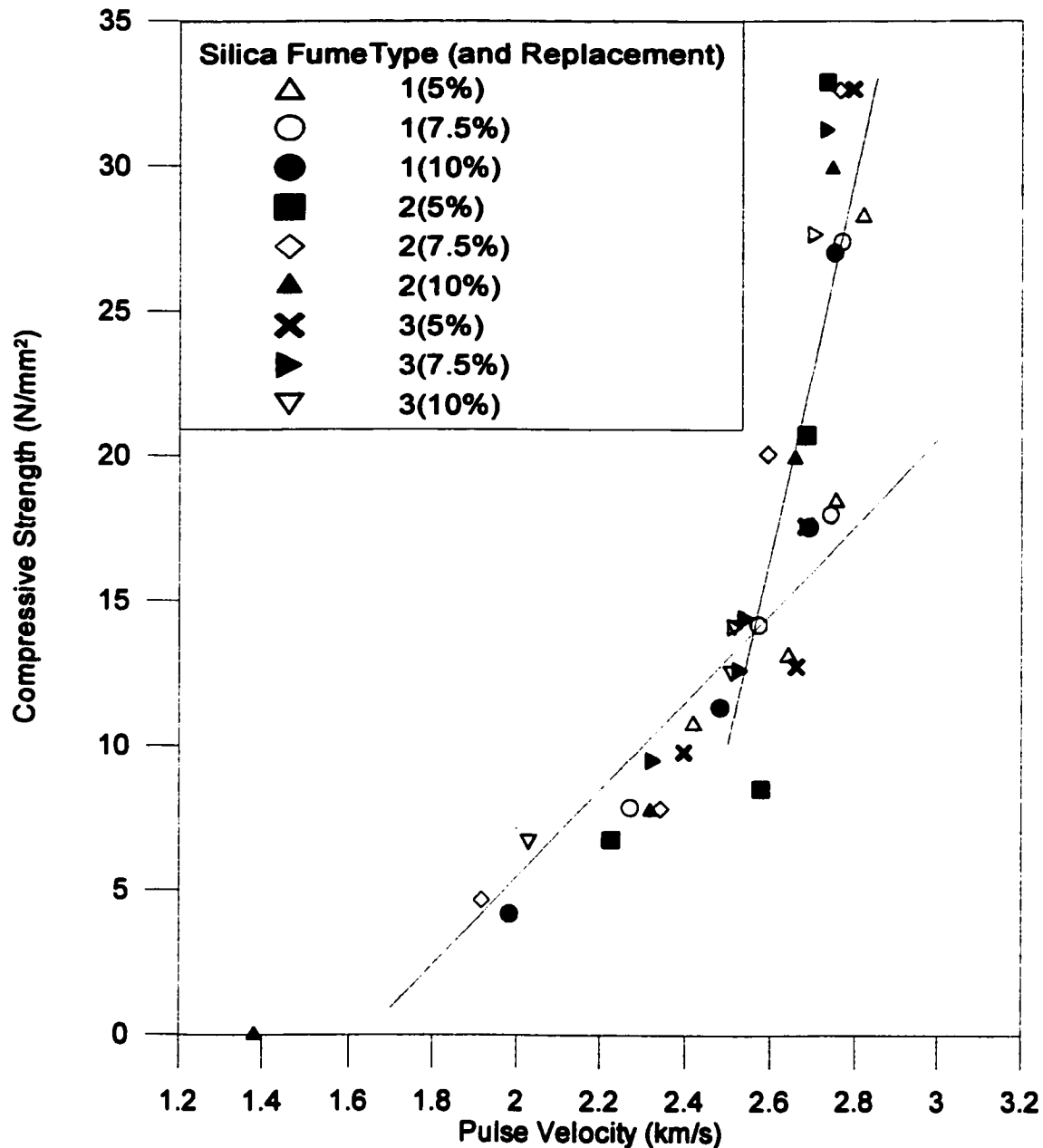


Figure 4.58: Relationship between compressive strength and pulse velocity for all three types of silica fume cement concrete (temperature of 45 °C, RH of 35% and wind velocity of 15 km/hr).

4.10.7 Split Tensile Strength of Silica Fume Cement Concrete

Figures 4.59 and 4.60 depict the variation of the split tensile strength with time of plain and blended cement concretes. In Figure 4.59, the split tensile strength increased with time, however, the rate decreased at later times for Type 1 silica fume cement concrete. A similar trend was observed for Types 2 and 3 silica fume cement concretes, the split tensile strength did not vary significantly between the three types of silica fume cement concretes.

In Figure 4.60, the split tensile strength of plain and fly ash and Superpozz® a cement concrete is shown. The plain cement concrete had a higher split tensile strength compared to any of the blended cement concretes. Fly ash cement concrete had the lowest values of the split tensile strength at all times.

Linear Regression of the Split Tensile Strength with Time for Silica Fume Cement Concretes

A regression analysis similar to that in the previous section is presented for the variation of the split tensile strength with time for the various types of silica fume cement concretes. Tables 4.32 and 4.33 depict the correlation coefficients for the different types of plain and blended cement concretes. The silica fume cement concretes were prepared

at a constant dosage of 7.5%. Here, a power fit produced better correlations compared to a linear one. The fitted relationship is of the following form:

$$f_t = A * X^b \quad (\text{Equation 4.3})$$

Where,

f_t = split tensile strength; MPa

A, and b are constants; and

X = time in hours.

The split tensile strength of the silica fume cement concretes could be represented by the following correlation irrespective of the type of silica fume:

$$f_t = 0.4771 * X^{0.2749} \quad (R^2 = 0.896) \quad (\text{Equation 4.4})$$

With an R^2 value of 0.896 (see row "All" in Table 4.32), this compares favorably with that of Type 1 silica fume cement concrete with an accuracy of $87.5\% \pm 5$ (Table 4.32). Thus, the type of silica fume did not have a significant effect on the split tensile strength of the resulting concrete, at the specified exposure and curing conditions. However, this accuracy level still falls below the generality acceptable statistical level of $95\% \pm 5$,

therefore, at this level the effect of the type of silica fume is significant.

Table 4.32: Correlation coefficients for the variation of split tensile strength with time of silica fume cement concretes (silica fume dosage: 7.5%).

Silica Fume	Coefficient (A)	Exponent (b)	R ²
All	0.477	0.276	0.896
Type 1	0.550	0.253	0.875
Type 2	0.397	0.308	0.925
Type 3	0.500	0.264	0.932

Table 4.33: Correlation coefficients for variation of the split tensile strength with time of plain, fly ash and Superpozz® cement concretes.

Type of Cement	Coefficient (A)	Exponent (b)	R ²
Plain	1.008	0.1555	0.996
Fly ash	0.492	0.218	0.852
Superpozz®	0.447	0.290	0.856

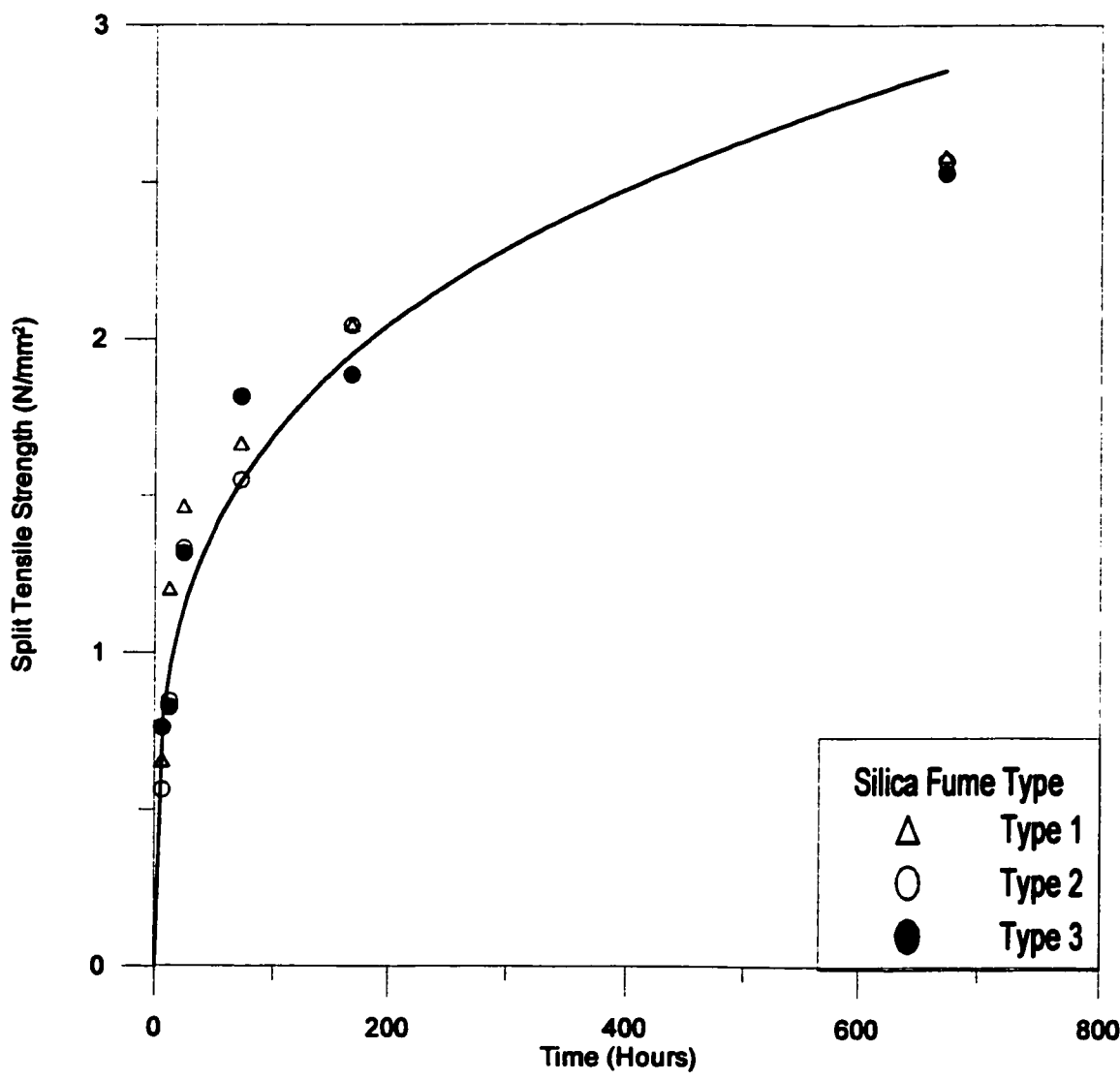


Figure 4.59: Variation of the split tensile strength with time for silica fume cement concretes at dosages of 7.5% (temperature of 45 °C, RH of 35% and wind velocity of 15 km/hr).

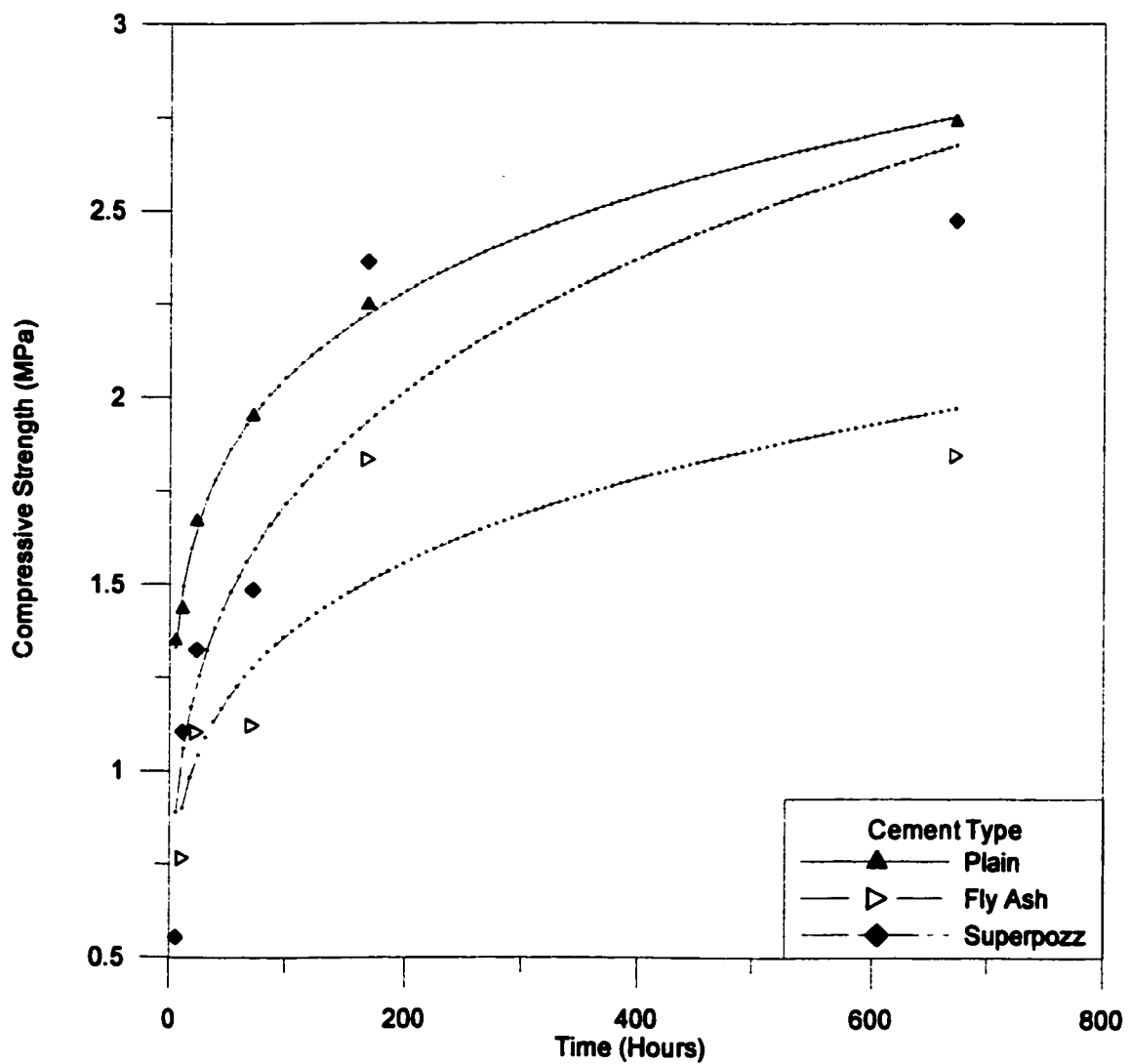


Figure 4.60: Variation of the split tensile strength with time for plain, fly ash and Superpozz[®] cement concretes (temperature of 45 °C, RH of 35% and wind velocity of 15 km/hr).

Split Tensile Strength of Plain, Fly ash and Superpozz® Concretes

Table 4.33 and Figure 4.60 depict the regression coefficients for plain, fly ash and Superpozz® concretes. Plain cement concrete had an R^2 value of 0.996, while for fly ash and Superpozz® cement concretes, these values were approximately 0.85.

4.10.8 Discussion on the Split Tensile Strength of Plain and Blended Cement Concretes

From the data presented in Tables 4.32 and 4.33 and Figures 4.59 and 4.60, it can be concluded that the type of blended cement material did not significantly affect the split tensile of the concrete at a level of accuracy of 85%, but became significant at higher levels of accuracy.

4.10.9 Correlation between the Split Tensile Strength and Compressive Strength of Blended Cements

Relationship Between Split Tensile Strength And Compressive Strength For Plain, Fly Ash And Superpozz® Concretes

Figures 4.61 and 4.62 depict the correlation between the split tensile strength and the compressive strength of silica fume cement concretes and that of plain, fly ash and Superpozz® cement concretes, respectively. Tables 4.34 and 4.35 show the correlation

coefficients. A linear regression model of the form shown below could be easily utilized:

$$Y = A * X + B \quad (\text{Equation 4.5})$$

Where,

Y = Compressive strength, MPa;

X = Split Tensile strength, MPa; and

A and B are constants.

Table 4.34 shows the statistical parameters for Types 1, 2 and 3 silica fume cement concretes at a constant dosage of 7.5%. The coefficient of correlation was more than 0.9 for all silica fume concretes. The relationship between compressive and split tensile strength for all the silica fume cement concretes, can be expressed by the following equation:

$$Y = 0.0788X + 0.0734 \quad (R^2 = 0.945) \quad (\text{Equation 4.6})$$

Equation 4.6 above can be utilized to predict the split tensile strength from the compressive strength and vice versa irrespective of the type of silica fume at this dosage

with an accuracy of 95% (Table 4.34).

Figure 4.62 depicts the relationship between the split tensile strength and compressive strengths for plain, Superpozz® and fly ash cement concretes. The statistical parameters are summarized in Table 4.35. Plain cement concrete had the best fit with a coefficient of 0.994. Rixom and Mailvaganam [95] presented similar relationships between the split tensile and compressive strength of concrete with and without chemical admixtures (plasticizer and superplasticizers) using the direct tensile, split tensile and flexural strength specimens, however, the R^2 values were not reported.

4.10.10 Discussion on the Relationship between the Split Tensile and Compressive Strength of Plain and Blended Cement Concretes

With reference to data in Figures 4.61 and 4.62 and Tables 4.34 and 4.35, a linear relationship model was found as the best fit, producing the highest values of R^2 of 0.945, but the reported relationship in the literature is not always linear. According to Wen *et al.* [137], a low S/C (split tensile/compressive strength) ratio of 0.1 and with a compressive strength of less than 40 MPa, the relationship was linear. However, at higher strength values, the relationship became non-linear. The results presented in this investigation had a S/C value of 0.0788 (Equation 4.6), which is less than 0.1, with the maximum value of

The other point of interest is whether or not the above relationship at a silica fume dosage of 7.5% could be used to represent all the other dosages and types of silica fume concrete under prevailing hot weather conditions. From the data presented in Figures 4.50 through 4.52, the compressive strength was highest at a dosage of 5% and lowest at 10% for all the types of silica fume, with maximum and minimum values of 32.9 and 27.0 MPa, respectively. Accordingly, the range of values is fairly narrow. The slope of the lines is also quite similar, which implies that the rate of strength gain with time is about the same in all the types of silica fume cement concretes under consideration. From the foregoing, the expression in Equation 4.6 could be used with caution with the stated accuracy between the types of silica fume. Following the trend of the values in Table 4.34 (the "All" row), it can be observed that additional error will be introduced in Equation 4.6 if it is to be used within dosages as well.

**Relationship between Split Tensile Strength and Compressive Strength for
Plain, Fly Ash And Superpozz® Concretes**

The relatively poor fit of fly ash cement concrete in Table 4.35, as compared with plain and Superpozz® cement concretes, was due to its low strength development, especially the split tensile strength that did not develop until after 12 hours. Superpozz® cement concrete had a better fit although its strength development (both split tensile and compressive) was similar to that of fly ash cement concrete. The use of a linear model

with no intercept for fly ash and Superpozz® cement concretes was found to produce a better value of R^2 compared with the linear model fitted with an intercept. Accordingly, no intercepts (coefficient B) were presented for both fly ash and Superpozz® cement concretes. From a practical point view, the presence or absence of an intercept is meaningless because concrete exhibits anisotropy.

From the above data, it is possible to discount the effect of type of silica fume in correlating the split tensile and compressive strengths, but the additional effect of the dosage of silica fume must be taken into account, although the magnitude of the error is of the same order as that of the effect type of silica fume as noted in Table 4.34.

Table 4.34: Relationship between split tensile and compressive strength for silica fume cement concretes (silica fume dosage: 7.5%).

Type of Cement Replacement	Coefficient (A)	Coefficient (B)	R ²
All	0.0788	0.073	0.945
Type 1	0.0987	-0.185	0.988
Type 2	0.0682	0.218	0.962
Type 3	0.0827	-0.042	0.970

Table 4.35: Relationship between split tensile and compressive strength for plain, fly ash and Superpozz® cement concretes.

Type of Cement Replacement	Coefficient (A)	Coefficient (B)	R ²
Plain	0.055	1.044	0.994
Fly Ash	0.077	0	0.839
Superpozz®	0.079	0	0.991

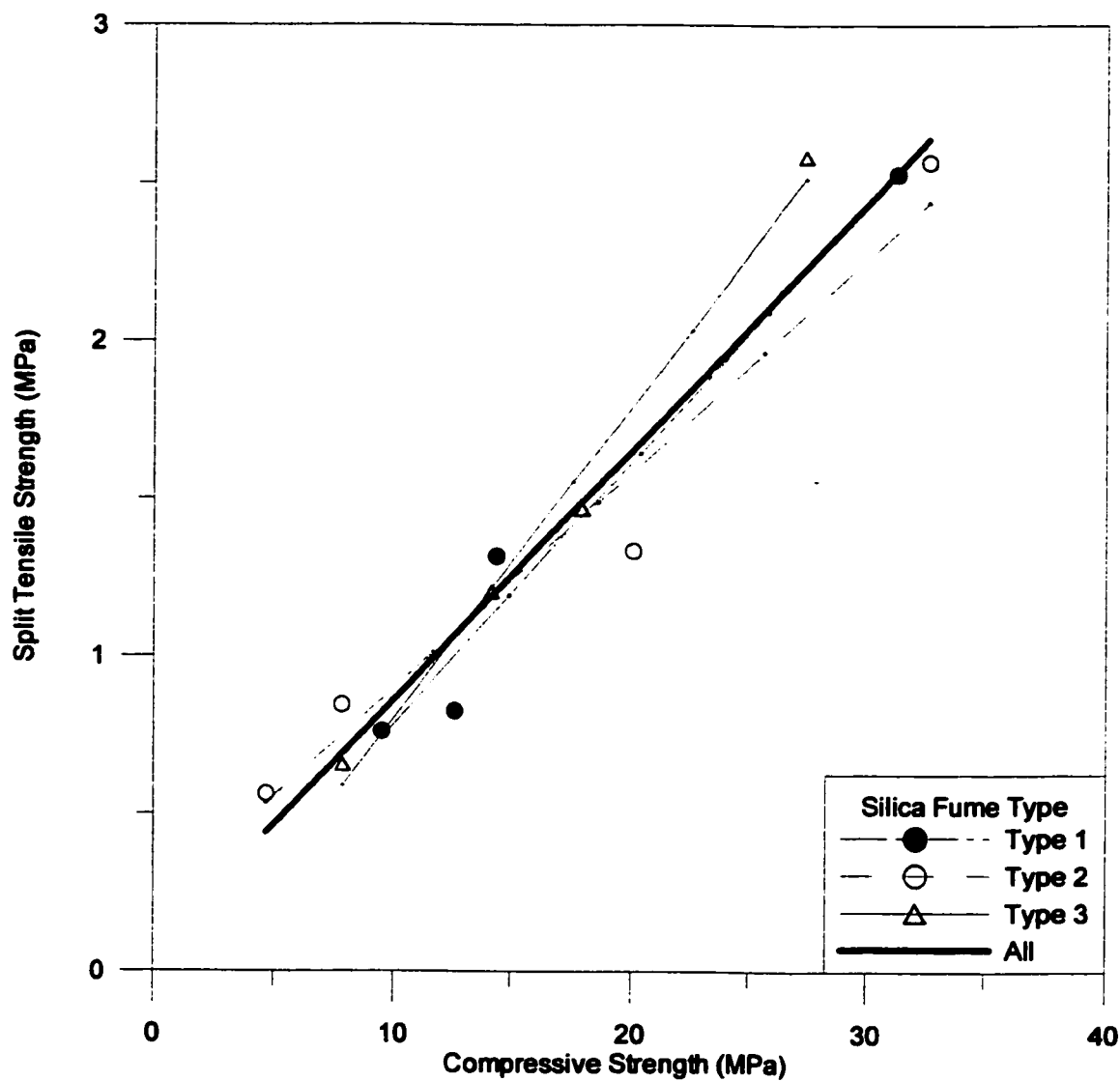


Figure 4.61: Relationship between the split tensile and compressive strength of silica fume cement concretes (temperature of 45 °C, RH of 35% and wind velocity of 15 km/hr).

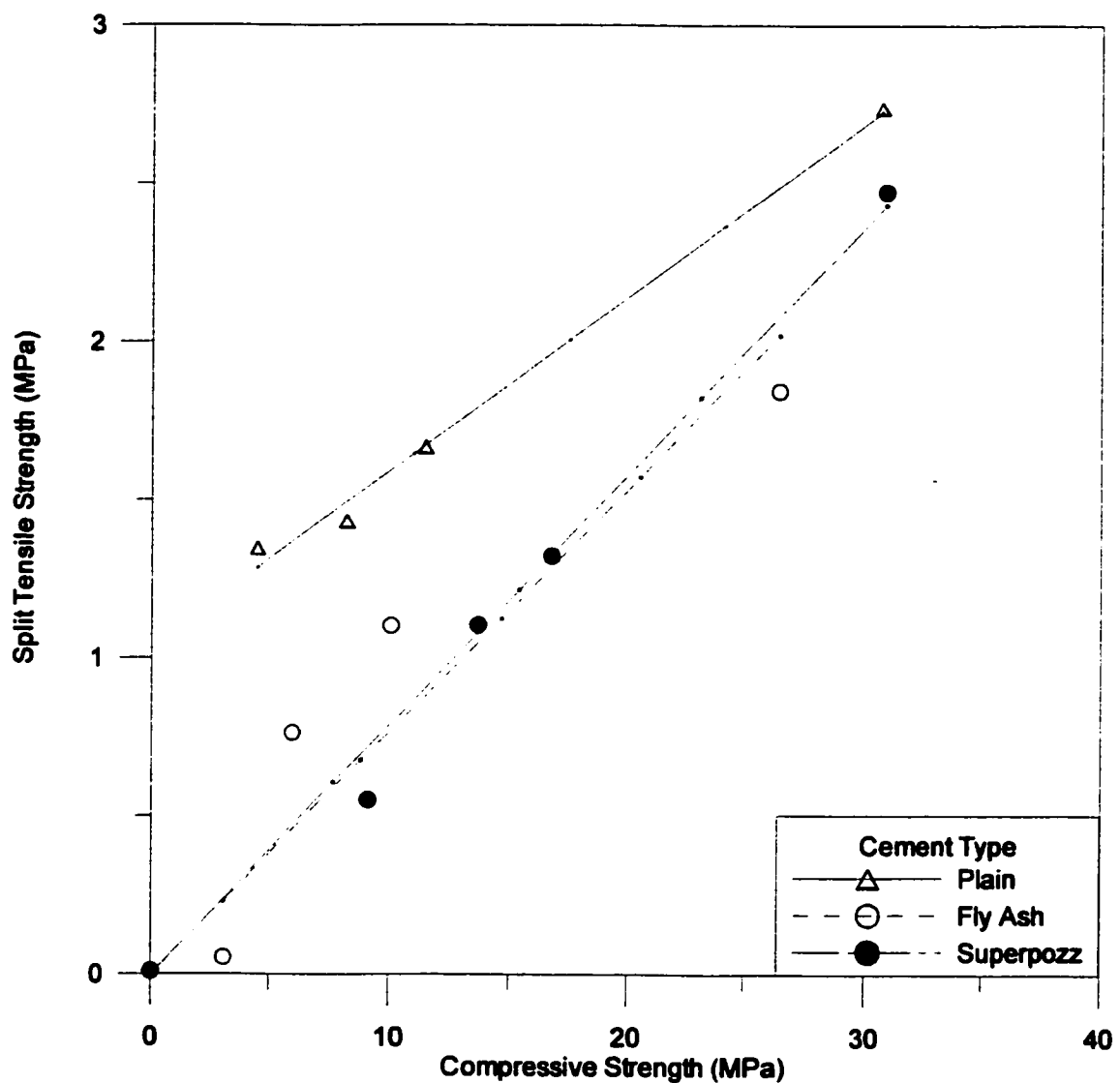


Figure 4.62: Relationship between the split tensile and compressive strength of plain, fly ash and Superpozz® cement concretes (temperature of 45 °C, RH of 35% and wind velocity of 15 km/hr).

CHAPTER 5

CONCLUSIONS AND RECOMMENDATIONS

The experimental program was conducted to study the effects of the type and dosage of silica fume on the plastic shrinkage cracking and strains in blended cement concretes under hot weather conditions. In addition, data on drying shrinkage, compressive strength, and split tensile strength and pulse velocity at early ages under hot weather conditions were developed. The compatibility of the selected silica fume and some types of superplasticizers was also evaluated.

5.1 CONCLUSIONS

The following most important conclusions can be drawn based on the data presented in Chapter 4:

1. The type and dosage of silica fume significantly affected the strains and cracking of the resulting concrete cast under hot weather conditions.
2. There exists a threshold value of plastic shrinkage strain of 1,100 μm that would initiate cracks. This threshold value of plastic shrinkage strain was found to be independent of the exposure conditions.
3. The plastic shrinkage strain in plain and blended cements was related directly to the fineness of the silica fume or blended cement material in question.
4. Statistical analysis has shown that the variability due to the type and dosage of silica fume in cement concrete is of the same order as material variability generally occurring in plain cement concrete. This is true for the compressive strength as well as the split tensile strength of concrete, with proper quality control.

Other conclusions of this study are presented in the following sections.

5.1.1 Effect of Type and Dosage of Blending Material on Plastic Shrinkage Strain

1. The plastic shrinkage strain increased with increasing the dosage of the silica fume irrespective of the type of silica fume used. Plastic shrinkage strains in the silica fume cement concretes were higher than those in plain cement concrete.
2. The plastic shrinkage strain in fly ash and Superpozz® cement concretes was higher than that of plain cement concrete but lower than that of the silica fume cement concretes.
3. The highest plastic shrinkage strain was noted in Type 2 silica fume cement concrete. This was attributed to its undensified nature that had less bulk density and a higher specific surface area compared to the other silica fumes.

5.1.2 Effect of Exposure Conditions on Plastic Shrinkage Strain and Cracks

4. The plastic shrinkage strains in the silica fume cement concretes increased with increasing the exposure temperature and decreasing the relative humidity and increasing the wind velocity.

5. A decrease in the relative humidity created the most severe exposure condition resulting in increased plastic shrinkage strain as compared to an increase in both the temperature and wind velocity.
6. Plastic shrinkage cracks occurred in three of the five types of silica fume cement concretes. No cracks were observed in plain, fly ash and Superpozz® cement concretes under the specified exposure conditions. No relationship was observed between the plastic shrinkage strains and the intensity of cracks.
7. The specific surface area-average pore radius (SSA/APR) ratio was found to have a direct relation with the plastic shrinkage strain and cracking.
8. In the Type 1 silica fume cement concrete that exhibited cracking at all dosages, the intensity and total area of cracks increased with increasing the dosage of silica fume. The time to cracking also varied with the dosage of the silica fume. Types 3 and 4 silica fume cement concretes both cracked at a dosage of 10% only.
9. In almost all the slabs that exhibited cracking, the cracks went through the full thickness of the 30 mm-thick slabs.

10. Cracks were developed at extreme exposure conditions (i.e. at a temperature of 45 °C) while no cracks were observed at lower temperatures. A decrease in the relative humidity produced the most severe conditions, with cracks developing at all the relative humidity values except at a RH of 60%. An increase in the wind velocity likewise led to the formation of cracks, a velocity of 15 km/hr was required to initiate cracks.

5.1.3 Incompatibility between Superplasticizer and Silica Fume Cement Concrete

11. The time to achieve maximum strain provided an approximate indication of the incompatibility between the superplasticizer and silica fume. The higher the time to achieve maximum strain the better would be the concrete in gaining the necessary tensile strength so as to be able to resist cracking. However, no correlation between the type and dosage of silica fume and the time to achieve maximum strain could be noted.
12. Incompatibility of silica fume and superplasticizers was assessed in terms of an excessive variation in time to achieve maximum strain with increasing the dosage of silica fume. Incompatibility was noted between PCE superplasticizer and plain and Types 1 and 3 silica fume cements.

5.1.4 Temperature Distribution in Concrete Slabs

13. The internal temperature in the concrete slabs increased marginally from the initial placement temperature to a peak value before decreasing to the exposure temperature. The internal concrete temperature due to the development of the heat of hydration alone could not be reliably assessed as the exposure “ambient” temperature dominated the temperature of the concrete. As such, very little variation was found in the temperature profiles of the different types of blended cement concretes.

5.1.5 Drying Shrinkage

14. Drying shrinkage in mortar bars increased with increasing the dosage of silica fume. All the five types of silica fume, fly ash and Superpozz® cement mortars exhibited drying shrinkage strains higher than that of plain cement concrete.
15. Concrete incorporating silica fumes and exposed to severe hot weather conditions exhibited differing drying shrinkage behavior that depended on both the type and dosage of silica fume. The extent to which the presence of silica fume in concrete mitigated or compounded drying shrinkage depended on the extent of curing, severity of exposure conditions and type and dosage of silica fume.

5.1.6 Pulse Velocity of Concrete Slabs

16. Ultrasonic pulse velocity in concrete slabs taken after a period of 90 days gave a good indication of the denseness of the concrete matrix although the effect of the presence of micro-cracks on the results cannot be ruled out. Fly ash, Superpozz,[®] Types 1, 2 and 3 silica fume cement concretes appeared to be denser than Types 4 and 5 silica fume cement concretes. Further points are noted below:

- The fact that the type of silica fume was densified or densified did not affect the pulse velocity of the resulting concrete.
- There was marginal or no difference in the pulse velocity values of plain cement concrete and that of silica fume cement concretes under the prevailing exposure conditions.

5.1.7 Strength of Concrete at Early Ages

17. The compressive strength development of silica fume cement concretes was different from that of plain cement concrete. The compressive strength development of fly ash and Superpozz[®] cement concrete was similar to that of plain cement concrete. However, the rate of strength development in the former was much slower than that of the latter. After 28 days of curing, the highest

compressive strength was noted in Type 2 silica fume cement concrete, while it was least in fly ash cement concrete.

18. In terms of the dosage of silica fume, 5% replacement of silica fume produced the highest compressive strength while the 10% replacement produced the lowest strength. This may be attributed to the effect of curing, which lasted for one day after casting. One would expect the reverse trend that is, the 10% replacement producing the highest strength to be true. This clearly emphasizes the importance of curing of blended cement concretes in achieving optimum strength, especially when exposed to hot weather conditions.
19. The development of the split tensile did not follow a similar pattern as that of the compressive strength. No significant differences could be observed in the development of the split tensile strength of plain and blended cement concretes. There were also very little differences in the split tensile strength as far as the dosage of silica fume was concerned. Only fly ash cement concrete showed a slight variation, due to its slow strength development.
20. Contrary to the compressive strength data, the pulse velocity in the 5% silica fume cement concrete was the highest while it was lowest in the 10% silica fume cement concrete. The pulse velocity in plain cement concrete was more than that

in the blended cement concrete.

5.1.8 Correlation between the Compressive Strength and Pulse Velocity in Blended Cement Concretes

21. The pulse velocity and compressive strength readings were correlated using a two-stage (i.e., bi-linear) regression model. The first line was fitted up to 24 hours, while the other line correlated the data between 1 and 28 days. Correlation coefficients were relatively high and consistent for the former while the values were generally poor for the latter due to the limited number of test data points.
22. The effect of the type of silica fume on the pulse velocity-compressive strength models was significant. The effect of the dosage of the silica fume on the pulse velocity-compressive strength models was also found to be significant and of the same order of magnitude as the effect of the type of silica fume.

5.1.9 Correlation between the Split Tensile Strength and Compressive Strength

23. The correlation between the split tensile and compressive strengths of plain and blended cement concretes was statistically very accurate. No differences were noted between the correlation for the split tensile and compressive strengths of

plain and blended cement concretes. Only fly ash cement concrete produced a relatively low correlation coefficient of variation.

5.1.10 Effect of Type of Superplasticizer on the Plastic Shrinkage Strain

24. The type of superplasticizer was found to affect the plastic shrinkage strain and the susceptibility of the concrete to plastic shrinkage cracking. For example, the use of superplasticizer in the silica fume cement concretes improved its ability to resist plastic shrinkage cracking. However, this effect could not be reproduced and is to be treated with caution.
25. In this investigation, the maximum plastic shrinkage strain was noted in Type 2 silica fume cement concrete, for all the four types of superplasticizer used. This was attributed to the undensified nature of this silica fume. The least plastic shrinkage strain was noted in the plain cement concrete.
26. No apparent relationship could be found between the volume change (i.e. plastic and drying shrinkage) of plain and blended cement concretes, and their pore volumes at the micro-structural level. The ratio of the specific surface area to the total pore volume in Types 4 and 5 silica fume and Superpozz® cement concretes was better than that in Types 1, 2 and 3 silica fume, fly ash and plain cement

concretes.

5.2 RECOMMENDATIONS

- 1) Where plastic and drying shrinkage cracks are not of concern, undensified silica fume could be used to produce concrete of higher compressive strength. There exists a threshold value of plastic shrinkage strain of $1,100 \mu\text{m}$ that would initiate cracking. This value of plastic shrinkage strain should be used with a silica fume of high SSA and bulk density.
- 2) The adverse effect of changes in the relative humidity and wind velocity on the properties of the concrete should be avoided. Early loss of moisture must be prevented by:
 - a. Continuous water curing, use of wet-burlap, use of curing compounds, etc;
 - b. Use of wind breakers; and
 - c. Avoid casting during summer days.
- 3) Superpozz[®] could also be used to reduce the plastic shrinkage cracking.

- 4) In order to minimize the drying shrinkage in blended cement concretes, silica fume with lower SSA should be used.
- 5) Modified lignosulfate polymer (MLP) type of superplasticizer is recommended for use in hot weather conditions to reduce the plastic shrinkage strain and cracking.
- 6) Trial mixes of blended cement and superplasticizer must be conducted to investigate the effect of superplasticizers on blended cement concretes to control the workability in order to detect any incompatibility that may arise. Where possible, these mixes should be prepared on site, i.e., under the same environmental media representative of the site conditions.

5.3 FUTURE STUDY

Based on the results presented herewith, it is recommended that further research be conducted in the following areas:

- 1) To study the effect of type and dosage of silica fume on the concrete properties at the micro-structural level using advanced techniques, such as the image intensity

mapping technique (IIT), scanning electron microscopy (SEM) and nuclear magnetic resonance (NMR) imaging, in order to further characterize the mechanisms of plastic and drying shrinkage.

- 2) Study the chemistry of the interaction between different types of superplasticizers and cement concrete incorporating blended cement materials.

REFERENCES

1. Rasheeduzzafar, "Fields Studies on the Durability of Concrete Construction in a High Chloride-Sulphate Environment", *House Science*, Vol. 4, No. 3, 1980, pp. 203-232.
2. Fooks, P.G. and Collis, L., "Problems in the Middle East Concrete", *Concrete*, Vol. 9, No. 7, July 1975, pp. 12-16.
3. Zein Al-Abideen H.M., "Concrete Practices in the Arabian Peninsula and the Gulf", *Materials and Structures*, Vol. 31, No. 208, May 1998, pp. 275-280.
4. Saricimen H., "Concrete Durability Problems in The Arabian Gulf Region- A Review", *Proceedings, Fourth International Conference on Deterioration and Repair of Reinforced Concrete* in the Arabian Gulf, Bahrain, 1993, pp. 943-959.
5. Mohammed Abdul-Waris, *Plastic Shrinkage Cracking in Hot Weather Conditions*, MS Thesis, Department of Civil Engineering, King Fahd University of Petroleum and Minerals, Dhahran, Saudi Arabia, 1996.
6. Maslehuddin, M., *Optimization of Concrete Mix Design for the Durability in the Eastern Province of Saudi Arabia*, MS thesis, Department of Civil Engineering King Fahd University of Petroleum and Minerals, Dhahran, Saudi Arabia, 1981.
7. Al-Saadoun S.S., Rasheeduzzafar, and Al-Gahtani, A.S., "Mix Design Considerations for Durable Concrete in the Gulf Environment", *Arabian Journal for Science and Engineering*, Vol. 17, No. 1, January 1992, pp. 17-33.
8. Venecanin, S.D., "Influence of Temperature on Deterioration of Concrete in the Middle East", *Concrete*, Vol. 8, No. 11, 1977, pp. 31-32.
9. Hsu, T.T.C., "Mathematical Analysis of Shrinkage Stresses in a Model of Hardened Concrete", *ACI Journal Proceedings*, Vol. 60, No.3, March 1963, pp. 371-390.

10. Slate, F.O., and Matheus, R.E., "Volume Changes upon Setting and Curing of Cement Paste and Concrete from Time Zero to Seven Days", *ACI Journal Proceedings*, Vol. 6, No.1 January 1967, pp. 34-39.
11. Rasheeduzzafar, and Al-Kurdi, S.M.A., "Effect of Hot Weather Conditions on the Microcracking and Corrosion Cracking Potential of Reinforced Concrete", *Durable Concrete in Hot Climates*, American Concrete Institute SP-139, Detroit 1993, pp. 1-20.
12. Al-Amoudi, O.S.B., Rasheeduzzafar, Maslehuddin, M., and Almusallam, A. A., "Improving Concrete Durability In the Arabian Gulf" *Proceedings, 4th International Conference on Deterioration and Repair of Reinforced Concrete in the Arabian Gulf*, Vol. 2, October 1993, pp. 929-940.
13. Rasheeduzzafar, Dakhil, F. H., and Mukkaram, K., "Influence of Cement Composition and Content on the Corrosion behavior of Reinforcing Steel in Concrete", *American Concrete Institute*, Special Publication SP-100, Detroit 1987, pp.1477-1503.
14. Maslehuddin, M., Al-Mana, A.I., Sacricimen, H., and Shamim, M., "Corrosion of Reinforcing Steel in Concrete Containing Slag or Pozzolans", *Cement, Concrete and Aggregates*, Vol. 12, No. 1, 1990, pp. 24-31.
15. Hussain, S.E., "Mechanisms of High Durability Performance of Plain and Blended Cements", PhD Dissertation, King Fahd University of Petroleum & Minerals, Dhahran, 1991.
16. Al-Amoudi, O. S. B., Abduljauwad, S.N., Rasheeduzzafar and Maslehuddin, M., "Effect of Chloride and Sulfate Contamination in Soils on the Corrosion of Steel and Concrete", *Transportation Research Record*, No. 1345, 1992, pp. 67-73.
17. Samman, T.A., Mirza, W.H., and Wafa, F.F., "Plastic Shrinkage Cracking of Normal and High Strength Concrete: A Comparative Study," *ACI Materials Journal*, Vol. 93, No. 1, Jan-Feb. 1996, pp. 36-40.
18. Uno, P.J., "Plastic Shrinkage Cracking and Evaporation Formulas," *ACI Materials Journal*, Vol. 95, No. 4, Jul-Aug. 1998, pp. 365-375.
19. ACI Committee 305, "Hot Weather Concreting", Committee Report 305 R-91, *American Concrete Institute*, 1991.

20. Jaegermann, C. H., Ravina, D., and Pundak, B., "Accelerated Curing of Concrete by Solar Radiation", *Proceedings, RILEM International Symposium on Concrete and Reinforced Concrete in Hot Countries*, Institute of Technology, 1971, pp. 339-362.
21. "Development of Building and Construction Materials Using Available Resources in Saudi Arabia", Technical Report, SANCST Project AR-4.
22. "Making Good Concrete in the Heat of Summer", *Concrete International*, Vol. 14, No. 4, April 1992, pp. 55-57.
23. Hover, K., "Keeping Concrete Cool in the Heat of Summer", *Aberdeen's Concrete Construction*, Vol. 38, No. 6, June 1993, pp. 433-436.
24. Bloom, R., and Bentur, A., "Free and Restrained Shrinkage of Normal and High-Strength Concrete", *ACI Materials Journal*, Vol. 92, No. 2, Mar-Apr. 1995, pp. 211-217.
25. Al-Amoudi, O.S.B., Mashlehuddin, M., and Bader, M.A., "Characteristics of Silica Fume and its Impact on Concrete in the Arabian Gulf," *Concrete*, Vol. 35, No. 2, February 2001, pp. 45-50.
26. Concrete Society Working Party, "Non-structural Cracks in Concrete", Technical Report, The Concrete Society, UK, Dec. 1982.
27. Chatterji, S., "Probable Mechanisms of Crack Formation at Early Ages of Concrete: A Literature Survey," *Cement and Concrete Research*, Vol. 12, 1982, pp. 371- 376.
28. Lea, F.M., *The Chemistry of Cement and Concrete*, 3rd edition, Arnold, London, 1970, pp. 269.
29. Radocea, A., *A Study on the Mechanism of Plastic Shrinkage on Cement-Based Materials*, PhD Dissertation, Chalmers University of Technology Gothenburg, Sweden, 1992.
30. Shalon, R., and Ravina, D., "Studies in Concreting in Hot Countries", *RILEM International Symposium on Concrete and Reinforced Concrete in Hot Countries*, 1960, pp. 1-46.
31. Jaegermann, C.H., and Glucklich, J., "Effect of Plastic Shrinkage on Subsequent

- Shrinkage and Swelling of the Hardened Concrete", *Proceedings, International Colloquium on the Shrinkage of Hydraulic Concretes*, Madrid 1968, Vol. 1, pp. 1-26.**
32. Shalon, R., and Ravina, D., "Shrinkage of Fresh Mortars Cast Under and Exposed to Hot Dry Climate conditions", *RILEM-CEMBUREAU Colloquium on the Shrinkage of Hydraulic Concretes*, Madrid 1968, Vol. 2, pp. 1-19.
 33. Shalon, R., and Ravina, D., "Plastic Shrinkage Cracking", *ACI Journal Proceedings*, Vol. 65, No. 4, April 1968, pp. 282-291.
 34. Kral, S., and Gabauer, J., "Shrinkage and Cracking of Concrete at Early Ages," *Proceedings, Conference Internationale sur le Dallas en Beton*, Dundee, Apr. 1979, pp. 412-420.
 35. Berhane, Z., "Evaporation of Water from Fresh Mortar and Concrete at Different Environmental Conditions", *ACI Journal Proceedings*, Vol. 81, No. 6, Nov-Dec. 1984, pp. 560-565.
 36. Almusallam, A.A., Maslehuddin, M., Abdul-Waris, M., Dakhil, F.H., and Al-Amoudi, O.S.B., "Plastic Shrinkage Cracking of Blended Cement Concretes in Hot Environments," *Magazine of Concrete Research*, Vol. 51, No. 4, August 1999, pp. 241-246.
 37. Blakey, B.E. and Beresford, F.D, "Cracking of Concrete", *Construction Review* (Sydney), Vol. 32, No. 4, February, 1959, pp. 100-108.
 38. Shaeles, C.A., and Hover, K.C., "Influence of Mix Proportions and Construction Operation on Plastic Shrinkage Cracking in Thin Slabs," *ACI Materials Journal*, Vol. 85, No. 6, Nov-Dec. 1988, pp. 495-504.
 39. Almusallam, A.A., Maslehuddin, M., Abdul-Waris, and Khan, M.M., "Effect of Mix Proportions in the Plastic Shrinkage Cracking of Concrete in Hot Environments," *Construction and Building Materials*, Vol. 12, 1998, pp. 353-358.
 40. Troxell, G.E., Raphael, J.M., and Davis, R.E., "Long-Term Creep and Shrinkage Tests of Plain and Reinforced Concrete," *Proceedings ASTM*, Vol. 58, 1958, pp. 1101-1120.
 41. Richard, T.E., *Creep and Drying Shrinkage of Lightweight and Normal Weight Concrete*, Technical Report, Monograph 74, National Bureau of Standards,

- Washington DC, 1964, pp. 30.
42. Powers, T.C., "Causes and Control of Volume Change," *Portland Cement Association Research and Development Laboratories*, No 1, Jan. 1959. pp. 29-39.
 43. Reeves, C.M., "The Use of Ground Granulated Blast Furnace Slag to Produce Durable Concrete," *How to Make Today's Concrete Durable for Tomorrow, Iceland*, UK. Thomas Telford, London, 1985, pp. 59-75.
 44. Cabrera, J.G., "The Use of Pulverized Fly Ash to Produce Durable Concrete," *How to Make Today's Concrete Durable for Tomorrow, Iceland*, UK. Thomas Telford, London, 1985, pp. 29-57.
 45. Cabrera, J.G., and Nwaubani, S. O., "The Influence of High Temperature on Strength and Pore Structure of Concrete Made with Natural Pozzolan," *Proceedings, 3rd International RILEM Conference on Concrete in Hot Climates*, Torquay, England, Sept. 1992, pp. 101-113.
 46. Wainright, P.J., Cabrera, J.G., and Al-Amri, A.M., "Performance and Properties of Pozzolanic Mortars Cured in Hot Dry Environments," *Proceedings, 3rd International RILEM Conference on Concrete in Hot Climates*, Torquay, England, Sept. 1992, pp. 115-128.
 47. Haque, M.N., and Kayyali, O.A., "Strength and Porosity of Hardened Paste-Cement-Fly-Ash Pastes in Hot Environments," *ACI Materials Journal*, Vol. 86, No. 2, 1989, pp. 128-134.
 48. Svenkerud, P.J., and Knusten, K., "The Use of Microsilica in the Arabian Gulf," *Proceedings, 4th International Conference on Deterioration and Repair of Reinforced Concrete in the Arabian Gulf*, Vol. 2, October, 1993, pp. 961-973.
 49. Al-Sugair, F.H., "Analysis of the Time-Dependent Volume Reduction of Concrete containing Silica Fume," *Magazine of Concrete Research*, Vol. 4, No.170, Mar. 1995, pp. 77-81.
 50. Sellevold, J., Bager, D.H., Jensen, E.K. and Knudsen, T., "Silica Fume Cement Paste - Hydration and Pore Structure," in: *Condensed Silica Fume in Concrete*, Gjorv, O.E., and Loland K.E. (Eds.), University of Trondheim, Norway, 1982, pp. 19-50.
 51. ACI Committee 226, "Silica Fume in Concrete," *ACI Materials Journal*, Vol. 84,

- No. 2, 1987, pp. 158-166.
52. Delage, P., and Aitcin, P.C., "Influence of Condensed Silica Fume on the Pore Size Distribution of Concretes," *Industrial Engineering Chemical Production Research and Development*, Vol. 22, No. 2, 1983, pp. 286-290.
 53. Detwiler, R.J., and Mehta, P.K., "Chemical and Physical Effects of Silica Fume on the Mechanical Behavior of Concrete, *ACI Materials Journal*, Vol. 86, No. 6 1989, pp. 609-614.
 54. Cong, X., "Role of Silica Fume in the Compressive Strength of Cement Paste, Mortar, and Concrete," *ACI Materials Journal*, Vol. 89, No. 4, 1992, pp. 375-387.
 55. Malhotra, V.M., and Carette, G.G., "Silica Fume Concrete - Properties, Applications and Limitations," *Concrete International*, Vol. 5, No. 5, 1983, pp. 40-46.
 56. Al-Khaja, W.A., "Strength and Time-Dependent Deformations of Silica Fume Concrete for Use in Bahrain," *Construction and Building Materials*, Vol. 8, No. 3, 1993, pp. 169-172.
 57. Cohen, M.D., Olek, J., and Dolch, W.L., "Mechanism of Plastic Shrinkage Cracking in Portland Cement and Portland-Cement-Silica Fume Paste and Mortar," *Cement and Concrete Research*, Vol. 20, No. 1, 1990, pp. 103-119.
 58. Al-Amoudi, O.S.B., *Studies on the Evaluation of Permeability and Corrosion Resisting Characteristics of Portland Pozzolanic Concrete*, MS thesis, Department of Civil Engineering, King Fahd University of Petroleum and Minerals, Dhahran, Saudi-Arabia, 1985.
 59. Wittman, F.H., "On the Action of Capillary Pressure in Fresh Concrete," *Cement and Concrete Research*, Vol. 6, No. 1, 1976, pp. 49-56.
 60. Powers, T.C., "Properties of Cement Paste and Concrete", *Proceedings, 4th International Symposium on the Chemistry of Cement*, Paper VI in session V, Washington D.C., 1960, pp. 577-608.
 61. Pihlajavaara, S.E., "A Review of Some of the Main Results of a Research on the

- Ageing Phenomena of Concrete: Effect of Moisture Conditions on Strength, Shrinkage and Creep of Mature Concrete" *Journal of Cement and Concrete Research*, Vol. 4, 1974, pp. 761-771.
62. Radocea, A., "A Model of Plastic Shrinkage," *Magazine of Concrete Research*, Vol. 46, No. 167, June 1994, pp. 125-132.
 63. Collepardi, M., "Admixtures Used to Enhance Placing Characteristics of Concrete," *Cement and Concrete Composites*, Vol. 20, No. 2/3, 1998, pp. 103-112.
 64. ACI Committee 212, "Chemical Admixtures for Concrete," *Manual of Concrete Practice*, Part 1, 1993, pp. 212.R1 to 212.R1-31.
 65. Ramachandran, V.S., and Malhotra, V.M., "Superplasticizers," in: "Concrete Admixtures Handbook", Edt. V.S. Ramachandran, Noyes Publications, New Jersey, 1984, pp. 211-265.
 66. Chandra, S., and Flodin, P., "Interaction of Polymers and Organic Admixtures on Portland Cement Hydration" *Cement and Concrete Research*, Vol. 17, No. 6, 1987, pp. 875-890.
 67. Chan, R.W.M., Ho, P.N.L., and Chan, E.P.W. *Concrete Admixtures for Waterproofing Construction*, Technical Report, Structural Materials Group, Structural Engineering Branch, Architectural Services Department, Government of Hong Kong, December 1999.
 68. Anderson, P.J., and Roy, D.M., "Effect of Superplasticizer Molecular Weight on Its Adsorption and Dispersion of Cement," *Cement and Concrete Research*, Vol. 18, No. 6, 1988, pp. 980-986.
 69. Uchikawa, H., Hanehara, S., Shirasaka, T., and Sawaki, D., "Effect of Admixture on Hydration of Cement, Adsorptive Behavior of Admixture, and Fluidity and Setting of Fresh Cement Paste," *Cement and Concrete Research*, Vol. 22, No. 6, 1992, pp. 1115-1129.
 70. Jolicoeur, C., Nkinamubanzi, P.C., Simard, M.A., and Piotte, M., "Progress in Understanding the Functional Properties of Superplasticizers in Fresh Concrete," *Proceedings, 4th CANMET/ACI International Conference on Superplasticizers and Chemical Admixtures*, SP-148, American Concrete Institute, Detroit, 1994, pp. 63-88.

71. Older, T., and Becker, T., "Effect of Some Liquefying Agents on Properties and Hydration of Portland Cement and Tricalcium Silicate Pastes," *Cement and Concrete Research*, Vol. 10, No. 3, 1980, pp. 321-331.
72. Simard, M.A., Nkinamubanzi, P.C., Jolicoeur, C., Perraton, D., and Aitcin, P.C., "Calorimetry, Rheology and Compressive Strength of Superplasticized Pastes," *Cement and Concrete Research*, Vol. 23, No. 4, 1993, pp. 939-950.
73. Gagne, R., Boisvert, A., and Pigeon, M., "Effect of Superplasticizer Dosage on Mechanical Properties, Permeability, and Freeze-Thaw Durability of High-Strength Concretes with and without Silica Fume," *ACI Materials Journal*, Vol. 93, No. 2, March-April, 1996, pp. 111-120.
74. Hanna, E., Luke, K., Perraton, D., and Aitcin, P.C., "Rheological Behavior of Portland Cement in the "Presence of a Superplasticizer," *Proceedings, Third International conference on, "Superplasticizers and other Chemical Admixtures in Concrete,"* ACI SP-119, Detroit, 1989, pp. 171-188.
75. Dodson, V., *Concrete Admixtures*, Van Nostrand Reinhold, London, 1990, pp. 211.
76. Aitcin, P.C., Jolicoeur, C., and Macgregor, J.G., "Superplasticizers: How They Work and Why They Occasionally Don't," *Concrete International*, Vol. 16, No. 5 May 1994, pp. 45-52.
77. Taghit-Hamou, A., Baalbaki, I.M., and Aitcin, P-C, "Calcium Sulfate Optimization in Low Water/cement Ratio Concrete for Rheological Purposes," *Proceedings, 9th International congress on the Chemistry of Cement*, New Delhi, 1992, pp. 21-25.
78. Ramachandran, V.S., Lowery, M.S., and Malhotra, V.M., "Behavior of ASTM Type V Cement hydrated in the Presence of Sulfonated Melamine Formaldehyde," *Materials and Structures*, Vol. 28, No. 177, May 1995, pp. 133-138.
79. RamezanianPour, A.A., and Malhorta, V.M., "Effect of Superplasticizers on the Microstructure and Strength of Concrete Made with ASTM Type V Cement," *Materials and Structures*, Vol. 29, No. 187, February 1996, pp. 141-148.
80. ACI Committee 234R-96, *Guide for the Use of Silica fume in Concrete*, Report by

- ACI Committee 234, ACI, Farmington Hills, Michigan, 1997.
81. Rosenberg, A.M., and Gaidis, J.M., "A New Mineral Admixture for High-Strength Concrete – Proposed Mechanism for Strength Enhancement," *Concrete International: Design and Construction*, Vol. 11, No. 4, 1989, pp. 31-36.
 82. De Larrard, F., "Method for Proportioning High-Strength Concrete mixtures," *Cement, Concrete, and Aggregates*, Vol. 12, No. 2, Summer 1990, pp. 47-52.
 83. Yogendran, V., Langan B.W., Haque, M.N., Ward, M.A., "Silica Fume in High-Strength Concrete," *ACI Materials Journal*, Vol. 84, No. 2, 1987, pp. 124-129.
 84. Al-Manaser, A.A., and Keil, D.L., "Physical Properties of Cement Grout Containing Silica Fume and Superplasticizer," *ACI Materials Journal*, Vol. 89, No. 2, 1992, pp. 154-160.
 85. Kucharska, L., and Moczko, M., "Influence of Silica fume on the Reological Properties of the Matrices of High-Performance Concretes," *Advances in Cement Research*, Vol. 6, No. 24, Oct. 1994, pp. 139-145.
 86. Soroka, I., and Ravina, D., "Hot Weather Concreting with Admixtures," *Cement and Concrete Composites*, Vol. 20, No. 2/3 1998, pp. 129-136.
 87. Previte, R.W., "Concrete Slump Loss". *Proceedings, ACI Materials Journal*, Vol. 74, No. 8, 1977 pp. 361-367.
 88. Hampton, J.S., "Extended Workability of Concrete Containing High-Range Water-Reducing Admixtures in Hot Weather," In: *Development in the Use of Superplasticizers*, ACI SP 68, American Concrete Institute, Detroit, 1981, pp. 409-22.
 89. Mailvaganam, N.P., "Factors Influencing Slump Loss in Flowing Concrete," In: *Superplasticizers in Concrete*, ACI SP 62, American Concrete Institute, Detroit, 1979, pp. 389-403.
 90. Fattuhi, N.I., "Influence of Temperature on the Setting of Concrete Containing Admixtures," *Construction Building Materials*, Vol. 2, 1988, pp. 27-30.
 91. El-Rayyes, M.S., "Remedies to Rapid Setting in Hot Weather Concreting," In *Proc. RILEM Symposium, Admixtures for Concrete*, Ed. E. Vazques, Chapman & Hall, London, 1992, pp. 120-134.

92. Pinto, R.C.A., and Hover, K.C., "Effect of Silica fume and Superplasticizer Addition on Setting behavior of High-Strength Mixtures," *Transportation Research Record No. 1574*, Washington, D.C., 1997, pp. 56-62.
93. Pinto, R.C.A., and Hover, K.C., "Superplasticizer and Silica Fume Addition Effects on Heat of Hydration of Mortar Mixture with low Water-Cementitious Materials Ratio" *ACI Materials Journal*, Vol. 96, No. 5 Sept-Oct. 1999, pp. 600-604.
94. Jolicoeur, C., Simard, M-A., "Chemical Admixture-Cement Interactions: Phenomenology and Physico-chemical Concepts," *Cement and Concrete Composites*, Vol. 20, No. 2/3, 1998, pp. 87-101.
95. Rixom, M.R., and Mailvaganam, N.P., *Chemical Admixtures for Concrete*, Second Edition, E. & F. N. SPON, London, 1986.
96. Mollah, M.Y.A., Palta, P., Hess, T.R., Vempati, R.K., and Cocke, D.L., "Chemical and Physical Effects of Sodium Lignosulfonate Superplasticizer on the Hydration of Portland Cement and Solidification/Stabilization Consequences," *Cement and Concrete Research*, Vol. 25 No. 3, 1995, pp. 671-82.
97. Bonen, D., and Sarkar, S.L., "The Superplasticizer Adsorption Capacity of Cement Pastes, Pore Solution Composition, and Parameters Affecting Flow Loss," *Cement and Concrete Research*, Vol. 25, No. 7, 1995, pp. 1423-1434.
98. Collerpardi, M., "Admixtures Used to Enhance Placing Characteristics of Concrete," *Cement and Composites*, Vol. 20, No.2/3, 1998, pp. 103-112.
99. Uchikawa., H., Hanehara, S., and Sawaki, D., "The Role of Steric Repulsive Forces in the Dispersion of Cement Particles in Fresh Pastes Prepared with Organic Admixture, *Cement and Concrete Research*, Vol. 27, 1997, pp. 37-50.
100. Guadong, X., and Beaudoin, J.J., "Effect of Polycarboxylate Superplasticizer on Contribution of Interfacial Transition Zone to Electrical Conductivity of Portland Cement Mortars," *ACI Materials Journal*, Vol. 97, No. 4, Jul-Aug. 2000, pp. 418-424.
101. Joana, R., *Effect of Superplasticizers on the Behavior of Concrete in the Fresh and Hardened States: Implication for High-Strength Concrete*, PhD dissertation, Universitat Politècnica de Catalunya, Barcelona, Spain, June 2000.

102. Abell, A.B., Willis K.L., and Lange D.A., "Mercury Intrusion Porosimetry and Image Analysis of Cement-Based Materials" *Journal of Colloidal and Interface Science*, Vol. 211, 1999, pp. 39-44.
103. Nicos, S.M., *Survey of Concrete Transport Properties and their Measurement*, United States Department of Commerce, Technology Administration, National Institute of Standards and Technology, Gaithersburg, MD 20899, February 1995.
104. Mehta, P.K., Monteiro, P. J. M., *Concrete, Structure, Properties and Materials* Prentice Hall, Second Edition, New Jersey, 1993.
105. Pentala, V.E., "Effects of Microporosity on the Compression Strength and Freezing Durability of High-Strength Concretes," *Magazine of Concrete Research*, Vol. 41, No. 148, September 1989, pp. 171-181.
106. Wing, K.S.W., "Historical Perspectives of Physical Adsorption" *Proceedings of the NATO Advanced Science Institute on Physical Adsorption: Experiment, Theory and Applications*, Edited by Fraissard, J., and Conner, C. W., Series C: Mathematical and Physical Sciences, Vol. 491, Kluwer Academic Publishers, Netherlands, 1997, pp. 3-8.
107. Wing, K.S.W., "Analysis of Physisorption Isotherms, Determination of Surface Area and Porosity" *Proceedings of the NATO Advanced Science Institute on Physical Adsorption: Experiment, Theory and Applications*, Edited by Fraissard, J., and Conner, C W., Series C: Mathematical and Physical Sciences, Vol. 491, Kluwer Academic Publishers, Netherlands, 1997, pp. 9-16.
108. ASTM C 1069-86 (1997) e1, *Standard Test Method for the Specific Surface Area of Alumina or Quartz by Nitrogen Adsorption*, American Society for Testing and Materials, Pennsylvania, 1997.
109. Yan, F., Ping G., Ping X., and Beaudoin, J. J., "Development of Eigenstress due to Drying Shrinkage in Hardened Portland Cement Pastes: Thermomechanical Analysis," *Concrete and Concrete Research*, Vol. 24, No. 6, 1994, pp. 1085-1091.
110. Persson, B., "Self Desiccation and its Importance in Concrete Technology", *The Nordic Seminar In Lund*, June 1997.
111. Bentz, D.P., Jensen, O.M., Hansen, K.K., Stang, H., and Haecker, C-J.,

- "Influence of Cement Particle Size Distribution on the Early Age Autogenous Strains and Stresses in Cement-Based Materials," *Journal of the American Ceramic Society*, Vol. 84, No. 1, 2001, pp. 129-135.
112. ASTM C 403-99, *Standard Test Method for Time of Setting of Concrete Mixtures by Penetration Resistance*, American Society for Testing and Materials, Pennsylvania, 1999.
 113. El Hindy, E., Buquan, M., Chaallah, O., and Aitcin, P-C., "Drying Shrinkage of High-Performance Concrete," *ACI Structural Journal*, Vol., 91, No. 3, May-June 1994, pp. 300-305.
 114. Whiting, D. A., Detwiler, R.J., and Lagergren, E.S., "Cracking Tendency and Drying Shrinkage of Silica Fume Concrete for Bridge Deck Applications," *ACI Materials Journal*, Vol., 97, No. 6, Nov-Dec. 2000, pp. 71-77.
 115. Burnett, I., "Silica Concrete in Melbourne, Australia", *Concrete International*, Vol. 13, No. 8, 1991, pp. 18-24.
 116. Moreno, J., "225W. Wacker Drive," *Concrete International*, Vol. 12, No.1, Jan. 1990, pp. 35-39.
 117. Bentur, A., and Cohen, M.D., "The Effect of Condensed Silica Fume on the Microstructure of the Interfacial Zone in Portland Cement Mortars," *Journal of the American Ceramic Society*, Vol. 84, No. 2, 1987, pp. 130-135.
 118. Cohen, M. D., Olek, J., and Bryant, M., "Silica Fume Improves Expansive-Cement Concrete" *Concrete International*, Vol. 13, No. 3, pp. 31-37, 1991.
 119. ACI Committee 226, "Silica Fume in Concrete," *ACI Materials Journal*, Vol. 84, No. 2, 1987, pp. 158-166.
 120. Malhotra, V.M., and Carette, G.G., "Silica Fume Concrete Properties, Applications and Limitations," *Concrete International*, Vol. 5, No. 5, 1983, pp. 40-46.
 121. Haque, M.N., and Kayali, O., "Properties of High-Strength Concrete Using a very Fine Fly Ash," *Cement and Concrete Research*, Vol. 28, No. 10, July 1998, pp. 1445-1452.
 122. Lura, K. van Breugel and Maruyama, I., "Autogenous and Drying Shrinkage of

- High Strength Lightweight Aggregate Concrete at Early Ages -The Effect of Specimen size, *Pre-proceedings RILEM International Conference on Early Age Cracking in Cementitious System*, (EAC'01), Hifa, 2001, pp.337-344.
123. Almudaiheem, J.A., and Hansen, W., "Prediction of Concrete Drying Shrinkage from Short-term Measurements," *ACI Materials Journal*, Vol. 86, No. 4, Jul-Aug. 1989, pp. 401-408.
 124. Persson, B., "Experimental Studies on Shrinkage of High-Performance Concrete," *Cement and Concrete Research*, Vol. 28, No. 7, pp. 1023-1036, 1998.
 125. Haque, M.N., "Strength Development and Drying Shrinkage of High-Strength Concretes," *Cement and Concrete Composites*, Vol. 18, No. 5, 1996, pp. 333-342.
 126. Almudaiheem, J.A., and Hansen, W., "Effect of Specimen Size and Shape on Drying Shrinkage of Concrete," *ACI Materials Journal*, Vol. 84, No. 2, Mar-Apr. 1987, pp.130-135.
 127. Swamy, R. N., and Lambert, G. H., "Shrinkage and Creep Behavior of Concrete made with PFA Coarse Aggregates," *Proceedings, Second International Conference on Fly ash, Silica fume, Slag ad Natural Pozzolan in Concrete*, 1986, Vol.1, pp. 145-170.
 128. Brull, L., Komlos, K., and Majzlan B., "Early Shrinkage of Cement Pastes, Mortars, and Concretes," *Materiaux et Constructions*, Vol. 13, No. 73, 1980, pp. 41-45.
 129. Jennings, H.M., Garci, M.C., Moss, G.M., Tennis, P.D., and O'Neil, E.F., "Why Volume Changes Matter: Relationship Between Microstructure and Shrinkage," *Concrete International*, Vol. 22, No. 5, May 2000, pp. 50-3.
 130. Jennings, H.M., and Tennis, P.D., "A model for the Developing Microstructure in Portland Cement Pastes," *Journal of the American Ceramic Society*, Vol. 77, No. 12, 1994, pp. 3161-72. Correction published in, *Journal of the American Ceramic Society*, Vol. 78, No. 9, 1995, pp. 2575.
 131. Jennings, H.M., Tennis, P.D., "A model for Two Types of C-S-H in the Microstructure of Portland Cement Pastes," *Cement and Concrete Research*, Vol. 30, No. 6, 2000, pp. 855-863.
 132. Gebler, S.H., and Klieger, P., "Effect of Fly Ash on the Physical Properties of

- Concrete," *Proceedings, 2nd International Conference on Fly Ash, Silica Fume, Slag and Natural Pozzolans in Concrete*, Vol. 1, 1986, pp.1-49.
133. Coppola, L., Troli, R., Borsoi, A., Zaffaroni, P., and Collepardi, M., "Influence of Superplasticizer Type on the Compressive Strength of RPM", *Proceedings, 5th CANMET/ACI International Conference on "Superplasticizers and other Chemical Admixtures in Concrete*, Roma, 7-10 October 1997, SP 173, pp. 512-536.
 134. Sicker, A., *Influence of Superplasticizer on the Autogeneous Shrinkage of High Performance Concrete*, Dr. rer. nat., Institut für Massivbau und Baustofftechnologie, Universität Leipzig, Leipzig Annual Civil Engineering Report (LACER) No. 4, 1999.
 135. Ramachandran, V.S., Feldman, R.F., Beaudoin, J.J., *Concrete Science. Treatise on Current Research*, Heyden, London, 1981.
 136. Elvery, R.H., and Ibrahim, L.A.M., "Ultrasonic Pulse Velocity of Concrete Strength at Early Ages," *Magazine of Concrete Research*, Vol. 28, No. 97, December 1976, pp. 180-190.
 137. Wen, H. X., Bagheri, A.R., and Plum, D.R., "The Strength Development of Silica Fume Concrete and Its Prediction under Varying Temperature Conditions," *Magazine of Concrete Research*, Vol. 41, No. 149, Dec. 1989, pp. 199-204.
 138. Neville, A.M., *Properties of Concrete*, Longman Scientific and Technical, Third edition, Essex, 1986.
 139. Gardener, N.J., "Effect of Temperature on the Early-Age Properties of Type I, Type III, and Type I/Fly Ash Concretes," *ACI Materials Journal*, Vol. 87, No. 1, Jan-Feb. 1989, pp. 68-78.
 140. 42-CEA Committee, Reports of Technical Committees, *Properties of Concrete at Early Ages*, 32nd Meeting of RILEM Permanent Committee, Rio de Janeiro, 1979.
 141. Bishr, H.A.M., Al-Amoudi, O.S.B., Basunbul, I.A., and Al-Sulaimani, G.J., "Assessment of Concrete Strength Using the Lok Test," *Construction and Building Materials*, Vol. 9, No. 4, August 1995, pp. 227-237.